PRODUCTION OF PETROCHEMICALS BY DEOXYGENATION OF MODEL LIGHT OXYGENATES FRACTION FROM BIO-OIL

AYUT WITSUTHAMMAKUL

A THESIS SUBMITTED IN PARTIAL FULFILLMENT
OF THE REQUIREMENT FOR THE DEGREE OF
DOCTOR OF PHILOSOPHY IN APPLIED CHEMISTRY
FACULTY OF SCIENCE
KING MONGKUT'S INSTITUTE OF TECHNOLOGY LADKRABANG
2015

KMITL-2015-SC-D-010-061

PRODUCTION OF PETROCHEMICALS BY DEOXYGENATION OF MODEL LIGHT OXYGENATES FRACTION FROM BIO-OIL

AYUT WITSUTHAMMAKUL

A THESIS SUBMITTED IN PARTIAL FULFILLMENT
OF THE REQUIREMENT FOR THE DEGREE OF
DOCTOR OF PHILOSOPHY IN APPLIED CHEMISTRY
FACULTY OF SCIENCE
KING MONGKUT'S INSTITUTE OF TECHNOLOGY LADKRABANG
2015
KMITL-2015-SC-D-010-061

หัวข้อวิทยานิพนธ์	การผลิตสารปิโตรเคมีโดยกระบวนการขจัดออกซิเจนออกจากส่วนที่เป็นออกซิจิเนตเบาจำลองในน้ำมันชีวภาพ
ชื่อนักศึกษา	นายอยุทธ์ วิทย์สุธรรมกุล
รหัสประจำตัว	54650301
ปริญญา	ปรัชญาดุษฎีบัณฑิต (เคมีประยุกต์)
ภาควิชา	เคมี
พ.ศ.	2558
อาจารย์ที่ปรึกษาวิทยานิพนธ์	รศ.ดร. ตะวัน สุขน้อย

บทคัดย่อ

งานวิจัยนี้มีจุดประสงค์เพื่อแปรรูปสารออกซิจิเนตเบาในน้ำมันชีวภาพเป็นสารปิโตรเคมีด้วยกระบวนการขจัดออกซิเจน โดยเลือกอะซิโตน เฟอร์ฟูรัล และกรดอะซิติก เป็นตัวแทนของสารกลุ่มคีโตน อัลดีไฮด์ และกรดอินทรีย์ การขจัดออกซิเจนออกจากสารเหล่านี้ด้วยวิธีดั้งเดิมต้องใช้อุณหภูมิและความดันสูง (สูงกว่า 673 เคลวิน และ 40 บาร์) ทำให้ได้ผลิตภัณฑ์เป็นพาราฟินเบาที่นำไปใช้ประโยชน์ได้จำกัดและมูลค่าต่ำ งานวิจัยนี้จึงมุ่งเน้นการแปรรูปด้วยสภาวะที่ไม่รุนแรง (ที่อุณหภูมิน้อยกว่า 573 เคลวิน และความดันบรรยากาศ) ซึ่งต้องอาศัยอนุกรมของปฏิกิริยาการขจัดออกซิเจนประกอบด้วย การขจัดน้ำ การเติมไฮโดรเจน คีโตไนเซชั่น และอัลดอล คอนเดนเซชั่น บนตัวเร่งปฏิกิริยาโลหะ โลหะออกไซด์ และซีโอไลต์ เพื่อผลิตสารเคมีที่มีมูลค่าสูง

สารประกอบคีโตนเบา เช่นอะซิโตน และเอทิลเมทิลคีโตน สามารถเกิดการขจัดออกซิเจนได้ในตัวเองเมื่ออยู่บนตัวเร่งปฏิกิริยาโปรตอนซีโอไลต์ ได้แก่ HZSM-5 HY H-β H-Mordenite และ H-Ferrierite ได้ผลิตภัณฑ์เป็นสารประกอบโอเลฟินและกรดคาร์บอกซิลิกที่อุณหภูมิสูงกว่า 448 เคลวิน จากการศึกษาพบว่ากระบวนการขจัดออกซิเจนเกิดผ่านปฏิกิริยาอัลดอล คอนเดนเซชั่น จากนั้นสารมัธยันตร์ที่เกิดขึ้นจึงสลายตัวเนื่องจากขนาดรูที่จำกัดของซีโอไลต์เกิดเป็นสารผลิตภัณฑ์ การขจัดออกซิเจนเพิ่มเติมสามารถทำได้ผ่านกระบวนการคีโตไนเซชั่นของกรดคาร์บอกซิลิกที่ถูกผลิตขึ้น เกิดเป็นคีโตนอีกครั้งที่อุณหภูมิสูงกว่า 503 เคลวิน นอกจากนี้ยังสามารถขจัดออกซิเจนออกจากคีโตนโดยการใช้ไฮโดรเจน (ไฮโดรดีออกซิจีเนชั่น) ผ่านอนุกรมปฏิกิริยาการเติมไฮโดรเจนและการขจัดน้ำบนตัวเร่ง

ปฏิกิริยา 2 หน้าที่ ซึ่งประกอบด้วยโลหะทองแดงบนตัวรองรับโปรตอนซีโอไลต์ (Cu/HY และ Cu/HZSM-5) จากการศึกษาพบว่า Cu/HY เป็นตัวเร่งปฏิกิริยาที่เหมาะสมกว่าเนื่องจากมีความสามารถในการเร่งปฏิกิริยาที่ดีสามารถแปรรูปอะซิโตน เอทิลเมทิลคีโตน และไซโคลเฮกซะโนนได้ 90% 25% และ 85% ตามลำดับ นอกจากนี้ยังมีความเลือกสรรต่อโอเลฟินอันได้แก่โพรพิลีน นอร์มัลบิวทิลีน และไซโคลเฮกซีนมากกว่า 80% กระบวนการนี้สามารถนำไปต่อยอดใช้กับกระบวนการคีโตไฮโดรดีออกซิจีเนชั่นเพื่อขจัดออกซิเจนออกจากกรดคาร์บอกซิลิก กระบวนการนี้เกิดผ่านอนุกรมปฏิกิริยาคีโตไนเซชั่น การเติมไฮโดรเจน และการขจัดน้ำ บนตัวเร่งปฏิกิริยาผสมระหว่างซีเรียมออกไซด์กับทองแดงบนตัวรองรับซีโอไลต์โปรตอนวาย (CeO_2-Cu/HY) จากการทดสอบพบว่าตัวเร่งปฏิกิริยานี้สามารถแปรรูปกรดอะซิติก 80% ไปเป็นโพรพิลีน 50% และมีความเสถียรนานถึง 30 ชั่วโมง ที่อุณหภูมิทดสอบ 573 เคลวิน นอกจากนี้ตัวเร่งปฏิกิริยา Cu/HY ยังสามารถนำไปใช้กับการขจัดออกซิเจนออกจากเฟอร์ฟูรัลเพื่อผลิต 2-เมทิลฟิวแรนในสภาวะที่มีกรดอะซิติกเจือปนโดยสามารถแปรรูปเฟอร์ฟูรัลทั้งหมดไปเป็น 2-เมทิลฟิวแรนได้ที่อุณหภูมิ 523 เคลวิน

คำสำคัญ : การขจัดออกซิเจน ตัวเร่งปฏิกิริยา น้ำมันชีวภาพ โอเลฟิน

Thesis Title	Production of petrochemical by deoxygenation of model light oxygenates fraction from bio-oil
Student Name	Mr.Ayut Witsuthammakul
Student ID	54650301
Degree	Doctor of Philosophy (Applied Chemistry)
Department	Chemistry
Year	2015
Thesis Advisor	Assoc.Prof.Dr. Tawan Sooknoi

Abstract

In this research, the light oxygenates from bio-oil are upgraded by controllable deoxygenation. Acetone, furfural and acetic acid are chosen as model compounds for ketone, aldehyde, and carboxylic acid, respectively. While the conventional upgrading process needs high temperature and pressure (> 673 K and > 40 bars) resulting in light parafins, this study emphasize the milder condition (< 573 K and atmospheric pressure) and production of high value chemicals. These can be achieved by the series of reaction including hydrogenation, dehydration, ketonization, and aldol condensation, over various metal, zeolite, and metal oxide catalysts.

For light ketones, acetone and ethyl methyl ketone can be self-deoxygenated over H-zeolites (HZSM-5, HY, H-β, H-Mordenite, and H-Ferrierite) to form olefin and carboxylic acid (*i*-butylene-acetic acid and methylbutenes-propanoic acid, respectively) at >448 K. This can be achieved by aldol-condensation then decomposition of intermediate within the zeolite confinements. The additional deoxygenation can be obtained by ketonization of the carboxylic acids produced within the self-deoxygenation cycle when the temperature is increased to >503 K. Alternatively, hydrodeoxygenation (HDO) of ketones is achieved by hydrogenation-dehydration over bi-functional catalysts of 5%Cu/HY and 5%Cu/HZSM-5. Cu/HY is suitable for ketones upgrading (90% acetone,

25% ethyl methyl ketone, and 85% cyclohexanone conversion) with >80% selectivity to corresponding olefins (propylene, n-butylene, and cyclohexene). This approach can be applied for keto-hydrodeoxygenation (KHDO) of carboxylic acid, in which the degree of oxygenated is gradually reduced by ketonization-hydrogenation-dehydration, over mixture of CeO_2 to Cu/HY. The acetic acid is converted to propylene (>80% conversion and 50% selectivity) with stability up to 30 hours on stream at 573 K. The acetic acid can be also directly converted to ethylene, acetaldehyde, ethanol, and ethyl acetate. The same HDO catalyst can be used for hydrodeoygenation of furfural to 2-methylfuran at 523 K (100% conversion and selectivity to 2-methylfuran), even in the presence of acetic acid.

Keywords : deoxygenation, catalyst, bio-oil, olefin

Acknowledgements

The author would like to appreciate his advisors, Assoc.Prof.Dr. Tawan Sooknoi and Prof.Dr. Daniel E. Resasco for knowledge in catalysis, skill coaching, suggestion, and experimental instrument and thanks for judgment and valuable comments by examination committees including Dr. Amnat Permsubscul, Asst.Prof.Dr. Montree Thongkam, Assoc.Prof.Dr. Siriporn Jongpatiwut, and Assoc.Prof.Dr. Jatuporn Wittayakun.

The author is grateful to his institutes (King Mongkut's Institute of Technology Ladkrabang and The University of Oklahoma) for work place and facility and also to The Royal Golden Ph.D. Program (Grant No. PHD/0137/2553) and PTT Public Co. Ltd., for financial support.

The author also shares this success to his colleagues in CCR group at KMITL and CBME group at OU.

Finally, the author dedicates this work to his parents, who gave a smart brain and a strong body for working.

Mr.Ayut Witsuthammakul

Contents

Contents (continue)

Contents (continue)

Contents (continue)

Contents (continue)

Contents (continue)

Contents (continue)

Contents (continue)

List of tables

Table **Page**

Chapter 2

Chapter 3

List of tables (continue)

Table **Page**

Chapter 4

Chapter 5

List of tables (continue)

Chapter 6

Chapter 7

List of tables (continue)

Table **Page**

List of figures

Figure **Page**

Chapter 2

List of figures (continued)

Figure **Page**

Chapter 3

List of figures (continue)

Figure **Page**

Chapter 4

List of figures (continue)

Figure **Page**

Chapter 5

List of figures (continue)

Figure **Page**

Chapter 6

List of figures (continue)

List of figures (continued)

Figure **Page**

Chapter 7

List of figures (continue)

Figure **Page**

Chapter 1

Introduction

As petroleum is running low, future of petrochemical is in risk. Cellulosic biomass is a new promising due to the most abundant around the world. The approximation of annual global biomass production is 1.05 x 10^{17} g carbon [1], half on land and half in ocean. Thailand is rich in biomass sources due to plentiful land, rain, and sunlight all year round [2]. The biomass utilization is not new agenda in Thailand. >90% of commercial renewable source are biomass from agricultural residue (rice, sugar cane, corn, cassava, and palm) [3]. The 2013 Thailand overall final energy consumption is 75,214 ktoe (kilo tons oil equivalent). 22% obtains from renewable source and tend to increase every year [4-5] mostly by combustion for power plant [6]. However, no report on application in Thailand for petrochemical production was found.

To utilize the cellulosic biomass as hydrocarbon source, polymeric structure of cellulose, hemicellulose, and lignin must be primarily broken down to small fragment generally by pyrolysis [7]. The bio-oil production (liquid yield form biomass pyrolysis) is low quality feedstock [8] hence the direct utilization is limited. This is due to the constituent of oxygenates (35-50% by weight) [9], including aldehydes and ketones, and carboxylic acids (totally 50 % of all oxygenate compounds) [8]. Accordingly, deoxygenation process is the necessary upgrading for the best of bio-oil utilization. The expectations are i) the deoxygenation of light oxygenates produce the light olefins for petrochemicals and ii) the deoxygenation of heavy oxygenates yield the liquid fuel comparable to gasoline and Diesel fuels.

Most of the developments in this study focus on removing the oxygen by hydrotreatment similar to conventional petroleum treatment [10]. However, it was found that the oxygenate compounds suffer uncontrolled deoxygenation particularly the light oxygenates resulting in low value products e.g. acetic acid to methane, acetaldehyde to ethane, and acetone to propane [11]. The operating is unsafe and high investment cost is charged to owner due to very high hydrogen pressure process (typically > 40 bars) [12]. Therefore, the controllable deoxygenation with mild condition is preferred for light oxygenates upgrading. For example, alcohols can be dehydrated at atmospheric pressure over acid catalysts and and aldehyde can be decarbonylated over

noble metals [13-14]. In contrast, the deoxygenation of ketones by decarbonylation is impossible. The decarboxylation of small carboxylic acid is not catalytic process [15].

The deoxygenation of small ketones and carboxylic acids can be accomplished by consecutive mild reaction with low activation energy. The reaction series is designated from common deoxygenation including hydrogenation and ketonization/hydrogenation for mild upgrading of light oxygenates. The intermediate is alcohol that can be simply dehydrated to olefin, an important feedstock for polymers and industrial chemicals [16-17]. The elimination of oxygen with reasonable hydrogen consumption are controlled through the water, carbon monoxide, and carbon dioxide removal from the light oxygenates. In this work, the acetone, furfural, and acetic acid are selected as model compound from bio-oil light oxygenates. The hydrogenation and decarbonylation are conducted over metal catalysts while the dehydration and ketonization are accelerated by acid and metal oxide catalysts, respectively. The multi-functional heterogeneous catalyst is targeted for upgrading of oxygenated mixture. The deoxygenation of the model mixture from bio-oil is also investigated.

1.1 Objectives and goals

1. To upgrading light oxygenates from bio-oil to petrochemicals by series of deoxygenation under mild condition
2. To provide the practical catalyst for controlled deoxygenation of the light oxygenates with minimum hydrogen consumption
3. To understand the reaction mechanism and role of catalyst for deoxygenation of the light oxygenates
4. To investigate the interference of mixture components on upgrading catalyst and process

1.2 Scope of the study

1.2.1 Ketones self-deoxygenation over H-zeolites

1. Characterize the H-zeolites (HZSM-5, HY, H-β, H-Mordenite, and H-Ferrierite) by N_2 adsorption, temperature programed desorption of *i*-propylamine (IPA-TPD), temperature programed desorption of reactants (TPD-MS of acetone, diacetone alcohol, mesityl oxide, and acetic acid), thermal desorption with GC-FID, X-ray powder diffraction (XRD), and temperature programed oxidation (TPO)
2. Catalytic self-deoxygenation of ketones to olefins in fixed-bed reactor using acetone and ethyl methyl ketone (MEK) as model compounds
3. Investigate the significant of enone intermediate by comparison of mesityl oxide and isobutyl methyl ketone conversion and secondary conversion of products, *i*-butylene and acetic acid
4. Examine the effect of contact time (37, 74, and 148 g.h.mol^{-1})
5. Investigate the effect of reaction temperature (423, 448, 473, 523, and 573 K)
6. Testing the effect of water in pulse-flow reactor
7. Study the effect of zeolite frameworks using HZSM-5, HY, H-β, H-Mordenite, and H-Ferrierite
8. Investigate the effect of zeolite site proximity with HZSM-5 (Si/Al = 13, 40, 140 and 250)

1.2.2 Hydrodeoxygenation (HDO) of ketones to olefins

1. Prepare 2 %wt metal/silica catalysts (metal; chromium, iron, cobalt, nickel, copper, and palladium) by incipient wetness impregnation
2. Prepare 2, 5, 10, 20, and 40 %wt nickel/silica and copper/silica by incipient wetness impregnation

3. Prepare 0, 25, 50, 75, and 100 %wt Cu of copper-nickel alloy/silica catalyst by co-impregnation

4. Prepare 5 %wt copper/HZSM-5 and copper/HY by incipient wetness impregnation

5. Characterize the metal support catalysts in 1.-4. by X-ray fluorescence (XRF), N_2 adsorption, temperature programed desorption of ammonia (NH_3-TPD), temperature programed reduction (TPR), temperature programed reduction of N_2O oxidizing metal surface (TPRs), and thermogravimetric analysis (TGA)

6. Study the effect of metal catalyst with chromium, iron, cobalt, nickel, copper, and palladium on silica support to acetone hydrogenation, acetone hydrogenolysis, and propylene hydrogenation in fixed bed reactor (373–623 K)

7. Investigate the effect of reaction temperature to ketone hydrogenation using acetone as model compound (373, 423, 473, 498, 523 and 573 K)

8. Examine the effect of contact time to acetone hydrogenation (14, 29, 59, and 119 g.h.mol^{-1})

9. Investigate the effect of metal loading on acetone hydrogenation (2, 5, 10, 20, and 40 %wt)

10. Examine the effect of metal alloy between nickel and copper acetone hydrogenation (0, 25, 50, 75, and 100 %wt of copper)

11. Investigate the effect of reaction temperature to alcohol dehydration using *i*-propanol as model compound (373, 398, 423, 448, and 473 K)

12. Examine the effect of contact time to *i*-propanol dehydration (0.8, 1.5, 3, and 5 g.h.mol^{-1})

13. Study the effect of zeolite frameworks *i*-propanol dehydration with HZSM-5, HY, H-β, and H-Mordenite

14. Catalytic HDO of ketone using acetone, ethyl methyl ketone (MEK), and cyclohexanone as model compounds, in fixed bed reactor

15. Testing the effect of catalyst combination to HDO of ketone by sequential bed catalyst, physical mixed catalyst, and bi-functional catalyst

1.2.3 Keto-hydrodeoxygenation (KHDO) of carboxylic acid to olefins

1. Catalytic KHDO of carboxylic acid to olefins over tri-functional catalyst of CeO_2/Cu/zeolite using acetic acid as model compound in fixed bed reactor
2. Compare the effect of zeolite frameworks (HZSM-5 and HY) to KHDO of acetic acid
3. Investigate the effect of reaction temperature to KHDO (548, 573, 598, 623, and-648 K)
4. Investigate the effect of catalyst composition to KHDO (60, 75, 86, and 93 %wt of CeO_2 in CeO_2/Cu/zeolite)
5. Compare the effect of catalyst combination to KHDO between sequential bed catalyst and physical mixed catalyst
6. Study the effect of feed concentration in stream to KHDO (1.2 and 2.3 %mol)
7. Examine the effect of water to KHDO by feed alternation between acetic acid and aqueous acetic acid
8. Produce the light distillated hydrocarbons from acetic acid using KHDO and HZSM-5 catalysts

1.2.4 Deoxygenation of furfural in acetic acid/water

1. Prepare 5 wt% palladium on SiO_2, γ-Al_2O_3, HY, TiO_2, ZnO, and CeO_2 and 5 wt% copper on SiO_2 and HY by incipient wetness impregnation
2. Characterize the catalyst in 1. by inductively couple plasma (ICP-MS), X-ray fluorescence (XRF), N_2 adsorption, temperature programed desorption of ammonia (NH_3-TPD), temperature programed reduction of N_2O oxidizing metal surface (TPRs), transmission electron microscope (TEM-EDS), and thermogravimetric analysis (TGA)

3. Catalytic decarbonylation of furfural to furan using palladium support catalyst from 1. in fixed bed reactor

4. Investigate the interference of acetic acid and water to light oxygenate upgrading using furfural decarbonylation to furan as model reaction by feed alternation between i) furfural and acetic acid ii) furfural and furfural/acetic acid solution

5. Compare the catalytic HDO of furfural to 2-methylfuran over Cu/ SiO_2 and Cu/HY in fixed bed reactor

6. Investigate the effect of contact time to HDO of furfural to 2-methylfuran (5, 10, and 20 $g.h.mol^{-1}$)

7. Investigate the interference of acetic acid and water to light oxygenate upgrading using HDO of furfural to 2-methylfuran as model reaction

1.3 Expected results

1.3.1 This research leads to excellence catalytic system design for light oxygenate upgrading.

1.3.2 The system in 1.3.1 can produce high quality fuels and petrochemicals including propylene, i-butylene, and furan derivatives selectively.

1.3.3 The knowledge obtained from this research leads to the fundamental and strategy for light oxygenate upgrading.

1.4 References

[1] Field C.B., Behrenfeld M.J., Randerson J.T. and Falkowski P. “Primary Production of the Biosphere: Integrating Terrestrial and Oceanic Components” **Science,** vol.281, no.5374, pp.237-240.

[2] Thailand meteorological department. 2013. “Annual report 2013”

[3] Khidhathong P., Wangjiraniran W. and Suriyawong A. "A Study on Spatial Potential of Biomass for Electricity Generation" **Journal of Energy Research,** vol.1, 2014, pp.63-76.

[4] Thailand ministry of energy. 2013. "Thailand alternative energy situation 2013"

[5] Thailand ministry of energy. 2013. "Energy in thailand: facts & figures"

[6] Thailand ministry of energy. 2013. "Thailand Energy Statistics 2013"

[7] Bridgwater A.V., Meier D. and Radlein D. "An overview of fast pyrolysis of biomass" **Organic Geochemistry,** vol.30, 1999. pp.1479-493.

[8] Basu P. **Biomass gasification and pyrolysis: practical design and theory.** Burlington: Academic Press. 2010.

[9] Özçimen D. "An Approach to the Characterization of Biochar and Bio-Oil" pp.1-18.

[10] Elliott D.C. and Baker E.G. **"Process for upgrading biomass pyrolyzates"** U.S. patent no.4795841, 3 Jan 1989.

[11] Zhao C., Kou Y., Lemonidou A.A., Li X. and Lercher J.A. "Highly Selective Catalytic Conversion of Phenolic Bio-Oil to Alkanes" **Angewandte Chemie,** vol.121, 2009. pp.4047-4050.

[12] Gagnon J. and Kaliaguine S. "Catalytic Hydrotreatment of Vacuum Pyrolysis Oils from Wood" **Industrial & Engineering Chemistry Research,** vol.27, 1988, pp.1783-1788.

[13] Sitthisa S., Pham T., Prasomsri T., Sooknoi T., Mallinson R.G. and Resasco D.E. "Conversion of furfural and 2-methylpentanal on Pd/SiO2 and Pd–Cu/SiO2 catalysts" **Journal of Catalysis,** vol.280, 2011, pp.17-27.

[14] Witsuthammakul A. and Sooknoi T. "Direct conversion of glycerol to acrylic acid via integrated dehydration–oxidation bed system" **Applied Catalysis A: General,** vol.413– 414, 2012, pp.109-116.

[15] Lee C.C. and Spinks J.W.T. "The Mechanism of the Ketonic Pyrolysis of Calcium Carboxylates" **University of Saskatchewan,** 1953. 1079-1086.

[16] Chaudhuri U.R. **Fundamentals of petroleum and petrochemical engineering.** Florida: CRC Press. 2011.

[17] Hagen j. **Industrial Catalysis: A Practical Approach.** 2nd ed. Darmstadt: WILEY-VCH Verlag GmbH & Co. 2006.

Chapter 2

Theories and literature reviews

2.1 Biomass

Biomass is biologically material obtained from nature e.g. trees, animals or crops. The basic elements in biomass are carbon, hydrogen and oxygen. However, biomass usually refers to plant based materials. The plants can capture the solar energy via chemical conversion called "photo-synthesis". Basically, the carbon dioxide in air is trapped and reacts with water to form three polymerized sugar i.e. cellulose, hemicellulose, and starch deposited in plant [1];

$$CO_2 + H_2O + \text{Sunlight} \xrightarrow{\text{Chlorophyll}} (CH_mO_n) + O_2 - 480\ \text{kJ/mol}$$

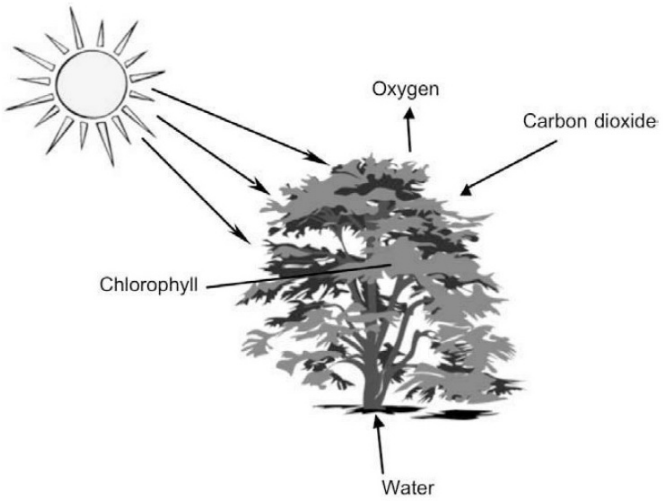

Various reactions take place in plant in the same time leading to the different chemical structure. The components composed in biomasses can be roughly divided into three majority; cellulose hemi-cellulose and lignin so called "lingocellulosic material". The quantity of each component depends on part of biomass as shown in Table 2.1.

Table 2.1 Proportion of major components (%) within Silver birch [2]

Parts	Cellulose	Hemicelluloses	Lignin	Extractives
Stem wood	43.9	28.9	20.2	3.8
Bark	10.7	11.2	14.7	25.6
Branches	33.3	23.4	20.8	13.5
Leaves	N/A	N/A	11.1	33.0
Stump	29.5	19.4	13.4	4.7
Roots	26.0	17.1	27.1	13.5

2.1.1 Cellulose

Cellulose; $(C_6H_{10}O_5)_n$, is a natural homopolymer made from 6 carbon monosaccharide named "D-glucose" ($C_6H_{12}O_6$). Figure 2.1 left illustrates two anhydroglucose unit (AGU) linked by ether bond between C1 and C4 called "β 1-4 glucosidic bond". This polymer chain is very strong with the degree of polymerization around 10,000-15,000 depend on source of material [3].

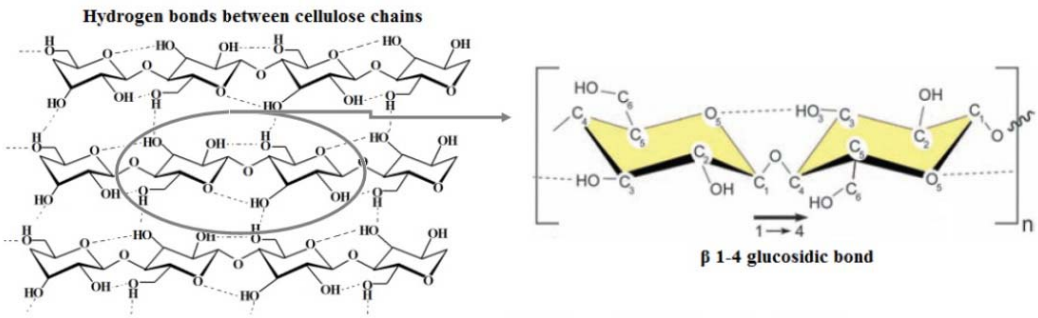

Figure 2.1 Structure of cellulose

Moreover, the remaining hydroxyls around the anhydroglucose ring can form hydrogen bond to hydroxyl of neighbor units or hydroxyl of beside cellulose chains themself shown by dash line in Figure 2.1. The intra-chain hydrogen bond enhances the physical strength and results in the linear configuration. While, the inter-chain hydrogen bonding and strong van der Waals force generates the aggregate of cellulose chains forming the fibril. The strong interaction between chains results in the rigidness, dense

packing, and insoluble in common solvent due to inaccessible. There are crystalline and amorphous regions in natural cellulose fibril.

2.1.2 Hemicellulose

Hemicellulose is a heteropolymer consist of 5 carbons monosaccharide (D-xylose and D-arabinose) and 6 carbon monosaccharide (D-mannose, D-galactose and D-glucose) as illustrated in Figure 2.2. The average formula is expressed by $(C_5H_8O_4)_n$ due to C5 >> C6. The amorphous nature and the degree of polymerization lower than cellulose (50-200) results to higher reactivity and soluble in many alkaline solutions [4].

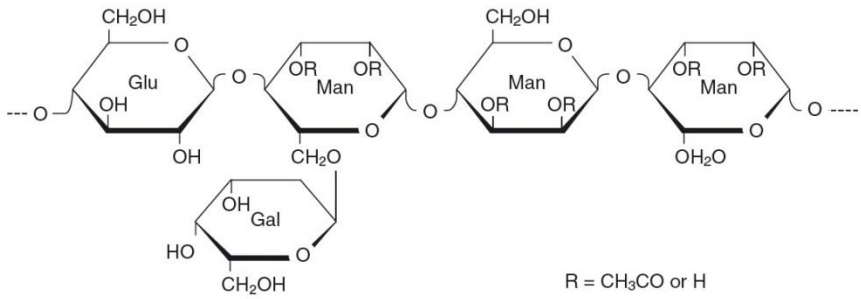

Figure 2.2 Structure of hemicellulose [5]

2.1.3 Lignin

Lignin is a polyphenolic material binding the cellulose fiber. It derives from three monomers, coniferyl alcohol, sinapyl alcohol, and p-coumaryl alcohol (Figure 2.3). The ether bond and carbon-carbon bond to the benzene ring results in 3 dimensional network like crosslinking polymer however there is no exact structure for lignin. The molecular weight is very wide varied (10^2-10^6) depend on source e.g. leaf, wood, etc. The amorphous structure leads to the glass transition temperature (T_g) and softening at high temperature. Without hydrogen bond as found in cellulose, many solvent dissolves lignin successively e.g. dioxane, acetone, dimethylsulfoxide, pyridine, and methyl cellosolve (2-methoxy ethanol) [6].

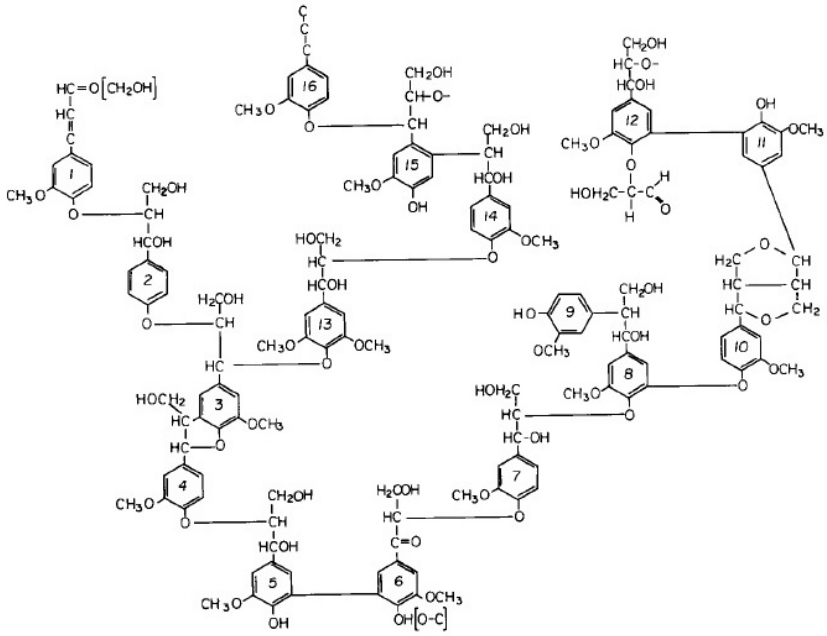

Figure 2.3 Structure model of spruce lignin

2.2 Biomass conversion

In the past, biomass was widely used for material (lumber, board, trunk and pallet). A little of it was carbonized to charcoal or burnt directly for energy. Nowadays, the fuels and chemicals from biomass gain the important. A major requirement is they should be in liquid or gas due to the versatility, transportation reason, and industrial application. Therefore, solid nature of biomass is a major obstacle [7]. The biomass can be transformed to meet the requirement by mechanical, biological, and thermal conversion as illustrated by Figure 2.4. The mechanical conversion is the easiest process for triglyceride from oily fruit, used for bio-diesel production [1]. The bio processing was known for a long time. Methane was produced by anaerobic microbial digestion of biomass residue for local energy using in India and China. Nowadays, ton of bio-ethanol used for vehicle energy can be produced by fermentation of agriculture products. These biological processes possess high selectivity but slow, typically days or weeks [7].

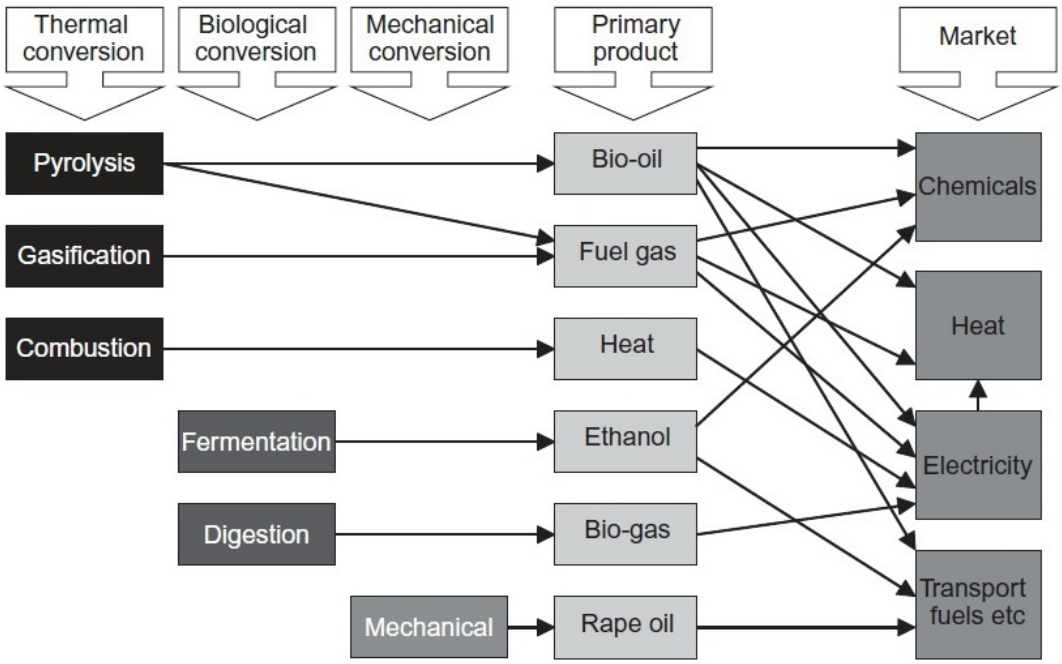

Figure 2.4 Overview of biomass conversion [1]

The thermal and thermochemical processes can provide more industrial practical, as compared to the bio processing, due to the faster production. The reaction time can be lower than a second for fast pyrolysis [1]. The thermal conversion of biomass found today can be broadly classified to four pathways

2.2.1 Combustion

The oldest process is the combustion. The simplest example is burning of wood generating the flame (see also Table 2.2 for condition). The reaction between hydrocarbon in biomass and oxygen in air can be expressed as;

$$\text{Biomass} + \text{Air} \longrightarrow CO_2 + H_2O + N_2 + \text{Heat} \quad [8]$$

Table 2.2 Comparison of biomass thermochemical processes [7]

Process	Temperature C°	Pressure MPa	Catalyst	Drying
Liquefaction	250-330	5-20	Essential	Not required
Pyrolysis	380-530	0.1-0.5	Not required	Necessary
Combustion	700-1400	>0.1	Not required	Not essential but may help
Gasification	500-1300	>0.1	Not essential	Necessary

Due to the exothermic nature, the heat released is used for cooking or warming in winter. Today, wood chip, pellet, and log are increasingly supplied to boiler. The steam produced from burning propels the gas turbine resulting in electric. However, the heating value is lower than coals, which still available most part of the world (Figure 2.5).

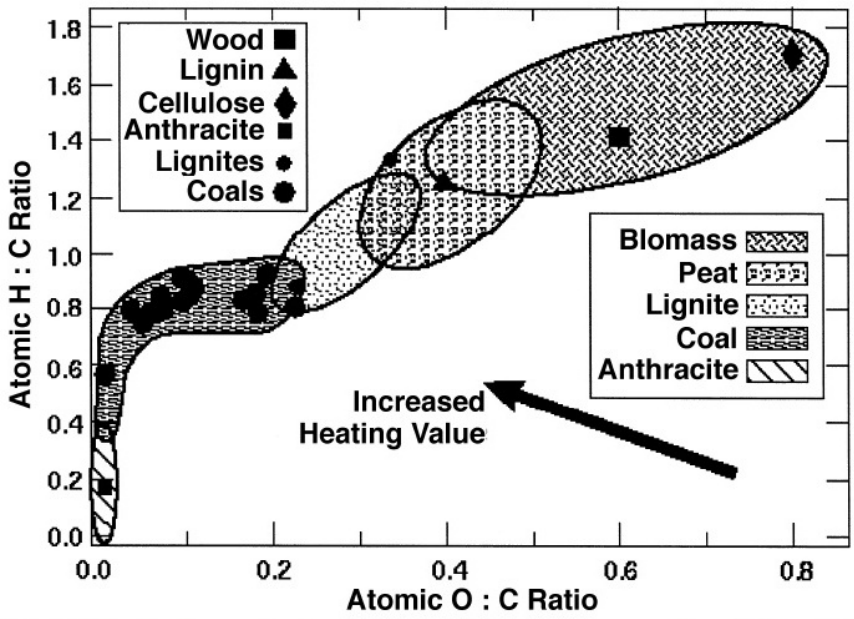

Figure 2.5 Heating value, O/C, and H/C ratios of different coal and biomass resources [9]

2.2.2 Gasification

The gasification is a conversion of hydrocarbon containing material to valuable gas, not CO_2 as found for combustion. The process needs a medium, which always be supercritical water or gas (subcritical steam or controllable air or oxygen) for reaction. Currently, gasification is a common process for synthetic gases production (carbon monoxide and hydrogen) from fossil source. Although the biomass gasification is not widely used, it still possesses motivation for the industry as pre-treatment process for electrical generator for two reasons. i) The elements, which are harmful for burner and environment e.g. sulfur, nitrogen, and metals, are eliminated for safety. ii) The heating value can be elevated by removing non-combustible components like oxygen and nitrogen. The oxygen is removed in form of water and carbon dioxide by dehydration and decarboxylation respectively as expressions below [7];

Dehydration: $C_mH_nO_q \longrightarrow C_mH_{n-2q} + q\ H_2O$

Decarboxylation : $C_mH_nO_q \longrightarrow C_{m-q/2}H_n + q\ CO_2$

The latter process also increases the H/C ratio of feed leading to the decrease of vaporization temperature. Moreover, the biomass gasification can delivers synthetic gases for chemical and fuel plants. For example, the gas and liquid hydrocarbons can be obtained by integrating to Fisher-Tropsch process.

2.2.3 Liquefaction

Liquefaction of biomass to liquid is achieved through pyrolysis, gasification, or hydrothermal processes, which is the most interesting today. For hydrothermal, biomass can be converted to hydrocarbon oil and gases (Figure 2.6) by contacting to high temperature water [7] in range of sub [10] or super-critical water [11]. The pressure is higher than other biomass thermal conversion, but lower reaction temperature (Table 2.2).

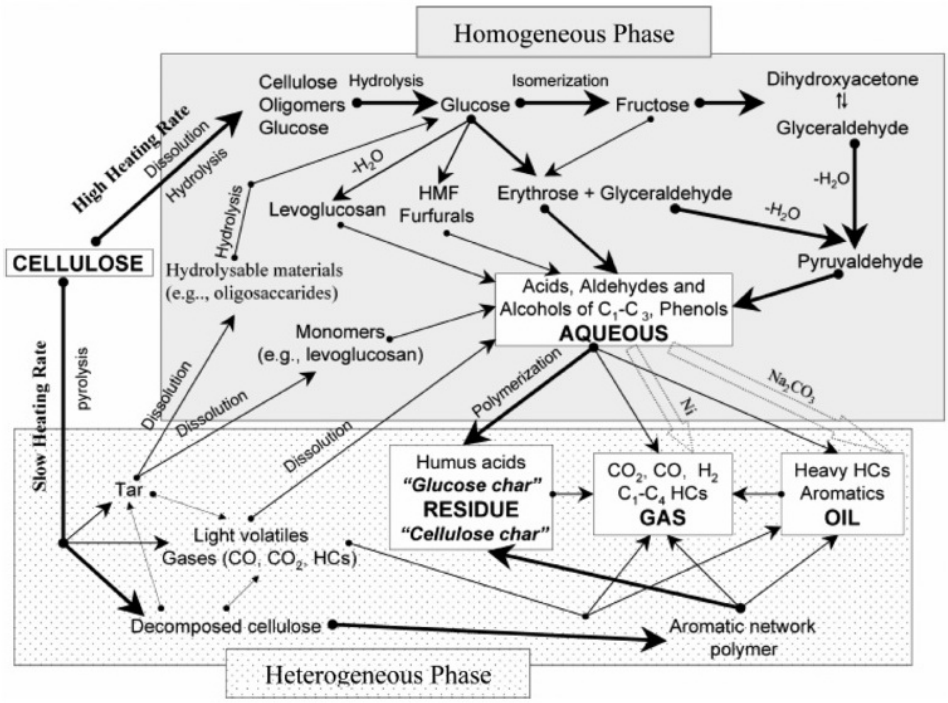

Figure 2.6 Reaction network for cellulose hydrothermal conversion in subcritical water catalyzed by nickel or sodium carbonate [1]

The catalyst is essential for this process. Metals, salts, and bases were found to be effective catalysts (Ni, NaOH, KOH, K_2CO_3, Na_2CO_3, and $Ca(OH)_2$). The deoxygenation mechanism is different depending on role of catalyst, for example Na_2CO_3 usage. The sodium carbonate reacts with water and carbon dioxide yielding the sodium formate [12];

$$Na_2CO_3 + 2\ CO + H_2O \longrightarrow 2\ HCO_2Na + CO_2$$

The vicinal hydroxy can be dehydrated to enol then tautomerized to keto form;

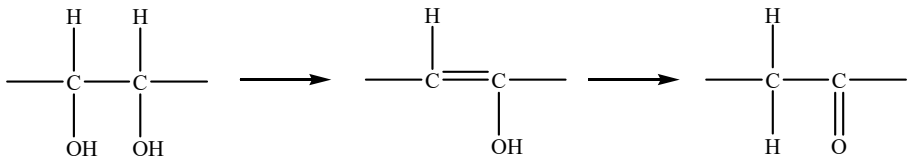

The formate ion and water can hydrogenate the carbonyl to hydroxyl, which can further dehydrate to hydrocarbon, and left hydroxyl ion;

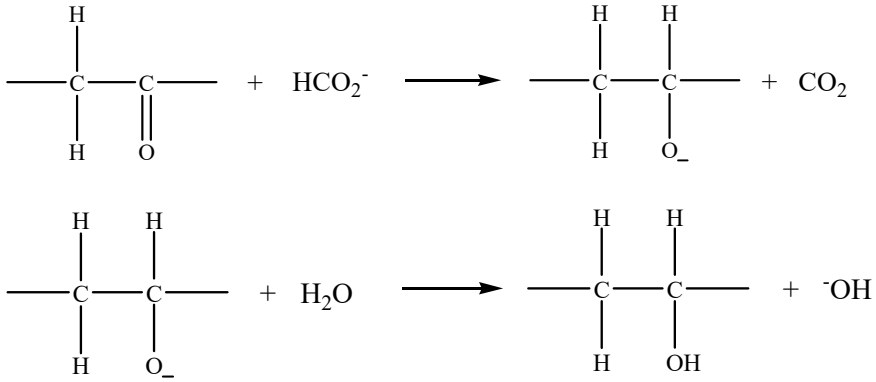

The hydroxyl ion reacts with carbon monoxide regenerating the formate ion;

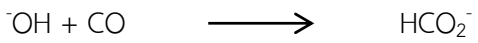

2.2.4 Pyrolysis

Pyrolysis is a process for biomass thermochemical decomposition. It possesses overlap of carbonization, cracking, devolatilization, destructive distillation, and thermolysis. The process is found as initial step for combustion and gasification but the oxidation does not occur due to the absence of oxygen. The pyrolysis requires the temperature lower than combustion and gasification because just the biomass breaks down is expected (Table 2.2). The setup is very simple without pressure adding on. There are many kinds of pyrolysis (Table 2.3) leading to the flexible of product distribution as expressed in Figure 2.7. Therefore, the pyrolysis is the most attractive thermochemical biomass conversion for today [7].

Table 2.3 Characteristic of different biomass pyrolysis modes [1, 7]

Mode	Residence time	Heating rate	Final temperature (C°)	Products
Carbonization	Days	Very low	400	Charcoal
Torrefaction	~ 30 min	Low	300	Solid, gas
Conventional	5-30 min	Low	600	Char, bio-oil, gas
Fast	<2 s	Very high	~ 500	Bio-oil
Flash	<1 s	High	<650	Bio-oil, chemicals, gas
Ultra-rapid	<0.5 s	Very high	~ 1000	Chemicals, gas
Vacuum	2-30 s	Medium	400	Bio-oil
Hydropyrolysis	<10 s	High	<500	Bio-oil
Methano-pyrolysis	<10 s	High	>700	Chemicals

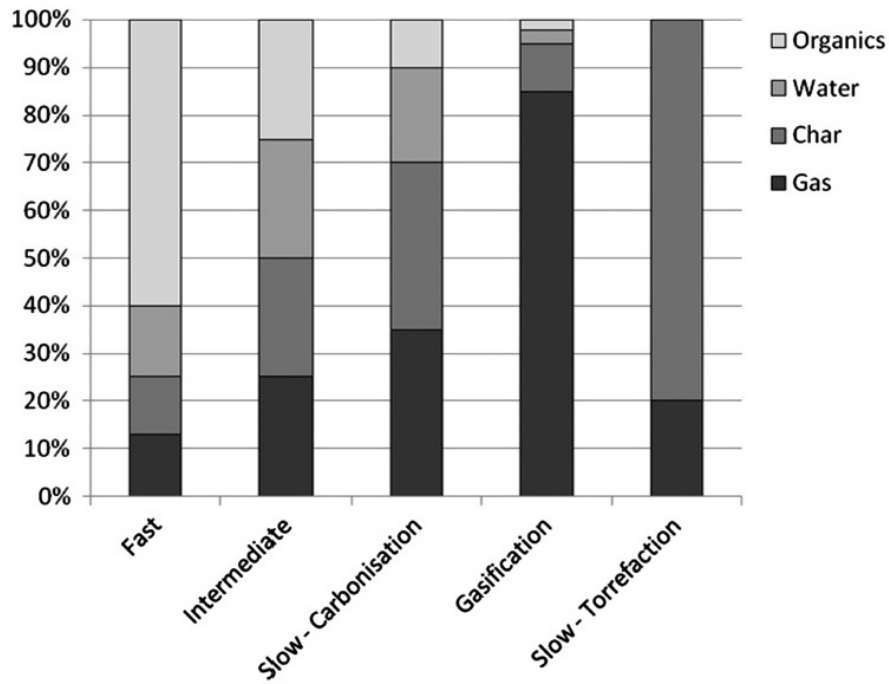

Figure 2.7 Product spectrum from different biomass pyrolysis modes [1]

Figure 2.8 shows a pyrolysis model of a biomass particle. The primary products are tar (condensable gas), and solid char. Tar can be further decomposed by gas phase

or heterogeneous gas-solid phase reaction to smaller molecules, non-condensable gas (CO, CO_2, H_2, and CH_4), water and solid char. The general reaction can be expressed by;

$$C_nH_mO_p \text{ (biomass)} \longrightarrow \Sigma_{liquid}C_xH_yO_z + \Sigma_{gas}C_aH_bO_c + H_2O + C \text{ (char)}$$

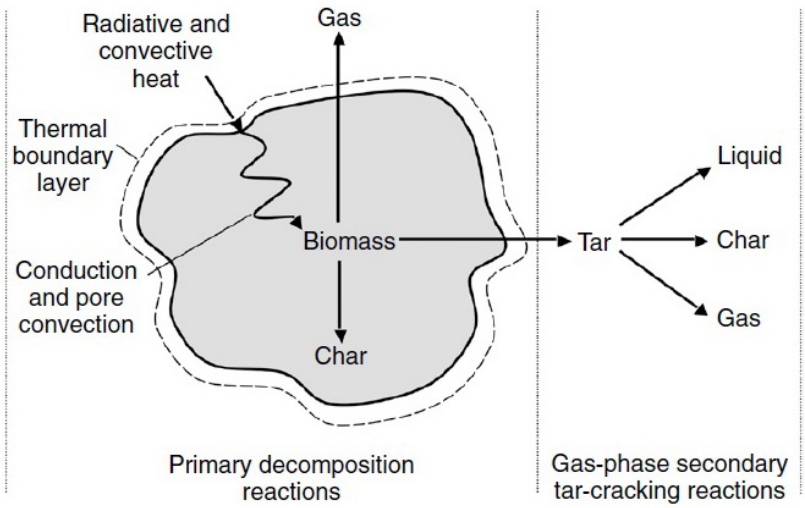

Figure 2.8 Pyrolysis of a biomass particle [7]

The decomposition phenomena arranging by temperature can be divided into four stages [7].

1. Drying stage (at ~ 100 °C): At low temperature, the heat can remove the free moisture in biomass by evaporation then conducting to inner core of biomass (Figure 2.8). For humid lignocellulosic biomass, the moisture can enhance the melting of lignin resulting to the softening. This is widely used for wood bending process.
2. Initial stage (at 100-300 °C): The dehydration of biomass occurs rapidly with the elimination of non-condensable gases (CO and CO_2).
3. Intermediate stage (at >200 °C): Biomass particle is decomposed to condensable gases (tar and liquid yield), non-condensable gas, and primary char. Most of bio-oil is produced in this stage.
4. Final stage (at ~ 300-900 °C): If the large molecular weight condensable products from third stage reside on remaining biomass particle for sufficient

time, these products can further crack to smaller molecule, non-condensable gas, and secondary char. Therefore, the condensable products should be released from reactor before this stage.

The biomass compositions also effect to pyrolysis products especially H/C ratio. As mentioned earlier, the biomass contents by three major components; cellulose, hemicellulose, and lignin. They prefers for pyrolysis at different temperature as described below;

- Hemicallulose: 150-350 °C
- Cellulose: 275-350 °C
- Lignin: 250-500 °C

The cellulose decomposition is multistage process initiated by pre-reaction (reaction I) as illustrated by Figure 2.9. Then, the competition between reaction II and reaction III take place. The dehydration dominates at low temperature and slow heating rate. The carbon rich biomass is further deoxygenated by decarboxylation and carbonization yielding coal. Meanwhile, the reaction III takes place via depolymerization, which favors at high temperature with fast heating rate. Levoglucosan was found to be a major intermediate for this route. The condensable gases are produced following four stage biomass conversion mentioned before. Therefore, the fast pyrolysis is suitable for liquid fuel and chemical feed stock production. For hemicellulose, it possesses rapid conversion more than cellulose and lignin. The decomposition produces more gas but less char, as compared to cellulose. Amount of aqueous product usually be the same [7].

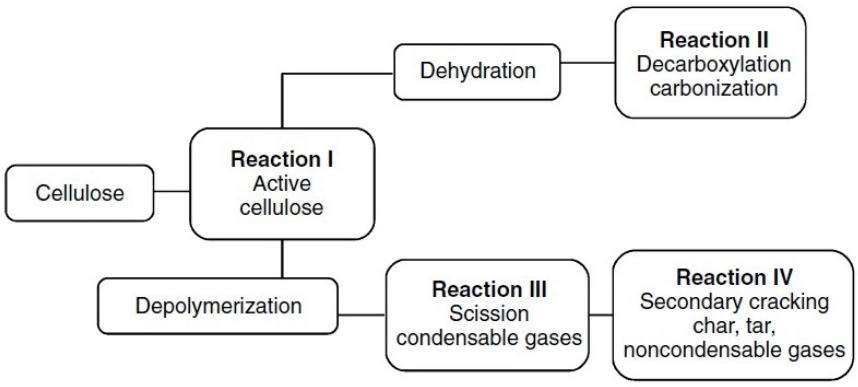

Figure 2.9 Decomposition model of cellulose [7]

The lignin cannot be dehydrated easily as found from cellulose and hemicellulose. The pyrolysis of lignin largely produces char (~ 55%). 15% Tar and 20% aqueous products are obtained from depolymerization with 12% gasses. Almost tar is phenolic compounds (green resin) [7].

2.3 Components in bio-oil

The liquid fraction from biomass pyrolysis is dark-brown and free-flow liquid with viscosity 40-100 cP at 40 °C, density 1200 kg/m^3 at 15 °C, and flash point 48-55 °C (2.4 cP, 820 kg/m^3, and 42 °C, respectively for diesel) [7] as displayed in Figure 2.10. The maximum yield of bio-oil is up to 80% (wet basis) of dry feed [13]. The fast (or faster) pyrolysis is the most suitable process for bio-oil production due to the highest organic yield (Figure 2.7). Bio-oil is a mixture of polar compound (75-80%), water (20-25%) and small amount of solid suspension (<1.0 %wt) [7]. The composition of bio-oil depends on type of biomass and processing (e.g. heating rate, pressure [14], reactor design [15-16], microwave assist [17], and catalyst [18]). Common oxygenates compounds including alcohols, aldehydes, ketones, and carboxylic acids were largely found in bio-oil as classified by Table 2.4.

Figure 2.10 Bio-oil [19]

Table 2.4 General composition bio-oil [7]

Group	Compound	Mass (%)
Water		20-30
Lignin fragments	Insoluble pyrolytic lignin	15-30
Aldehydes	Formaldehyde, acetaldehyde, hydroxyacetaldehyde, glyoxal	10-20
Carboxylic acids	Formic, acetic, propionic, butyric, pentanoic, hexanoic, glycolic	10-15
Carbohydrates	Cellobiosan, α-D-levoglucosan, oligosaccharides, 1, 6 anhydroglucofuranose	5-10
Phenols	Phenol, cresols, guaiacols, syringols	2-5
Alcohols	Methanol, ethanol	2-5
Ketones	Acetone, acetol (1-hydroxy-2-propanone), cyclopentanone	1-5
Furfurals		1-4

2.3.1 Carboxylic acids: acetic acid

Carboxylic acids are made up from carbonyl bond to hydroxyl group (R-(CO)-OH). They are polar molecules, which can form hydrogen bond to each other or water, so the boiling point is usually high and show good solubility in water. The solubility decreases with the increase of carbon chain length (R-) [20]. Due to the acidic property, the presence of carboxylic acids in bio-oil leads to low pH (2.0-3.0) [7]. Carboxylic acids are widely found in nature. Long chain carboxylic acid such as lauric acid, palmitic acid, stearic acid, oleic acid, and linoleic acid are major constituent in fats and oils. Citric acid and niacin are known as vitamin. Formic acid, pyruvic acid and biotin are found in lives [21].

Acetic acid (CH_3-(C=O)-OH) is a corrosive organic acid; appear in form of clear and colorless liquid. General physical and chemical properties are displayed in Table 2.5. Acetic acid >99% is called “glacial acetic acid”. Water is major impurity of acetic acid with trace of acetaldehyde, acetic anhydride, formic acid, biacetyl, methyl acetate, and ethyl acetoacetate.

Table 2.5 Physical and chemical properties of acetic acid [22]

Properties	
Appearance	Colorless, clear liquid
Odor	Pungent
pH	2.4 at 60.05 g/L
Melting point	16.2 °C
Boiling point	117 °C
Flash point	No data available
Upper/lower explosive limit	19.9%/4% (V)
Auto ignition temperature	485.0 °C
Vapor pressure	15.2 hPa at 20 °C, 73.3 hPa at 50 °C
Relative density	1.049 g/cm^3 at 25 °C
Surface tension	28.8 mN/m at 10.0 °C
Water solubility	Completely miscible

In natural, acetic acid can be found in plant and animal liquid due to the central of biological energy pathways and also in ocean water, and rain. The oldest acetic acid manufacture is vinegar production by fermentation of fruit and vegetable juice. Anaerobic bacterias (*Clostridium* or *Acetobacterium*) can convert sugar to 2-12% acetic acid solution [23];

$$C_6H_{12}O_6 \longrightarrow 3\ CH_3COOH$$

In 2012, global demand of acetic acid was 14 million tons approximately [24]. The commercial acetic acid is produced from liquid phase methanol carbonylation called “Monsanto process”. The rhodium complex is a working catalyst as the following scheme;

$$CH_3OH + CO \xrightarrow[HI,\ H_2O]{cis\ [Rh(CO)_2I_2]^-} CH_3COOH$$

The selectivity to acetic acid is > 99% at 150-200 °C and 33-65 atm. The loss of efficiency is due to the water-gas shift producing CO_2 and H_2. The most second important acetic acid production is the oxidation of acetaldehyde as shown below;

$$CH_3CH_2OH + O_2 \longrightarrow 2\ CH_3COOH$$

As acetaldehyde is produced easily by oxidative dehydrogenation of ethanol over silver, brass or bronze catalysts, the aldehyde can be further oxidized to carboxylic acid over manganese or cobalt salts in liquid phase with yield > 95% [23]. For bio-mass pyrolysis, vapor phase thermal decomposition of levoglucosan, derived from cracking of cellulose, yields various oxygenate C2-C3 through C5 intermediate as displayed in Figure 2.11. The ketene can be ultimately hydrated to acetic acid. The decomposition of C5 and C6 anhydrosugars composed in hemicellulose such as xylan also adds the acetic acid to bio-oil as shown by Figure 2.12 [25].

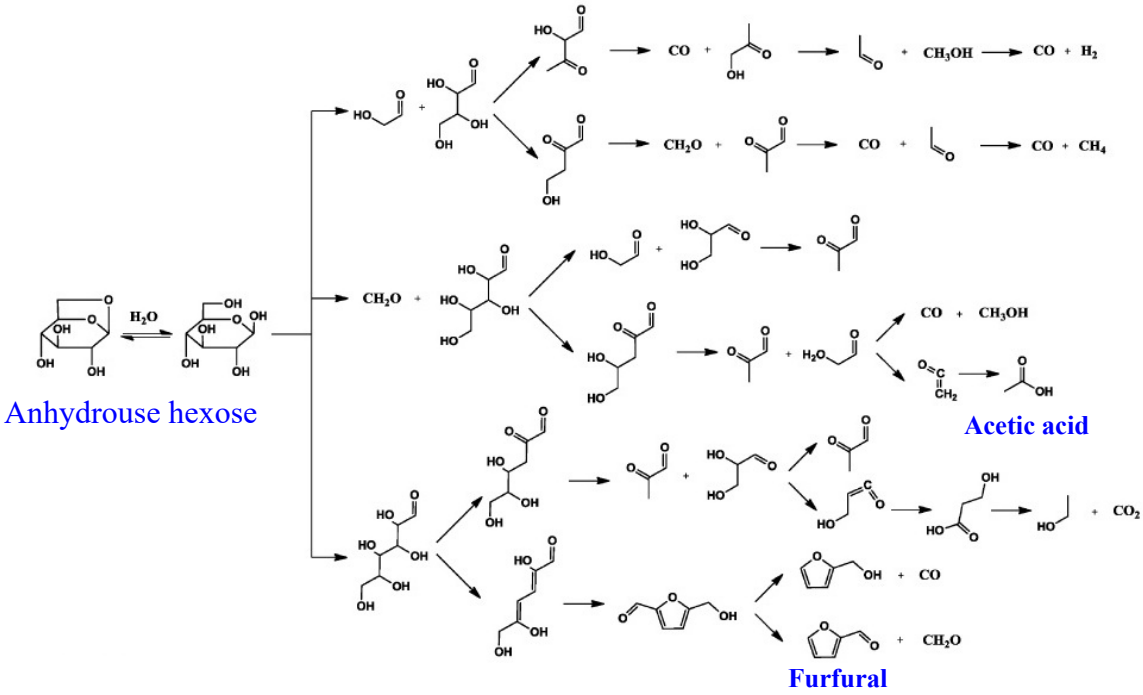

Figure 2.11 Proposed reaction pathways of levoglucosan thermal decomposition by fast pyrolysis [25]

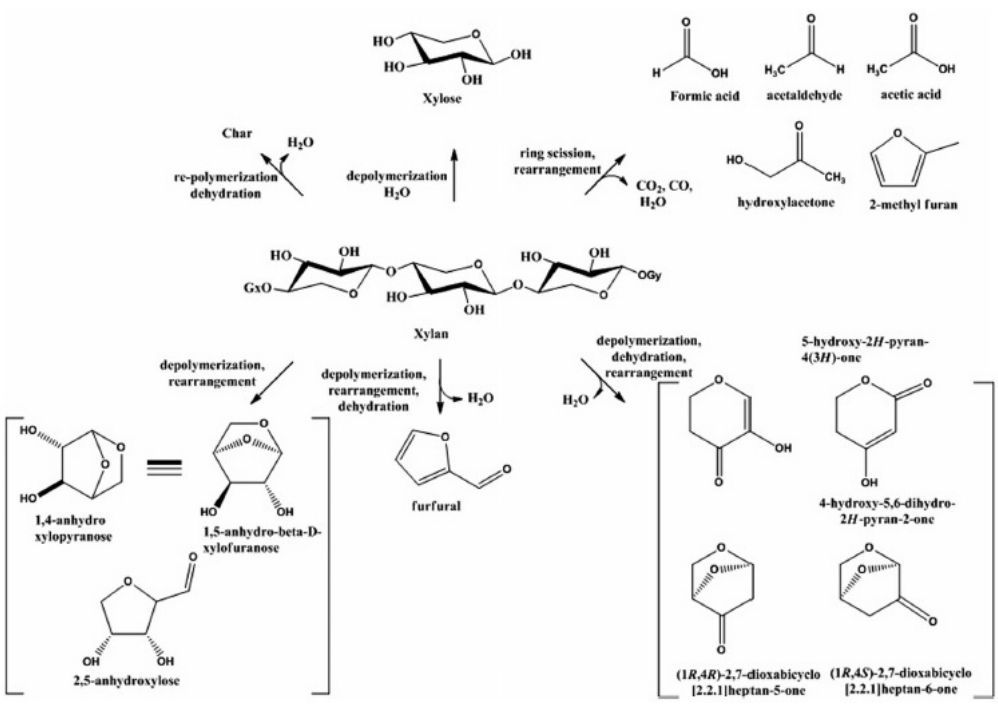

Figure 2.12 Proposed reaction scheme of hemicellulose thermal decomposition by fast pyrolysis [25]

Acetic acid is mainly used for vinyl acetate production (41%), cellulose acetate and acetic anhydride (36%), and solvent for terephthalic acid (7%). Acetic acid is a corrosive material following U.S. DOT (department of transportation) regulations. Metal or plastic bottles may be used for shipping at <0.45 kg. Aluminium container will be corroded slowly forming acetate layer, which can prevent further corrosion. The corrosion rate is increased by water. The acetic acid greater than 0.45 kg may be shipped by glass bottle or plywood drum. The solution with >50% acetic acid is considered as corrosive acid. Concentrate or aqueous solution can damage the skin seriously. Sharp odor can penetrates tissue to make the blister. The exposure in air at <10 mg/m^3 seem not to be harmful [23].

2.3.2 Ketones and aldehydes: acetone and furfural

Ketones have carbons bond to carbonyl at the both side (R_1-(C=O)-R_2) while aldehydes have carbon and hydrogen bond to each side of carbonyl (R_1-(C=O)-H).

Carbonyl is polar functional group so ketones and aldehydes possess higher boiling point than hydrocarbons. Ketones and aldehydes themself cannot form hydrogen bond. The boiling point is always lower than corresponding carboxylic acids and alcohols. However, oxygen of carbonyl can form hydrogen bond to water therefore small ketones and aldehydes like acetone and acetaldehyde are soluble in water at every ingredient. Ketones and aldehydes are naturally found in perfumes and fragrances. (*Z*)-Jasmone, α-damascone, and ionones are used as odor of jasmine, roses, and violet, respectively [20].

Acetone (CH_3-(C=O)-CH_3) is colorless, flammable liquid with mild pungent as tabulate in Table 2.6. It is the smallest and most important ketone due to good miscible in water and every organic solvent. Gums, resins, fats, oils, grease, waxes, and die-stuff, that are dissolved difficulty, are also miscible in acetone.

Table 2.6 Physical and chemical properties of acetone [26]

Properties	
Appearance	Colorless, clear liquid
Odor	No data available
pH	No data available
Melting point	-94 °C
Boiling point	56 °C
Flash point	-17.0 °C (closed cup)
Upper/lower explosive limit	13%/2% (V)
Auto ignition temperature	465.0 °C
Vapor pressure	245.3 hPa at 20.0 °C
Relative density	0.791 g/cm^3 at 25 °C
Water solubility	Completely miscible

Acetone was firstly found in 1595 from distillation of lead sugar (lead acetate). The acetone from fermentation of carbohydrate (cornstarch and molasses) by bacterial was used until loss the competitive ~ 1960 [27]. Global demand of acetone was 6 million tons in 2012 [28]. In petroleum age, most of acetone is manufactured by cumene process (Hoch process);

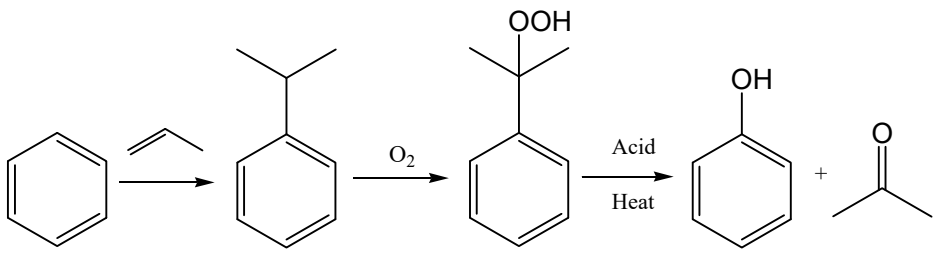

Two cheap petrochemicals including benzene and propylene are converted to cumene over Lewis acid catalyst. Cumene is then oxidized to cumene hydroperoxide, which can be decomposed to acetone and phenol by heating with acidic catalyst. The co-product phenol is a valuable feedstock for polymer industry. Alternatively, the dehydrogenation of isopropyl alcohol is also used due to unbalance of acetone and phenol demand in global market. The isopropyl alcohol is produced easily via liquid or gas phase hydration of propylene. The dehydrogenation, which is endothermic reaction and the equilibrium favorable at high temperature, is carried out over ZnO, ZrO_2 or copper catalysts at 325 °C [27];

$$CH_3CH(OH)CH_3 \longrightarrow CH_3(C{=}O)CH_3 + H_2$$

Acetone from biomass begins in 19th century through pyrolysis of citric acid and destructive distillation of wood and carbohydrate with lime [27]. Recently, acetone from thermal decomposition of biomass is interested. The cellulose direct decomposition majority yields the C3 especially acetone as proposed in Figure 2.13 [29].

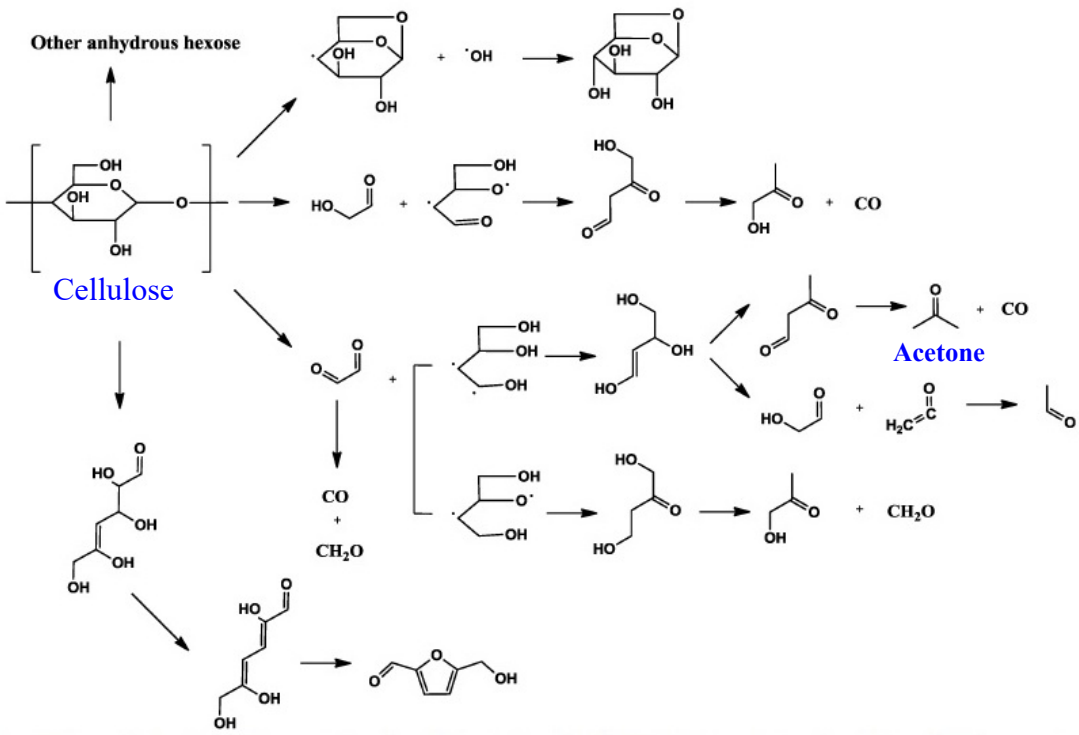

Figure 2.13 Proposed reaction pathways of cellulose thermal decomposition by fast pyrolysis [29]

The acetone is a most important feedstock for consumer products. 45% is used for acetone cyanohydrine for poly methyl methacrylate (PMMA) synthesis. 20% is supplied for bis-phenol A and 25% for aldol chemicals (MIBK and MIBC). It also widely used as solvent due to good solubility in various materials. DOT (department of transportation) classifies the acetone to flammable liquid. The glass container is used for < 5 L. The volume over 5 L should contains by carbon steel drum, stainless steel, or aluminium tank. Acetone is low toxic solvent. High vapor concentration may lead to eyes, nose, and throat irritant. No injury from skin contact has been reported. Fire is a major hazard due to low flash point and flammability. It should be used and kept in well-ventilation area and kept away from ignition source [27].

Furfural ((OC_4H_3)-(C=O)-H) is a heterocyclic aldehyde. The physical and chemical properties are tabulated in Table 2.7. The fresh distilled furfural is colorless clear liquid with pungent aromatic odor similar to almond. The darkness of furfural to yellow or light brown is due to the exposure to the air or long time storage.

Table 2.7 Physical and chemical properties of furfural [30]

Properties	
Appearance	Light brown, clear liquid
pH	No data available
Melting point	-36 °C
Boiling point	162 °C
Flash point	60 °C (closed cup)
Upper/lower explosive limit	19.9%/2.1% (V)
Vapor pressure	2.3 hPa at 20 °C
Relative density	1.16 g/cm^3 at 25 °C
Surface tension	43.5 mN/m at 20.0 °C
Water solubility	Soluble

Furfural was first discovered as a yellow oily by-product from formic acid synthesis in the early 19th century by Dobereiner, and also found from boiling vegetables such as corn and oat with aqueous sulfuric acid by many scientists. It was sometime used as an ingredient in perfume at that time. Furfural became an important commercial chemical in 20th century. The Quaker Oats Company developed the oat hulls utility by acid hydrolysis and achieves several tons per month. The first industrial application was solvent for wood rosin purification. Today, it is still manufactured from renewable agriculture sources such as corncobs, rice hulls, oat hulls, cotton seed hulls, and bagasse, which have pentosan polysaccharides (also known as hemicellulose) including xylan and arabinan. The synthesis is conducted in a batch or continuous digester. The pentosan is hydrolyzed to pentose then cyclodehydrated to furfural;

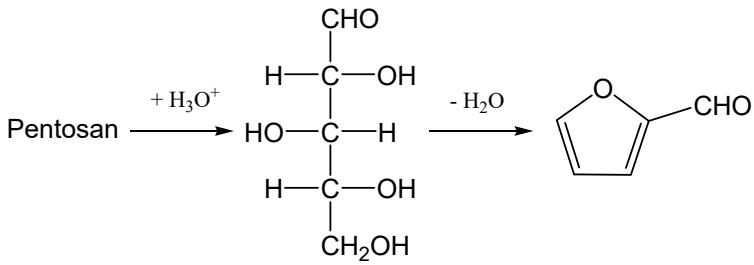

The strong inorganic acid is widely used as catalyst, however, it was found that the acetic acid by-product, producing at high temperature, can also accelerate the reaction. The weight yield of furfural depends on the hemicellulose in starting material (usually ~ 10% of dry weight) [31]. Alternatively, furfural was also found in bio-oil. It is derived from thermal decomposition of hemicellulose and cellulose parts (via anhydroglucose) as expressed in Figure 2.11-2.12 [25]. The direct application of furfural is extractive distillation solvent for the separation of saturation and unsaturation hydrocarbons in petroleum refinery especially C4. More than 90% of furfural is used as a feedstock for other compounds that is furan by decarbonylation, tetrahydrofuran by subsequent hydrogenation, and furfuryl alcohol resins. It is moderate toxic. Slight irritant can occur when contact to eyes and skin.

However, there are at least other 85 chemicals in bio-oil detecting by GC-MS [32-33] while more than 40% of water fraction remain unidentified [34]. The separation of bio-oil to pure chemicals is somewhat difficult and worthless in the commercial view. The multi steps extraction can fractionation the bio-oil into similar functional group, which will aid the utilization of bio-oil, as shown by Table 2.8 [35].

Table 2.8 Fractionation of bio-oil from Pine [35]

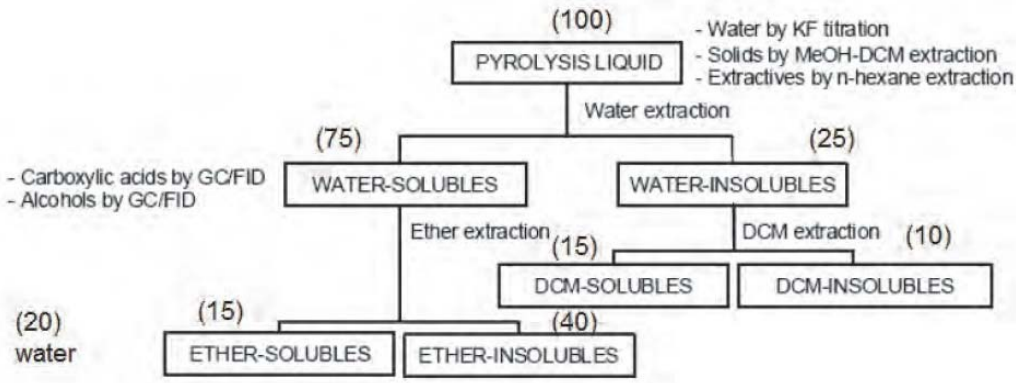

	wt %	COMPOUND TYPES	C	H	N	O
	(wet basis)		wt % (dry basis)			
WATER-SOLUBLES	75-85					
Acids, alcohols	5-10		36.0	6.0	0	58.0
Ether-solubles	5-15		60.0	6.0	0.1	33.9
Ether-insolubles	30-40		46.0	6.3	0.3	47.4
Water	20-30		0	11.1	0	88.9
WATER-INSOLUBLES	15-25		66.2	6.6	0.3	26.9
n-Hexane-solubles	2-6	$CH_3 - (CH_2)_n - CO_2H$ n = 10-30 $HOCH_2 - (CH_2)_n - CO_2H$ n = 10-28	77.4	10.4	0	12.2
DCM-solubles	5-10		68.1	6.7	0.4	24.7
DCM-insolubles	2-10	degraded lignin	64.1	5.9	1.5	28.4

2.4 General aspect of fuels and petrochemicals

After the beginning of industrial age, the global energy and chemicals hang on the fossil sources. It is well known that they are derived from biomasses (animal and plant crops), which composed by carbon, hydrogen, and hetero atom (oxygen, nitrogen or sulfur). The organic compounds decompose and penetrate through the soil and rock, where the natural spent many million years to transform them to hydrocarbon base materials like natural gas and crude oil, and coals. While the natural gas (> 90%

methane) [36] and coals (mostly carbon) are directly supplied to electric generator, the mixture of different carbon chain length (C3-C80) [37] in crude oil (also known as petroleum) can be broadly fractionated leading to different application including LPG, gasoline fuel, jet oil. Diesel fuel, gas oil, and asphalt as illustrated in Figure 2.14.

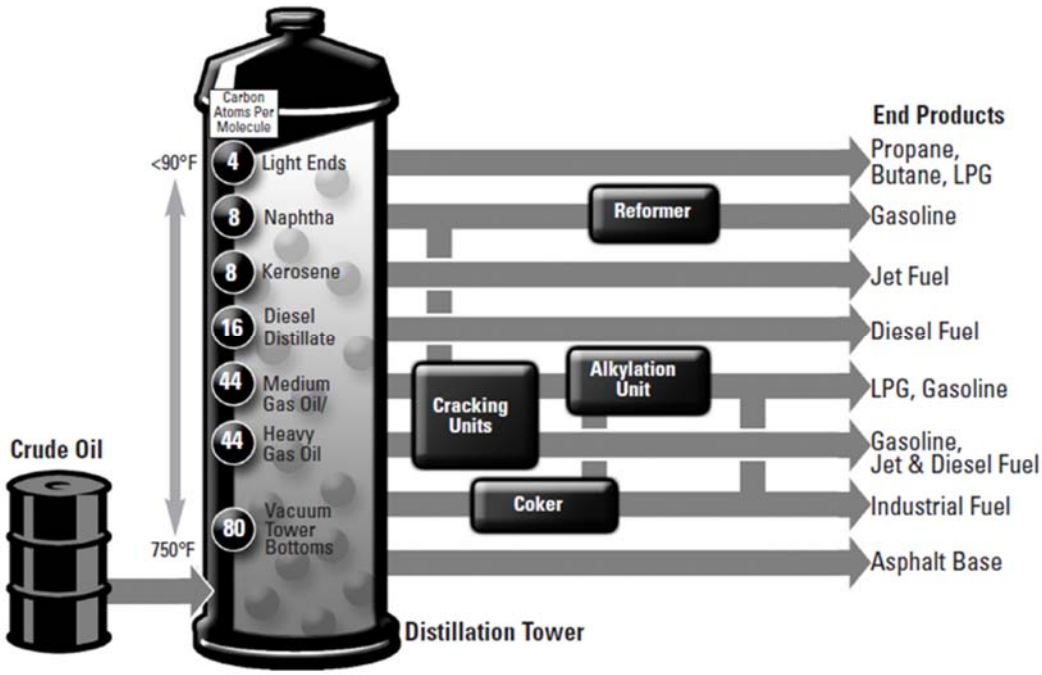

Figure 2.14 Crude oil distillation and oil refinery [37]

The hydrocarbons compose in crude oil are classified to paraffins (alkanes), naphthenes (cycloparaffins), and aromatics (Figure 2.15), which were widely used as liquid fuel for vehicle [38].

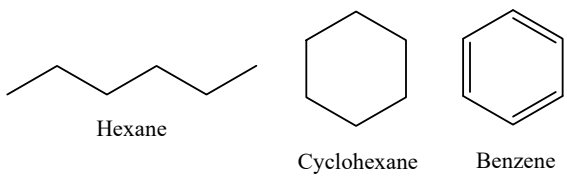

Figure 2.15 Example of paraffin, naphthene, and aromatic C6 found in crude oil [39]

Alternatively, value of the liquid fraction can be gained by cracking to olefins especially ethylene, propylene, and butenes. They and aromatics are feedstock for petrochemical industry due to higher reactivity, as compared to olefins. The C3 petrochemical network, which is the most important, starting from propylene to many consumable products is expressed by Figure 2.16 [39]. Notably, olefins are sometime found in fuel from cracking unit [38].

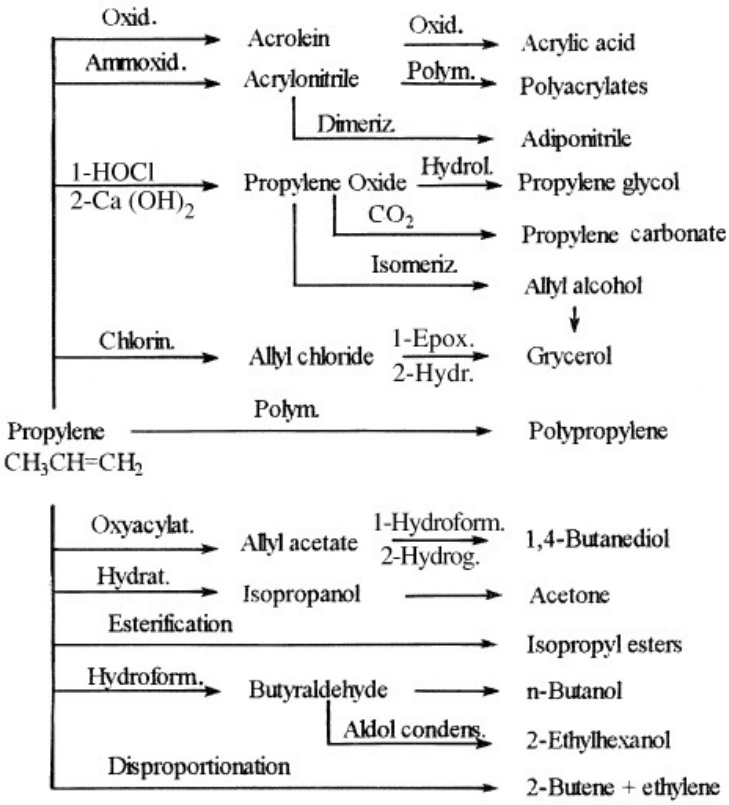

Figure 2.16 C3 petrochemical industry [39]

2.5 Catalytic upgrading of bio-oil

The heating value of bio-oil is relatively low (18-20 MJ/kg), as compared to fossil fuels (42-44 MJ/kg for gasoline and diesel) [7] due to high O:C ratio as shown by Figure 2.5. Bio-oil is classified as a low quality fuel and cannot be used as chemicals.

Moreover, the oxygenate compound are very reactive leading to unstable and short shelf-life [40]. The quality and stability of bio-oil need upgrading. The chemical conversion is the most powerful methodology for chemical and physical properties improvement. This is accomplished by catalytic processes.

2.5.1 Chemistry of catalysis

Since the catalytic process was found, many impossible reactions become true. The catalyst never changes the final state of reaction but changes the reaction pathway to the activation energy lower than uncatalyzed pathways as shown by Figure 2.17.

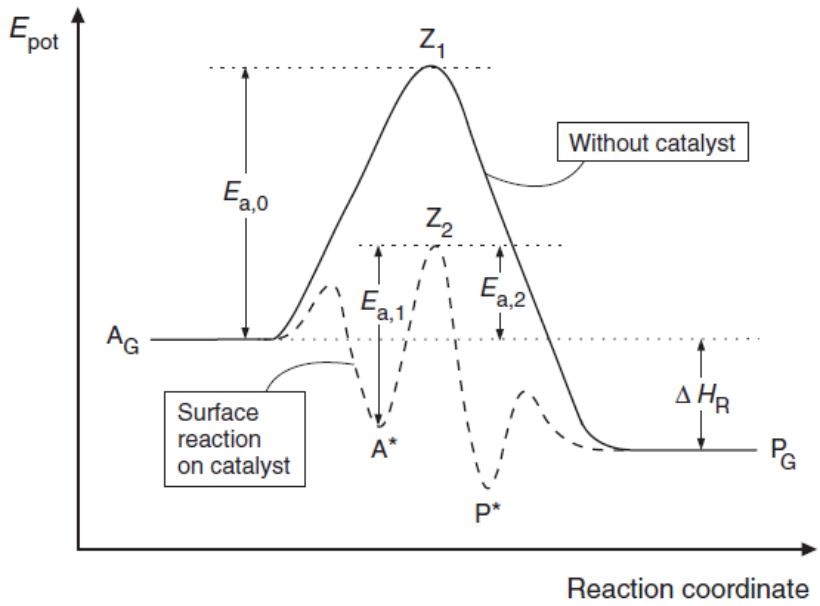

Figure 2.17 Comparison of activation energy between catalytic and uncatalytic reactions [41]

Today, almost all chemical processes need catalyst. It does not only help reaction drive easily but also help reaction occurred specifically. They are important parts of industrial growth for examples ammonia synthesis and catalytic hydrogenation. A definition of catalysis that still valid today belongs to Ostwald (1985): “a catalyst accelerates a chemical reaction without effecting the position of equilibrium.” It had

been assumed that the catalyst remained unchanged in the course of reaction. Nowadays, it is known that the catalyst can bond to reactant transforming to the intermediate of catalyst (Cat-R), which is highly reactive and difficult to detect. The product is then released and the catalyst is back to the initial state. Thus, the catalyst works as cycle as shown below;

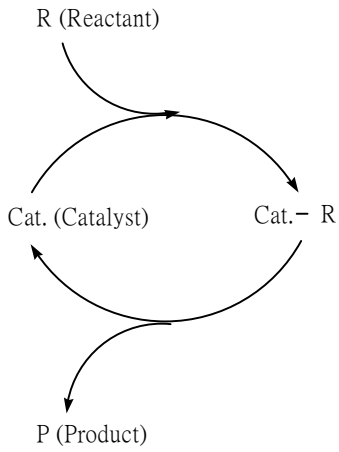

Catalyst will not be theoretically consumed. However, there are other competitive reactions resulting in chemical change of the catalyst so the activity become lower (deactivation). The regeneration of catalyst is necessary [42].

The catalysts can be classified by many criteria (Figure 2.18), i.e. states, structures, acid-base, compositions, and applications. However, the state, which they act, is the most preferable classification. The catalysts can be divided into two main groups including heterogeneous and homogeneous catalysts, and there are intermediate forms also known as heterogenized homogeneous catalysts (immobilized catalysts) such as homogeneous catalysts attached to support and biocatalysts (enzymes).

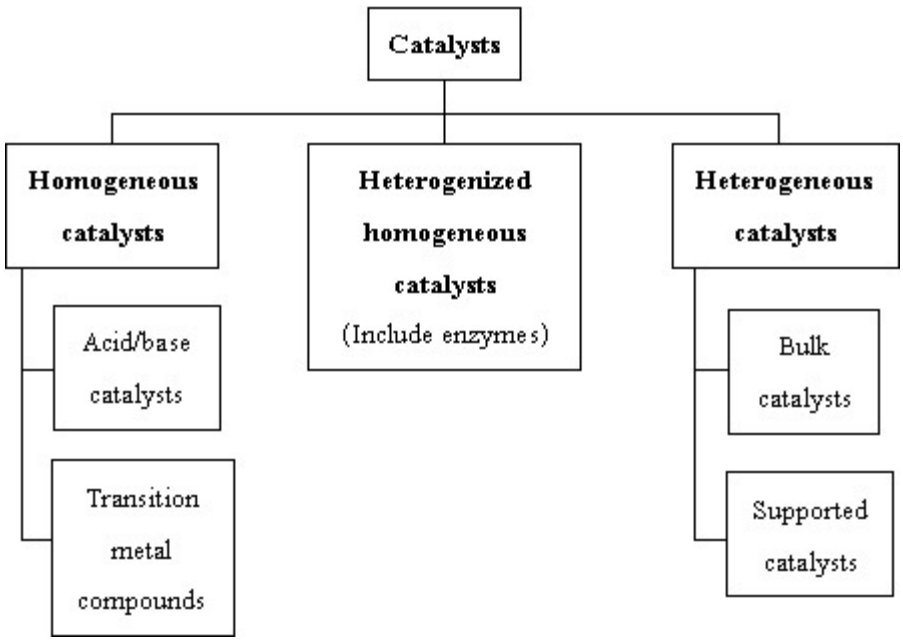

Figure 2.18 Classification of catalysts [42]

Catalytic processes taken place between two phases are classified as heterogeneous catalysis. Only surface of the catalysts are active. In contrast, homogeneous catalysis takes place in uniform phase. The homogeneous catalysts, which every catalyst molecules can be active sites, have higher degree of dispersion than the heterogeneous ones.

2.5.1.1 Heterogeneous catalysts

Generally, the industrial prefers the heterogeneous catalyst due to high thermal stability, compatible with various reactor designs, low loss during processing, easy separation from product, and regeneration ability. The catalytic process over porous heterogeneous catalyst can be considered by seven steps according this scheme;

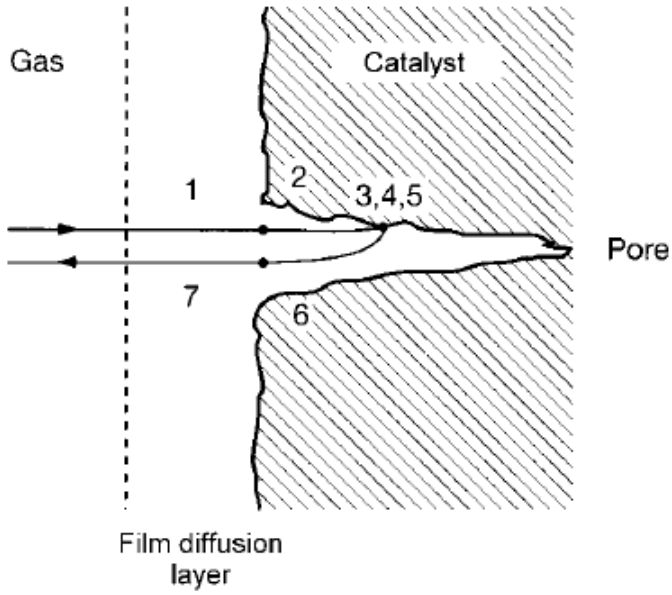

1) Diffusion of reactant to the boundary layer of catalyst surface
2) Diffusion of reactant into the pore of catalyst
3) Adsorption of reactant to the surface of catalyst (active site)
4) Catalytic conversion of reactant to product promoted by active site
5) Desorption of the product from active site
6) Diffusion of product leaving the pore
7) Diffusion of product to the environment

For heterogeneous catalysis, the adsorption is an important step. It is an exothermic process and the potential energy is lower than the normal state as illustrated by the dissociative adsorption of hydrogen gas to hydrogen atom over nickel surface in Figure 2.19. Therefore, the reaction can be carried out over catalyst surface with low energy [41].

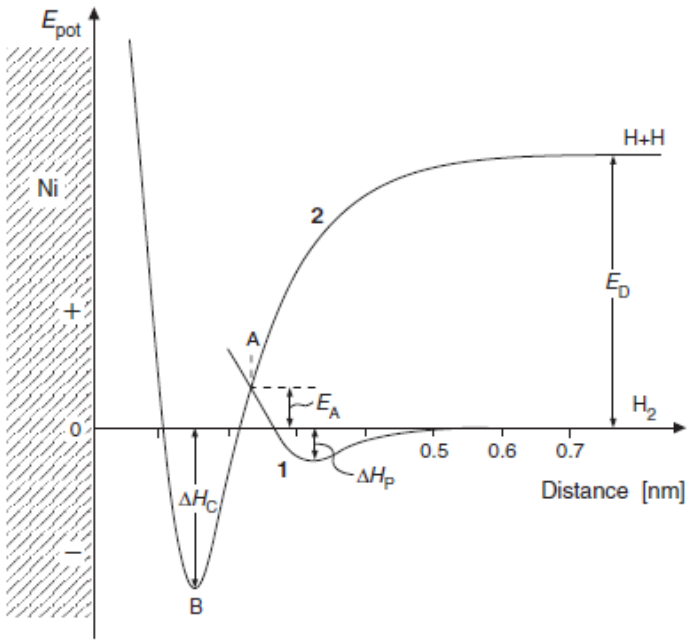

Figure 2.19 Potential energy of hydrogen and hydrogen atom with the distance from nickel surface, 1 is hydrogen physisorption distance and B is the chemisorption distance [41]

Nowadays, the frequent used heterogeneous catalysts almost are in solid phase including metal, metal oxide, and shape selectivity catalysts.

Metal catalysts are the simplest solid catalyst by single crystal structure. They are usually considered as flat surface with elaborate arrangement of atom in different direction leading to plans as shown below;

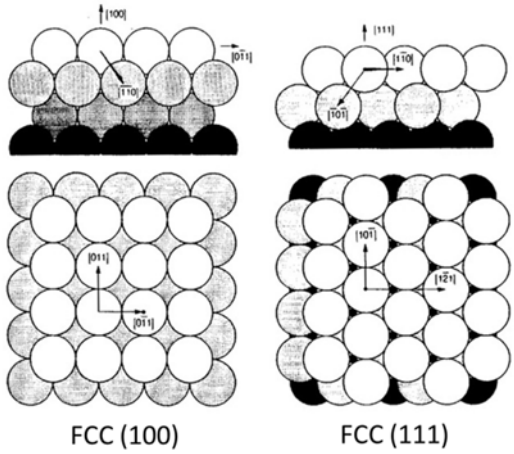

The surface atom possesses unsaturated coordination, which act as active site for adsorption due to the electronic effect [42];

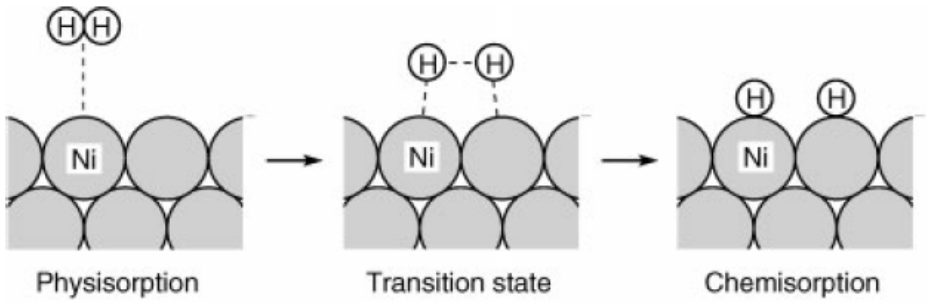

Actually, the metal surface does not perfectly flat. The loss of an atom or a part of layer generates the defect such as step, kink, and terrace that decreases the coordination number of metal at surface [43] as given below;

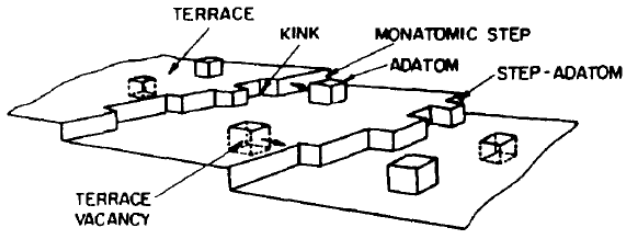

Therefore, these defects are active more than perfect surface and suitable for acceleration. The defects also lead to the different adsorption mode due to geometrical effect resulting in different reaction mechanism [42];

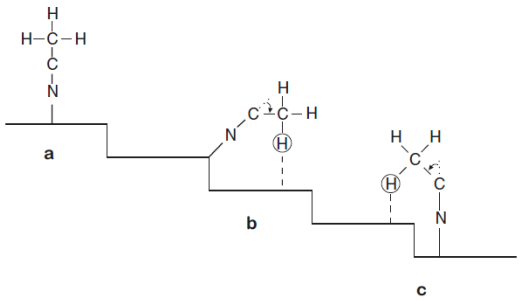

Metal oxide catalysts compose by metal and oxygen in structure so they generally have two different sites including + of matals and – of oxygen. The complexity of metal oxides (e.g oxidation state, phase, coordination, and surface specie) leads to different mechanism [44]. As the homolytic cleavage of hydrogen adsorbed on nickel surface is mentioned previously, the heterolytic cleavage promoted by pair-ion takes place over metal oxide surface like chromium (III) oxide;

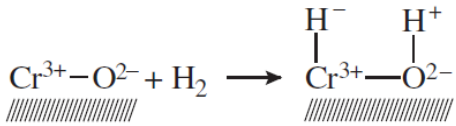

On the other hand, the redox property of metal can generate the two mole of hydride from a hydrogen mole when the cleavage is taken place over chromium (II) oxide [41];

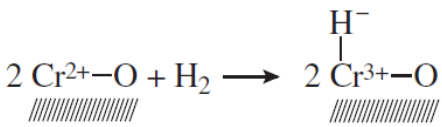

Shape selectivity catalysts are also known as zeolites. They are solid crystalline of aluminosilicates, which consist of SiO_4 and AlO_4^- tetrahedral, and interlinked to be three dimension network of porous structure. Inside of zeolites pore has cations e.g. metal ion, ammonium, and proton balancing the negative charge from the aluminium anionic framework. The general formula of zeolite is given below;

$$M_v(AlO_2)_x(SiO_2)_y.zH_2O$$

where M are metal cations

The Si/Al atomic ratio is a favorite way to identify the composition of zeolite. The structure of zeolites is confined by template and gel composition during the synthesis. The aperture of pore usually be 8 (small), 10 (medium), and 12 (large) T-atom (metals without oxygen), that could be around 4-8 Å. The pore can be oriented in one, two or three dimension as illustrated by Figure 2.20.

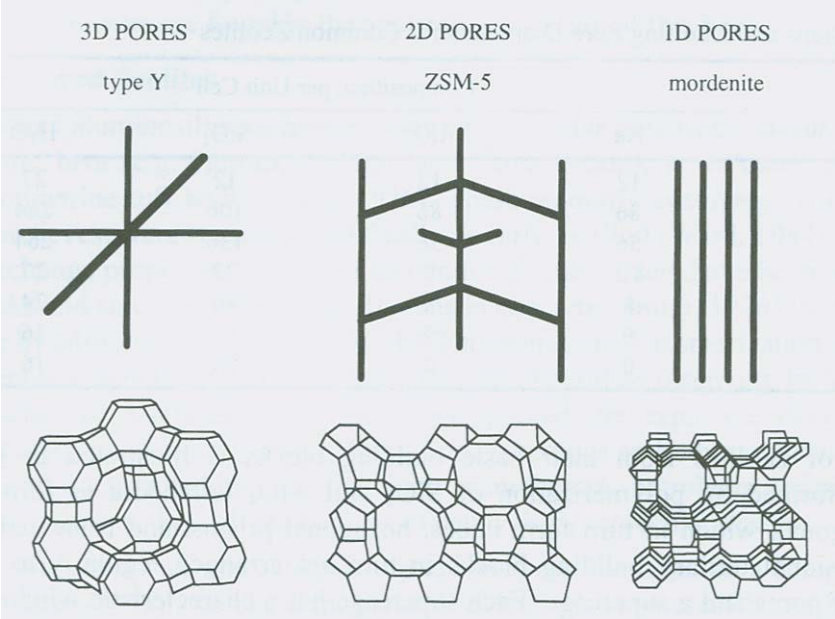

Figure 2.20 Three commercial zeolites of difference dimensionalities

Due to their high surface area, zeolites have high capacity for molecular adsorption. The reactant, which possesses kinetic diameter (diameter when moving, vibrate, and rotate) less than pore aperture, will diffuse to inside the pore for adsorption then conversion. This is the reactant selectivity (Figure 2.21). Once the reactant can be adsorbed to the pore, the intermediate forming during the reaction are also controlled by well-define pore structure leading to transition state selectivity. While, the only the product smaller than pore exit can be diffused out of pore resulting to product selectivity. With these reasons, the zeolite is call shape selective catalyst;

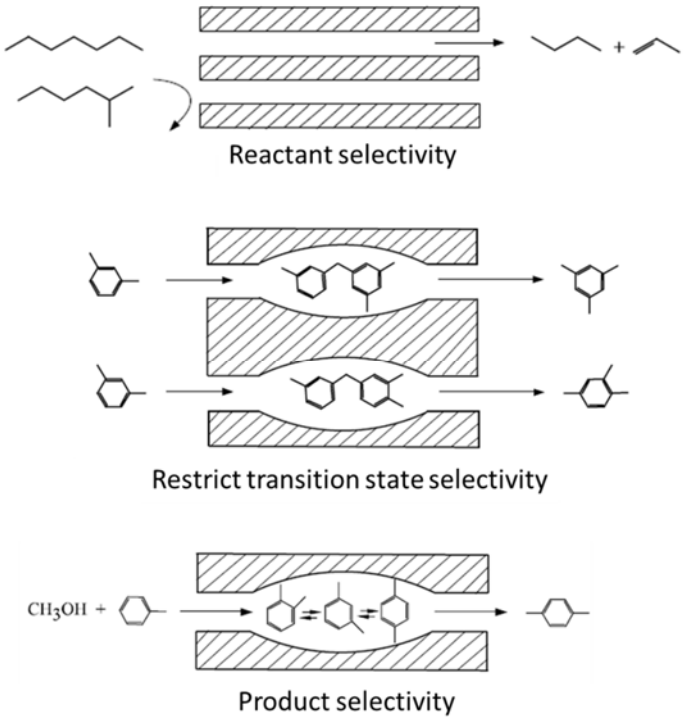

Figure 2.21 Selectivity by pore of zeolite [42]

Another catalytic activity of zeolite is acid-base property. This is the result from the difference between – of aluminium framework and + of balancing cation. For acidic zeolite, the acid strength (power of acid) can be varied over wide range depending on the metal cation (H >> La > Mg > Ca > Sr > Ba > Na). Zeolites in H form are strongest acid. They can be prepared by exchanging of alkaline metal ion by NH_4^+ ions then eliminate NH_3 by calcinations in air which results in proton balancing;

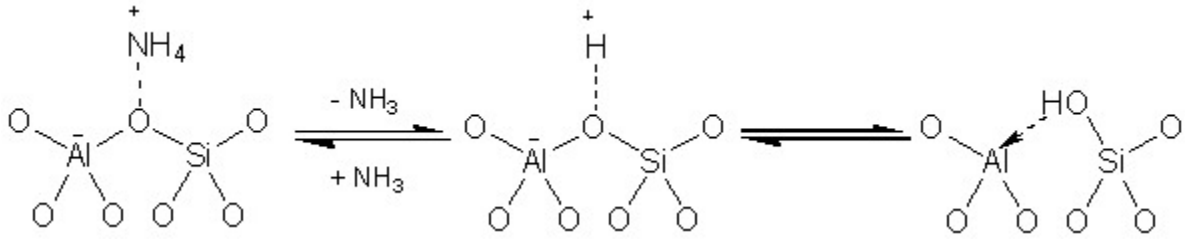

When H-zeolites are heated to high temperature (>500 °C), waters are eliminated from the zeolites leading to defect of frameworks. These defects are electron deficient sites so they can act as Lewis acid catalyst [45];

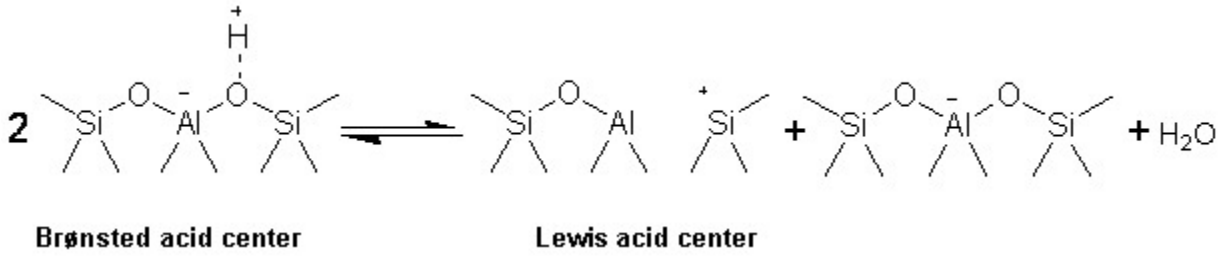

2.5.1.2 Action modes of catalyst

To determine how well of the catalyst, it can be considered from three modes including activity, selectivity, and stability (deactivation behavior).

Activity**:** Activity is a measure of how fast of reactions proceed in the presence of catalyst. Activity can be expressed many ways e.g. reaction rate (*r*), rate constant (*k*) and activation energy (E_a). In practice, instant measurement of activity by the comparison of conversion under constant reaction condition is often sufficient for catalyst evaluation.

The conversion (X_A) is the ratio between amount of reactant A, which is reacted, and amount of reactant A, which is introduced into reactor;

$$X_A = \frac{n_{A,0} - n_A}{n_{A,0}} \qquad \text{(mol/mol or \%)}$$

where, $n_{A,,0}$: amount of reactant at initial time

n_A : amount of reactant at end point

Catalysts are often operated in continuous process, which conversions at constant space velocities or contact times are compared. The space velocity is ratio of volume flow rate (V_0) to catalyst mass (m_{cat});

$$Space\ velocity = \frac{V_0}{m_{cat}} \qquad (\mathrm{m^3\,kg^{-1}\,s^{-1}})$$

Another important measurement of catalyst activity is “turn over number” (*TON*), which is number of reactant molecules converted per active center before the catalyst is completely deactivated. In case of homogeneous catalyst, TON can be determined directly because every catalyst molecules present in solution. For heterogeneous catalyst, it is quite complicate to measure because only surface molecules of catalyst are active centers so number of active sites depends on area of catalyst surface. However the active sites can be determined indirectly by chemisorption methods.

Selectivity**:** Not only desired reaction happens during the processing but also side reactions. When a reactant converts to two or more products, it is called parallel reaction as illustrated in Figure 2.22. And, when a product is further converted to other product, it is a sequential reaction. Both phenomenon give undesired products (P_1, P_2).

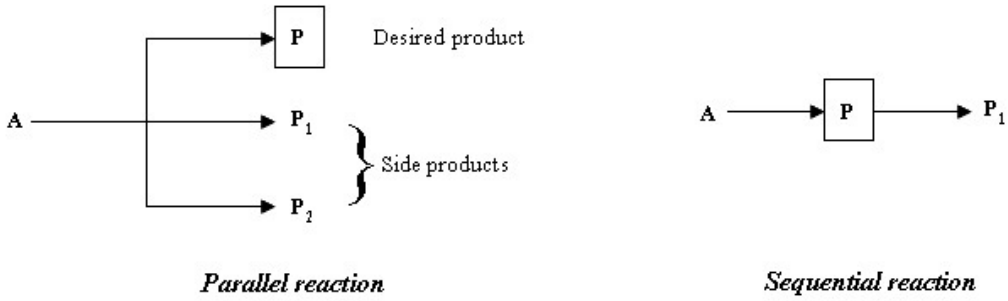

Figure 2.22 Parallel and sequential reaction

The selectivity (S_P) to a product is the ratio of desired product (P) to converted reactant (or conversion). The selectivity is comparison between reactant and product, which is usually difference in mole, so the stoichiometric coefficients (v_i) must be taken into account;

$$S_P = \frac{n_P / \nu_P}{(n_{A,0} - n_A) / |\nu_A|} \qquad \text{(mol/mol or \%)}$$

where, $n_{A,,0}$: amount of reactant at initial time

n_A : amount of reactant at end point

v_i : stoichiometric coefficients

Stability**:** The chemical, thermal and mechanical stability of catalyst determine lifetime of the catalytic process. They are influenced by several factors including decomposition, coking and poisoning. Catalyst deactivation can be followed by measuring activity and selectivity during processing time. The catalyst lifetime can be extended by regenerating the deactivated catalysts. The total lifetime is an important consideration for processing method and economic.

Generally, the priority of catalyst evaluation is in order of: selectivity > stability > activity [41]

2.5.2 Deoxygenation of bio-oil

As mentioned previously, the oxygen is barrier for bio-oil utilization. The deoxygenation process, which the oxygen is removed catalytically, seems to be the most attractive upgrading and stabilization for now. The hydrocarbons obtained from the process will be ready to use as fuel and petrochemicals similar to the hydrocarbon from crude oil refinery. The separation of bio-oil by multistage pyrolysis [46] or extraction as given in Table 2.8 can help the chemistry choose the suitable chemical reaction for deoxygenation of each fraction e.g. hydrogenation, dehydration, ketonization, decarbonylation, and decarboxylation.

2.5.2.1 Hydrogenation and hydrogenolysis

Hydrogenation (also known as reduction) is the addition of hydrogen to pi-bond [47]. Although the process is not the fully deoxygenation, the saturation can stabilize the bio-oil by elimination of unsaturated compound e.g. alkenes, ketones and aldehydes, which is very reactive. The active catalyst for hydrogenation is transition metals [48]. The unsaturated organic molecules chemisorb to metal surface by π-electron donating to vacant *d*-orbitals of metal [49]. In the same time, hydrogens also chemisorb to the surface then breaking to adsorbed hydrogen atoms. These radicals can add to the organic intermediate leading to hydrogenation as illustrated by the *Horiuti-Polanyi* mechanism of ethylene hydrogenation below [48];

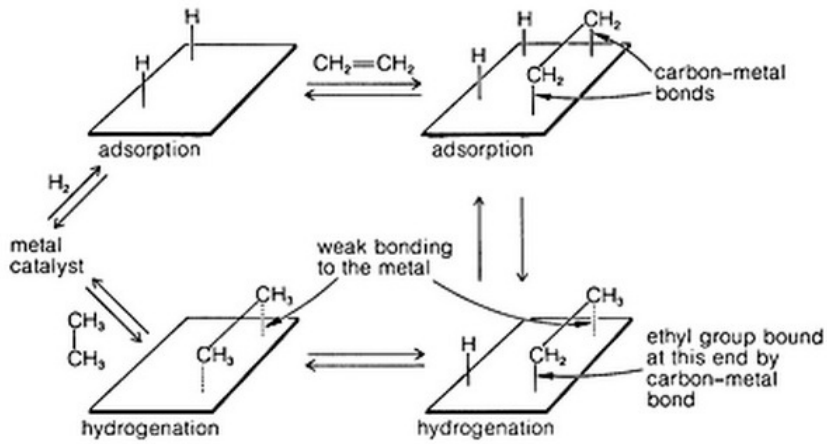

The hydrogenation by plane metal surface mostly dominates by electronic effect. The metals, which bond weakly to reactant, are inert due to low adsorptivity. Meanwhile, the over strong bonding leads to unbreakable bond and low desorptivity. These results lead to the volcano plot of metals catalyst along the periodic table as the example given in Figure 2.23. The suitable metal catalysts for hydrogenation must have the balance between adsorptivity and desorptivity [49], which are transition metal in group 8B and 1B in sometime (Fe, Ni, Rh, Pt, and Cu). The metal base hydrogenation catalyst can be deactivated easily by poisoning at the surface with halogens, sulfur, nitrogen, and phosphorus compounds, pore blocking by coke, and attrition [45].

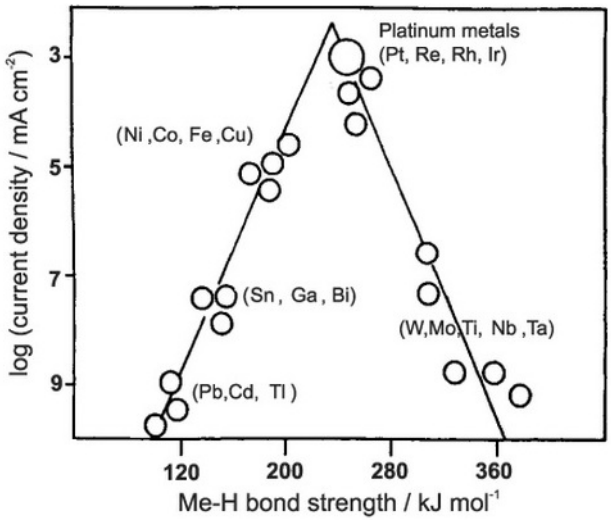

Figure 2.23 Volcano plot of activity and metal-H bond strength of CO hydrogenation by electro catalysis [50]

Metal oxides like zinc oxide are also promotes the hydrogenation at room temperature. Surface of the metal oxide is considered to two different active sites including metal and oxide. The dissociative adsorption of gas phase hydrogen takes place one atom on metal and the other on oxide, and possesses the mobility as illustrated below;

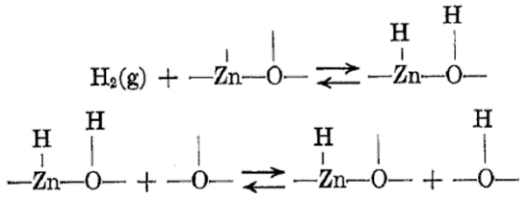

When ethylene is adsorbed, the addition of hydrogen atoms occurs rapidly through stepwise mechanism resulting in ethane [42, 51];

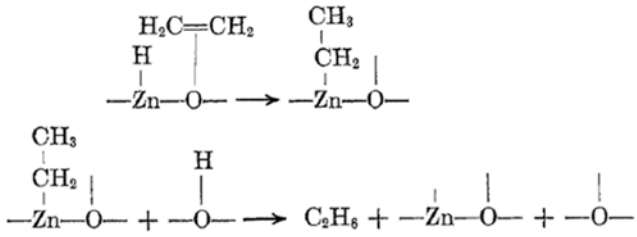

For, the catalytic hydrogenation of carbonyl compounds, it was found that the ketones are hydrogenated more difficult than aldehydes due to the steric hindrance. The working catalyst are supported platinum group metal (PGM) including ruthenium, platinum, rhodium, and iridium. The mild temperature (20 – 80 ^{o}C) is often used with some pressure (<10 bars) and operated by batch reactor. The good solvents are ethyl acetate, alcohols, and water. Nickel is sometime used due to cheapest in PGM but the operating temperature should be increased. Hydrogenation of carboxylic acid to aldehyde or alcohol over conventional metal catalysts is more difficult than aldehyde and ketone due to higher hydrogen pressure. The reaction through acid chloride (need $SOCl_2$) or other hydrogen donor such as formic acid is alternative methods for small scale production. On the other hands, the metal oxides are successive catalysts for reduction of carboxylic acid. Iron oxide was first discovered catalyst for benzoic acid hydrogenation to benzaldehyde. Today, Y_2O_3 and ZrO_2 are the most effective catalyst at 400-450 ^{o}C and low pressure (0.1 MPa). Other optional catalysts are γ-Al_2O_3, MgO, TiO_2, and ZnO [49].

Hydrogenolysis is the cleavage of σ-bond (e.g. C-C, C-X, C-O, and C-N) by hydrogen. It is a structure sensitive reaction [52]. Palladium, platinum, and nickel base catalysts are generally used for simple structure e.g. aliphatic compound. The general mechanism C-C cleavage of ethane over active metal surface (*) in excess of hydrogen (route I) and ethane (route II) are given below [53];

1. $H_2 + 2* = 2\underset{*}{H}$
2. $C_2H_6 + 2* = \underset{*}{C_2H_5} + \underset{*}{H}$
3. $\underset{*}{C_2H_5} + * = \underset{*}{CH_3} + \underset{*}{CH_2}$
4. $\underset{*}{CH_2} + \underset{*}{H} = \underset{*}{CH_3} + *$
5. $\underset{*}{CH_3} + \underset{*}{H} = CH_4 + 2*$

Route I

1. $H_2 + 2* = 2\underset{*}{H}$
2. $C_2H_6 + 2* = \underset{*}{C_2H_5} + \underset{*}{H}$
3. $\underset{*}{C_2H_5} + * = \underset{*}{C_2H_4} + \underset{*}{H}$
4. $\underset{*}{C_2H_4} + * = \underset{*}{C_2H_3} + \underset{*}{H}$
5. $\underset{*}{C_2H_3} + * = \underset{*}{C_2H_2} + \underset{*}{H}$
6. $\underset{*}{C_2H_2} + * = 2\underset{*}{CH}$
7. $\underset{*}{CH} + \underset{*}{H} = \underset{*}{CH_2} + *$
8. $\underset{*}{CH_2} + \underset{*}{H} = \underset{*}{CH_3} + *$
9. $\underset{*}{CH_3} + \underset{*}{H} = CH_4 + 2*$

Route II

For deoxygenation by C-O bond cleavage, the rate is in order of OCOR > OAr >> OR > OH. This rate is determined by the leaving group belong to S_N-type reaction. The hydrogenolysis cyclic ethers are much more easy than open chain structure. Three and four membered rings are reactive even at room temperature while five and six membered rings require higher temperature [49]. The phenolic compounds require some modification of catalyst such as acidic support [54].

2.5.2.2 Dehydration

The dehydration is the deoxygenation of alcohols in from water forming alkenes by intra-molecular elimination or ethers by intermolecular elimination. The practical catalysts can be acidic, basic or bi-functional acid-base ones.

When monohydric alcohols is dehydrated, alkenes can be formed by the loss of water through β (or 1, 2-) elimination. Selective products are obtained as terminal alkenes (α olefin) when primary alcohols are dehydrated by appropriate solid catalysts. In contrast, either 1- or 2- alkenes can be produced by secondary alcohols dehydration. The reactivity of alcohols is ordered following the sequence: tertiary > secondary > primary. The mechanistic studies of dehydration are established over acidic oxides follow two major routes;

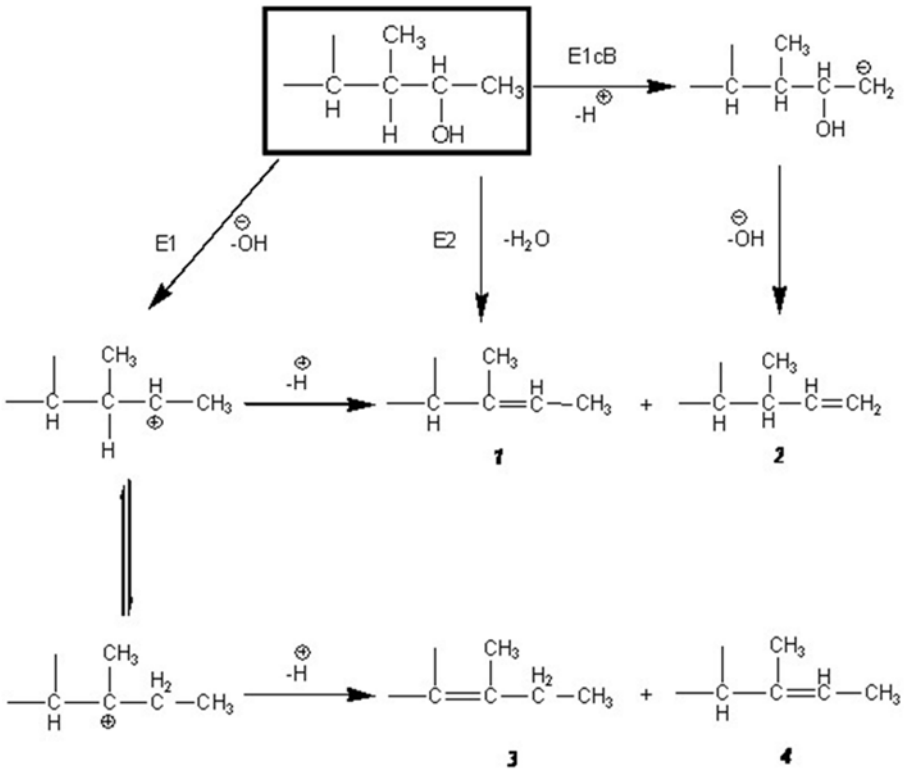

The single step mechanism (concerted E2) results in alkenes according Saytzev's rule (more substituted alkene isomers, product 1). For the two-step elimination (E1), the mechanism starts with $^{-}$OH removal leading to carbocation intermediate generation. It can then be rearranged to stable form, which gives rise to mixture of isomeric alkenes (product 3, 4). For basic oxide, E1cB mechanism initiates by proton removal from β carbon. The rearrangement of the intermediate is in line with Hofmann rule (less substituted alkenes, product 2) [49].

Acidic oxide like alumina is a common dehydration catalyst. It is always treated with alkaline metal cations, ammonia or organic bases because pure strong acidic of alumina can promote carbocations rearrangement and double bond migration as observed from comparison of cyclohexanol dehydration over alumina and alumina treated with potassium (Table 2.9)

Table 2.9 Dehydration of cyclohexanol [49]

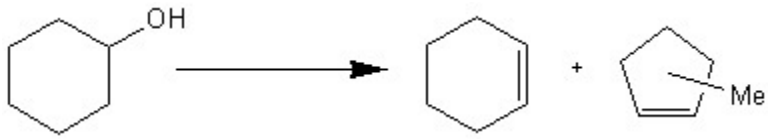

Catalysts	Temperature (K)	Conversion (%)	Selectivity (%)	
			Cyclohexene	Methyl cyclopentene
Al_2O_3 with 1%K	683	95	100	0
Al_2O_3	623	95	89	11
	693	99	40	60

Numerous studies are performed with molecular sieves as dehydration catalysts. Influence of E1 mechanism, which generates reactive carbocationic intermediates followed by rearrangement and inter and intra molecular parallel reaction, results in mixture of alkene isomer products and ethers. However, some specific structural alcohols can be transformed selectively. For example, 1-phenyl-1-ethanol is converted to styrene with 95% yield over HZSM-5 zeolite at 493 K. Ethers formation occur when α-(*p*-tolyl) ethanol is reacted over HY zeolite. Low concentration of reactant in zeolite pores is required to prevent inter molecular reaction.

In contrast to alumina, thoria (thorium dioxide) is a typical E1cB catalyst which converts 2-alkanols to 1-alkenes. From the studies of lanthanide and alkaline earth dehydration with various alcohols, it was suggested that selectivity depends on the relative strength and concentration of acidic and basic centers. The E1cB mechanism is known to be associated with dehydrogenation (removed hydrogen gas). It was observed that dehydration activity increased with covalent characteristic of metal-oxygen bond while ionic characteristic one enhances dehydrogenation activity [49].

Recently, the global focuses on dehydration of biomasses, which almost are polyols. Hexose and fructose dehydrations to 5-hydroxymethylfurfural (HMF) are apparent example. This compound can be used as starting materials for various fine chemicals and polymers;

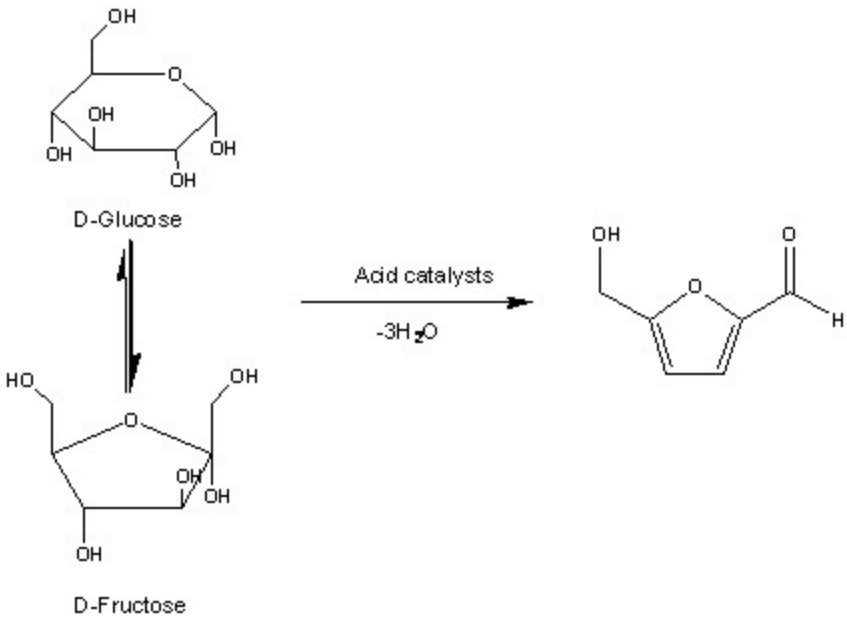

Dehydrations usually conduct in aqueous media with continuous extraction. Strong acids such as ion-exchange resins and zeolites have been studied. Zeolites are selective catalysts because side reactions and C-C cleavage are less important. Moreover, they are regenerated easily and can be operated at high temperature. Moredenite has excellence characteristic due to shape selectivity and low mesoporosity. Heterogeneous niobium catalysts (niobic acid, H_3PO_4 treated niobic acid and niobium phosphate) have recently been found to be selective catalysts [49].

2.5.2.3 Decarbonylation, decarboxylation, and ketonization

Decarbonylation is the deoxygenation in form carbon monoxide. In contrast to dehydration, the decarbonylation gains the interesting due to the useful of carbon monoxide as synthesis gas for petrochemicals. The decarbonylation generally requires high temperature [55]. The carbonyl compounds including aldehydes [56] and ketones [55, 57] can be decarbonylated through various mechanisms depending on catalyst. The common mechanism is found in homolytic α-cleavage of carbonyl radical, which needs the radical initiater or photo energy in case of ketones, to alkane and carbon monoxide [57];

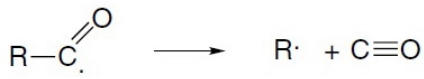

The most success catalyst are organometallic complex of metals in group 8B especially palladium and rhodium. The reaction can be carried out in liquid phase with low temperature (190 °C) [56]. The catalytic cycle of benzaldehyde decarbonylation by rhodium complex occurs through migratory elimination as investigated by [58];

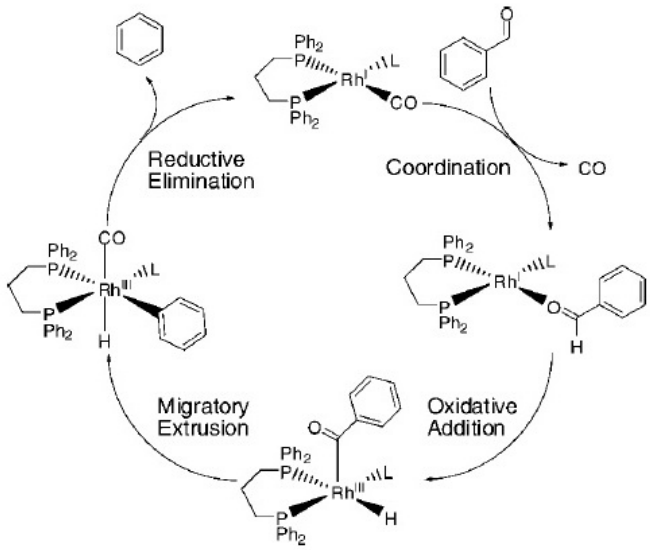

The decarbonylation of carboxylic acids can be promoted by iron and palladium complex [59-60]. The reaction is more complicate than the decarbonylation of aldehyde because acid anhydride generation is essential step. The carbon monoxide is eliminated with water, which is trapped by acetic anhydride, and yields alkene according to the general catalytic cycle below;

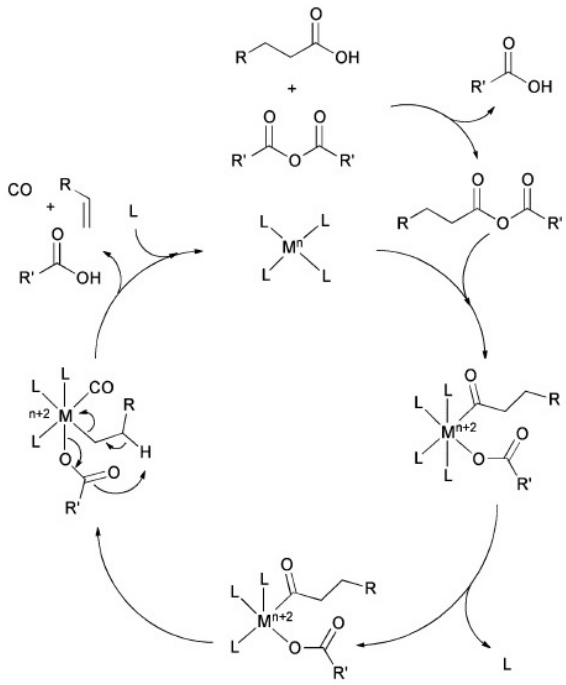

Decarboxylation is the deoxygenation in form of carbon dioxide. Carboxylic acids and some esters can be decaboxylated easily to alkane and ketone, respectively due to thermal unstable of carboxylic group at high temperature. This is an exothermic process. The rate is very slow without catalyst [20]. In general, the decarboxylation proceeds through heterolytic cleavage;

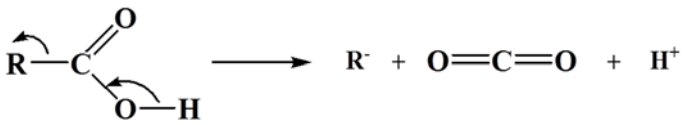

The simplest method is heat the carboxylic acid with sodium hydroxide and lime (CaO) the carbon dioxide will be removed in form of sodium carbonate [61];

$$CH_3CH_2COOH + 2\ NaOH \rightarrow CH_3CH_3 + Na_2CO_3 + H_2O$$

However, the β-ketoacids, which have a carbonyl group at the next two carbon, were found to be decarboxylated easily at low temperature (100-150 °C). The six membered ring is a suitable configuration for decarboxylation as express below;

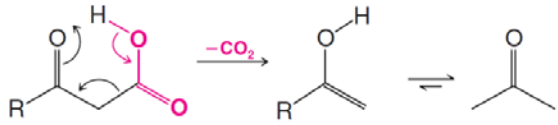

Moreover, the decarboxylation takes place easily under the basic condition due to the stability of resonance anion [20];

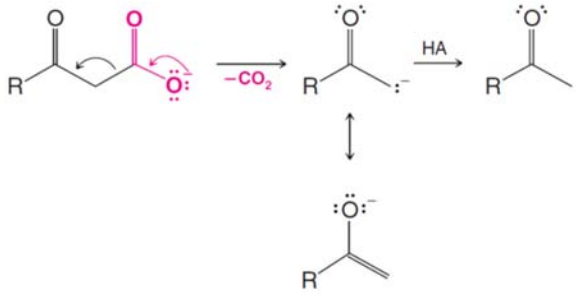

The β-ketoesters can also be decarboxylated in similar manner to β-ketoacids [20]. Today, the decarboxylation of fatty acid to hydrocarbons for liquid fuel is most the attractive process. The catalyst is mostly based on the base metal oxide especially MgO. However, the catalyst deactivates fast due to carbonate formation similar to above process. The catalyst can be regenerated by calcination [62]. Meanwhile, there are evidences for decarboxylation by radical mechanism. They were widely found in photo catalysis. The reaction is really different to decarbonylation due to the β-scission as shown below [57];

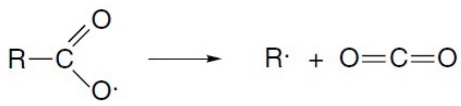

Ketonization: Not only decarboxylation but also ketonization (also known as ketonic decarboxylation) can occur to the carboxylic acids at high temperature (typically >300 °C). The ketonization is old practical process for acetone production from metal acetate salts, which obtain from the reaction between metal carbonates or hydroxides and carboxylic acids, during the World War I [27]. It is believed that the decomposition occurs through two steps ionic mechanism [63];

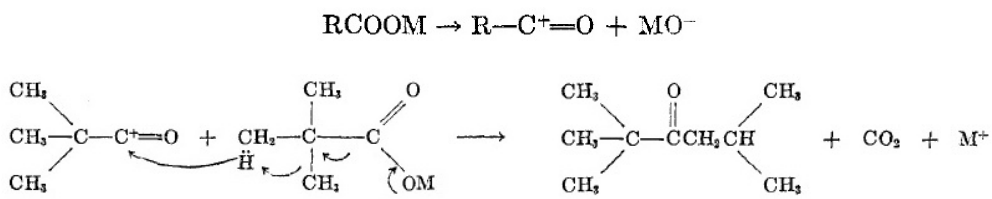

where, M = metals

R = $(CH_3)_3C$-

The direct fed of carboxylic acid is more attractive than decomposition of carboxylate salts for today. The mechanism of alkaline and alkaline earth oxides including BaO, MgO, CaO, and SrO starts from carboxylate salt generation due to the strong interaction between metals and carboxylic acid. It is then decomposed same as mentioned above [64]. This leads to the deoxygenation by elimination of carbon dioxide and water simultaneously. The transition metal oxides such as TiO_2 [65], ZrO_2 [64], and CeO_2 base mixed oxides [66] are also interested but the mechanism still unclear depending on the catalyst and operating system. The α-hydrogens are very active leading to the formation of β-ketoacids, which is further decarboxylated easily as mentioned in the decarboxylation section [64, 67];

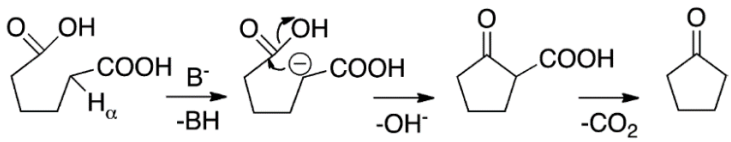

As the dehydration of carboxylic acids can be promoted at high temperature, the ketonization via ketene is also proposed as shown below [64];

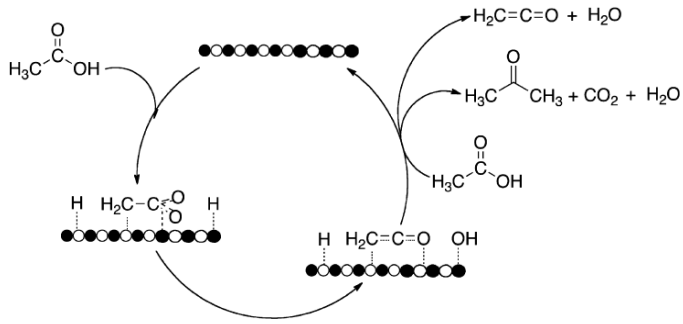

2.6 Overview of the thesis

In this thesis, acetone, acetic acid, and furfural were selected as model compounds for ketone, carboxylic acid, and aldehyde in light fraction of bio-oil. They were upgrading to olefins used in petrochemical via deoxygenation. The sequential of reactions were established from simple catalytic processes including hydrogenation, dehydration, ketonization, and condensation to remove oxygen content at relatively mild condition (< 573 K and atmospheric pressure). These require multi-functional catalysts synthesized from metals, metal oxides, and zeolites working synchronously. Therefore, the catalyst design is emphasized for a selective olefin production from these model oxygenates.

In **Chapter 3**, preparation of the catalysts (metal support, metal oxide, zeolites, and bi-functional catalysts) as well as the characterization procedures were generally described. Setting up and parameters for catalytic upgrading of the model oxygenates over those catalysts were then explained with diagram.

In **Chapter 4**, the self-deoxygenation of ketones (acetone and ethyl methyl ketone) to olefins and carboxylic acid was mentioned. The reaction was carried out over proton zeolites at relatively low temperature (448 K) and atmospheric pressure of inert (nitrogen). As a certain mechanism had never been investigated, flow reaction with

different contact time and temperature (i), pulse reaction (ii), temperature programmed desorption (iii), and thermal desorption (iv) were performed. The reaction pathway for self-deoxygenation was proposed to involve the catalytic conversion of several intermediates (mesityl oxide, diacetone alcohol, isobutyl methyl ketone, *i*-butylene, acetic acid, and water). The suitable zeolite catalysts used were also evaluated with various frameworks (HZSM-5, H-β, HY, H-Mordenite, and H-Ferrierite) and Si/Al (13, 40, 100, and 150).

Alternatively, the upgrading of ketones (acetone, ethyl methyl ketone, and cyclohexanone) to their corresponding olefins under atmospheric pressure of hydrogen is referred in **Chapter 5**. The hydrodeoxygenation (HDO) via hydrogenation-dehydration at relatively low temperature (< 473 K) was proposed. The study was initiated with each individual catalytic processes; hydrogenation with metal catalysts (chromium, iron, cobalt, nickel, copper, palladium, and nickel-copper alloy) and dehydration with proton zeolites (HZSM-5, H-β, HY, and H-Mordenite). The metal-zeolite combinations as HDO catalyst were then evaluated by sequential process (Ni/SiO_2+HZSM-5), mixed catalyst (Cu/SiO_2-HZSM-5 and Cu/SiO_2-H-β) and bi-functional catalyst (Cu/HZSM-5 and Cu/HY). The temperature programmed reduction (TPR), temperature programmed desorption of ammonia (NH_3-TPD), and transmission electron microscope (TEM) were employed to identify the aspect of catalyst that leads to different catalytic activity.

The deoxygenation of the most abundant compound in bio-oil; acetic acid, was mentioned in **Chapter 6**. As a part of oxygen in the carboxylic acid is removed selectively by ketonization over CeO_2, further deoxygenation of the ketone produced to olefin would be possible in a manner similar to that described in Chapter 5, except that the reaction must be carried out at >573 K. Therefore, the sequential process of ketonization-hydrogenation-dehydration of acetic acid to propylene was proposed, so called “keto-hydrodeoxygenation” (KHDO). The mixture of CeO_2-Cu/HY and CeO_2-Cu/HZSM-5 were an advance in catalyst combination, particularly designed for KHDO. The catalyst composition and reaction temperature were optimized to obtain high propylene yield with low direct HDO of acetic acid. The extension of KHDO to light distillated hydrocarbons was also performed to produce higher value chemicals such as

toluene, xylenes, and *n*-butylenes in this section. The effect of water in bio-oil as well as the stability of the catalysts were discussed.

In **Chapter 7**, the interference of acetic acid and water to the bio-oil upgrading was examined over HDO of furfural. The furfural decarbonylation to furan over palladium catalysts (Pd/C, Pd/CeO_2, Pd/HY, Pd/SiO_2, Pd/ZnO, Pd/γ-Al_2O_3, Pd/ TiO_2) and furfural HDO to 2-methylfuran over copper catalysts (Cu/SiO_2 and Cu/HY) were tested. The single and mixed feed (furfural, furfural/water, furfural/acetic acid, and furfural/acetic acid/water) as well as the feed alternation (furfural-furfural/acetic acid and furfural-acetic acid) were employed. The deactivation by carbon deposition, competitive adsorption and corrosion was followed in combination with the change in catalyst morphology and composition as observed by TEM-EDS. The simultaneous conversion of furfural and acetic acid was also emphasized to improve the corrosion and stability of bio-oil.

The catalyst design and condition for upgrading of ketones, aldehyde, and carboxylic acid in light fraction of bio-oil were summarized in **Chapter 8**. The suggestions were also given for further development.

2.7 References

[1] Crocker M. **Thermochemical Conversion of Biomass to Liquid Fuels and Chemicals.** Cambridge: RSC Publishing. 2010.

[2] Räisänen T. and Athanassiadis D. **Basic Chemical Composition of the Biomass Components of Pine, Spruce and Birch.** Sweden: Forrest Refine. 2013.

[3] Van De Ven T. and Godbout L., Editors. **Cellulose–Fundamental Aspects.** Rijeka: InTech. 2013.

[4] Yokoyama S. and Matsumura Y., Editors. **The Asian Biomass Handbook: A Guide for Biomass Production and Utilization.** Japan: The Japan Institute of Energy. 2008.

[5] Blaschek H.P., Ezeji T.C. and Scheffran J., Editors. **Biofuels from Agricultural Wastes and Byproducts.** Singapore: Blackwell Publishing. 2010.

[6] Lin S.Y. and Dence C.W., Editors. **Methods in Lignin Chemistry.** Berlin: Springer-Verlag. 1992.

[7] Basu P. **Biomass gasification and pyrolysis: practical design and theory.** Burlington: Academic Press. 2010.

[8] Sadaka S. and Johnson D.M. **Biomass Combustion.** Arkansas: University of Arkansas.

[9] Jenkins B.M., Baxter L.L., Miles Jr. T.R. and Miles T.R. "Combustion properties of biomass" **Fuel Processing Technology,** vol.54, 1998. pp.17-46.

[10] Toor S.S., Rosendahl L. and Rudolf A. "Hydrothermal liquefaction of biomass: A review of subcritical water technologies" **Energy,** vol.36, 2011. pp.2328-2342.

[11] Toor S.S, Reddy H., Deng S., Hoffmann J., Spangsmark D., Madsen L.B., Holm-Nielsen J.B. and Rosendahl L.A. "Hydrothermal liquefaction of *Spirulina* and *Nannochloropsis salina* under subcritical and supercritical water conditions" **Bioresource Technology,** vol.131, 2013. pp.413-419.

[12] Demirbas A. "Mechanisms of liquefaction and pyrolysis reactions of biomass" **Energy Conversion & Management,** vol.41, 2000. pp.633-646.

[13] Bridgwater A.V., Meier D. and Radlein D. "An overview of fast pyrolysis of biomass" **Organic Geochemistry,** vol.30, 1999. pp.1479-1493.

[14] De Jongh W.A., Carrier M. and Knoetze J.H. "Vacuum pyrolysis of intruder plant biomasses" **Journal of Analytical and Applied Pyrolysis,** vol.92, 2011. pp.184-193.

[15] Sepman A.V. and De Goey L.P.H. "Plate reactor as an analysis tool for rapid pyrolysis of biomass" **Biomass and bio energy,** vol.35, 2011. pp.2903-2909.

[16] Amutio M., Lopez G., Artetxe M., Elordi G., Olazar M. and Bilbao J. "Influence of temperature on biomass pyrolysis in a conical spouted bed reactor" **Resources, Conservation and Recycling,** vol.59, 2012, pp.23-31.

[17] Yin C. "Microwave-assisted pyrolysis of biomass for liquid biofuels production" **Bioresource Technology,** vol.120, 2012, pp.273-284.

[18] French R. and Czernik S. "Catalytic pyrolysis of biomass for biofuels production" **Fuel Processing Technology,** vol.91, 2010. pp.25-32.

[19] Brown R.C. and Holmgren J. **Fast Pyrolysis and Bio-Oil Upgrading.** [Slide]. Iowa: Iowa State University and UOP.

[20] Solomons G. and Fryhle C.B. **Organic Chemistry**. 10thED. USA. John Wiley & Sons, Inc. 2011.

[21] Reusch W. 2013. **Carboxylic Acids.** [online]. Available: https://www2.chemistry.msu.edu/faculty/reusch/virttxtjml/crbacid1.htm

[22] Sigma-Aldrich. 2014. **Acetic acid Safety Data Sheet.** Singapore.

[23] Seidel A., Editor. "Acetic acid" **Kirk-Othmer encyclopedia of chemical technology.** vol.1: 115-133.

[24] Xie J. 2013. **Global Acetic Acid Outlook.** [Slide]. Singapore: Methanol Market Service s Asia.

[25] Liu C., Wang H., Karim A.M., Sun J. and Wang Y. "Catalytic fast pyrolysis of lignocellulosic biomass" **Chemical Society Reviews,** vol.43, 2014. pp. 7457-7956.

[26] Sigma-Aldrich. 2014. **Acetone Safety Data Sheet.** Singapore.

[27] Seidel A., Editor. "Acetone" **Kirk-Othmer encyclopedia of chemical technology.** vol.1: 160-175.

[28] Pandia R.M. 2013. **The Phenol-Acetone Value Chain: Prospects and Opportunities.** [Slide]. Seoul.

[29] Van De Ven T. and Kadla J. **Cellulose-Biomass Conversion.** Rijeka: InTech. 2013.

[30] Sigma-Aldrich. 2014. **Furfural Safety Data Sheet.** Singapore.

[31] Seidel A., Editor. "Furan derivatives" **Kirk-Othmer encyclopedia of chemical technology.** vol.12: 259-281.

[32] Alsbou E. and Helleur R. "Whole sample analysis of bio-oils and thermal cracking fractions by Py-GC/MS and TLC–FID" **Journal of Analytical and Applied Pyrolysis,** vol.101, 2013. pp.222-231.

[33] Mullen C.A. and Boateng A.A. "Chemical Composition of Bio-oils Produced by Fast Pyrolysis of Two Energy Crops" **Energy & Fuels,** vol.22, 2008. pp.2104-2109.

[34] Vispute T. "**Pyrolysis Oils: Characterization, Stability Analysis, and Catalytic Upgrading to Fuels and Chemicals**" Ph.D. Thesis of University of Massachusetts. 2011.

[35] Bernardes M.A., Editor. **Biofuel's Engineering Process Technology.** Rijeka: InTech. 2011.

[36] Shell Alaska. **Offshore 101.** Alaska: Shell. 2011.

[37] Exxon Mobile. **A Simple Guide to Oil Refining.**

[38] Chaudhuri U. R. **Fundamentals of petroleum and petrochemical engineering.** USA: CRC Press. 2011.

[39] Matar S. and Hatch L.F. **Chemistry of Petrochemical Processes.** 2nd ED. Houston: Gulf Publishing Company. 2000.

[40] Chen D., Zhou J., Zhang Q. and Zhu X. "Evaluation methods and research progresses in bio-oil storage stability" **Renewable and Sustainable Energy Reviews,** vol.40, 2014. pp.69-79.

[41] Hagen J. **Industrial Catalysis: A Practical Approach.** 2nd ED. Darmstadt: WILEY-VCH Verlag GmbH & Co. KGaA, 2006.

[42] Gates B.C. **Catalytic Chemistry.** 1stED. USA: John Wiley & Sons, Inc. 1991.

[43] Baragiola R. **Surface structure.** Virginia: University of Virginia. 2001.

[44] Wachs I.E. and Routray K. "Catalysis Science of Bulk Mixed Oxides" **ACS Catalysis,** vol.2, 2012. pp.1235-1246.

[45] Bartholomew C.H. and Farrauto R.J. **Fundamental of Industrial Catalytic Processes.** 2nd ED. Hoboken: John Wiley & Sons, Inc. 2006.

[46] Lobban L. **Fast Pyrolysisfor Biomass Conversion to Fungible Fuels.** [Slide]. Oklahoma: Oklahoma Bioenergy Center

[47] Carey F.A. and Sundberg R.J. **Advanced Organic Chemistry Part B: Reactions and Synthesis.** 5th ED. New York: Springer Science+Business Media, LLC. 2007.

[48] Campbell I.M. **Catalysis at Surfaces.** 1st ED. New York: Chapman and Hall. 1988.

[49] Sheldon R.A. and Van Bekkum H. **Fine Chemicals through Heterogeneous Catalysis.** Morlenbach: WILEY-VCH Verlag GmbH. 2001.

[50] Wendt H., Spinacé E.V. and Linardi A.M. "Electrocatalysis and Electrocatalysts for Low Temperature Fuel Cells: Fundamentals, State of the Art, Research and Development" **Quimica Nova,** vol.28, 2005. pp.1066-1075.

[51] Dent A.L. and Kokes R.J. "Hydrogenation of Ethylene by Zinc Oxide. II: Mechanism and Active Sites" **The Journal of Physical Chemistry,** vol.73, 1969. pp.3781-3790.

[52] Sarkany A. and Tetenyi P. "On the structure sensitivity of ethane hydrogenolysis on Ni catalysts" **Reaction Kinetics and Catalysis Letters,** vol.12, 1979. pp.297-301.

[53] Gudkov B.S., Guczi L. and Tetenyi P. "Kinetids and Mechanism of Ethane Hydrogenolysis on Silica-Supported Platinum and Platinum-Iron Catalysts" **Journal of Catalysis,** vol.74, 1982. pp.207-215.

[54] Tavoularis G. and Keane M.A. "Gas phase catalytic dehydrochlorination and hydrodechlorination of aliphatic and aromatic systems" **Journal of Molecular Catalysis A: Chemical,** vol.142, 1999. pp.187-199.

[55] Hartwig J. **Organotransition metal chemistry: from bonding to catalysis.** USA: Edwards Brothers, Inc. 2010.

[56] Konopka J. "**Green Decarbonylation of Aldehydes using Palladium (II) Acetate**" Senior Thesis of Salve Regina University. 2011.

[57] Carey F.A. and Sundberg R.J. **Advanced Organic Chemistry Part A: Structure and Mechanisms.** 5th ED. New York: Springer Science+Business Media, LLC. 2007.

[58] Fristrup P., Kreis M., Palmelund A., Norrby P and Madsen R. "The Mechanism for the Rhodium-Catalyzed Decarbonylation of Aldehydes: A Combined Experimental and Theoretical Study" **Journal of the American Chemical Society,** vol.130, 2008. pp.5206-5215.

[59] Miranda M.O., Pietrangelo A., Hillmyer M.A. and Tolman W.B. "Catalytic decarbonylation of biomass-derived carboxylic acids as efficient route to commodity monomers" **Green Chemistry,** vol.14, 2012. pp.490-494.

[60] Maetani S., Fukuyama T., Suzuki N., Ishihara D. and Ryu I. "Iron-catalyzed decarbonylation reaction of aliphatic carboxylic acids leading to a-olefins" **Chemical Communications,** vol.48, 2012. pp.2552-2554.

[61] Everlong, Hagindaz, Jomegat, Pdavis68, Horning R., Swift, Whiteknight, Contributors. **Organic Chemistry/ Print version.** Creative Commons.

[62] Na J.G., Yi B.E., Kim J.N., Yi K.B., Park S.Y., Jong-Ho Park, Kim J.N. and Ko C.H. "Hydrocarbon production from decarboxylation of fatty acid without hydrogen" **Catalysis Today,** vol.156, 2010. pp.44-48.

[63] Lee C.C. and Spinks J.W.T. "The Mechanism of the Ketonic Pyrolysis of Calcium Carboxylates" **University of Saskatchewan,** 1953. 1079-1086.

[64] Pham T.N., Sooknoi T., Crossley S.P. and Resasco D.E. "Ketonization of Carboxylic Acids: Mechanisms, Catalysts, and Implications for Biomass Conversion" **ACS Catalysis,** vol.3, 2013. pp.2456-2473.

[65] Gonzalez F., Munuera G. and Prieto J.A. "Mechanism of Ketonization of Acetic Acid on Anatase TiO_2 Surfaces" **Journal of the Chemical Society, Faraday Transactions 1: Physical Chemistry in Condensed Phases,** vol.74, 1978. pp.1517-1529.

[66] Klimkiewicz *R.,* Teterycz H., Grabowska H., Morawski I., Syper L. and Licznerski B.W. "Ketonization of Fatty Methyl Esters over Sn-Ce-Rh-O Catalyst" **Journal of the American Oil Chemists' Society,** Vol.78, 2001. pp.533-535.

[67] Renz M. “Ketonization of Carboxylic Acids by Decarboxylation: Mechanism and Scope” **European Journal of Organic Chemistry,** vol.2005, 2005. pp.979-988.

Chapter 3

Experimental details

3.1 Reagents

Table 3.1 List of reagents

	Reagents; trade names	Grade; purity	Manufacturers
1	Acetone	HPLC; ≥ 99.8%	Sigma-Aldrich®
2	Acetic acid	Reagent; ≥ 99.7%	Sigma-Aldrich®
3	Furfural	99%	Sigma-Aldrich®
4	Deionized water		
5	*i*-Propanol	≥ 99.9%	RCI Labscan
6	Mesityl oxide	99%	Acros Organics™
7	Diacetone alcohol	≥ 99%	Sigma-Aldrich®
8	Isobutyl methyl ketone	≥ 98.5%	Sigma-Aldrich®
9	*t*-Butanol	HPLC; ≥ 99.5%	Sigma-Aldrich®
10	Ethyl methyl ketone	Technical; ≥ 99.5%	Carlo Erba®
11	Cyclohexanone	Technical; ≥ 99.5%	Carlo Erba®
12	Compressed nitrogen gas	UHP; >99.999%	Praxair
13	Compressed hydrogen gas	UHP; >99.999%	Praxair
14	Compressed helium gas	UHP; >99.999%	Airgas®
15	Compressed air	Zero grade; 20-21% O_2	Praxair
16	Chromium (III) nitrate nonahydrate	> 96%	Ajax Fine Chem
17	Iron (III) nitrate nonahydrate	> 98%	Ajax Fine Chem
18	Cobalt (II) nitrate hexahydrate	> 98%	Ajax Fine Chem
19	Nickel (II) nitrate hexahydrate	> 98%	Carlo Erba®

Table 3.1 (Continue)

	Reagents; trade names	Grade; purity	Manufacturers
20	Copper (II) nitrate trihydrate	> 98%	Ajax Fine Chem
21	Palladium acetate	99.98%	Sigma-Aldrich®
22	Precipitated silica		Carlo Erba®
23	HZSM-5 (13)*; Zeocat PZ-2/25H		Zeochem®
24	NH_4^+ZSM-5 (40)*; CBV 8014		Zeolyst®
25	NH_4^+ZSM-5 (180)*; CBV 28014		Zeolyst®
26	HZSM-5 (250)*; Zeocat PZ-2/500H		Zeochem®
27	NH_4^+-Ferrierite (10)*		Alfa Aesar®
28	H-Mordenite (15)*; HSZ660HOA		Tohso®
29	H-β (14)*; HSZ930NHA		Tohso®
30	HY (100)*; HSZ390HUA		Tohso®
31	Palladium on activated charcoal	5% Palladium	Sigma-Aldrich®
32	Activated charcoal	100 mesh particle	DARCO®
33	13X Molecular sieve	8-12 mesh bead	Sigma-Aldrich®
34	Nitrous oxide	99.99%	Praxair
35	5% Oxygen balanced helium		Airgas®
36	10 % Hydrogen balanced argon		TIG
37	1% Ammonia balanced helium		TIG
38	*i* – Propylamine	99%	Sigma-Aldrich®
39	Liquid leak detector; Snoop®		Swagelok®
40	Cerium (IV) oxide	> 99.0%	Sigma-Aldrich®
41	Titanium dioxide	P25	Degussa
42	Titanium dioxide	99.9%, anatase	Alfa Aesar®
43	Alumina	99.97%, γ-phase	Alfa Aesar®
44	Zinc oxide	99.9%	Alfa Aesar®
45	HY (15)*		Zeolyst®

* is Si/Al molar ratio

3.2 Apparatuses

Table 3.2 List of apparatuses

	Apparatuses; specification	Manufacturer; model
1	Borosilicate glass tube reactor; 4 mm and 6 mm inside Ø	Pyrex®
2	Quartz tube reactor; 4 mm and 6 mm inside Ø	
3	316 Stainless steel tube, fitting, valve, and safety kit	Swagelok®
4	PTFE sealant kit and Viton® O-ring	Swagelok®
5	Mass flow controller and meter	Brooks instrument
6	Vertical tube furnace; 25 mm chamber Ø X 30 cm	Carbolite®; MTF 12/25/250
7	Syringe pump	Kd Scientific; KDS100
8	Gas tight syringe; 1 mL, 5 mL ,and 10 mL with 1’ stainless steel needle	Hamilton®
9	Stand, clamp, and lab jack	
10	Glass wool and quartz wool	Grace
11	Glass bead; 0.5 mm Ø	
12	Gas chromatography with FID (packed column type)	Buck Scientific; 910
13	Hayesep® P packed column; 1/8”X8’	Alltech®
14	Gas chromatography with FID (capillary column type)	Agilent; 6890
15	EC-wax capillary column; 0.25 mm X 30 m	Alltech®
16	Thermal conductivity detector with controller	VICI®; TCD2-NIFED-220
17	Gas chromatography syringe; 1 µL	Hamilton®
18	X–Ray Fluorescence Spectrometer	Philips®; PW2400

Table 3.2 (Continue)

	Apparatuses	Manufacturer; model
19	X-ray diffractometer	Siemens®; D8 Advance
20	Gas absorption analyzer	Quantachrome; Autosorb-1
21	Gas regulator	CONCOA
22	Thermo gravimetric analyzer	Perkin Elmer®; Pyris 1
23	Transmission electron microscope	FEI™; Tecnai G2
24	Mass spectrometer	MKS instrument; Cirrus™
25	Personal computer	
26	Flow meter	Agilent; ADM1000
27	Thermocouple with monitor	
28	Rubber gloves	Sempermed®
29	Goggle	3M
30	Lab coat	
31	Mask	3M
32	Carbon monoxide alarm	Kidde
33	Gas chromatography with MS detector	Agilent; 6890N (GC) 5973N (MS)
34	Pelletizer with 1 cm Ø mold	Shimadzu
35	USA standard sieve; 600 and 850 micron	
36	Agate mortar	
37	Power regulator	
38	Heating rod with insulator	
39	Analytical balance	Sartorius
40	Borosilicate glass beaker, stirring rod	Pyrex®
41	Oven	
42	Polypropylene beaker, strirring rod, and dropper	

Table 3.2 (Continue)

	Apparatuses	Manufacturer; model
43	Ceramic boat	
44	Horizontal tube furnace; 65 mm chamber Ø X 65 cm	Vecstar
45	Weighting paper	VWR®
46	Volumetric flask; 10 and 25 mL	Pyrex®

3.3 Experimental methods

3.3.1 Catalyst preparation

All oxide supports and zeolite powders were packed within ceramic boats and calcined in a horizontal tube furnace under the flow of air (60 $mL.min^{-1}$) at 723 K for 5 hours (2 $K.min^{-1}$) before use. For ammonium zeolites, they will be transformed to proton zeolites after the calcination. No calcination needs for charcoal base catalysts and support.

The metal support catalysts including chromium, iron, cobalt, nickel, and copper were prepared by impregnation of the calcined supports with the metal nitrate precursors. The precursors were weighted into glass beakers and supports were weighted into polypropylene beakers as listed in Table 3.3-3.4. The precursors were dissolved in deionized water and adjust the total volume to 25 mL in volumetric flask. The metals were introduced into support by incipient wetness impregnation (IWI). The metal precursor solutions were carefully dropped into support till wet. The mixture was then dried in oven at 333 K (typically 15 minutes). The impregnation was repeated until the metal precursor solutions were run out. The mixtures were left in oven overnight for final drying. Each batch could yield the product equivalent to 3 grams of supported catalyst in metal form (after reduction).

For palladium catalyst, the precursor is in acetate form. The weighting is also given in Table 3.3. Palladium (II) acetate ($Pd(OAc)_2$) was dissolved well in acetone and adjusted the volume to 15 mL in volumetric flask. The solution was kept cool in a refrigerator (below 288 K) all the time. The metal was introduced into support by incipient wetness impregnation similar to other metal nitrates except that it was dried in a hood at 298 K then left in oven overnight for final drying. Each batch can yield the product equivalent to 0.3 grams of supported catalyst in metal form (after reduction).

After impregnation, the metal precursors were decomposed to metal oxides by calcination in a horizontal tube furnace in a manner similar to the support. The catalyst sample including metal support catalysts of chromium, iron, cobalt, nickel, and copper, and zeolites, were pressed into discs at 3 tons then crushed and sieved into 600-850 μm pellets (or 20-30 meshes, ASTM E-11). The palladium catalysts were used in powder form. The catalysts and zeolites were kept dry in a desiccator at 298 K. The metal catalysts in oxide form must be *in-situ* reduced to metal form under the hydrogen flow in reactor at the temperature above the reduction temperature (following the TPR result) before use.

Table 3.3 Monometallic supported catalyst preparation

	Catalysts wt% metal/support	Precursor; weight (g)	Support; weight (g)
1	2%Cr/SiO_2	$Cr(NO_3)_3.9H_2O$; 0.4615	SiO_2; 2.940
2	10%Cr/SiO_2	$Cr(NO_3)_3.9H_2O$; 2.308	SiO_2; 2.700
3	2%Fe/SiO_2	$Fe(NO_3)_3.9H_2O$; 0.4329	SiO_2; 2.940
4	10%Fe/SiO_2	$Fe(NO_3)_3.9H_2O$; 2.164	SiO_2; 2.700
5	2%Co/SiO_2	$Co(NO_3)_2.6H_2O$; 0.2959	SiO_2; 2.940
6	2%Ni/SiO_2	$Ni(NO_3)_2.6H_2O$; 0.2971	SiO_2; 2.940
7	5%Ni/SiO_2	$Ni(NO_3)_2.6H_2O$; 0.7428	SiO_2; 2.850
8	8%Ni/SiO_2	$Ni(NO_3)_2.6H_2O$; 1.189	SiO_2; 2.760
9	20%Ni/SiO_2	$Ni(NO_3)_2.6H_2O$; 2.971	SiO_2; 2.400
10	40%Ni/SiO_2	$Ni(NO_3)_2.6H_2O$; 7.428	SiO_2; 1.500
11	2%Cu/SiO_2	$Cu(NO_3)_2.3H_2O$; 0.2282	SiO_2; 2.940
12	5%Cu/SiO_2	$Cu(NO_3)_2.3H_2O$; 0.5705	SiO_2; 2.850
13	10%Cu/SiO_2	$Cu(NO_3)_2.3H_2O$; 1.141	SiO_2; 2.700
14	15%Cu/SiO_2	$Cu(NO_3)_2.3H_2O$; 1.711	SiO_2; 2.550
15	40%Cu/SiO_2	$Cu(NO_3)_2.3H_2O$; 4.564	SiO_2; 1.800
16	5%Cu/HZSM-5(250)*	$Cu(NO_3)_2.3H_2O$; 0.5705	HZSM-5(250); 2.850
17	5%Cu/HY(100)*	$Cu(NO_3)_2.3H_2O$; 0.5705	HY(100); 2.850
18	5%Pd/SiO_2	$Pd(OAc)_2$; 0.0316	SiO_2; 0.285
19	5%Pd/γ-Al_2O_3	$Pd(OAc)_2$; 0.0316	γ-Al_2O_3; 0.285
20	5%Pd/TiO_2	$Pd(OAc)_2$; 0.0316	TiO_2; 0.285
21	5%Pd/ZnO	$Pd(OAc)_2$; 0.0316	ZnO; 0.285
23	5%Pd/CeO_2	$Pd(OAc)_2$; 0.0316	CeO_2; 0.285
24	5%Pd/HY(100)*	$Pd(OAc)_2$; 0.0316	HY(100); 0.285

Table 3.4 Bimetallic nickel-copper supported catalyst preparation

	Catalysts [Ni:Cu molar%] wt% bimetallic/support	**Precursor weight** (g) $Ni(NO_3)_2.6H_2O$; $Cu(NO_3)_2.3H_2O$	**SiO_2 support weight** (g)
25	[20:80] 2%NiCu/ SiO_2	0.0558; 0.1854	SiO_2; 2.940
26	[30:70] 2%NiCu/ SiO_2	0.0843; 0.1634	SiO_2; 2.940
27	[50:50] 2%NiCu/ SiO_2	0.1427; 0.1186	SiO_2; 2.940
28	[75:25] 2%NiCu/ SiO_2	0.2184; 0.0605	SiO_2; 2.940
29	[50:50] 5%NiCu/ SiO_2	0.3568; 0.2964	SiO_2; 2.850

3.3.2 Characterization of Catalysts

3.3.2.1 Elemental Analysis

Elemental composition of catalysts was determined by an X-ray fluorescence spectrometer (XRF; Philips® PW2400). The sample could be prepared by mixing 0.50 g of catalysts with 4.5 g of boric acid binder and ground in a ball-mill (Rock Lab grinder). The mixture was pressed into an aluminium pan at 150 kN. The analysis was carried out by placing a sample pan into a sample chamber. The lithium fluoride, pentaerythrite and W/Si multilayer were used as diffracting crystal and the rhodium was X-ray source for measurement at 50 kV, 60 mA.

Inductive coupled plasma with mass-spectroscopy was also used. The certain amount of sample was weighted. The metal was eluted from support by immerging in concentrated nitric acid for 15 minute. The sample was filtrated and washed by deionized water. The filtrated solution was collected and adjusted to 50 mL in volumetric flask. To reduce the concentration of metal to < 0.5 ppm, 2 mL of sample solution was pipetted then adjusted to 100 mL. The diluted solution was measured against blank. The metal content was calculated using calibration curve.

In case of low amount sample, the analysis could be carried out by TEM-EDX technic (see sample preparation from 3.3.2.4). After image caption, analysis area was chosen then scanned for the spectrum of X-ray energy.

3.3.2.2 Crystal Structure

Crystal structure of the catalysts was determined by an X-ray diffractometer (XRD; Siemens D8 Advance). CuKα was an analytical X-ray source at 30 kV, 30 mA. The samples were prepared by spreading catalyst powder over sample holder and placed into the instrument. The samples were scanned from 2θ of 5° to 80° with 1sec/step time and 0.04 2θ /step increment. X-ray diffraction pattern of samples were then compared with standard X-ray diffraction pattern for the determination of structure.

3.3.2.3 Surface Area

Surface area of the catalysts was measured by a gas absorption analyzer (Quantachrome Autosorb-1). Nitrogen (N_2) was used as probe molecules. The sample was prepared by weighting 0.02-0.05 g of the catalysts into a sample cell. The cell was loaded to outgassing station for catalyst surface cleaning by vacuum at 573 K before test. The cell was filled by nitrogen then moved to analysis station rapidly. Adsorption isotherm was measured in a pressure range of 10^{-6} to 1.0 P/P_0 at 70 K cooling by liquid nitrogen. After the analysis, the cell was uninstalled and closed immediately. The cell with catalyst was weighted and compared to the blank cell for certain amount of catalyst without humidity. The surface area of the catalysts was calculated by using Brunauer, Emmett, and Teller equation (BET).

3.3.2.4 Particle size of metal on support

A transmission electron microscope (TEM; FEI^{TM}; Tecnai G2) was employed for elucidating the metal particle on supports. The catalyst powder was crushed in a mortar and suspended in ethanol by sonication. The suspension was dropped onto copper coated Formvar grid and left dry at 298 K overnight. The grid was loaded into TEM then image the picture maximum at 440 kX magnitude. The LaB_6 is an X-ray emitter up to 200 kV. The captions were imported to Image J$^{©}$ program for metal particle size measurement.

3.3.2.5 H_2-Temperature programmed reduction

The reducibility of metals was investigated by temperature programmed reduction (TPR) in a tubular down flow system. The 0.100 gram of catalyst pellets in oxide form were packed into a quartz tube reactor by placing on the quartz wool. The tube was connected to the flow system and surrounding with a vertical tube furnace.

The catalyst was treated in air (30 mL.min^{-1}) at 773 K (2 K.min^{-1}) for 5 hours and cooled down to 323 K under the flow of helium (30 mL.min^{-1}). The gas was switched to 10% hydrogen balance argon at 30 mL.min^{-1} for 30 minutes then the test was started by temperature ramping at 10 K.min^{-1} from 323 to 1173 K. The water produced from reduction was trapped before the detector at 223 K above the vapor of liquid nitrogen. The electronic signal from hydrogen consumption was recorded by an on-line thermal conductivity detector (TCD; VICI® TCD2-NIFED-220). The hydrogen consumption can be calculated from integration of the thermogram and comparing the area with the reduction of certain amount of copper (II) oxide.

3.3.2.6 Copper dispersion on supports

The dispersion of copper on support was also determined in the same system with TPR. The testing was initiated by normal TPR but at 323-723 K as mentioned in [1]. The first thermogram corresponds to total amount of copper in catalyst. After that, the catalyst was cooled down to 333 K in helium flow (30 mL.min^{-1}) then oxidized by nitrous oxide at 30 mL.min^{-1} for 2 hours. With this technique, only surface of copper was oxidized. The excess nitrous oxide was then removed by 30 mL.min^{-1} of helium for 30 minutes and the second TPR was *in-situ* repeated. The second thermogram corresponds to quantity of copper only at the surface. The calculation of hydrogen consumption is similar to TPR. The copper surface and molar dispersion of copper can be calculated following the [2] as shown in appendix B.

3.3.2.7 NH_3-Temperature programmed desorption

Acidity and acid strength of catalysts were determined by temperature programmed desorption of ammonia (NH_3-TPD) in the same system with TPR. The 0.200 gram of catalyst pellets were packed into quartz tube and installed similar to TPR. The catalyst was treated in air (30 mL.min^{-1}) at 773 K for 5 hours and cooled down to 303 K under the flow of helium (30 mL.min^{-1}). Ammonia was adsorbed onto acid site by flowing 30 mL.min^{-1} of 1% ammonia in helium through the catalyst bed for 2 hours. The physisorbed ammonia was then removed by 30 mL.min^{-1} helium for 2 hours. The ammonia desorption was carried out by ramping the temperature from 303-973 K at 10 K.min^{-1} in flow of 30 mL.min^{-1} helium. The desorbed ammonia was detected by an on-line thermal conductivity detector. The complicated thermogram was deconvoluted by Origin Pro®. The amount of ammonia was calculated by comparing with certain volume of the 1% ammonia in helium from standard loop.

3.3.2.8 Brønsted acidity of zeolites

Number of Brønsted acid site in zeolites was determined by temperature programmed desorption of *i*–propylamine (IPA–TPD) in a tubular down flow system. The 0.100 gram of zeolite pellets were packed into a quartz tube reactor by placing on the quartz wool. The tube was connected to the flow system and surrounding with a vertical tube furnace. The catalyst was treated in air (20 $mL.min^{-1}$) at 773 K (2 $K.min^{-1}$) for 5 hours and cooled down to 373 K under the flow of helium (20 $mL.min^{-1}$). A mass spectrometer (MS; MKS instruments Cirrus™) was used as a detector. It was set to detect the masses at 44 *m/z* for *i*–propylamine, 41 *m/z* for propylene and 17 *m/z* for ammonia with the chamber vacuum of 6 X 10^{-7} torr. The MS filament was turned on and the *i*–propylamine was manually adsorbed onto zeolites by a GC syringe as pulses at 323 K until signal of 44 *m/z* was consistent. The zeolites were left in helium stream until no 44 *m/z* signal was detected (minimum 3 hours) for physisorbed *i*–propylamine removal. The analysis was started by temperature ramping at 10 $K.min^{-1}$ from 373 to 973 K resulting in the propylene and ammonia signal. The calibration was carried out by injection of propylene through certain volume loop.

3.3.2.9 Temperature program desorption of reactant

The TPD of reactants was used for the investigation of reaction sequent. The experimental procedure was similar to IPA-TPD but the adsorbed was changed to reactant used in this work. The pre-adsorption was carried out at 348 K. The analysis was then achieved under the flow of helium (20 $mL.min^{-1}$) at 10 $K.min^{-1}$ from 373 to 973 K. The mass detection of products was set as summarized in Table 3.5.

Table 3.5 Mass collection for TPD of reactants

Product	Mass collection (*m/z*)
Water	18
i-Butylene	39
Ethenone	42
Carbon dioxide	44
Acetone	58
Acetic acid	60
Toluene	65
Xylenes	77
Mesityl oxide	83
Trimethylbenzenes	120

3.3.2.10 Thermogravimetric analysis

The thermogravimetric analyzer (TGA; Perkin Elmer® Pyris 1) was well known instrument for the analysis of carbon deposited over the catalysts. The 0.002-0.020 gram of spent catalysts were loaded into platinum pan then hanged from microbalance in the closed system of TGA. The combustion of carbonaceous was carried out and tracking the sample weight from 323-1173 K at 10 $K.min^{-1}$ under the stream of air (50 $mL.min^{-1}$).

3.3.2.11 Temperature programmed oxidation

Temperature programmed oxidation (TPO-MS) of spent catalyst was performed in the same system to IPA-TPD. The 0.05 gram of spent catalysts were packed into a quartz tube reactor and installed to the system. They were dried in helium (20 $mL.min^{-1}$) at 423 K for 2 hours before test and cools down to 323 K. The TPO was then carried out in 5% oxygen in helium (20 $mL.min^{-1}$) at 10 $K.min^{-1}$ from 323-973 K. The MS was set for carbon dioxide detection at *44 m/z*.

3.3.3 Catalytic activity testing

3.3.3.1 Continuous flow reactor

The catalytic activity was studied by a fixed bed flow reactor as illustrated in Figure 3.1. The catalyst pellets were packed into a glass tube reactor covering top and bottom by glass wool to form the catalyst bed. The glass beads were loaded above of

the bed to facilitate feed flow dispersion. In case of two beds system, a glass bead layer, thickness similar to a catalyst bed, was set between the catalyst beds to prevent the back flowing. The flow system was assembled from 316 stainless steel tube and fitting and controlled the gas from cylinder by two mass flow controllers, one for hydrogen and another for nitrogen or air. The reactor was installed at the center of a vertical furnace then sealed to the flow system by Teflon® kit or O-rings. The flow was measured by a bubble flow meter or electronic flow meter at the end of line. Gas leakage at connectors was checked before running. The oxide support and zeolites catalysts were treated in air (30 $mL.min^{-1}$) at 773 K (2 $K.min^{-1}$) for 5 hours. The reduction was necessary only for metal support catalysts by flowing with nitrogen (30 $mL.min^{-1}$) for 30 minutes and hydrogen (30 $mL.min^{-1}$) for 3 hours. The catalysts were then cooled down under the stream of reaction carrier (hydrogen or nitrogen) to reaction temperature. For charcoal base catalysts, they were heated under the hydrogen stream to the reaction temperature (2 $K.min^{-1}$) without any treatment. The liquid reactant was kept in a syringe and fed by a pump. The reaction was started by punching a 1' needle through the reactor head septum. The products were delivered through the heating line at the bottom of reactor and sampling by a 6 port valve with 25 µL loop to a gas chromatography for further analysis. The unsampling stream was drained to ventilation system.

For analysis, the products were separated by a chromatography column. Hayesep® P was used with the samples from acetone and acetic acid conversion to olefins and EC-wax was used with the samples from furfural conversion to furan derivatives. The amount of products was transformed to signal by flame ionization detector connected with a personal computer. The area of each product in chromatogram was calculated to %molar of carbon by adjustment with response factor then normalization as shown in apendix. The structure of products was confirmed by gas chromatography with mass spectrometry (GC-MS; Agilent 6890N, 5973N) of products collected by a cold trap or a gas sampling bag.

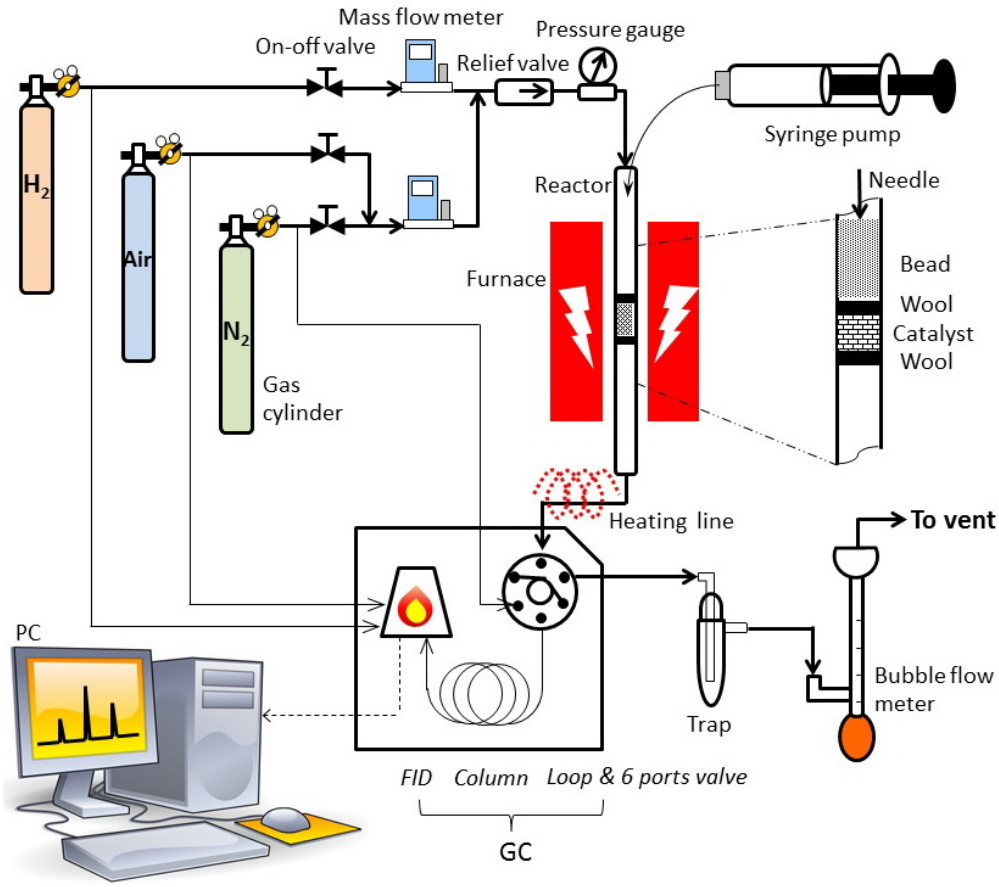

Figure 3.1 Diagram of continuous flow system and reactor packing pattern

3.3.3.2 Pulse flow reactor

The catalytic activity was also examined in a pulse flow reactor. The setting up is displayed in Figure 3.2. The catalyst pellets were packed into a quartz tube reactor covering top and bottom by glass wool to form the catalyst bed. The flow system was assembled from the same material as the continuous process. Gases from cylinder were controlled by two mass flow controllers, one for helium and another for air. The reactor was centered in a vertical furnace then sealed to the flow system by O-rings. The flow could be checked by an electronic flow meter at the reactor outlet. The catalysts were treated in air (20 mL.min^{-1}) at 773 K (2 K.min^{-1}) for 5 hours. The catalysts were then cooled down in helium to reaction temperature. The reactant was introduced into reactor as pulses at 0.5 μL by a syringe. The products were sampled through a heated transfer line at the bottom of reactor. The unsampling stream was drained to ventilation system.

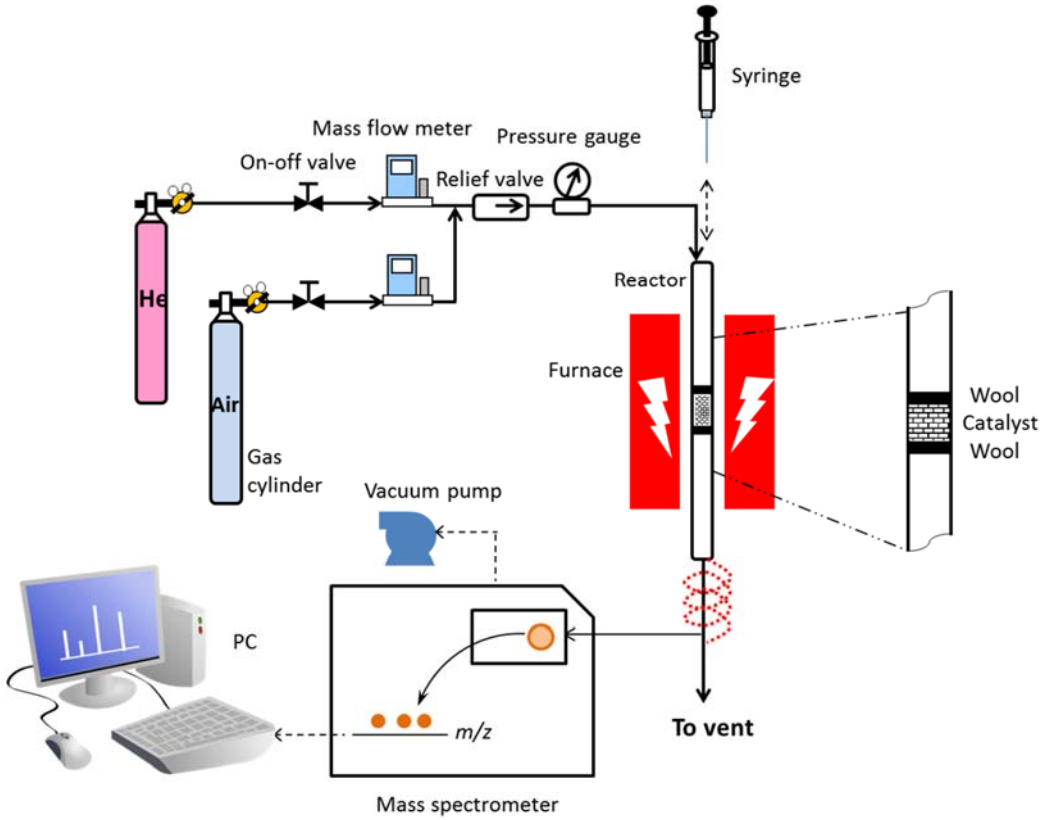

Figure 3.2 Diagram of pulse flow system and reactor packing pattern

3.4 References

[1] Hoang D.L., Dang T.T.H., Engeldinger J., Schneider M., Radnik J., Richter M. and Martin A. "TPR investigations on the reducibility of Cu supported on Al2O3, zeolite Y and SAPO-5" **Journal of Solid State Chemistry,** vol.184, 2011. pp.1915–1923.

[2] Sagar G.V., Rao P.V.R., Srikanth C.S. and Chary K.V.R. "Dispersion and Reactivity of Copper Catalysts Supported on Al_2O_3-ZrO_2" **Journal of Physical Chemistry B,** vol.110, 2006. pp.13881-13888.

Chapter 4

Self-deoxygenation of ketones to olefins

4.1 Introduction

To produce the chemical feedstocks, in which the olefins are the most preference, from biomass derived ketones, the deoxygenation is necessary. Direct hydrogenation is a most common deoxygenation, and can be promoted by several metals catalysts (Ni [1], Pd [2], Pt [3], and Ru [4-5]). However, operation with high hydrogen pressure, is a major concern (typically >75 bars) [2]. Moreover, the paraffins produced is useless chemicals, required further treatment e.g. dehydrogenation to produce olefins.

Alternatively, the self-deoxygenation of ketones to olefins becomes an important state that hydrogen is absent. The use of proton zeolites (HZSM–5 [6-9] and H–β [10]) as catalyst is a major key to success. Acetone was 100 % converted to olefins (~ 20 % selectivity), paraffin (~ 10 %) and aromatics (~ 65 %) over HZSM-5 at 723 K and atmospheric pressure [6]. There are several attempts to improve the selectivity to an individual product by zeolite modification. Alkaline metal exchanged β catalysts were studied at 773 K by Tago *et al.* [11] The selectivity to *i*–butylene was improved by Cs–β (>90%) while K–β was excellent in catalyst stability. Transition metals exchanged β including Cr, Mn, Fe, Co, Ni, Cu, Zn, Al, and Pb were also studied by Cruz-Cabeza *et al.* [10]. Almost zero selectivity to naphthalene derivative was reported from these catalysts. Ni-β and Cu–β preferred the production of aliphatic hydrocarbons while Cr-β, Mn–β and Zn–β were good catalysts for aromatic production. While product selectivity depends on the reaction mechanism, these works propose that the *i*-butylene is obtained from aldol-condensation. The further condensation of the aldol-condensation products results in higher hydrocarbon and aromatic compounds. However, the certain reaction pathway for conversion of acetone to *i*-butylene has never been investigated.

In this work, the deoxygenation of acetone and ethyl methyl ketone were studied with proton zeolites including HZSM-5, H-Ferrierite, H-Moredenite, H-β, and HY at low temperature (448-498 K) and atmospheric pressure. The reaction pathway was investigated using TPD and pulse reaction of acetone and possible intermediates

including diacetone alcohol, mesityl oxide, *t*-butanol, and acetic acid. The effect of acid site proximity, water and reaction temperature on product selectivity were also emphasized.

4.2 Experimental details

Acetone (Chromasolve® for HPLC, ≥99.9%), diacetone alcohol (99%), methyl isobutyl ketone (ACS reagent, ≥98.5%), *t*–butanol (Chromasolve® for HPLC, ≥ 99.5%) and acetic acid (ACS reagent, ≥99.7%) were purchased from Sigma–Aldrich® and used as receive. The mesityl oxide (99 %) was obtained from Acros Organics™ and dried over molecular sieve 13X before used. Briefly, pellets of 13X molecular sieve were calcined at 623 K for 12 hours. Then, they were cooled down to 373 K and transferred to mesityl oxide while hot.

HZSM-5 (Si/Al=13) and HZSM-5 (Si/Al=150) were obtained from Zeochem®. HZSM-5 (Si/Al=40), HZSM-5 (Si/Al=100) and HY (Si/Al=15) were obtained from Zeolyst®. NH_4^+-β (Si/Al=13) and H-Mordenite (Si/Al=15) were supplied by Tohso Co., Ltd. and H-Ferrierite (Si/Al=11) was purchased from Alfa Aesar®. To balance a total acidity in catalyst bed, silica (SiO_2, Carlo Erba), which is catalytically inert at testing condition, was used as diluent. The zeolites and silica were calcined in air (60 mL.min^{-1}) at 773 K for 3 hours before used. The calcined HZSM-5 and silica were physically mixed and then pelletized to 600–850 μm.

Elemental composition was determined by X-ray fluorescence spectrometer (XRF; Siemens). Specific surface area (BET) of catalysts was measured using nitrogen adsorption analyzer (Quantachrome) at 77 K and 0.05–0.30 P/P_0. Number of Brønsted acid site in zeolites was determined by temperature programed desorption of *i*–propylamine (IPA–TPD) [12-13]. A mass spectrometer (MS, Cirrus™; MKS instruments) was used as detector. Mass collected is described in section 3.3.2.8. The zeolites were packed into a quartz tube and treated in air (20 mL.min^{-1}) at 773 K (2 K.min^{-1}) for 3 hours before test then cooled down in helium (20 mL.min^{-1}) to 373 K. *i*–Propylamine was adsorbed on zeolites by pulsing at 323 K until signal of *i*–propylamine was consistent. Excess amine was removed from catalysts by flushing in helium stream (20 mL.min^{-1}) until no *i*–propylamine signal was detected (minimum 3 hours). The analysis was carried out by ramping the temperature from 373–973 K at 10 K.min^{-1}. The calibration was

performed by injecting of certain amount of standard propylene. The temperature programed desorption (TPD) of reactants (acetone, dried mesityl oxide, diacetone alcohol, and acetic acid) was conducted in the procedure similar to IPA-TPD. A reactant was adsorbed in helium at 348 K then flushing at that temperature. The TPD was carried out from 348 to 973 K (10 $K.min^{-1}$). The MS setting is shown in Table 3.5. The decomposition of diacetone alcohol was investigated by a thermal desorber (Unity™; Markes international). Certain amount of diacetone alcohol was impregnated directly onto zeolite then left standing at 298 K for 6 hours. The mixture was re-weighted and packed into a cell. Physisorbed reactant was removed by flushing in helium (60 $mL.min^{-1}$) at 348 K for 10 minutes. The test was carried out in helium at 40 K/min to 448 K. The products were transferred to a GC–FID (Varian 3800) with a DB–5 column (0.25 mm X 30 m) for analysis. The type of carbon deposit on zeolite was examined by temperature programmed oxidation (TPO) in a tubular down flow reactor equipped with MS [14-15]. The spent catalyst was dried in helium (20 $mL.min^{-1}$) at 423 K for an hour and cooled down to 323 K. The TPO was then carried out in 5% O_2/He (20 $mL.min^{-1}$) at 323-973 K (10 $K.min^{-1}$). The MS was set as mentioned in section 3.3.2.11.

Catalytic activity testing was conducted in a fixed bed reactor (4 mm i.d. Pyrex®) connected with an online gas chromatograph–flame ionization detector (GC-FID, Agilent 6890). A Hayesep® P (1/8" X 8") was used as separating column. The zeolites were packed in reactor and activated at 773 K (2 $K.min^{-1}$) in air (30 $mL.min^{-1}$) for 3 hours. The system was cooled down in nitrogen to the reaction temperature (423–573 K) then feed was introduced by a syringe pump. The reaction was carried out in nitrogen (30 $mL.min^{-1}$) for 6 hours on stream. A pulse flow system was also used in catalytic activity testing. It was operated in a tubular down flow reactor with MS connected at the outlet. The mass collection is shown in Table 3.5. The zeolite was treated in air (20 $mL.min^{-1}$) at 773 K for 3 hours (2 K/min) then cooled down to reaction temperature in helium (20 $mL.min^{-1}$) to 448 K. The reaction was achieved by injecting a 1 µL of reactant into the reactor.

4.3 Result and discussion

4.3.1 Characterization of catalyst

The characterizations of zeolites are summarized in Table 6.1. In this work, HZSM-5 with Si/Al 13-150 are selected. The other zeolites (Ferrierite, Mordenite, β, and Y; Si/Al between 13 and 15) possess Si/Al comparable to HZSM-5 (13).

Table 4.1 Si/Al, surface area, and Brønsted acidity of zeolites

Zeolites	Si/Al	BET surface area m^2/g	Brønsted acidity (mmol/g)
HZSM-5 (Si/Al=13)	13	352	0.78
HZSM-5 (Si/Al=40)	40	447	0.40
HZSM-5 (Si/Al=100)	102	482	0.16
HZSM-5 (Si/Al=150)	152	376	0.07
H-Ferrierite (Si/Al=11)	11	324	0.83
H-Mordenite (Si/Al=15)	15	454	0.90
H-β (Si/Al=13)	13	523	0.95
HY (Si/Al=15)	15	733	0.45

All sample possess high surface area (>350 m^2/g). The large pore zeolites (Mordenite, β, and Y) obviously exhibit higher surface area, as compared to medium pore zeolites (ZSM-5 and Ferrierite). The increase in pore dimension results in the increase in surface area as well. While, a remarkable high surface area of Y (>700 m^2/g) is observed due to the large cavity in cage structure, as compared to the channel of β.

For HZSM–5, the increase in Si/Al (reduce Al in the other word) results in a decrease in Brønsted acidity (Table 6.1). This is very common when the number acid site depends on aluminium in framework of zeolite. With a comparable Si/Al, HZSM-5, H-Ferrierite, H-Mordenite, and H-β exhibit a similar Brønsted acidity. The Brønsted acidity obtained in this work is somewhat similar to those reported in the literatures (0.71, 1.0, 0.53, 0.61, and 0.34 mmol/g for HZSM-5, H-Mor, H-β, HY (Si/Al=11-15) and HZSM-5 (Si/Al=40), respectively [16-20]). Meanwhile, the noticeable lower Brønsted acidity of HY, as compared to other zeolites is probably due to the preparation procedure. As the synthesis of HY with high Si/Al cannot be achieved directly, the steaming is applied to dislodge aluminium out from framework HY with low Si/Al. The dislodged aluminium is

eluted difficultly resulting in external framework aluminium e.g. Al_2O_3, that has no Brønsted acidity.

4.3.2 Catalytic activity testing

4.3.2.1 Effect of contact time

In order to understand the reaction pathway for acetone self-deoxygenation, the study on effect of contact time was carried out between 0-150 g.h.mol^{-1} at 448 K to minimize the secondary reactions of the primary products. It is observed that *i*-butylene and acetic acid are major products (Figure 4.1a) and proportionally increase with conversion.

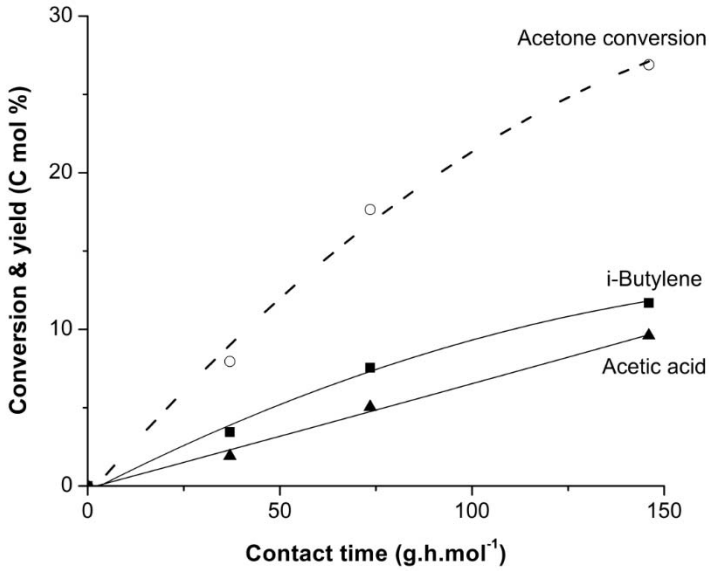

Figure 4.1a Effect of contact time to acetone self-deoxygenation over HZSM–5 (Si/Al=13); conversion, *i*-butylene, and acetic acid

N_2 (30 mL.min^{-1}) at 448 K, result at 15 min on stream

From Figure 4.1b, the mesityl oxide, C5-C8 olefins, propylene, and toluene are produced as minor products. A sharply increase in mesityl oxide yield points out that it is a primary product.

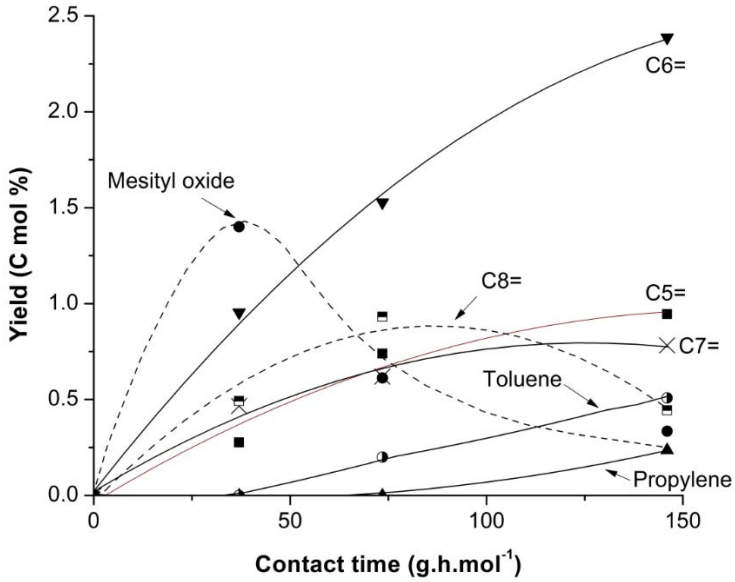

Figure 4.1b Effect of contact time to acetone self-deoxygenation over HZSM–5 (Si/Al=13); mesityl oxide, propylene, toluene, and C5-C8 olefins

N_2 (30 mL.min^{-1}) at 448 K, result at 15 min on stream

However, it is consumed rapidly as seen from a declined yield at contact time > 37 g.h.mol^{-1}. Meanwhile, an increase in yield of hydrocarbons (C5-C8 olefins, toluene, and propylene) indicates that they are secondary products. The *i*-butylene and acetic acid are continually increased with a comparable rate to mesityl oxide.

From the above observations, it can be postulated that the self-deoxygenation may occur via bimolecular reaction of acetones (C3 x 2) so called “aldol condensation” forming a mesityl oxide (C6). The C6 ketone may be an intermediate that could be decomposed to an *i*-butylene (C4) and an acetic acid (C2). TPD of acetone (Figure 4.2) agrees with the above suggestion. Mesityl oxide (*m/z = 83*) is the first product evolved from acetone adsorbed on HZSM-5 at approximately 480 K (the first peaks of acetone

(*m/z = 58*) and water (*m/z = 18*) are not counted as they are physisorbed acetone and moisture from the feed, respectively).

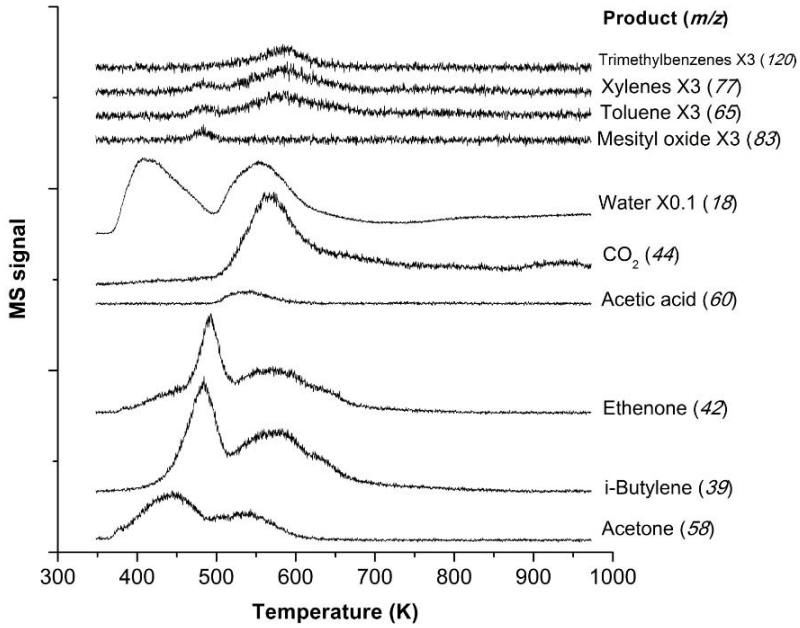

Figure 4.2 TPD of acetone over HZSM–5 (Si/Al=13) in He at 10 K.min^{-1}

It is clearly observed that the physisorbed water peak does not completely reach the initial base line during the mesityl oxide production. This result indicates that the mesityl oxide is derived from dehydration of diacetone alcohol, an adduct from aldol condensation of acetone. Hence, these C6 intermediates including mesityl oxide and diacetone alcohol can be decomposed to *i*-butylene and acetic acid. At 485 K, hydrocarbons (*i*-butylene along with small amount of toluene and xylenes secondary products) and ethenone are evolved. While, the acetic acid co-product comes off later at 550 K. During the decomposition of the adducts (mesityl oxide or diacetone alcohol), one oxygen from acetone must be transferred to an acetic acid, presumably as water. The *i*-butylene and an acetic acid would undergo secondary reaction to wide range of hydrocarbons. The immediately observed carbon dioxide with second peak of water and acetone, when acetic acid is presented in system, indicates that the acetic acid can be ketonized to acetone at that temperature. This results in the additional evolution of *i*-butylene, ethenone as well as the secondary products at 580 K. However, the

ketonization of acetic acid produced is the case only at high temperature. Therefore, no ketonization of acetic acid produced can be obtained at 448K (Figure 4.1). The self-deoxygenation pathways from the discussions above can be demonstrated as shown below;

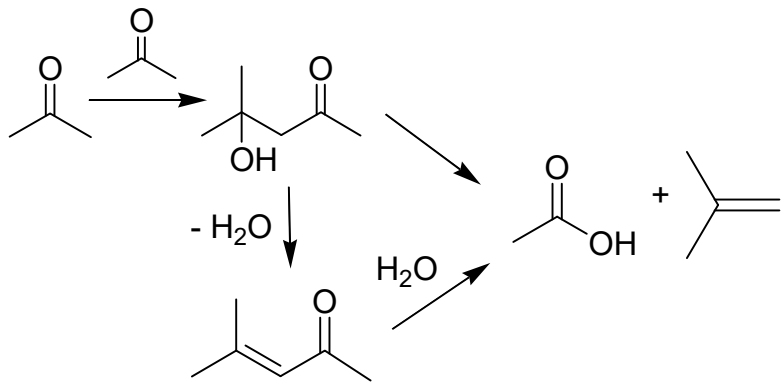

4.3.2.2 TPD of reaction intermediates

From the proposed deoxygenation pathways, it is clear that the oxygen is transferred from acetone to acetic acid via decomposition of the aldol-condensation products either mesityl oxide or diacetone alcohol. Accordingly, decomposition of the mesityl oxide and diacetone alcohol over HZSM-5 is investigated.

(i) Decomposition of mesityl oxide

From Figure 4.3, the TPD of mesityl oxide shows the production of *i*-butylene at the same temperature with TPD of acetone (*m/z = 39*, at 485 K).

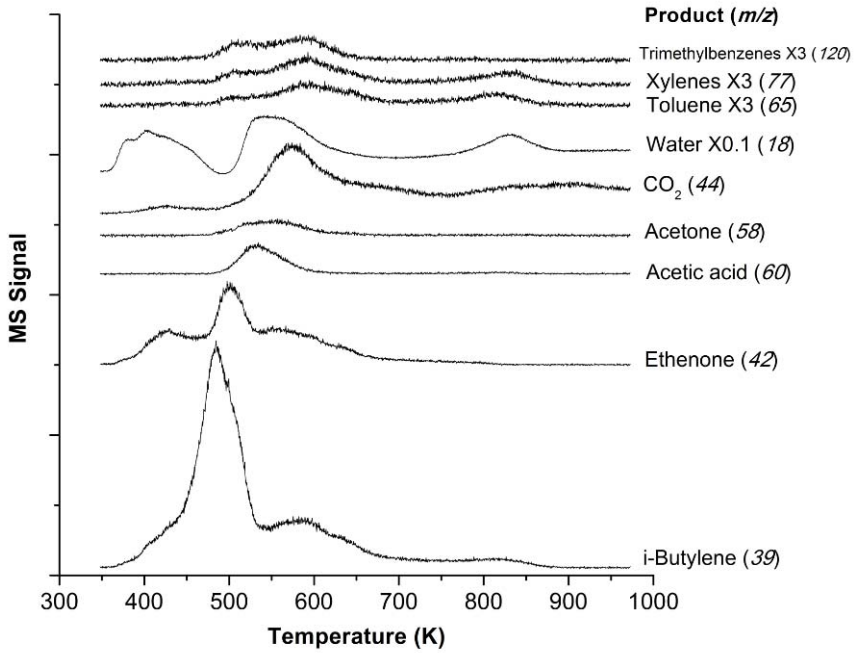

Figure 4.3 TPD of mesityl oxide over HZSM–5 (Si/Al=13) in He at 10 K.min^{-1}

However, the acetic acid, that is one of the major product observed in Figure 4.1a, is not evolved at same temperature as the *i*-butylene (Figure 4.3). An ethenone peak (*m/z = 42*, 490 K) is instead observed along with the *i*-butylene production. Therefore, the proposed decomposition of mesityl oxide can be illustrated by the following scheme;

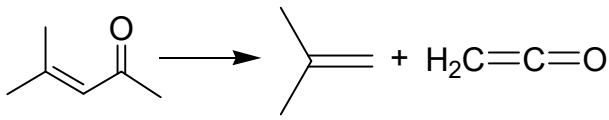

A slightly delay of ethenone evolution, as compared to that of *i*-butylene, is due to a strong adsorption on Brønsted acid site as acyl intermediate shown below;

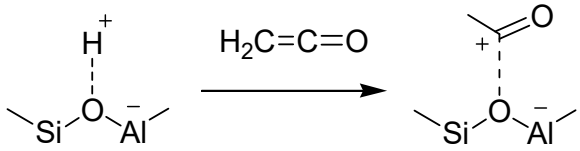

One could expect that protonation of mesityl oxide leads to cracking to *i*-butylene and ethenone. Theoretically, the carbenium ion derived from protonation at C=O (at 1) can be stabilized by C=C (at 2) as illustrated below;

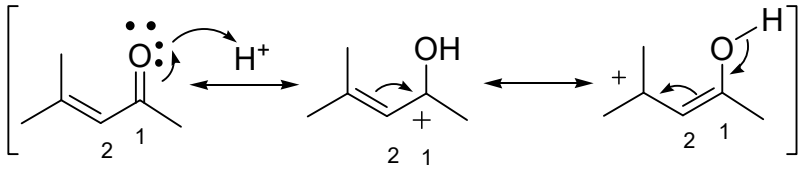

With those resonance structure, the decomposition of the protonated mesityl oxide at 1, 2-[C-C] cleavage is not possible. Therefore, the cracking of mesityl oxide to *i*-butylene and ethenone cannot occur via the protonation at C=O. Alternatively, the mesityl oxide can be protonated at C=C (at 2). This will generates tertiary carbenium ion from which the β-scission and deprotonation is then taken place immediately producing *i*-butylene and ethenone, as illustrated below;

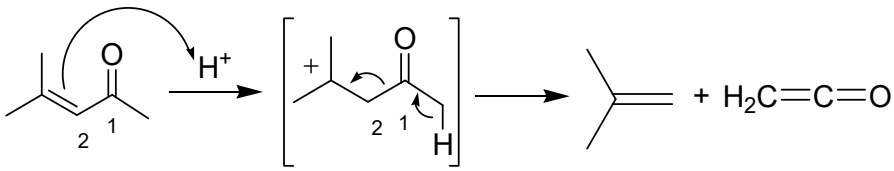

The important of C=C protonation was simply investigated by catalytic decomposition of mesityl oxide, an α-enone, and its corresponding saturated ketone that is isobutyl methyl ketone (MIBK) over HZSM-5.

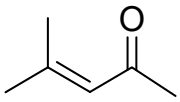

Mesityloxide

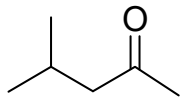

Isobutyl methyl ketone (MIBK)

It is found that the results from the two compounds are obviously different as shown in Figure 4.4. At initial time on stream (15th minute), conversion of the mesityl oxide (32%, Figure 4.4a) is much higher than that of MIBK (8% conversion, Figure 4.4b).

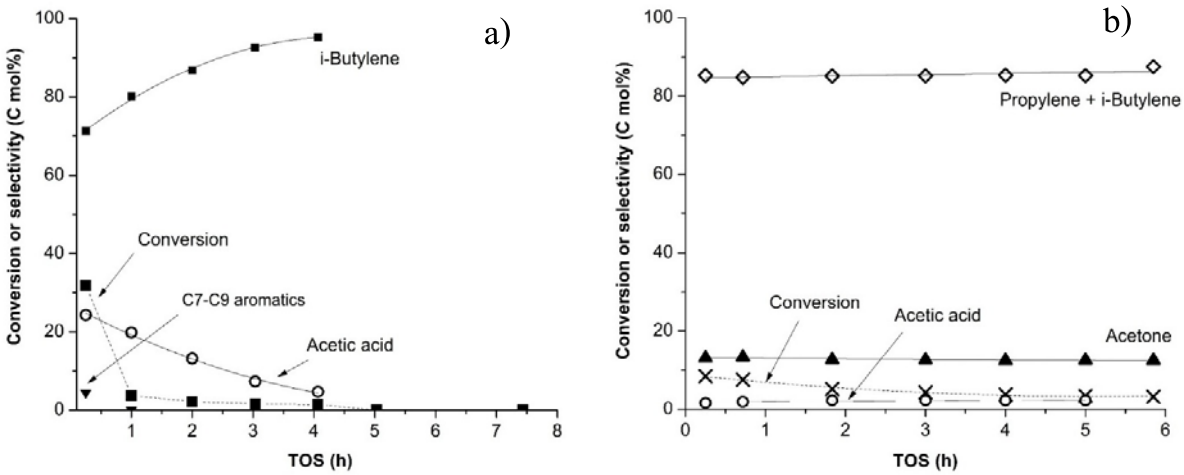

Figure 4.4 Catalytic decomposition of a) mesityl oxide b) isobutyl methyl ketone over HZSM–5 (Si/Al=13)

He (20 mL.min^{-1}) at 498 K and 148 g.h.mol^{-1}

In line with the acetone self-deoxygenation (Figure 4.1), the *i*-butylene, acetic acid along with aromatic compounds are produced from mesityl oxide decomposition. However, it is noted that the selectivity to acetic acid from mesityl oxide decomposition is drastically dropped (Figure 4.4a). This is because the acetic acid is not the primary co-product but ethenone (Figure 4.3). The ethenone is strongly adsorbed on zeolite leading to severe deactivation, within the first hour on stream as seen from Figure 4.4a.

Meanwhile, the products obtained from MIBK conversion are propylene and acetone (Figure 4.4b). For MIBK, the protonation can take place only at C=O. The secondary carbenium ion generated is relatively less feasible, as compared to the tertiary carbenium ion obtained from mesityl oxide. Therefore, the MIBK is relatively inert. It is suggested that the first MIBK decomposition gives propylene and acetone via protonation then β-scission. The acetone produced is subsequently self-deoxygenated to *i*-butylene and acetic acid as shown below;

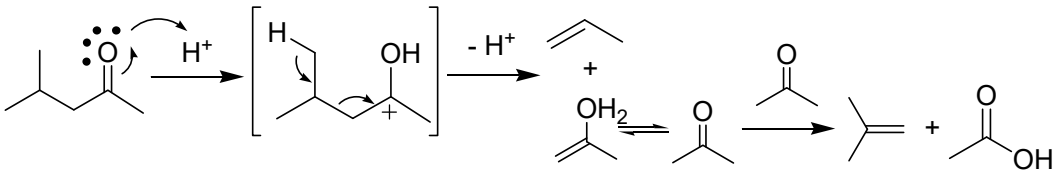

These results confirm that decomposition step of self-deoxygenation occurs via protonation at C=C of mesityl oxide. While the TPD results reveal that the ethenone is a primary co-product derived from mesityl oxide decomposition (Figure 4.3), the acetic acid is notably observed from acetone self-deoxygenation in continuous flow process (Figure 4.1a). It is possible that the ethenone and water can combine to form acetic acid, as the water is always present in the process from aldol condensation of either acetone or mesityl oxide. Accordingly, a comparison between dried mesityl oxide and wet mesityl oxide (50 mol% mesityl oxide in water), was carried out in a pulse flow reactor as shown in Figure 4.5.

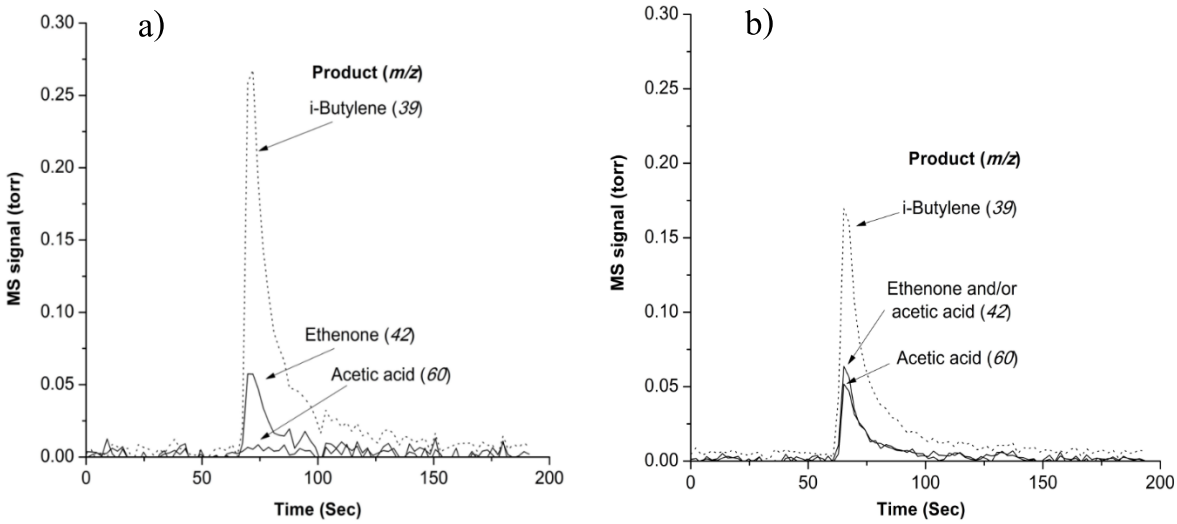

Figure 4.5 Pulse reaction of a) dried mesityl oxide b) wet mesityl oxide (50 mol% of mesityl oxide in water) over HZSM–5 (Si/Al=13)

He (20 mL.min^{-1}) at 448 K

From Figure 4.5a, it is again confirmed that only *i*-butylene and ethenone are produced from dried mesityl oxide decomposition. In the presence of water (Figure 4.5b), the acetic acid is notably evolved when mesityl oxide is decomposed. From this result, it is clear that the ethenone can react with water to form the acetic acid at the reaction condition. In fact, the acetic acid (*m/z = 60*, 530 K) is also observed from TPD of acetone and mesityl oxide (Figure 4.2-4.3) at the temperature higher than that of ethenone (490 K). The decomposition of mesityl oxide in presence of water can be demonstrated as shown below;

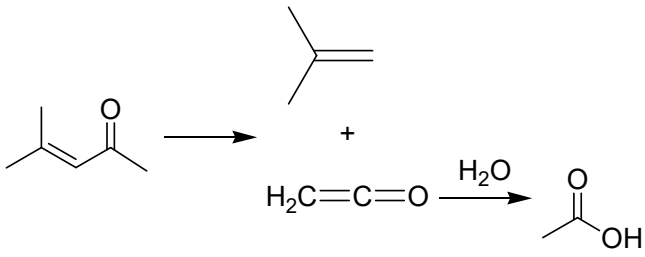

As compared to wet mesityl oxide, pulsing of acetone gives relatively less acetic acid as shown in Figure 4.6.

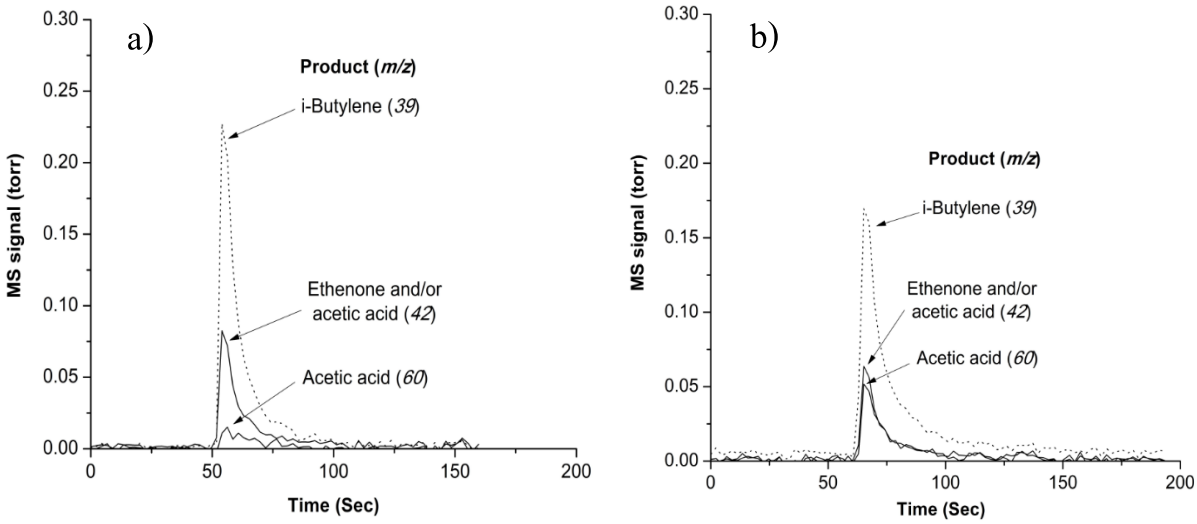

Figure 4.6 Pulse reaction of a) acetone b) wet mesityl oxide (50 mol% of mesityl oxide in water) over HZSM–5 (Si/Al=13)

He (20 mL.min^{-1}) at 448 K

This is because a pulse of acetone generates the pre-adsorbed acetone. The water from aldol condensation can be flushed off catalyst bed when the active site is occupied. While, a pulse of wet mesityl oxide generates a large amount of pre-adsorbed water, available for hydration. Moreover, the acetic acid is largely produced in continuous process (Figure 4.1a) because the water is continually supplied by the condensation of the incoming acetone.

(ii) Decomposition of diacetone alcohol

In addition to mesityl oxide, the decomposition of diacetone alcohol could also lead to *i*-butylene and acetic acid. In order to verify this hypothesis, TPD of the diacetone alcohol is investigated as shown in Figure 4.7.

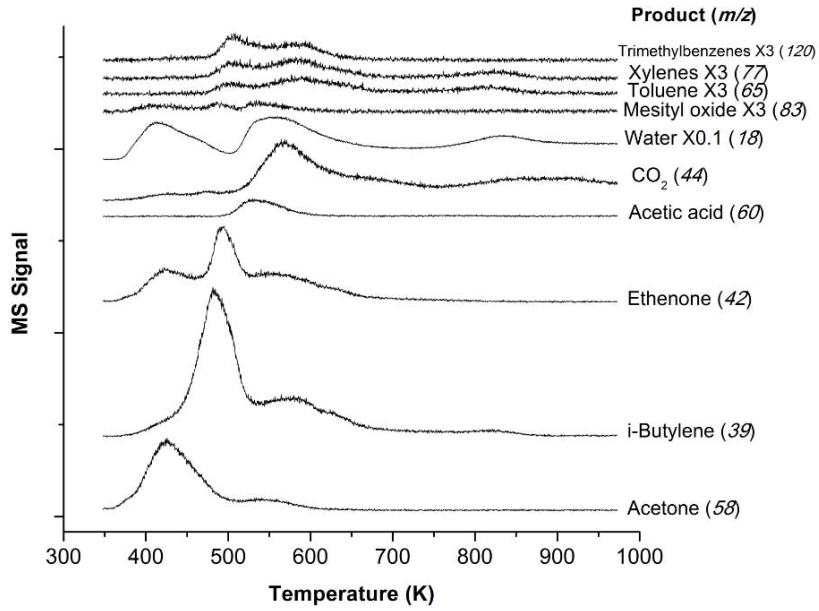

Figure 4.7 TPD of diacetone alcohol over HZSM–5 (Si/Al=13) in He at 10 K.min^{-1}

It is found that a high intensity peak of acetone is obtained at low temperature presumably due to the thermal decomposition of diacetone alchol. The mesityl oxide is produced simultaneously with the major products *i*-butylene and ethenone. While, the mesityl oxide is derived from the dehydration of diacetone alcohol as evidenced by the water peak at 450 K, *i*-butylene and ethenone may be derived from direct decomposition of diacetone alcohol or the mesityl oxide produced. Therefore, the dehydration and decomposition over Brønsted acid can be either parallel or sequential process. For the parallel process, the carbenium ion is an important intermediate. The diacetone alcohol can be protonated at hydroxyl group generating tertiary carbenium ion. The intermediate may undergo two parallel reactions a) deprotonation (as a part of stepwise dehydration mechanism (E1)) to form mesityl oxide and b) β-scission to *i*-butylene and ethenone as expressed below;

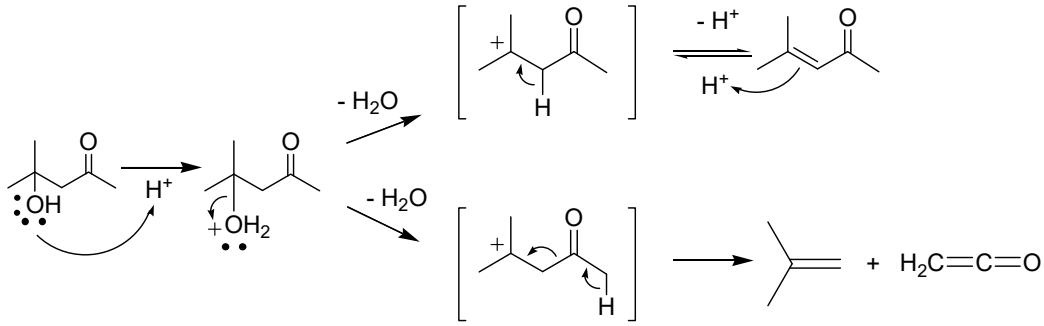

The mesityl oxide produced can be re-protonated to the carbenium ion intermediate and decomposed to *i*-butylene and ethenone as mentioned earlier. Alternatively, one could expect that the dehydration and decomposition may take place sequentially as the dehydration is relatively fast via concerted mechanism (E2). In this sequential process, mesityl oxide is readily formed from diacetone alcohol dehydration. However, it can strongly adsorb and be protonated over the acid site. The decomposition of mesityl oxide is subsequently taken place in a manner similar to the earlier discussion (section 4.3.2.2 (i)) as shown below;

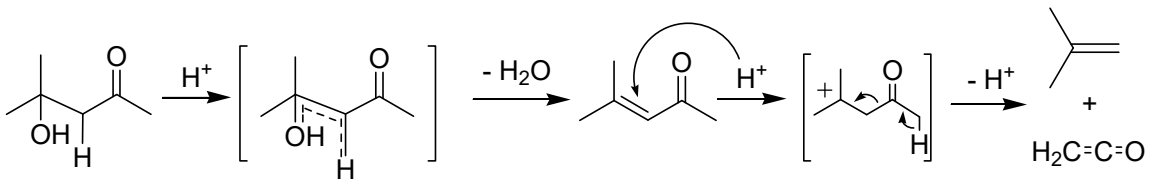

To verify the above hypothesis, the thermal desorption of diacetone alcohol is tested over the catalyst with limited and excess acid site. The diacetone alcohol was adsorbed over HZSM-5 at room temperature with different reactant/acid site ratio (4 and 0.5) then heated at 40 $K.min^{-1}$ to the reaction temperature (448 K). The result is shown in Table 4.2.

Table 4.2 Diacetone alcohol conversion over HZSM-5 (Si/Al=13) by thermal desorber

	Dosing of reactant/acid site	
	4	**0.5**
Conversion (C mol%)	54	100
Yield (C mol%)		
Acetone	36	54
Mesityl oxide	18	4
i-Butylene	-	22
Acetic acid	-	9
Olefins C6-C9	-	11

40 K/min from 348 to 448 K, in He

It is found that only mesityl oxide is obtained when the catalyst is limited (reactant/acid site dosing ration = 4). As the acid site is fully occupied by diacetone alcohol, this result indicates that only the dehydration takes place. The water generated would be strongly bounded to the surface leaving desorption of the mesityl oxide as product. When the excess catalyst is used (reactant/acid site dosing ratio = 0.5), *i*-butylene and acetic acid are significantly observed with small amount of the mesityl oxide. This result indicates that the mesityl oxide generated can be protonated on the excess acid sites. This leads to the subsequent decomposition of mesityl oxide to *i*-butylene and acetic acid. The higher olefins (C6-C9) obtained are generated from protonation of the *i*-butylene produced on the remaining acid sites. With these results, it can be concluded that the dehydration of diacetone alcohol is a very fast and the dehydration-decomposition to *i*-butylene and acetic acid is a sequential process.

4.3.2.3 Formation of secondary products

As the *i*-butylene and acetic acid are major products, it seems like they can be converted to higher hydrocarbons including C5-C8 olefins and toluene, and propylene at

relatively high contact time (Figure 4.1b). Accordingly, *i*-butylene and acetic acid conversion over HZSM-5 were carried out. Table 4.3 shows that higher hydrocarbons are obtained from *i*-butylene conversion over HZSM-5.

Table 4.3 *i*-Butylene and acetic acid conversion over HZSM-5 (Si/Al=13)

	***i*-Butylene**	**Acetic acid**
Conversion (C mol%)	67	-
Yield (C mol%)		
C5-C8 Olefins	59	-
C6-C9 Aromatics	8	-

448 K and 148 g.h.mol^{-1}, N_2 60 mL.min^{-1}, result at 15 min on stream

** i-Butylene was in-situ produced from t-butanol dehydration over HZSM-5 (Si/Al=13) at 448 K*

Meanwhile, the acetic acid is relatively inert at the testing temperature. According to these results, it is concluded that these higher hydrocarbons are virtually generated from *i*-butylene conversion. As the tertiary carbenium ion generated by protonation of *i*-butylene is feasible, it can be oligomerized to higher olefins as seen from the increase in C8 olefin (Figure 4.1b).

However, the decline of the C8 olefin yield is observed at contact time > 74 g.h.mol^{-1} while the yields of C5-C7 olefins increase continually. An equivalent yield between C5 and C7 and approximately two folded yield of C6 (Figure 4.1b) reveal that they are derived from cracking of C12. As the oligomerization occurred consecutively, it is likely that the *i*-butylene is oligomerized to C12 olefin pool that undergoes cracking to the smaller olefins (C5-C7). A late production of toluene at contact time of 37 g.h.mol^{-1} and propylene at contact time 74 g.h.mol^{-1} in Figure 4.1b, is probably due to the aromatization and dealkylation of the aromatic fraction in the pool, respectively. The secondary conversion of *i*-butylene to wide range of hydrocarbons via pool formation can be summarized as expressed below;

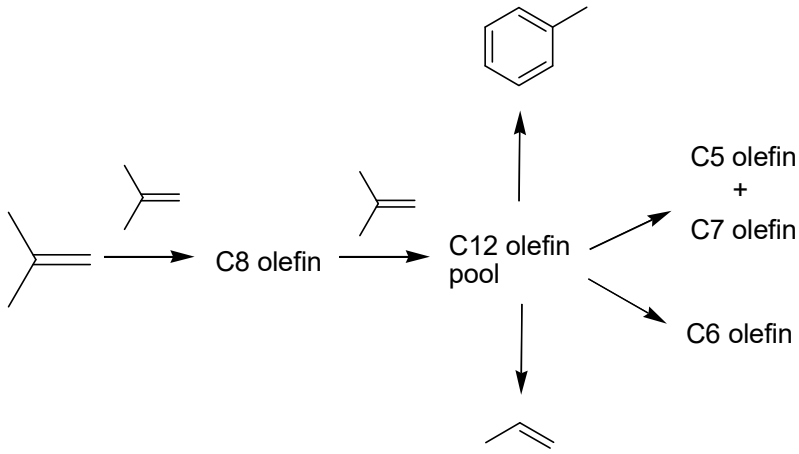

4.3.2.4 Effect of reaction temperature

Although the TPD of acetone (Figure 4.2) shows the evolution of various products e.g. carbon dioxide, acetone, and xylenes, they are not found from the reaction at low temperature (448K, Figure 4.1a-b). It is likely that the product selectivity depends on the reaction temperature. Accordingly, self-deoxygenation of acetone was studied at 423-573 K as expressed in Figure 4.8.

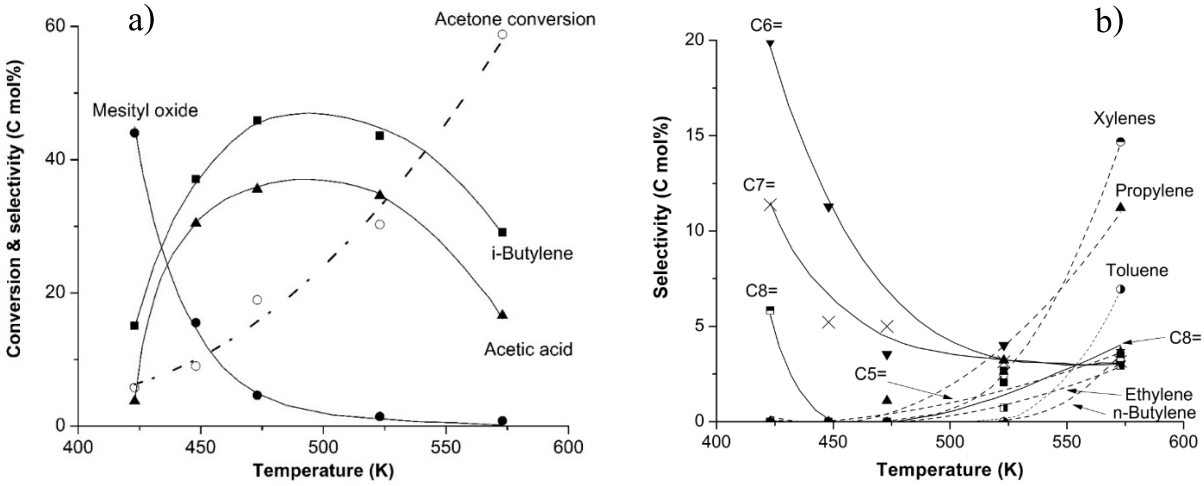

Figure 4.8 Effect of reaction temperature to acetone self-deoxygenation over HZSM–5 (Si/Al=13)

a) conversion, mesityl oxide, *i*-butylene, and acetic acid

b) C2-C8 olefins and aromatics

N_2 (30 mL.min^{-1}) at 74 g.h.mol^{-1}, result at 15 min on stream

At 423 K, low acetone conversion and selectivity to the major products (*i*-butylene, and acetic acid, Figure 4.8a) are observed while a large amount of mesityl oxide (Figure 4.8a) is obtained. These results show that the aldol condensation of acetone as well as the decomposition of mesityl oxide produced are not readily promoted at this temperature. However, the *i*-butylene produced can be oligomerized to the higher olefins. The increase in temperature to 498 K results in an increase in conversion and selectivity to the major products with a decrease in mesityl oxide selectivity. This is because the decomposition of mesityl oxide is promoted. The selectivity to higher olefins drop severely with the evolution of other secondary products including aromatics (toluene and xylenes) and smaller olefins (ethylene and propylene). This indicates that the hydrocarbon pools can be further aromatized or cracking at > 498 K.

While the conversion is continually increased from > 498 K, a decline in selectivity to the major products (*i*-butylene, and acetic acid) is observed. As the

temperature is increased, the *i*-butylene oligomerization and the aromatization and cracking of hydrocarbon pools is promoted. The rate of secondary reaction is higher than the rate of *i*-butylene generation. In a different manner, the acetic acid may be consumed via ketonation at high temperature, as mentioned in section 4.3.2.1;

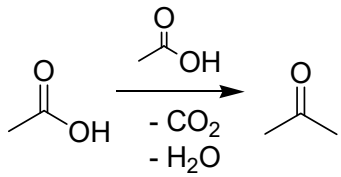

In line with this view, the TPD of acetic acid shows the ketonization as evidenced by carbon dioxide evolution at 550 K (Figure 4.9).

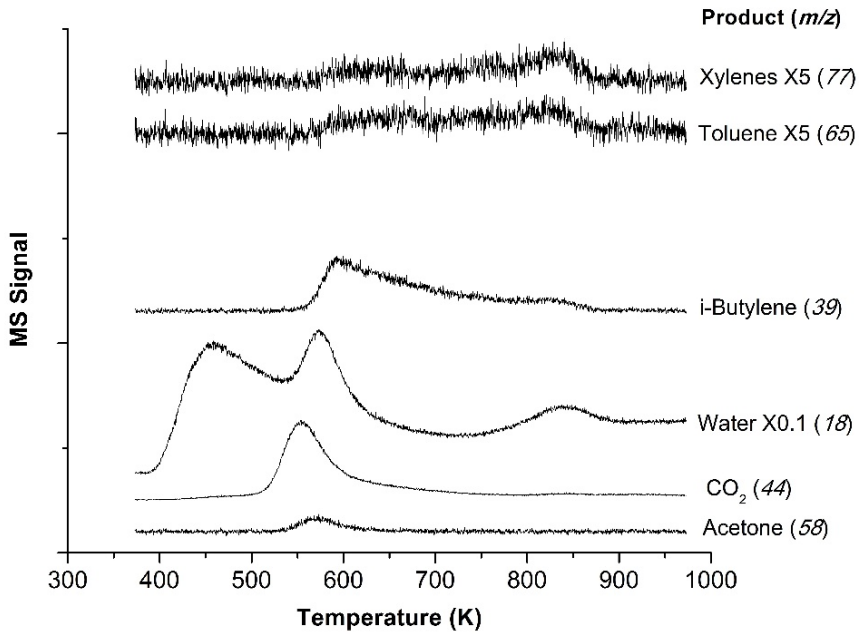

Figure 4.9 TPD of acetic acid over HZSM–5 (Si/Al=13) in He at 10 K.min^{-1}

From Figure 4.9, it is also found that the acetone and water are initially produced from acetic acid at temperature similar to that of the observed decline in acetic acid

selectivity (520 K). The regenerated acetone can be self-deoxygenated to additional *i*-butylene as seen from the peak at 600 K (Figure 4.9)

For the mechanistic point of view, it can be summarized at this stage that acetones are condensed to a diacetone alcohol then dehydrated to a mesityl oxide. The mesityl oxide is readily decomposed over Brønsted acid to an *i*-butylene and ethenone. The *i*-butylene is a highly reactive compound and can be further oligomerized to hydrocarbon pools that can undergo aromatization, dealkylation, and cracking to various olefins and aromatic compounds. On the other hand, an oxygen is transferred as water to ethenone forming acetic acid. In case of high temperature (> 498 K), acetic acids can be ketonized regenerating an acetone for additional self-deoxygenation. The oxygens are removed from acetic acid in form of a carbon dioxide and a water as illustrated below;

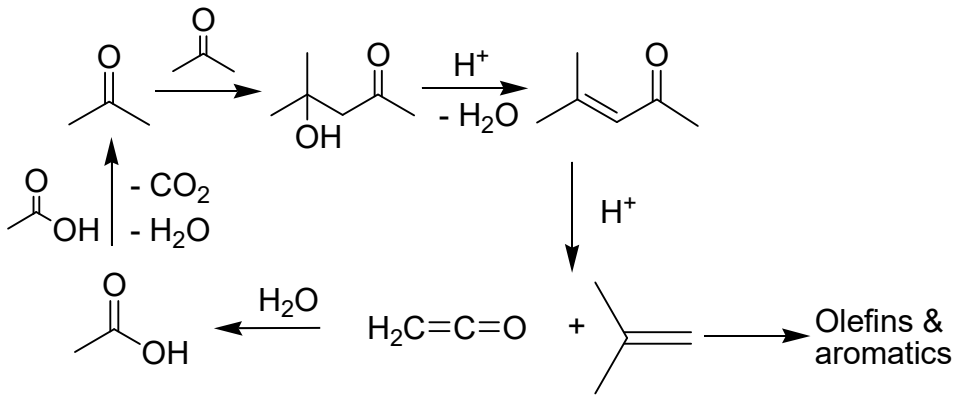

4.3.2.5 Effect of zeolite frameworks

With comparable Si/Al (11-15), the effect of zeolite framework was studied with HZSM-5, H-β, HY, H-Mordenite, and H-Ferrierite as shown in Table 4.4.

Table 4.4 Effect of zeolite framworks to acetone self-deoxygenation; conversion and selectivity at 1st hour

Framework	Conversion	Selectivity (C mol%)				
	(C mol%)	*i*-Butylene	Acetic acid	Mesityl oxide	C6-C9 Olefins	C7-C9 aromatics
H-Mordenite	4	60	33	1	-	6
HZSM-5	23	59	33	2	2	4
H-β	53	54	30	2	6	8
HY	17	54	31	0.7	0.3	14
H-Ferrierite	2	64	33	3	-	-

N_2 (60 mL.min^{-1}) at 498 K and 74 g.h.mol^{-1}

It is found that the order of initial activity is β > ZSM-5 > Y > Mordenite > Ferrierite. When the two dimensional pore zeolites (ZSM-5 and Ferrierite) are compared, it is found that the ZSM-5 obviously gives higher acetone conversion, as compared to Ferrierite. This is because ZSM-5 consist of medium pore in two dimension (~ 5.1-5.6 Å) while the Ferrierite composed by two kind of pore, one is medium pore (~ 5.4 Å) and the other dimension is small pore (~ 3.5 Å). Hence, the mass transfer of reactant and products is limited for Ferrierite, as compared to ZSM-5. When the zeolites with large pore size (β and Mordenite) are compared, it is clear that β is more active than Moredenite. This is because the β possesses 3 dimensional pore system. Therefore, the β facilitates the mass transfer of reactant and product, as compared to the Mordenite with 2 dimensional pore system. The comparison between three dimension large pore zeolites (β and Y) shows that the β possesses the activity higher than that of Y. This is because the reactant and products can be transferred easily in the channel structure of β while the cage structure of Y can trap reactant and products. However, all zeolites exhibit a severe deactivation as shown in Figure 4.10.

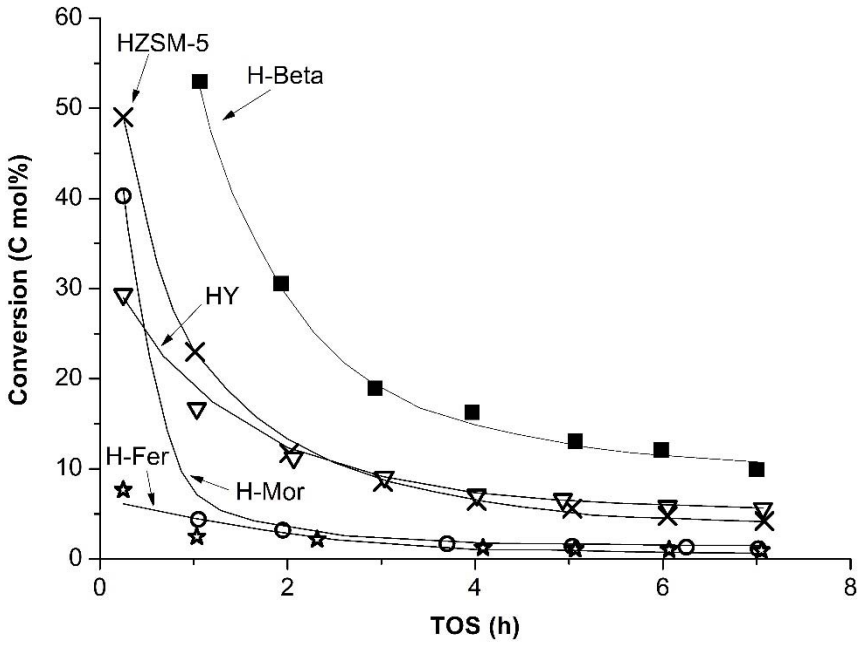

Figure 4.10 Effect of zeolite frameworks to acetone self-deoxygenation; conversion

N_2 (60 mL.min^{-1}) at 498 K and 74 g.h.mol^{-1}

This is presumably due to the coke deposit on the pore structure of zeolite. Since the *i*-butylene produced are strongly adsorbed on acid site, it can be oligomerized to higher olefins and hydrocarbon pools. The pool can be evolved to coke as the time is passed. A further investigation by temperature programmed oxidation with used HZSM-5 with acetone and mesityl oxide reveals that there is a coke deposit on zeolite surface as seen from oxygen consumption at 550-950 K (Figure 4.11).

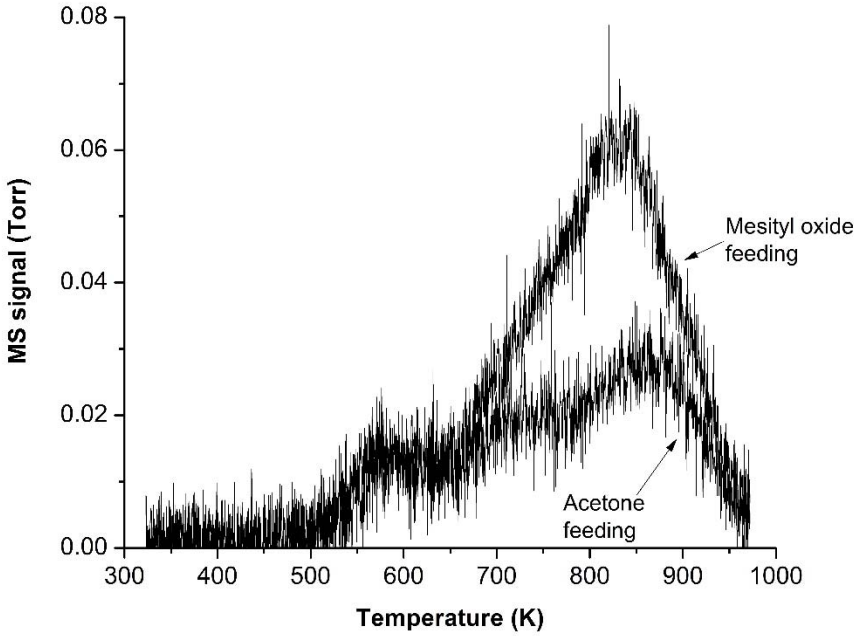

Figure 4.11 TPO-MS of spent HZSM–5 (Si/Al=13) with acetone and mesityl oxide fed, signal *m/z = 44* of CO_2, at 10 K.min^{-1}

For the product selectivity (Table 4.4), it can be seen that the selectivity to acetic acid from each catalyst is not different. A higher selectivity to *i*-butylene is obtained from the catalyst with lower in activity (Moredenite and Ferrierite) while the highly active catalyst (β and Y) generates a remarkable amount of secondary product (higher olefins and aromatics). This is because the large pore allow the formation of pools that is a source of the secondary products.

4.3.2.6 Effect of site proximity

As the self-deoxygenation of acetone involves with multistep reactions (protonation-deprotonation) over acid site, this reaction would be largely depended on acid density. Accordingly, the effect of site proximity is studied using HZSM-5 with various Si/Al. In this section, the total acidity of the catalyst bed is maintained at Brønsted acidity/bed = 6.3 μmol by adjusting the amount of loaded zeolite. Silica is used as diluent to maintain the catalyst bed high. The result is tabulated in Table 4.5.

Table 4.5 Effect of site proximity to acetone self-deoxygenation over HZSM–5/SiO_2

Si/Al	**Brønsted acidity**	**Conversion**	**Selectivity** (C mol%)				
	mmol/g	(C mol%)	*i*-Butylene	Acetic acid	Mesityl oxide	C6-C9 Olefins	C7-C9 Aromatics
13	0.78	6.8	63	31	4	0.5	2
40	0.40	6.0	64	34	0.4	0.6	1
102	0.12	5.5	67	32	-	0.9	-
152	0.063	4.6	67	33	-	-	-

N_2 (60 mL.min^{-1}) at 498 K and 148 g.h.mol^{-1}, 6.3 μmol of Brønsted acidity/bed, reactant/Brønsted acidity=1.78 min^{-1}, result at 15th min

It can be seen that the catalyst with lower Si/Al gives higher acetone conversion. A plot between acidity of the catalyst in Table 4.5 and turnover frequency reveals the increase in acid density of zeolite leads to the increase in turnover frequency as shown in Figure 4.12.

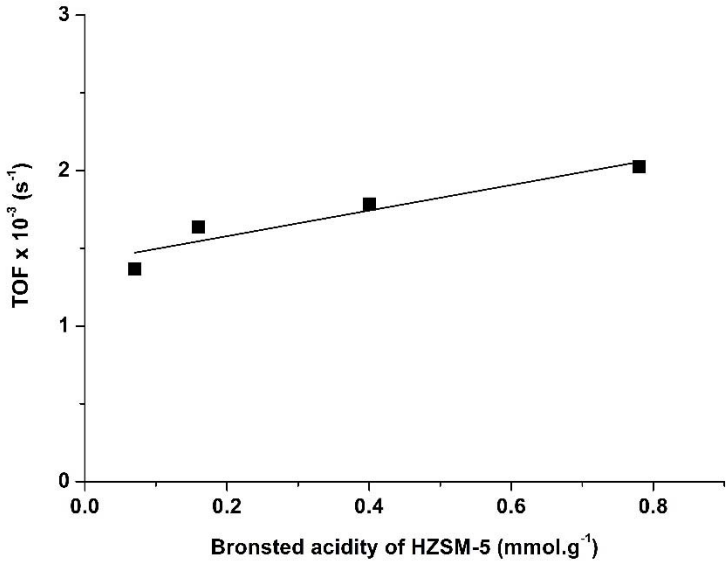

Figure 4.12 Effect of site proximity to acetone self-deoxygenation over HZSM–5/SiO_2; turnover frequency vs. acidity

N_2 (60 mL.min^{-1}) at 498 K and 148 g.h.mol^{-1}, molar ratio of Brønsted acidity/feed = 0.56 min, result at 15th min

This is because the self-deoxygenation of ketone is a sequential process as mentioned in section 4.3.2.2 (ii). The aldol condensation of acetone to mesityl oxide is promoted by an acid site. As water is generally bounded with the acid site after dehydration. The mesityl oxide would be re-adsorbed onto adjacent acid site for decomposition. The high acid density catalyst (low Si/Al zeolite on the other word) can provide a shorter range proximate site between those two acid sites, as compared to that with high Si/Al. Therefore, the decomposition of mesityl oxide produced can be readily promoted. With the similar reason, the bi-molecular process, such as oligomerization of *i*-butylene is also accelerated by the catalyst with high acid density as seen from the production of secondary products (C6+ olefins and aromatics).

4.3.2.7 The self-deoxygenation of ethyl methyl ketone

For a larger ketone, i.e. ethyl methyl ketone (MEK) self-deoxygenation can be accomplished as shown in Table 4.6.

Table 4.6 Comparison between ethyl methyl ketone (MEK) and acetone self-deoxygenation over HZSM-5 (Si/Al=13)

	MEK	Acetone
Conversion (C mol%)	11	30
Selectivity (C mol%)		
Butenes	4	44
Methyl butenes	37	2
Carboxylic acid	40 (C3)	35 (C2)
Aldol condensation product	0	2
C2-C3 Olefins	9	4
C6-C10 Olefins & aromatics	10	13

523 K and 74 g.h.mol^{-1} in N_2 (30 mL.min^{-1}), result at 15 min on stream

It is found that the conversion from self-deoxygenation of MEK is lower, as compared to self-deoxygenation of acetone. This is because the condensation products derived from MEK is more steric than that from acetone (mesityl oxide and diacetone alcohol) as demonstated below;

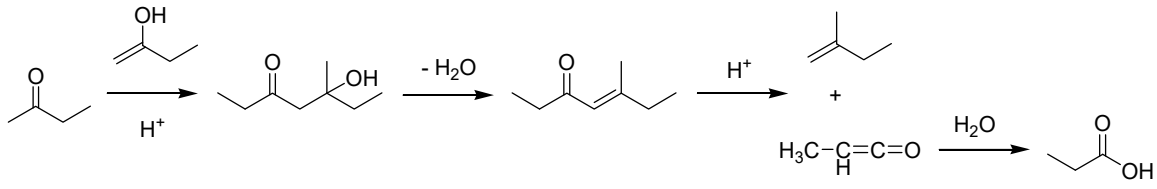

The C-C is formed at the terminal methyl of enol yielding an unsaturated C8 ketone. The subsequently decomposition of the ketone produced gives C5 olefins and propanoic acid as shown in Table 4.6.

As MEK is an asymmetric ketone, one could expect that the C-C formation may also takes place at adjacent methylene of enol. The decomposition of C8 ketone produced yields C6 olefins and acetic acid (20-30 %, [21]) as shown below;

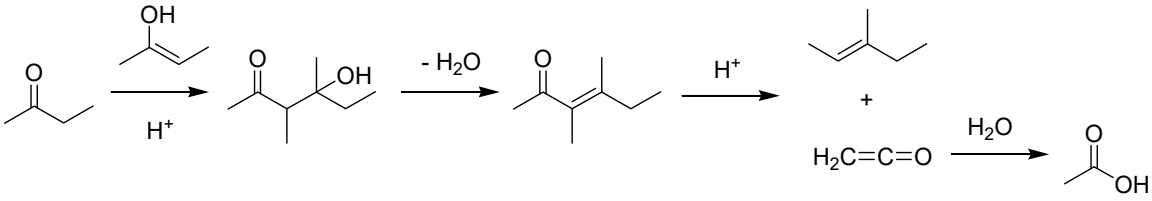

From Table 4.6, no C6 olefins and acetic acid is obtained from MEK self-deoxygenation. This is because C-C forming at methylene generates more steric condensation products, as compared to the C-C forming at methyl. Hence, the C-C forming at methylene is suppressed by pore of HZSM-5 and only C-C forming at methyl is allowed.

4.4 Conclusion

Ketone can be deoxygenated itself without H_2 consumption to an olefin and a carboxylic acid over acid zeolites even at low temperature (> 423 K) and atmospheric pressure. Using acetone as model compound, the process consists three sequential reactions including (i) aldol-condensation of two acetones to mesityl oxide and water, (ii) decomposition of the mesityl oxide to *i*-butylene and ethenone, (iii) hydration of the ethenone and water to acetic acid. The catalyst with good mass transfer (large three dimensional pore with channel structure; H-β) and high acid density (low Si/Al) is preferred. The additional deoxygenation can be obtained via ketonization of the acetic acids produced regenerating acetone to further self-deoxygenation only at > 503 K. The oligomerization, aromatization and cracking of the *i*-butylene produced is observed for the production of higher olefins and aromatic compounds.

4.5 References

[1] Elliott D.C. and Baker E.G. "**Process for upgrading biomass pyrolyzates**" U.S. patent no.4795841, 3 Jan 1989.

[2] Elliott D.C., Hart T.R., Neuenschwander G.G., Rotness L.J. and Zacher A.H. "Catalytic Hydroprocessing of Biomass Fast Pyrolysis Bio-oil to Produce Hydrocarbon Products" **Environmental Progress & Sustainable Energy,** vol.28, 2009. pp.441-449.

[3] Fisk C.A., Morgan T., Ji Y., Crocker M., Crofcheck C. and Lewis S.A. "Bio-oil upgrading over platinum catalysts using in situ generated hydrogen" **Applied Catalysis A: General,** vol.358, 2009. pp.150–156.

[4] Wildschut J., Melián-Cabrera I. and Heeres H.J. "Catalyst studies on the hydrotreatment of fast pyrolysis oil" **Applied Catalysis B: Environmental,** vol.99, 2010. pp.298-306.

[5] Bernardes M.A., Editor. **Biofuel's Engineering Process Technology**. Rijeka: InTech. 2011.

[6] Tago T., Sakamoto M., Iwakai K., Nishihara H., Mukai S.R., Tanaka T. and Masuda T. "Control of acid-site location of MFI zeolite by catalytic cracking of silane and its application to olefin synthesis from acetone" **Journal of Chemical Engineering of Japan**, vol.42, 2009. pp.s162–s167.

[7] Tago T., Konno H., Nakasaka Y. and Masuda T. "Selective synthesis for light olefins from acetone over ZSM-5 zeolites with nano- and macro-crystal sizes" **Applied Catalysis A: General**, vol.403, 2011. pp.183–191

[8] Slamet S. and Nasikin M., " Catalytic conversion of acetone to monoaromatic chemicals using HZSM-5" **International Journal of Engineering & Technology**, vol.11, 2011. pp.65-72.

[9] Konno H., Tago T., Nakasaka Y., Watanabe G. and Masuda T. "Characterization and catalytic performance of modified nano-scale ZSM-5 for the acetone-to-olefins reaction" **Applied Catalysis A: General**, vol.475, 2014. pp.127–133.

[10] Cruz-Cabeza A.J., Esquivel D., Jiménez-Sanchidrián C. and Romero-Salguero F.J. "Metal-exchanged β zeolites as catalysts for the conversion of acetone to hydrocarbons" **Materials**, vol.5, 2012. pp.121-134.

[11] Tago T., Konno H., Ikeda S., Yamazaki S., Ninomiya W., Nakasaka Y. and Masuda T. "Selective production of isobutylene from acetone over alkali metal ion-exchanged BEA zeolites" **Catalysis Today**, vol.164, 2011. pp.158–162

[12] Ausavasukhi A., Huang Y., To A.T., Sooknoi T. and Resasco D.E. "Hydrodeoxygenation of m-cresol over gallium-modified beta zeolite catalysts" **Journal of Catalysis**, vol.290, 2012. pp.90–100.

[13] Anaya F., Zhang L., Tan Q. and Resasco D.E. "Tuning the acid–metal balance in Pd/ and Pt/zeolite catalysts for the hydroalkylation of m-cresol" **Journal of Catalysis,** vol.328, 2015. pp.173–185.

[14] To A.T. and Resasco D.E. "Hydride transfer between a phenolic surface pool and reactant paraffins in the catalytic cracking of m-cresol/hexanes mixtures over an HY zeolite" **Journal of Catalysis,** vol.329, 2015. pp.57–68.

[15] To A.T. and Resasco D.E. "Role of a phenolic pool in the conversion of m-cresol to aromatics over HY and HZSM-5 zeolites" **Applied Catalysis A: General,** vol.487, 2014. pp.62–71.

[16] You S.J, and Park E.D "Effects of dealumination and desilication of H-ZSM-5 on xylose dehydration" **Microporous and Mesoporous Materials**, vol.186, 2014. pp.121–129.

[17] Hoang T.Q, Zhu X., Lobban L.L., Resasco D.E. and Mallinson R.G. "Effects of HZSM-5 crystallite size on stability and alkyl-aromatics product distribution from conversion of propanal" **Catalysis Communications**, vol.11, 2010. pp.977–981

[18] Opalka S.M., Willigan R.R., Zhu T., Dardas Z., Colket M.B. and Haas M. **Influence of Zeolite Reaction Site Characteristics on Hydrocarbon Cracking Mechanisms** [Slide]. United Technologies Research Center.

[19] Pieterse J.A.Z. **Low Temperature Alkane Activation over Zeolites**. Enschede: Print Partners Ipskamp. 2000.

[20] Rakiewicz E.F, Peters A.W., and Wormsbecher R.F. "Characterization of acid sites in zeolitic and other inorganic systems using solid-state ^{31}P NMR of the probe molecule trimethylphosphine Oxide" **Journal of Physical Chemistry B**, vol.102, 1998. pp.2890-2896.

[21] Kelly G.J. "Aldol condensation reaction and catalyst therefor" U.S. patent no.6706928B2, 16 Mar 2004.

Chapter 5

Hydrodeoxygenation of ketones to olefins

5.1 Introduction

The self-deoxygenation of the ketones to olefins in Chapter 4 expresses the opportunity to upgrade the ketones without hydrogen consumption but the rapid deactivation is a major concern. Meanwhile, the decarbonylation as simply done with aldehydes is impossible for the deoxygenation of ketones. Many works achieve the oxygen removal by hydrotreatment process over noble metal such as Ni. However, a large amount of hydrogen is consumed. The direct reduction usually leads to formation of paraffin [1-4], a cheap feedstock, when drastic condition is used. Accordingly, mild hydrodeoxygenation (HDO) is emphasized to remove oxygen functional groups with reasonable hydrogen consumption, and produce olefin as reactive hydrocarbon feedstock. For example, mild hydrodeoxygenation of acetone yields propylene that is a parent of C3 building block e.g. acrylic acid and acrylates [5-7], acrylonitrile [8-9], pyridine [10], propylene oxide and 1,2-propane-diol [11-13] and a most consumed polymer, polypropylene [14-15]. As a single reaction fails to produce olefin directly from ketone, a new approach for olefin production would be invented from sequential processes including i) treatment of ketone to alcohol by partial hydrogenation and ii) selective deoxygenation of the alcohol to olefin by dehydration as illustrated below;

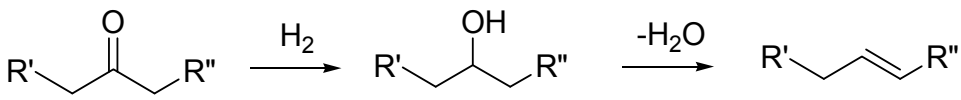

From Chapter 4, the self-deoxygenation of ketone shows that it is difficult to use a single type of catalyst for a process involving with several reactions. For example, oligomerization of the olefin produced and poisoning of the acid site by the ketene intermediate can lead to severe deactivation for self-deoxygenation. It seems that the treating each individual reactions with specific catalyst component is a better choice.

Therefore, bi or more functional catalyst is required for multi-step process like HDO of ketone to olefin.

In this Chapter, a catalytic system designed for mild HDO of ketone to olefin was investigated. Hydrogenation of ketone to alcohol (i) was accomplished over metal catalysts (Ni, Cu, Fe, Co, Pt and their alloys) [16-19]. The alcohol produced was subsequently dehydrated (ii) over acidic catalysts (γ-Al_2O_3, HZSM-5, HY and H-β) [20-23]. To understand the role of each catalytic reactions, hydrogenation (i) and dehydration (ii) were separately studied. However, the nature of these sub-reactions is different. For example, hydrogenation (i) is preferred at relatively low temperature and high pressure while dehydration (ii) is promoted at higher temperature and lower pressure. In the catalytic point of view, the metal should be selective for hydrogenation of the ketone to alcohol, not the olefin produced to paraffin. The acid function should facilitate dehydration of the alcohol produced, but not aldol condensation of the ketone fed. Accordingly, several parameters have to be adjusted and controlled including competitive adsorption of feed, intermediates and products on each individual active site. Then, the integrated hydrogenation-dehydration over sequential bed, mixed bed and single bed of bi-functional catalyst were then optimized for a least hydrogen-consumption required for olefin production from ketone.

5.2 Experimental details

HZSM-5 (Si/Al=13) and HZSM-5 (Si/Al=150) were obtained from Zeochem®. NH_4^+-β (Si/Al=13), H-Mordenite (Si/Al=15), NH_4^+Y (Si/Al=8) and HY (Si/Al=150) were supplied by Tohso. The NH_4^+-zeolites were converted to H^+-zeolites by calcination at 773 K under flow of air (60 mL/min) for 5 h with a heating rate of 2 $K.min^{-1}$. CeO_2 (99.9%, Sigma-Aldrich®) was also treated in similar manner to the zeolites. Metal supported catalysts were simply prepared by incipient wetness impregnation. Metal nitrate precursors ($Cu(NO_3)_2.3H_2O$ by Ajax Fine Chem, $Ni(NO_3)_2.6H_2O$, $Cr(NO_3)_3.9H_2O$ $Fe(NO_3)_3.9H_2O$, and $Co(NO_3)_2.6H_2O$ by Carlo Erba®) were dissolved in deionized water (~ 0.01 M) and slowly drop onto supports (SiO_2; Carlo Erba, HZSM-5(150), or HY (150)) until wet. The sample was dried at 333 K in an oven for 15 min, and then the loading was repeated until desired metal content was reached. The samples were kept to dry at 333 K overnight and calcined in air (60 $mL.min^{-1}$) at 723 K for 5 h. All samples were pelletized to the size of 600–850 μm before used.

Elemental composition was determined by X-ray fluorescence spectrometer (XRF; Siemens). Specific surface area (BET) of catalysts was measured using nitrogen adsorption analyzer (Quantachrome) at 77 K and 0.05–0.30 P/P_0. Residue retained in the used catalysts was analyzed by thermo-gravimetric analysis (Perkin Elmer) under air or N_2 stream from 323-1173 K at rate of 10 $K.min^{-1}$. Reducible metal oxide species in the catalysts was analyzed by temperature programmed reduction (TPR). The catalysts were treated in air at 723 K for 5 hours prior to heating from 323-1173 K in 10% H_2/Ar. The hydrogen consumption was recorded with an on-line thermal conductivity detector (VICI) [24-25]. Copper dispersion on support was also analyzed by selective surface TPR technique. Briefly after typical TPR, the sample was *in situ* treated with N_2O at 333 K for 2 hours. Then, the surface-oxidized sample was subjected to a secondary TPR [26]. The number of moles of surface copper can be calculated as described by Sagar *et al.* [27]. Acidity of HY and Cu/HY was quantified by NH_3-TPD. 1 % NH_3/He was pre-adsorbed at 323 K. TPD was carried out in He at 10 $K.min^{-1}$ from 323–973 K [28].

The catalytic testing was conducted in a fixed bed flow reactor (6 mm i.d. Pyrex®). The catalysts were primarily activated at 723 K (2 $K.min^{-1}$) under stream of air (30 $mL.min^{-1}$) for 5 h. Subsequently the metal supported catalysts were treated in H_2 at 723 K for 2 h. The system was cooled down to the reaction temperature (373–573 K) and the reactant was introduced by a syringe pump at a rate of 0.07-0.7 $g.h^{-1}$. The products were analyzed by an on-line GC-FID every 70 minutes. A Hayesep® P (1/8" X 8') was used as separating column. The analysis condition for gas chromatography is shown in Appendix A.

5.3 Result and discussion

5.3.1 Characterization of catalyst

Metal content, Si/Al and surface area of all catalyst samples are tabulated in Table 5.1. All catalysts possess relatively high surface area.

Table 5.1 % Metal content and surface area of metal catalysts and supports

Catalyst	Metal content	BET surface area	Si/Al
	%wt	(m^2/g)	
2%Cr/SiO_2	2.0	244	-
2%Fe/SiO_2	2.1	243	-
2%Co/SiO_2	1.8	245	-
2%Pd/SiO_2	1.7	238	-
2%Ni/SiO_2	2.1	239	-
5%Ni/SiO_2	5.0	234	-
8%Ni/SiO_2	8.1	212	-
20%Ni/SiO_2	20.3	208	-
40%Ni/SiO_2	42.0	137	-
2%Cu/SiO_2	2.1	242	-
5%Cu/SiO_2	5.1	240	-
10%Cu/SiO_2	10.7	220	-
15%Cu/SiO_2	16.4	214	-
40%Cu/SiO_2	36.1	144	-
2%NiCu/SiO_2 (25%Cu)	0.58(Cu);1.64(Ni)	240	-
2%NiCu/SiO_2 (50%Cu)	1.04(Cu);1.10(Ni)	241	-
2%NiCu/SiO_2 (70%Cu)	1.58(Cu);0.56(Ni)	238	-
2%NiCu/SiO_2 (80%Cu)	1.90(Cu);0.43(Ni)	238	-
SiO_2	-	246	-
Cu/HY	5.1	568	166
Cu/HZSM-5	5.2	361	173

Table 5.1 Continue

Catalyst	Metal content %wt	BET surface area (m^2/g)	Si/Al
HY (Si/Al=150)	-	713	153
HY (Si/Al=8)	-	734	8
HZSM-5 (Si/Al=150)	-	376	152
HZSM-5 (Si/Al=13)	-	352	13
H-β (Si/Al=13)	-	523	13
H-Mordenite (Si/Al=15)	-	454	15

The reducible metal species in metal catalysts is examined by TPR shown in Figure 5.1. It can be seen that at 2 %wt loading on silica, high temperature is required for reduction of Cr >Co ~ Fe >Ni >Cu oxides, respectively [29].

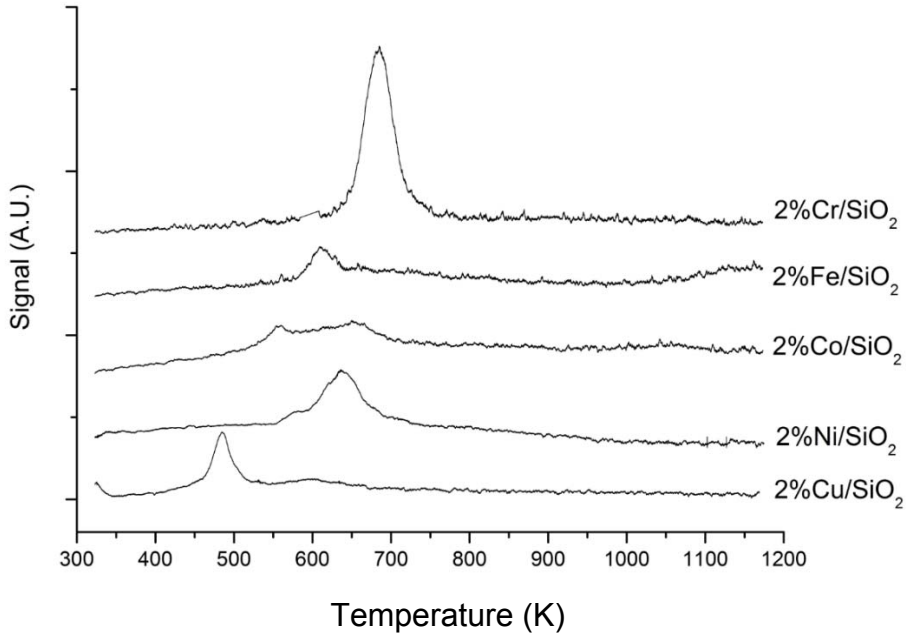

Figure 5.1 Temperature program reduction of 2%wt metals on SiO_2

Broad reduction peaks at the shoulder of CuO and NiO at 650-800 K are attributed to various metal-support interactions including copper or nickel silicate [30-31]. While, cobalt oxide expresses two peaks at 548 and 643 K, corresponded to Co_3O_4 ⟶ CoO and CoO ⟶ Co, respectively [32-33]. For iron oxide, the first reduction peak of iron composed by two overlap stages Fe_2O_3 ⟶ Fe_3O_4 and Fe_3O_4 ⟶ FeO (603 K) [34]. However, fully reduction of FeO to Fe cannot be achieved up to 1173 K, due to formation of Fe_2SiO_4 [35]. The TPR profile of chromium oxide corresponds to the reduction of dichromate and poly chromate to Cr_2O_3 (700 K) [36]. However, chromium (III) is very stable and cannot be reduced in this temperature range [37].

When nickel and copper are co-impregnated on silica, the complete alloys are obtained at every composition resulting in combination of reduction temperature (Figure 5.2). The good miscibility is due to the substitution of element with similar atomic size.

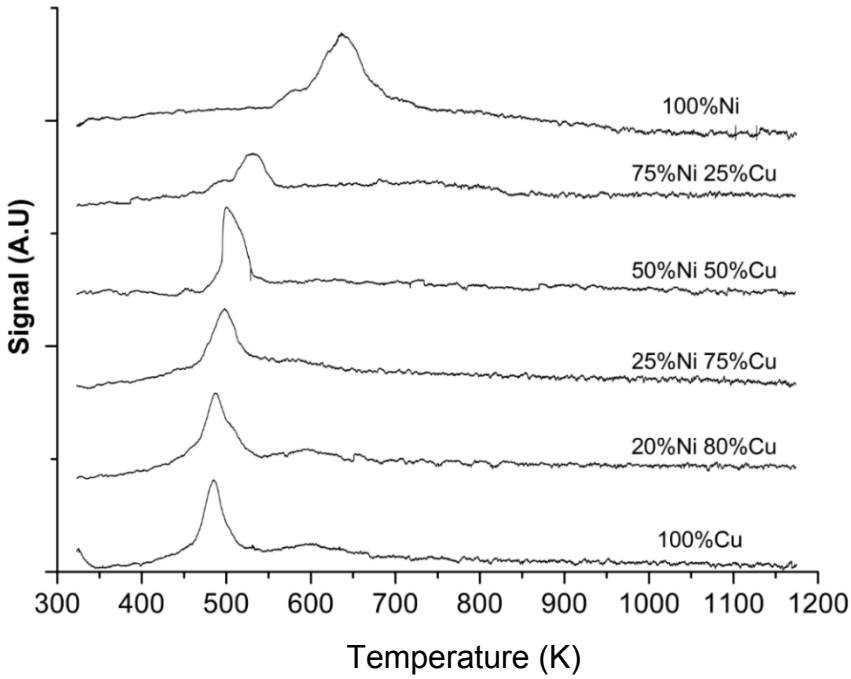

Figure 5.2 Temperature program reduction of 2%wt Ni-Cu alloy on SiO_2

For copper catalyst, the dispersion on SiO_2 decrease from 95 to 24 % when loading is increased from 5-15% (Table 5.2) due to the agglomeration.

Table 5.2 Copper surface area, copper dispersion, and acidity of Cu catalysts

Catalyst	Cu content	Si/Al	Cu area	% Cu dispersion	Acidity (μmol/g)	
	%wt		(m^2/g_{Cu})		Weak	Strong
2%Cu/SiO_2	2.1	-	257	n/a	-	-
5%Cu/SiO_2	5.1	-	646	95	-	-
10%Cu/SiO_2	10.7	-	437	66	-	-
15%Cu/SiO_2	16.4	-	220	24	-	-
Cu/HY	5.1	166	499	65	158	62
Cu/HZSM-5	5.2	173	414	54	92	20
HY	-	153	-	-	54	65
HZSM-5	-	152	-	-	56	65-

The good dispersion of 5% Cu/SiO_2 results in flat and thin copper particle, which is barely visible when observed by TEM (Figure 5.3).

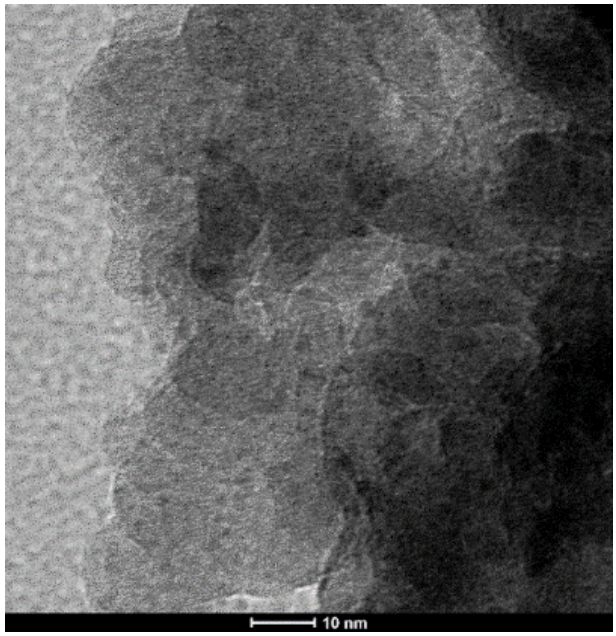

Figure 5.3 TEM image of Cu/SiO_2 at 440 kX; 5% Cu loading

It is noted that the dispersion of 2% Cu/SiO_2 cannot be accurately determined, presumably due to an incomplete surface oxidation by N_2O and a deviated hydrogen consumption measurement when the Cu loading is relatively small.

The relatively lower Cu dispersion (54–65 %) is observed when zeolites (HZSM-5 and HY at Si/Al ~ 150) are used as support. This is because a part of the surface Cu oxide may well become exchangeable, forming Cu cation that is difficult to reduce. The evidence of exchangeable copper cation in HY and HZSM-5 is shown in Table 5.2. For H-zeolite like HZSM-5 and HY, the acidity is derived from adsorption of an ammonia on a proton. Replacing the proton to a larger cation like copper cation (Cu/HY and Cu/HZSM-5) results in the increase in co-ordination number of ammonia per cation particularly weak interaction, as compared to the parent zeolites (HY and HZSM-5). This is because the copper cation possesses more available orbitals (*d*-orbitals), for the ammonia adsorption, as compared to the proton (*s*-orbital). The Cu/HY and Cu/HZSM-5 show two reduction peaks at 473 and 520 K (Figure 5.4), corresponding to copper oxide aggregates and highly dispersed copper oxide in the pore of zeolite, respectively [38,39].

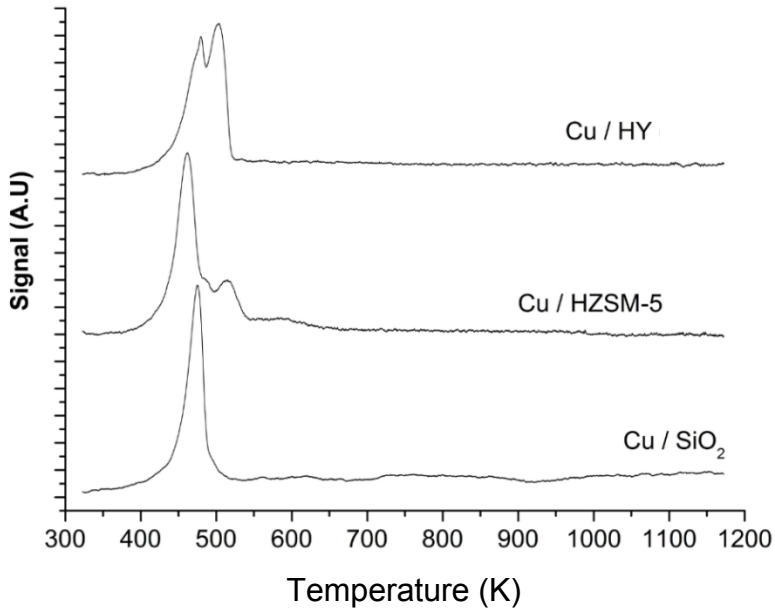

Figure 5.4 Temperature program reduction of Cu/zeolites; 5%wt Cu loading

The copper dispersion on HY is higher than that on HZSM-5 (peak at ~ 520 K), presumably due to a better diffusion of the Cu precursor in the larger pore of HY. This is consistent with the TEM images shown in Figure 5.5-5.6. The Cu/HY possesses relatively small Cu particles (Figure 5.5 (a-b)) and a part of them (dark spot) are aligned in the pore of HY (light grey plane) as expressed by insertion in Figure 5.5 (c).

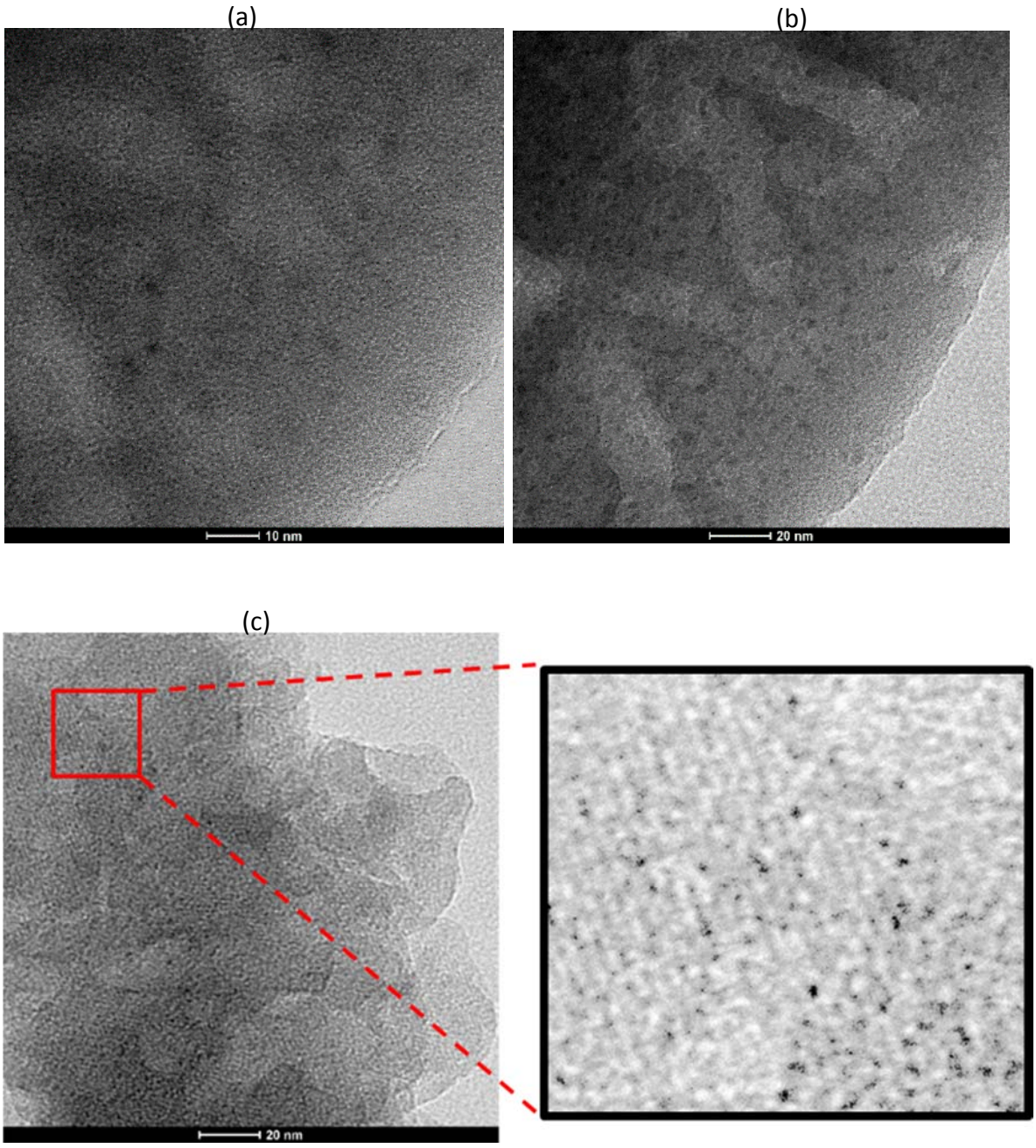

Figure 5.5 TEM image of Cu/HY (a) at 440 kX (b) at 285 kX (c) Cu particle well aligned in the HY pore at 285kX and insertion at 1,580 kX; 5% Cu loading

Meanwhile, a relatively lower Cu dispersion on HZSM-5 is observed from large semicircle Cu particles, deposited on the external surface of HZSM-5 crystals (Figure 5.6).

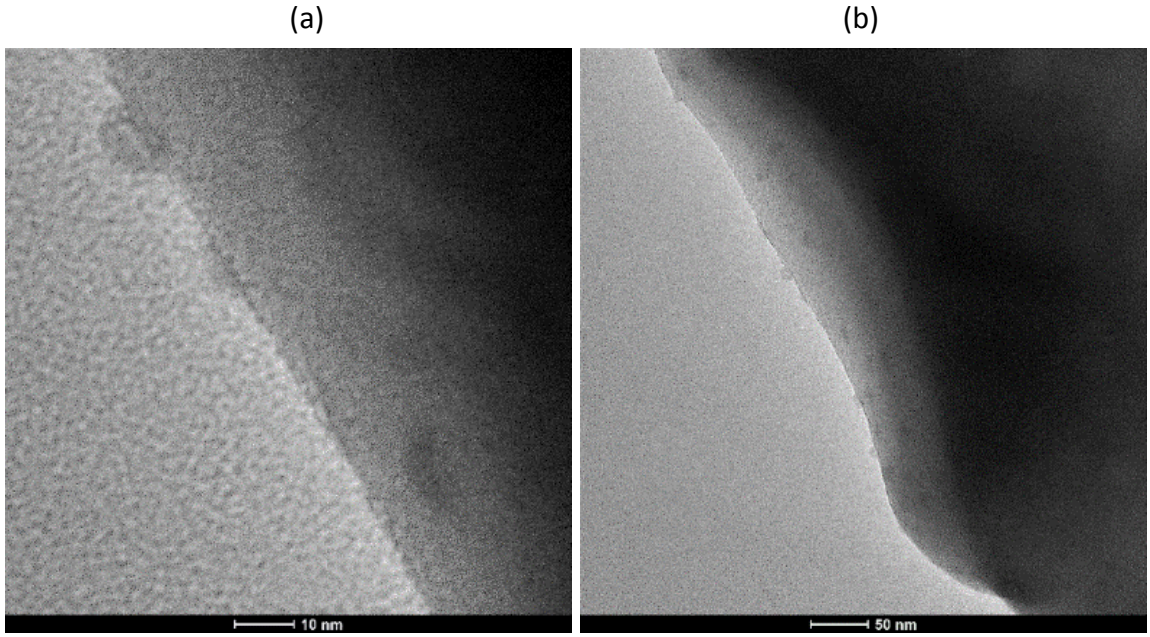

Figure 5.6 TEM image of Cu/HZSM-5 (a) at 440 kX (b) at 97 kX; 5% Cu loading

5.3.2 Hydrogenation of acetone

5.3.2.1 Effect of metal

As the hydrogenation of olefin product is not preferred, different metal catalysts are scanned for selective hydrogenation of ketone, but not for olefin hydrogenation. The initial activated temperature for hydrogenation of acetone and propylene model compounds over various metal catalysts are compared in Table 5.3. It is clear that chromium and iron are inactive for hydrogenations of acetone and propylene at low temperature.

Table 5.3 Initial activated temperature for hydrogenation and hydrogenolysis over metal catalysts from 373 – 623 K

Catalyst	Initial activated temperature[a]		
	Acetone hydrogenation to *i*-propanol	Acetone hydrogenolysis to paraffins	Propylene hydrogenation to propane
2%Cr/SiO_2	inactive	inactive	-
2%Fe/SiO_2	inactive	inactive	-
2%Co/SiO_2	523K	523K	498K
2%Ni/SiO_2	< 373K	473K	< 398K
2%Cu/SiO_2	< 373K	Inactive	Inactive
2%NiCu/SiO_2 [50:50]	< 373K	573K	< 473K
2%Pd/SiO_2	423K	573K	Active [40-41]

This is due to an incomplete reduction of the metal phase under the investigated condition (H_2, 723 K). Cobalt, nickel, palladium catalysts are active for both acetone and propylene hydrogenation [40-41]. Hydrogenolysis is also promoted over these metals at relatively higher temperature. The activity for acetone hydrogenation appears to be in the order of Ni > Pd > Co. In the opposite view, Pd is more active than Co and Ni for propylene hydrogenation.

According to Table 5.3, copper seems to be the best catalyst for mild hydrogenation of acetone to olefin with essential amount of hydrogen. Acetone can be hydrogenated (< 373 K) to alcohol without further conversion of propylene produced. This is because the copper prefers only η^1 (O) adsorption of carbonyl [42] rather than the η^2 of olefin.

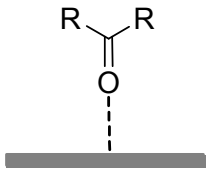

η^1 (O) adsorption of carbonyl

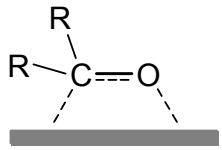

η^2 (C=O) adsorption of carbonyl

While, the nickel favors the adsorption at carbon (e.g. η^2 (C=C));

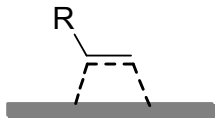

η^2 (C=C) adsorption of olefin

The alloy with Ni (NiCu) significantly decreases both hydrogenation of propylene and hydrogenolysis acivity, as compared to the Ni alone. This would increase the oxophillicity of the catalyst when Cu is alloyed. Hence, the adsorption of C=C is decreased. In addition, the Cu alloying strongly affects a structure sensitive reaction, in which the reactivity strongly depends on the size of active site, such as hydrogenolysis. The copper alloyed can separate the continuous Ni-Ni plan that promotes the hydrogenolysis via η^2 (C-O) adsorption. Hence, the hydrogenolysis is suppressed and high temperature is required for such reaction (Table 5.3). Both Ni and Cu catalyst possesses excellence catalyst stability. No carbon deposit is observed from TGA of the spent catalysts (Table 5.4).

Table 5.4 Thermo-gravimetric analysis of spent catalysts

Catalyst	Feed	Temp	Contact time	Weight loss (%)		
		K	(g.h.mol^{-1})	473-573 K	>573 K	Total
5%Ni/SiO_2	Acetone	448	15	-	-	-
5%Cu/SiO_2	Acetone	473	15	-	-	-
HY(Si/Al=8)	Acetone	448	3	-	2.6	2.6
H-*β*(Si/Al=13)	Acetone	448	3	-	5.5	5.5
H-Mordenite(Si/Al=15)	Acetone	448	15	2.1	5.4	7.5
HZSM-5(Si/Al=13)	Acetone	448	15	6.1	0.88	7.0
HZSM-5(Si/Al=13); TGA in N_2	Acetone	448	15	5.9	0.00	5.9
5%Cu/SiO_2+HZSM-5	Acetone	473	76+7	1.9	2.2	4.1
(Si/Al=13)	MEK	473	76+7	2.1	2.4	4.5
	Cyclohexanone	473	76+7	2.0	2.0	4.0
5%Cu/SiO_2+H-*β*	Acetone	473	76+7	1.3	1.9	3.2
(Si/Al=13)	Acetone	473	76+2	1.6	1.0	2.6
Cu/HY	Acetone	473	19	1.9	1.3	3.2
(Si/Al=13, 5%wt Cu)	MEK	473	19	4.3	2.1	6.4
	Cyclohexanone	473	19	2.8	1.6	4.4

5.3.2.2 Effect of reaction temperature

As Ni and Cu selectively promote hydrogenation of ketone at low temperature, these catalysts are selected for acetone hydrogenation at 373-573 K. For both metals, acetone conversion increases with temperature (Figure 5.7-5.8), according to kinetic.

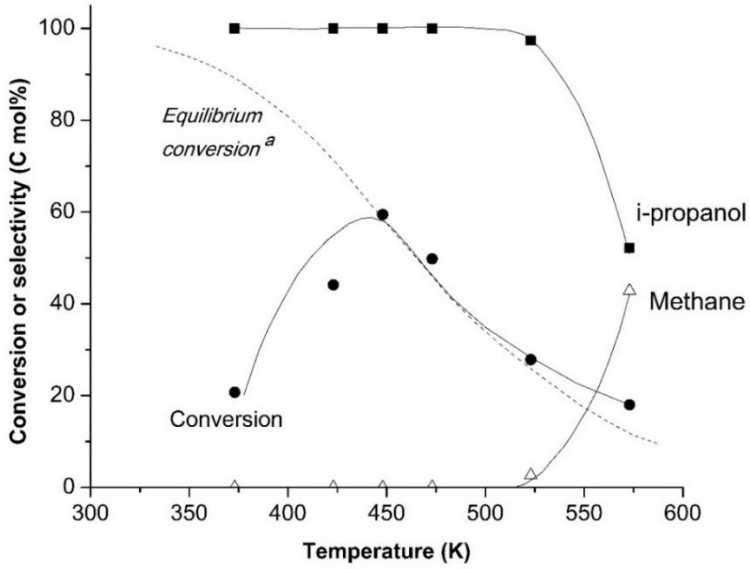

Figure 5.7 Effect of reaction temperature to acetone hydrogenation on 2%Ni/SiO_2

H_2 as carrier 30 mL/min, W/F 30 g.h.mol^{-1}

[a]Data taken from E. Buckley et al. [43]

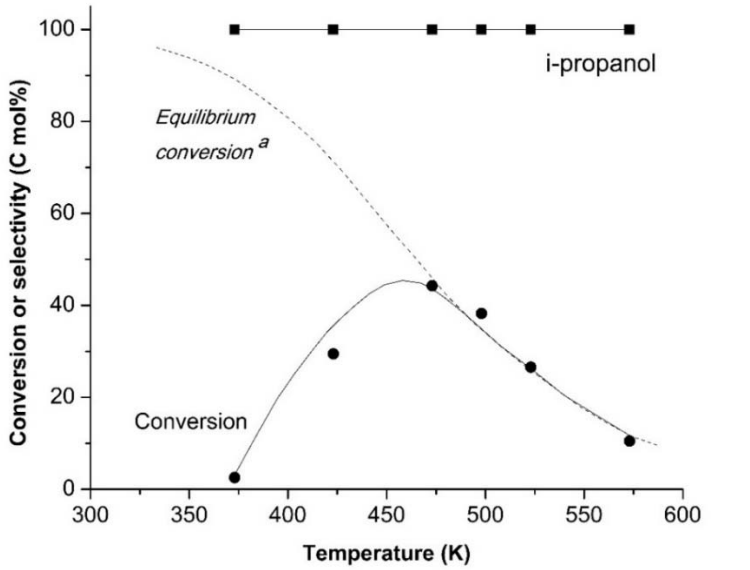

Figure 5.8 Effect of reaction temperature to acetone hydrogenation on 2%Cu/SiO_2

H_2 as carrier 30 mL/min, W/F 30 g.h.mol^{-1}

[a]Data taken from E. Buckley et al. [43]

However, the decline of conversion is observed when thermodynamic limitation (hydrogenation-dehydrogenation equilibrium) [43-45] is reached for the operating conditions. The maximum conversion is obtained at 448 K for nickel and 473 K for copper. It is clear that the nickel is more active than the copper. 100% selectivity to *i*-propanol is obtained over the nickel catalyst at 373-448 K. However, hydrogenolysis to methane can be observed at > 473 K. As the hydrogenolysis is endothermic and irreversible process, the hydrogenated acetone can be further decomposed to smaller compound at elevated temperature. Accordingly, the conversion obtained at this temperature is slightly higher than the equilibrium conversion of acetone to *i*-propanol [46]. Meanwhile, C-O single bond breaking is unusual because the copper prefers only η^1 (O) adsorption mode [42]; hence, 100% selectivity to *i*-propanol is obtained over the copper at temperature up to 573 K. Figure 5.9 emphasizes the thermodynamic limitation for acetone hydrogenation over copper catalyst by increasing the contact time. Although higher rate is obtained at higher reaction temperature (473 K), the conversion is limited at ~ 50%.

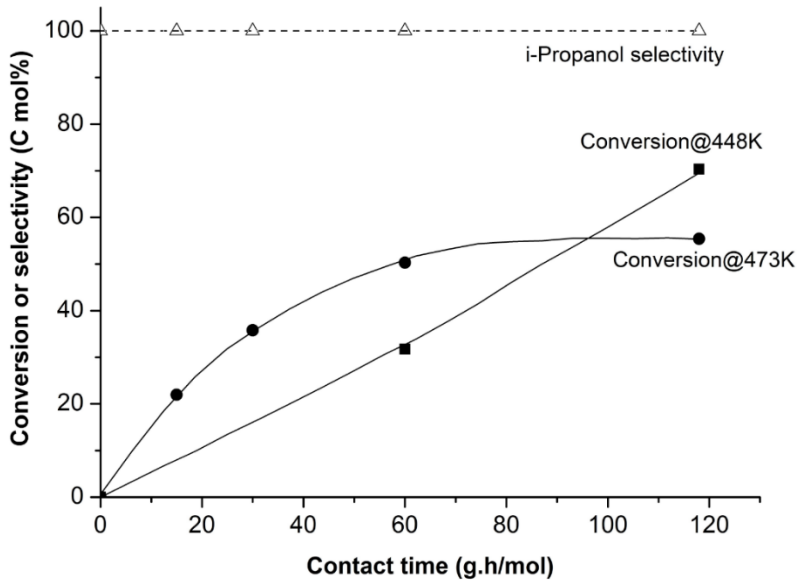

Figure 5.9 Effect of contact time for acetone hydrogenation on 2%Cu/SiO_2

448 and 473 K, H_2 as carrier 30 mL/min

At lower temperature (448 K), the thermodynamic limitation allows higher hydrogenation of acetone, as compared to that at 473 K. The conversion can be boosted up at higher contact time. For further investigation, the contact time in this work was tested below the equilibrium conversion (< 80 g.h.mol^{-1}).

5.3.2.3 Effect of metal loading

Effect of nickel and copper loading on SiO_2 was studied (5-40 %wt). When the metal loading is increased, acetone conversion is enhanced due to an increase in number of active sites (Figure 5.10).

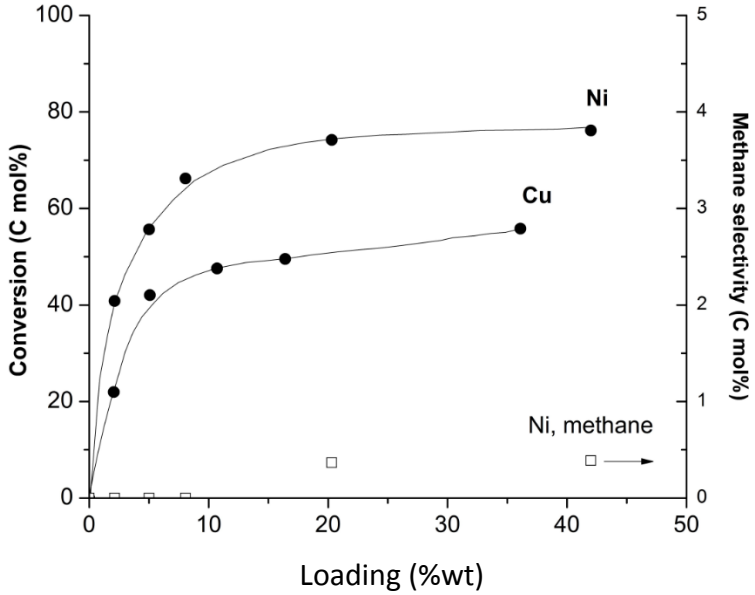

Figure 5.10 Effect of metal loading on SiO_2 to acetone hydrogenation; conversion and methane selectivity

448 K for Ni and 473 K for Cu, H_2 as carrier 30 mL/min; W/F 30 g.h.mol^{-1}

The turnover frequency for all Cu/SiO_2 catalyst is roughly 2.1-2.8 x 10^{-3} sec^{-1}, as shown in Table 5.5.

Table 5.5 Turn over frequency for acetone hydrogenation of Cu/SiO_2 catalysts

Catalyst	Cu content	Cu area	TOF
	%wt	(m^2/g_{Cu})	$x10^{-3}$ (sec^{-1})
5%Cu/SiO_2	5.08	646	2.6
10%Cu/SiO_2	10.7	437	2.1
15%Cu/SiO_2	16.4	220	2.8

473 K, W/F 30 g.h.mol^{-1}, H_2 as carrier 30 mL/min

However, the normalized rate for nickel and copper (Figure 5.11) is decreased due to agglomeration of the metal particles, which notably reduces the active metal surface per gram of metals (Table 5.5).

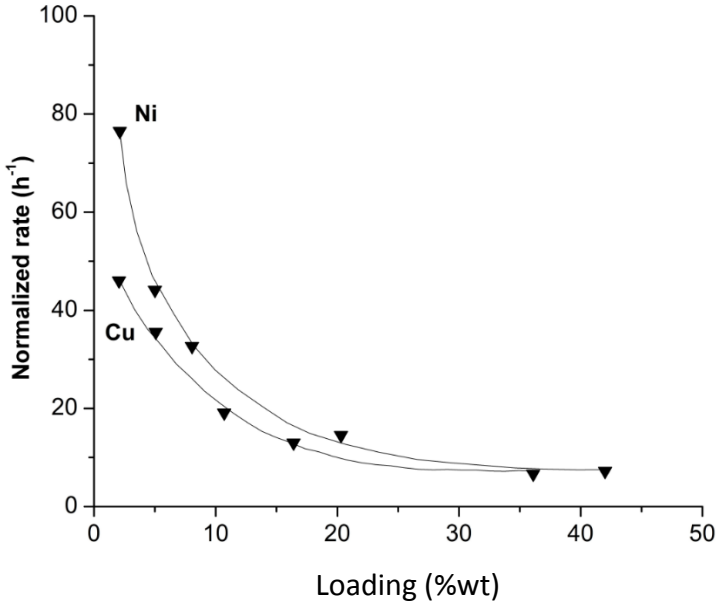

Figure 5.11 Effect of metal loading on SiO_2 to acetone hydrogenation, molar normalize rate

448 K for Ni and 473 K for Cu, H_2 as carrier 30 mL/min; W/F 30 g.h.mol^{-1}

In the case of nickel catalyst, the agglomeration enhances hydrogenolysis, as seen from Figure 5.10. The Ni catalysts with >20% loading yield significant amount of methane (~ 7% selectivity). Meanwhile, only η^1 (O) adsorption is allowed for C=O on Cu surface [42]. Hence, 100% selectivity to *i*-propanol is obtained over Cu catalyst up to 40% loading.

5.3.2.4 Effect of metal alloying

As methane was produced over the nickel catalyst at > 473 K, copper was alloyed into the nickel catalyst to retard the methane formation. Theoretically, nickel and copper are miscible in every component [47], as shown by TPR (Figure 5.2). As the copper is less reactive than nickel, it is clear from Figure 5.12 that the conversion is generally decreased with copper content in the alloy.

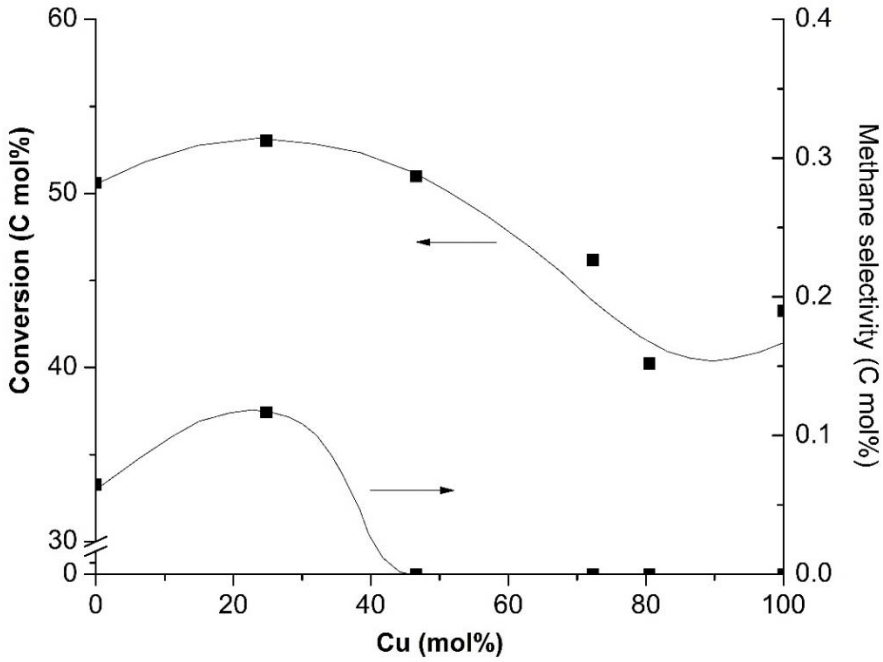

Figure 5.12 Effect of Ni-Cu alloying to acetone hydrogenation on 2% Metal/SiO_2

473 K; W/F 30 g.h.mol^{-1}, H_2 as carrier 30 mL/min

A slight improved activity at ~ 25% Cu is presumably due to a better dispersion of the metal phase. No methane is observed from the catalysts with > 40% Cu. This is because of the hydrogenalysis is a structure sensitive reaction. Alloying with copper can readily inhibits the η^2 (C=C, C=O) adsorption mode, that leads to C-C cleavage [46], by separating two adjacent nickel as mentioned in 5.3.2.1.

5.3.3 Dehydration of isopropanol

5.3.3.1 Effect of contact time

Dehydration of the hydrogenated product, *i*-propanol was separately investigated over H-β catalyst at 448 K. Figure 5.13 shows that *i*-propanol conversion is increased with the contact time. Propylene and diisopropyl ether are initially produced in parallel from intra-molecular dehydration and inter-molecular dehydration, respectively.

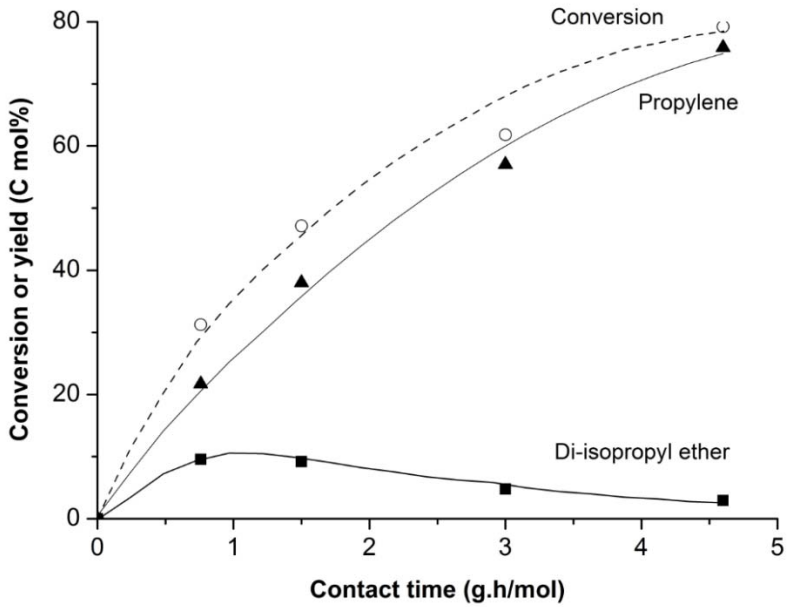

Figure 5.13 Effect of contact time on *i*-propanol dehydration on H-β (Si/Al=13)

448 K, H_2 as carrier 30 mL/min

However, yield of the ether drops gradually at higher contact time (> 1.5 g.h.mol^{-1}). While, no additional product is obtained. It is likely that ether is converted to propylene *i*-propanol as evidenced by the conversion of diisopropyl ether over H-β (Table 5.6).

Table 5.6 Di-isopropyl ether dehydration over H-β (Si/Al = 13)

	C mol %
Conversion	84
Selectivity	
Propylene	69
i-Propanol	29
C6 olefins	2

Results at 6th hour on stream, 448K, H_2 as carrier 30 mL/min, W/F 15 g.h.mol^{-1}

The protonation of ether can occur readily because it is highly nucleophilic. This leads to the dehydration of the ether to an olefin, regenerating a feed, alcohol [48]. The reaction pathways for *i*-propanol can be demonstrated below;

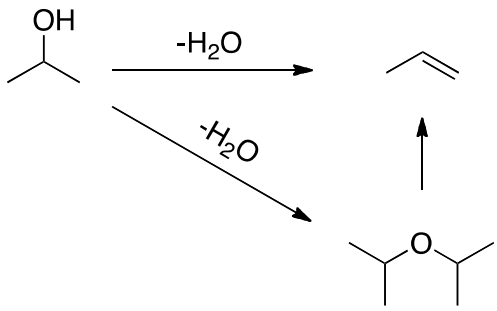

5.3.3.2 Effect of zeolite framework

From Table 5.7, it is observed that zeolite Y and β provide relatively higher activity, as compared to other zeolites (at 15 g.h.mol^{-1}).

Table 5.7 Effect of zeolite frameworks to *i*-propanol dehydration

Zeolite	Si/Al	Contact time (g.h.mol^{-1})	Conversion (C mol%)	Selectivity (C mol%)	
				Propylene	Di-isopropyl ether
HY	8	3	18	51	49
H-β	13	3	59	90	10
HY	8	15	90	99	0.5
H-β	13	15	100	100	-
H-Mordenite	15	15	28	80	20
HZSM-5	13	15	55	98	2

Results at 6th hour on stream, 448K, H_2 as carrier 30 mL/min

However, the cage structure of Y can retain both feed and products, which promotes the inter-molecular dehydration, as observed from high diisopropyl ether selectivity at low contact time (3 g.h.mol^{-1}). At higher contact time (15 g.h.mol^{-1}), it is clear that the catalyst with three dimensional pore opening (H-β) provides higher activity, as compared to those with two and one dimensional pore opening (HZSM-5 and H-Mordenite), respectively. With a comparable Si/Al, this result suggests that diffusivity of the feed and products plays important role on dehydration at relative low temperature (448 K). As the three dimensional pore system possesses better mass transfer, the feed can access the active site more rapidly and the less products is retained. On the other hand, the catalyst with poor mass transfer (one and two dimension pore), re-hydration may well take place at high contact time. Moreover, the long retention time of products obstructs the access of incoming feed. Hence, Mordenite gives lower activity; as compared to ZSM-5 despite the larger pore size. In

addition, ZSM-5 yields only 2% diisopropyl ether at 55 % conversion while β gives 10% di-isopropyl ether at similar conversion. The result indicates that the medium pore size of ZSM-5 constrains the size of bi-molecular intermediates as well as products while the large pores of β provides intrinsic space for the bimolecular reaction. In contrast, the large one-dimensional pore system particularly enhances the inter-molecular dehydration as the feed can be exceedingly retained in the pore. In line with this view, thermogravimetric analysis shows that < 1 % hard coke is detected on the used zeolite with medium pore while > 3% is observed for the larger ones (Table 5.4). The TGA under N_2 defines that most of deposits in HZSM-5 are the high molecular weight compounds probably from oligomerization of olefin. They cannot diffuse out of pore at testing temperature.

5.3.3.3 Effect of reaction temperature

Due to the endothermic nature of dehydration, the increased *i*-propanol conversion over HZSM-5 is expected when the reaction temperature is increased (Figure 5.14).

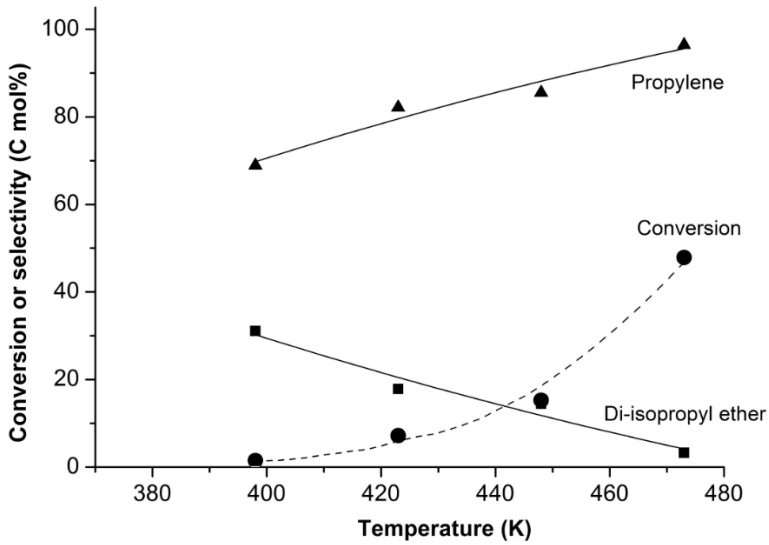

Figure 5.14 Effect of reaction temperature on *i*-propanol dehydration over HZSM-5 (Si/Al=13)

W/F 8 g.h.mol^{-1}; H_2 as carrier 30 mL/min

With similar reason, the further dehydration of di-isopropyl ether to propylene is also promoted as seen from the increase in propylene with the decrease in di-isopropyl ether selectivity, when the temperature is increased. Again, the effect of pore size is revealed particularly at lower temperature. When H-β was used (Figure 5.15), similar pattern to H-ZSM-5 was observed.

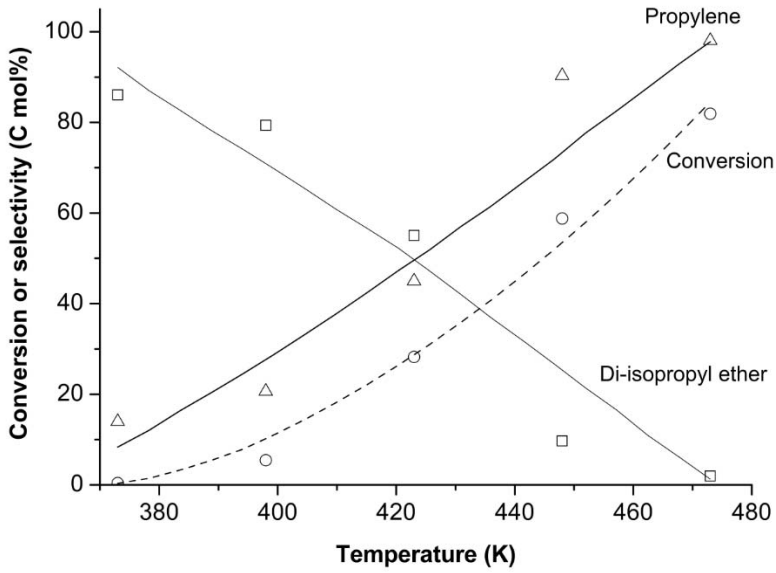

Figure 5.15 Effect of reaction temperature on *i*-propanol dehydration over H-β (Si/Al=13)

W/F 3 g.h.mol^{-1}; H_2 as carrier 30 mL/min

As discussed in 5.3.3.2, β possesses higher activity, as compared to ZSM-5, but higher selectivity to di-isopropyl ether at low temperature. No higher hydrocarbon was detected up to 473 K for both catalysts at this temperature range, presumably due to the strong adsorption of the alcohol and ether over the acid sites.

5.3.4 Ketones hydrodeoxygenation to olefins

To combine the hydrogenation–dehydration with exothermic and endothermic nature into one process, temperature has to be primarily optimized. For nickel-zeolite system, hydrogenation with no hydrogenolysis takes place at 373-448 K (Figure 5.7). While, the dehydration rate increases continuously above 423 K (Figure 5.14). Accordingly, only small gap from 423 to 448 K is allowed for a consecutive hydrogenation-dehydration over Ni/SiO_2-zeolite system, as illustrated below;

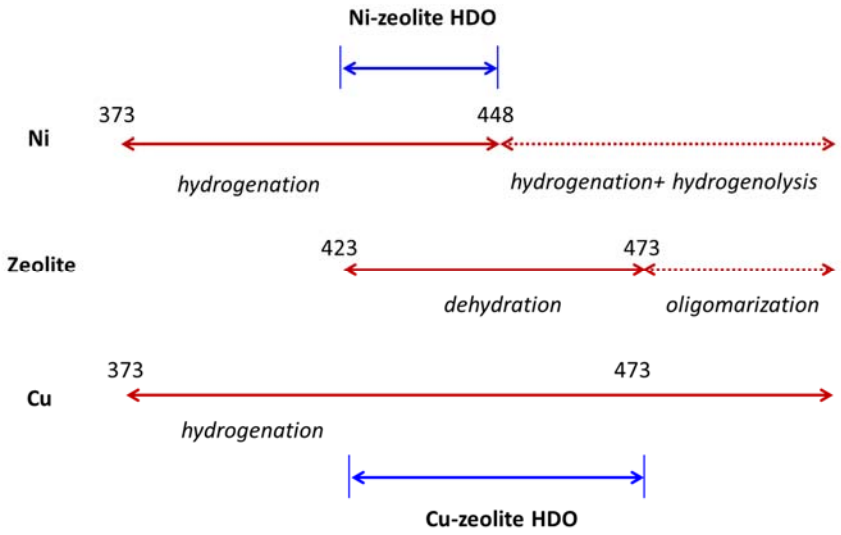

For Cu/SiO_2-zeolite system, no hydrogenolysis is promoted up to 575 K (Figure 5.8). However, the reaction over acid site is limited at 473 K to avoid the drastic oligomerization [49]. Accordingly, the window for hydrodeoxygenation over Cu/SiO_2-zeolite system is widely opened from 423 to 473 K.

In this section, the temperature at 448 K was selected for Ni/SiO_2-zeolite system to obtain the maximum dehydration rate without hydrogenolysis. Since olefin hydrogenation can also be promoted over Ni/SiO_2 (Table 5.3), the hydrodeoxygenation was conducted in two-bed system to prevent the re-adsorption of olefin on metal. The ketone was hydrogenated over Ni/SiO_2 to an alcohol that became a feed for the dehydration to olefin over the zeolite bed. For Cu/SiO_2-zeolite system, hydrogenation of olefin is not promoted. Hence, a single bi-functional bed system can be used for mild HDO over Cu/SiO_2-zeolite catalyst. A higher temperature (at 473 K) was chosen to

obtain high hydrogenation and dehydration rate without oligomerization of the olefin products. However, an undesirable condensation of acetone may take place over the acid sites as shown in section 4.3.2.1 (Chapter 4). Moreover, the ketone hydrogenation activity is relatively low, as compared to that of the alcohol dehydration. Accordingly, the metal component in the bi-functional bed system has to be greater than that of the zeolite.

5.3.4.1 Double bed system of Ni/SiO_2–zeolite

For this system, HZSM-5 (Si-Al=13) was used to minimize the ether formation. Table 5.8 shows that up to 60% conversion can be obtained at 76+7 g.h.mol^{-1}.

Table 5.8 Ketones hydrodeoxygenation on 5%Ni/SiO_2-HZSM-5 double-bed system

Feed	**Contact time** (g.h/mol) 1st bed + 2nd bed	**Conversion** (C mol%)	**Selectivity** (C mol%)			
			Alcohols	Ethers	*n*-Alkenes	*i*-Alkenes
Acetone	76+7	62	52	0.6	47	-
	76+29	60	16	-	84	-
MEK	76+7	62	39	-	52	9
	76+29	59	-	-	87	13

Result at 6th hour on stream, 448 K, (1st bed+2nd bed), H_2 as carrier 30 mL/min, HZSM-5 (Si/Al=13)

However, *i*-propanol and diisopropyl ether, which are intermediates, still remain in large amount. By increasing the zeolite bed (76+27 g.h.mol^{-1}), only 10 % *i*-propanol is observed without ether. The propylene is produced selectively (90% mol). Only a hydrogen is consumed for HDO of an acetone to a propylene as shown below;

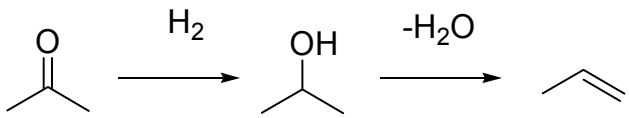

No aldol product derived from the condensation of acetone on zeolite is detected. This is probably because of strong adsorption of alcohol that prevents aldol condensation of the ketone. However, a slight deactivation can be observed for the dehydration bed. This is concluded from a gradual decline in propylene selectivity while the acetone conversion remains unchanged over 7 hours on stream (Figure 5.16).

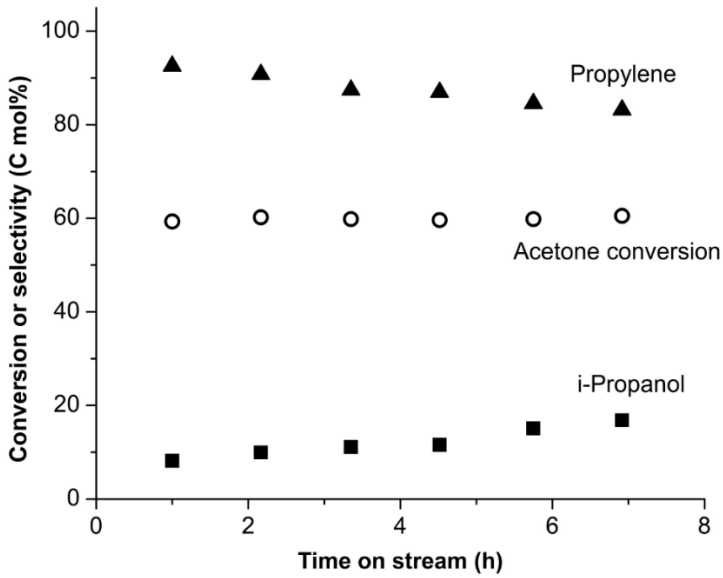

Figure 5.16 Hydrodeoxygenation of acetone over 5%Ni/SiO_2-HZSM-5 double-bed system for 7 hours on stream

H_2 as carrier 30 mL/min, 448 K, 76+7 g.h.mol^{-1} (1st bed+2nd bed), HZSM-5 (Si/Al=13)

In line with the deactivation, the TGA of spent HZSM-5 with *i*-propanol dehydration reveals the production of high molecular weight compound that may block the accessibility of the alcohol to the active sites (Table 5.4). When a larger ketone,

methyl ethyl ketone (MEK), is tested, a similar activity is obtained (~ 60%). However, relative low selectivity to the alcohol (2-butanol) is observed due to the higher dehydration reactivity of butanol, as compared to *i*-propanol. Again, no ether and aldol product are detected for hydrodeoxygenation of MEK. This is presumably due to a larger steric constrain of any C4 species in the zeolite pore which inhibits the bi-molecular reaction (either etherification of the alcohol and aldol condensation of the ketone). Hence, the butanol produced from MEK hydrogenation is selectively dehydrated to *n*-butene (1-butene + 2-butene; 87%) as displayed below;

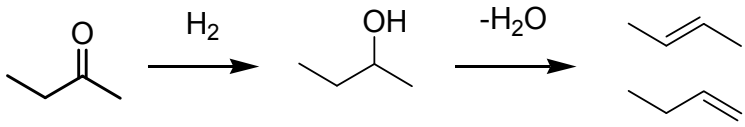

Over the Brønsted acid site in zeolite, these butenes can be isomerized to *i*-butene (13%) due to the higher stability of tertiary carbenium ion, as compared to the secondary carbenium ion, as illustrated below;

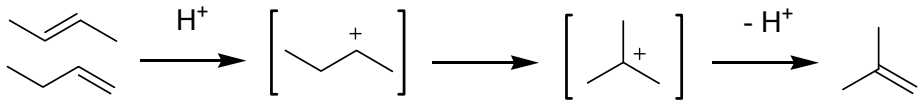

5.3.4.2 Cu/SiO_2–zeolite mixed bed

For a single mixed bed, 5% Cu/SiO_2 was mixed with the zeolites using high metal/zeolite ratio at 473 K to prevent the condensation of ketone, facilitated by the zeolites. From Table 5.9, it is seen that 68 % conversion with excellent selectivity to propylene (96 %) is obtained over the 76+7 bed (For contact time, 76+7 refers to 76 g.h.mol^{-1} of Cu/SiO_2 and 7 g.h.mol^{-1} of HZSM-5 (Si/Al=13); 83 g.h.mol^{-1} in total).

Table 5.9 Ketones hydrodeoxygenation on mixed 5%Cu/SiO_2–zeolites

Feed	Catalyst	Temp. (K)	Contact time (g.h/mol) Metal+Zeolite	Conversion (C mol%)	Selectivity (C mol%)				
					Alcohols	n-Alkenes/ cycloalkenes	i-Alkenes/ methyl cycloalkenes	Acetic acid	Mesityl oxide
Acetone	5%Cu/SiO_2 +HZSM-5	473	76+7	68	4	96	-	-	-
	5%Cu/SiO_2+H-β	473	76+7	21	-	75	4	2	19
		473	76+2	41	7	93	-	-	-
MEK	5%Cu/SiO_2 +HZSM-5	473	76+7	56	4	82	14	-	-
Cyclohexanone	5%Cu/SiO_2 +HZSM-5	473	76+7	100	-	96	4	-	-
		473	27+3	46	43	57	-	-	-
		423	76+7	58	64	36	-	-	-

Result at 6th hour on stream, H_2 as carrier 30 mL/min, Si/Al of HZSM-5 and H-β are 13

A significant improvement in acetone conversion over the mixed bed, as compared to the equilibrium value (45% at 473 K, Figure 5.8) for acetone-alcohol, is due to a simultaneous conversion of *i*-propanol to propylene over the acid catalyst. Therefore, a part of *i*-propanol is removed and the concentration of alcohol in system is decreased. This will subsequently reduce the rate of *i*-propanol dehydrogenation to acetone and hence lift the conversion of the acetone beyond such equilibrium level. With this catalyst composition and reaction conditions, no condensation products from acetone is observed. In fact, small amount *i*-propanol (3%) is intentionally retained to competitively adsorb and inhibit the condensation of the ketone.

However, when H-β (Si/Al=13) is mixed with Cu/SiO_2 (76+7 g.h.mol^{-1}), the acetone conversion at 6 hours on stream (21%) drops drastically, as compared to HZSM-5. This is because β possesses a larger pore size, as compared to ZSM-5. This facilitates a better diffusion and adsorprtion of acetone in the pore of β. Hence, relatively less fraction of the acetone interact with the metal surface and hydrogenation is limited. In line with this view, the aldol condensation and cracked products namely mesityl oxide, acetic acid and *i*-butylene ($\sim$ 20% in total) are instead produced, as previously observed in section 4.3.2.1 (Chapter 4) and literatures [50-51]. Since aldol condensation is largely pronounced, high molecular weight deposits (Table 5.4) and a rapid deactivation can be expected as discussed in section 4.3.2.5 (Chapter 4). Accordingly, reducing the contact time of β to 2 g.h.mol^{-1} provides 92% propylene selectivity without the condensation products. However, the acetone conversion is still lower than that over Cu/SiO_2+HZSM-5.

When larger ketone (i.e. MEK) is tested over 5% Cu/SiO_2+HZSM-5 mixed catalyst (Table 5.9), the conversion (56%) is slightly lower than the acetone. This is probably due to steric hindrance of the adsorbed ketone on the metal surface. High selectivity to 1-butene and 2-butene (82%) is observed with some isomerization products (*i*-butylene; 14%) and 2-butanol (4%). For larger cyclic ketone, cyclohexanone is more reactive than the aliphatic ketone. This is due to the stronger adsorption of cyclohexanone, as compared to those of acetone and MEK. 96% selectivity to cyclohexene is obtained via HDO as demonstrated below;

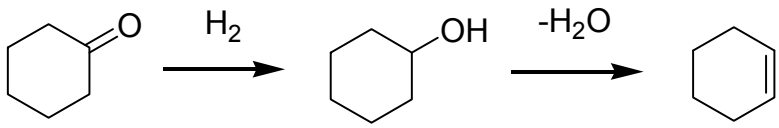

In similar manner to butenes, the cyclohexene can then be isomerized to methylcyclopentenes (4%);

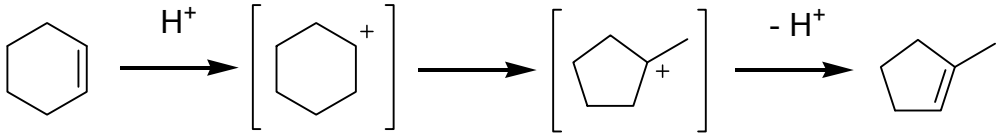

It is also worth noting that reducing the reaction temperature (423 K) or contact time (27+3 g.h.mol^{-1}) can prevent the secondary reaction like isomerization as seen in Table 5.9. However, this also decreases the dehydration rate significantly.

5.3.4.3 Bi-functional catalyst: Cu/zeolites

As high selectivity to olefin was observed over Cu/SiO_2+HZSM-5 system, Cu incorporated HZSM-5 (Cu/HZSM-5 (Si/Al=150, 5%wt Cu loading)) was primarily tested for acetone conversion. It is worth noting that zeolites with higher Si/Al (150) were used for the bi-functional catalyst in order to keep the number of acid sites and metal loadings similar to the mixed bed system. From Table 5.10, 100% acetone conversion can be obtained at 83 g.h.mol^{-1}, as compared to 67.5% from the mixed bed at 76+7 g.h.mol^{-1} (Table 5.9).

Table 5.10 Ketones hydrodeoxygenation on Cu/zeolites

Feed	Catalyst	Contact time (g.h/mol)	Conversion (C mol%)	Selectivity (C mol%)			
				Alcohols	n-Alkenes / cycloalkene	*i*-Alkenes / methyl	Alkanes
Acetone	Cu/HZSM-5	83	100	-	69	-	31
	Cu/HZSM-5	19	52	16	82	-	2
	Cu/HY	19	91	6	89	-	5
MEK	Cu/HY	19	25	-	87	13	-
Cyclohexanone	Cu/HY	19	85	18	82	-	-

Result at 6th hour on stream, H_2 as carrier 30 mL/min, 473 K, Si/Al of HZSM-5 and HY are 150, 5%wt Cu loading for all catalysts

A remarkable increase in activity, as compared to the mixed catalyst, is due to the close proximity for the metal and the acid sites. The hydrogenated intermediate, *i*-propanol, may well be removed immediately by dehydration over a near-by acid site, diminishing reversible dehydrogenation of the *i*-propanol to acetone. While, for the mixed catalysts, the dehydrogenation can be partially occurred due to relative longer range in a proximity between the catalyst particles, as compared to the adjacent metal-acid in bi-functional catalyst. This successive dehydration of *i*-propanol to propylene results in a significant increase in acetone hydrogenation over the Cu catalysts. As a result, the turnover frequency for hydrodeoxygenation over Cu/HZSM-5 (8.1×10^{-3} sec^{-1}) is approximately three-fold higher than that of hydrogenation over Cu/SiO_2 (2.6×10^{-3} sec^{-1}) at 473 K (Table 5.5).

Table 5.11 Turn over frequency for acetone hydrogenation of Cu/zeolite catalysts

Catalyst	Cu area (m^2/g_{Cu})	Contact time (g.h/mol)	TOF $x10^{-3}$ (sec^{-1})
Cu/HY	499	19	11.8
Cu/HZSM-5	414	19	8.1
Cu/SiO_2	646	30	2.6

473 K, H_2 as carrier 30 mL/min, Si/Al of HZSM-5 and HY are 150, 5%wt Cu loading for all catalysts

However, propane is also produced over the bi-functional catalyst, probably via the hydrogen transfer. It is likely that, at high contact time, propylene can be adsorbed onto the acid site. The hydrogenation of the adsorbed propylene may well be promoted by metal-acid site interaction. In other words, the adsorbed hydrogen on the metal can be source of hydrogen transfer to the adsorbed olefin on the proximate acid site;

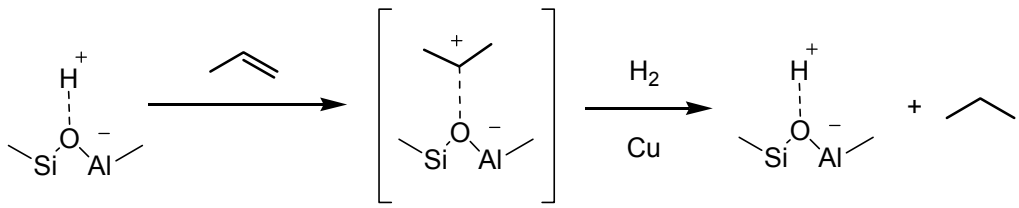

It should be noted that direct hydrogenation of propylene over copper metal surface is not the case, as evidenced and discussed in section 5.3.2.1. As the *i*-propanol possesses high adsorptivity on the acid site, the propylene hydrogenation over Cu/zeolites can be diminished by a decrease in contact time. This will decrease adsorbed propylene on the acid site when large amount of alcohol is present in the reaction stream. For a comparison of zeolite frameworks, Cu/HY (Si/Al=150, 5%wt Cu loading) shows a higher acetone conversion than Cu/HZSM-5. This is because the HY, the large and three dimension pore, possesses a better mass transfer, adsorption, and

dehydration activity, as compared to HZSM-5 as discussed in section 5.3.3.2. Moreover, the dispersion of copper in the pore of HY is higher than that of HZSM-5. As seen from Figure 5.5-5.6, formation of adjacent metal-acid is observed from Cu in HY and the external Cu particle is obtained in HZSM-5. For further catalytic testing, Cu/HY is the selected catalyst due to i) higher hydrogenation and dehydration rate ii) excellence specificity for hydrogenation-dehydration.

Over Cu/HY, the activity is in the order of acetone > cyclohexanone > MEK, respectively. As *i*-butylene, from HDO-isomerization of MEK, is the most reactive olefins among this comparison (others are propylene and cyclohexene), the observed low activity for MEK is due to a rapid deactivation as seen by relatively higher carbon deposit shown in Table 5.4. The oligomerization of the *i*-butylene takes place rapidly when tertiary carbenium ion is generated by zeolites even at low temperature (448 K), as mentioned in section 4.3.2.3 (Chapter 4). For cyclohexene, the oligomerization is also promoted particularly over the catalyst with larger pore opening such as HY. Accordingly, as the catalyst is deactivating, the observed activity of cyclohexanone conversion at 6^{th} hours on stream become slightly lower than that of acetone. Although the cyclohexanone shows a higher conversion over the 5%Cu/SiO_2+HZSM-5 mixed catalyst (Table 5.10), the large pore size with the cage structure of Y enhances the oligomerization of cyclohexanone, as compared to that over the medium channel of HZSM-5. The amount of coke deposit is in line with the observed activity (Table 5.4).

5.4 Conclusion

The optimization of reaction conditions and catalyst system for both hydrogenation and dehydration leads to a potential approach for ketone deoxygenation to olefins. Nickel catalyst is more reactive than the copper, but it is also capable to promote hydrogenation of the olefin produced. For the dehydration, the large pore zeolite like H-β and HY is excellence in activity while medium pore of HZSM-5 is outstanding for ether suppression. Accordingly, a double bed system containing Ni/SiO_2 and HZSM-5 is ideal for ketone hydrodeoxygenation to olefins. On the other hand, the mixed Cu/SiO_2+HSZM-5 and bi-functional Cu/zeolites catalysts can be used for single bed system. For the mixed catalyst, copper can hydrogenate ketone to alcohol without hydrogenolysis and it is somewhat inert for olefin hydrogenation. While, zeolites can promote dehydration of the alcohol formed at the same temperature range ($\leq$ 473 K).

The simultaneous conversion of ketone to alcohol and alcohol to alkene boosts the ketone conversion to exceed the ketone-alcohol equilibrium level. However, when the copper is incorporated into zeolites as bi-functional catalyst, the dispersion of copper in HZSM-5 is limited by its pore size. While, a close-proximity of copper-acid formed in large pore of HY offers the activity higher than copper in HZSM-5 as the alcohol formed is immediately removed over the neighboring acid sites. The reactivity of various ketones strongly depends on the deactivation by olefin produced. The order of reactivity is acetone > cyclohexanone > MEK.

5.5 References

[1] Elliott D.C., Hart T.R., Neuenschwander G.G., Rotness L.J. and Zacher A.H. "Catalytic Hydroprocessing of Biomass Fast Pyrolysis Bio-oil to Produce Hydrocarbon Products" **Environmental Progress & Sustainable Energy,** vol.28, 2009. pp.441-449.

[2] Baker E.G. and Elliott D.C. **Catalytic Hydrotreating of Biomass-Derived Oils.** 1st ED. Washington DC: American Chemical Society. 1988.

[3] Wildschut J., Melián-Cabrera I. and Heeres H.J. "Catalyst studies on the hydrotreatment of fast pyrolysis oil" **Applied Catalysis B: Environmental,** vol.99, 2010. pp.298-306.

[4] Fisk C.A., Morgan T., Ji Y., Crocker M., Crofcheck C. and Lewis S.A. "Bio-oil upgrading over platinum catalysts using in situ generated hydrogen" **Applied Catalysis A: General,** vol.358, 2009. pp.150–156.

[5] Naylor M.A. **"Liquid Phase Oxidation of Propylene to Acrylic Acid in the Presence of an Mn or Ni Catalyst"** U.S. patent no.3271447, 6 Sep 1966.

[6] Sert E. and Atalay F.S. "Esterification of Acrylic Acid with Different Alcohols Catalyzed by Zirconia Supported Tungstophosphoric Acid" **Industrial & Engineering Chemistry Research,** vol.51, 2012. pp.6666-6671.

[7] Kautter C.T. and Baumann U. **"Esterification of Acrylic Acid"** U.S. patent no.3458561, 29 Jul 1969.

[8] Wu L., Wang G. and Chen X. "**Fluidize-Bed Catalyst for Propylene Ammoxidation to Acrylonitrile**" U.S. patent no.6420307B1, 16 Jul 2002.

[9] Menon P.G. "On the Mechanism of Ammoxidation of Propylene to Acrylonitrile" **Journal of Catalysis,** vol.50, 1979. pp.314-316.

[10] Forni L., Tescari M., and Zambelli P. "Pyridines by Propylene Ammoxidation: Catalyst Structure and Reaction Selectivity" **Journal of Catalysis,** vol.65, 1980. pp.470-474.

[11] Liu Y., Murata K., Inaba M. and Mimura N. "Selective oxidation of propylene to propylene oxide by molecular oxygen over Ti-Al-HMS catalysts" **Catalysis Letters,** vol.89, 2003. pp.49-53.

[12] Ghosh S., Acharyya S.S., Tiwari R., Sarkar B., Singha R.K., Pendem C., Sasaki T. and Bal R. "Selective Oxidation of Propylene to Propylene Oxide over Silver-Supported Tungsten Oxide Nanostructure with Molecular Oxygen" **ACS Catalysis**, vol.4,. 2014. pp.2169–2174.

[13] Robeson M.O. and Webb T.P. **"Hydrolysis of 1,2-Propylene Oxide to 1,2-Propylene Glycol"** U.S. patent no. 2623909, 30 Dec 1952.

[14] Silva L.P. and Barbosa E.F., Editor. **In Polypropylene**. Nova Science Publishers, Inc. 2013.

[15] Zhang L.Y., Fan G.Q., Guo C.Y., Dong J.Y., Hu Y.L. and Huang M.B. "Synthesis of polypropylene block copolymers from brominated styrene-terminated isotactic polypropylene" **European Polymer Journal,** vol.42, 2006. pp.1043–1050.

[16] Rahman A. "Catalytic Hydrogenation of Acetone to Isopropanol: An Environmentally Benign Approach" **Bulletin of Chemical Reaction Engineering & Catalysis,** Vol.5 2010. pp.113–126.

[17] Stoddart C.T.H., Kemball C. "The Catalytic Hydrogenation of Acetone on Evaporated Metallic Films" **Journal of Colloid Science**, vol.11, 1956. pp.532-542.

[18] Qia S., Cheney B.A., Zheng R., Lonergan W.W., Yub W. and Chen J.G. "The effects of oxide supports on the low temperature hydrogenation activity of acetone over Pt/Ni bimetallic catalysts on SiO_2, γ-Al_2O_3 and TiO_2" **Applied Catalysis A: General,** vol.393, 2011. pp. 44–49.

[19] Yurieva T.M., Plyasova L.M., Makarova O.V. and Krieger T.A. "Mechanisms for hydrogenation of acetone to isopropanol and of carbon oxides to methanol over copper-containing oxide catalysts" **Journal of Molecular Catalysis A: Chemical,** vol.113, 1996. pp.113 455-468.

[20] Vidruk R., Landau M.V., Herskowitz M., Ezersky V. and Goldbourt A. "Control of surface acidity and catalytic activity of γ-Al_2O_3 by adjusting the nanocrystalline contact interface" **Journal of Catalysis,** vol.282, 2011. pp.215–227.

[21] Wade W.H., Teranishi S. and Durham J.L. “The Dehydration of Methanol and Isopropanol on Aluminas of Various Specific Surface Areas” **Journal of Colloid and Interface Science**, vol.21, 1966. pp.349-357.

[22] Jacobs P.A., Mortier W.J. and Uytterhoeven J.B. “Properties of Zeolites in Relation to Their Electronegativity: Acidity, Carboniogenic Acitivity and Strength of Interaction in Transition Metal Complexes” **Journal of Inorganic and Nuclear Chemistry,** vol.40, 1987. pp.1919-1923.

[23] Stone F.S. and Agudo A.L. “The Dehydration of Isopropanol Over Zeolite Catalysts” **Zeitschrift für Physikalische Chemie Neue Folge,** Bd. vol.64, 1969. pp.161—170.

[24] Ausavasukhi A. and Sooknoi T. “Additional Brønsted acid sites in [Ga]HZSM-5 formed by the presence of water” **Applied Catalysis A: General**, vol.361, 2009. pp.93–98.

[25] Peamaroon N. and Sooknoi T. “Aromatization of cyclopentane over ZSM-5 catalysts: a proposal of reaction pathway” **Petroleum Science and Technology**, vol.30, 2012. pp.1647–1655.

[26] Hoang D.L., Dang T.T.H., Engeldinger J., Schneider M., Radnik J., Richter M. and Martin A. “TPR investigations on the reducibility of Cu supported on Al_2O_3, zeolite Y and SAPO-5” **Journal of Solid State Chemistry**, vol.184, 2011. pp.1915–1923.

[27] Sagar G.V., Rao P.V.R., Srikanth C.S. and Chary K.V.R. “Dispersion and Reactivity of Copper Catalysts Supported on Al_2O_3-ZrO_2” **Journal of Physical Chemistry B,** vol.110, 2006. pp.13881-13888.

[28] Ausavasukhi A., Suwannaran S., Limtrakul J. and Sooknoi T. “Reversible interconversion behavior of Ag species in AgHZSM-5: XRD, ^{1}H MAS NMR, TPR, TPHE, and catalytic studies” **Applied Catalysis A: General**, vol.345, 2008. pp.89–96.

[29] Chen W.S., Chang F.W., Roselin L.S., Ou T.C. and Lai S.C. “Partial oxidation of methanol over copper catalysts supported on rice husk ash” **Journal of Molecular Catalysis A: Chemical**, vol.318, 2010. pp.36–43.

[30] Roh H.S., Dong W.S, Jun K.W., Liu Z.W., Park S.E. and Oh Y.S. “Partial oxidation of methane over Ni/SiO_2” **Bulletin-Korean Chemical Society**, vol.23, 2002. pp.669-673.

[31] Yao N., Ma H., Shao Y., Yuan C., Li D. and Li X. "Effect of cation–oligomer interactions on the size and reducibility of NiO particles on NiRu/SiO_2 catalysts" **Journal of Materials Chemistry**, vol.21, 2011. pp.17403-17412.

[32] Esposito S., Vecchio S.D., Ramis G., Bevilacqua M., Turco M., Bagnasco G., Cammarano C., Aronne A. and Pernice P. "Sol-gel synthesis of silicon cobalt mixed oxide nanocomposites" **Chemical Engineering Transaction**, vol.11, 2007. pp.83-88.

[33] Tang C.W., Wang C.B. and Chien S.H. "Characterization of cobalt oxides studied by FT-IR, Raman, TPR and TG-MS" **Thermochimica. Acta**, vol.473, 2008. pp.68–73.

[34] Nasir N.A.M., Zabidi N.A.M. and Kait C.F. "Synthesis and characterization of silica-supported iron nanocatalyst by modified colloidal method" **Journal of Applied Science**, vol.11, 2011. pp.1391-1395.

[35] Zhang C. H., Wan H. J., Yang Y., Xiang H. W. and Li Y. W. "Study on the iron–silica interaction of a co-precipitated Fe/SiO_2 Fischer–Tropsch synthesis catalyst" **Catalysis Communications**, vol.7, 2006. pp.733–738.

[36] Ge X., Zou H., Wang J. and Shen J. "Modification of Cr/SiO_2 for the dehydrogenation of propane to propylene in carbon dioxide" **Reaction Kinetics and Catalysis Letters**, vol.85, 2005. pp.253-260.

[37] Kim C.S. and Woo S.I. "Characterization of Cr/silica ethylene polymerization catalyst by TPO/TPR and FT-IR" **Jouml of Molecular Catalysis**, vol.73, 1992. pp.249-263.

[38] Strassberger Z., Alberts A.H., Louwerse M.J., Tanase S. and Rothenberg G. "Catalytic cleavage of lignin β-O-4 link mimics using copper on alumina and magnesia–alumina" **Green Chemistry**, vol.15, 2013. pp.768-774.

[39] Huo C., Ouyang J. and Yang H. "CuO nanoparticles encapsulated inside Al-MCM-41 mesoporous materials via direct synthetic route" **Scientific Reports**, vol.4, 2014. pp.1-9.

[40] Mann R.S. and Lien T.R. "Hydrogenation of propylene over group VIII metals" **Journal of Catalysis**, vol.15, 1969. pp.1-7.

[41] Brandao L., Fritsch D., Madeira L.M. and Mendes A.M. "Kinetics of propylene hydrogenation on nanostructured palladium clusters" **Chemical Engineering Journal**, vol.103, 2004. pp.89–97.

[42] Sitthisa S. and Resasco D.E. "Hydrodeoxygenation of furfural over supported metal catalysts: a comparative study of Cu, Pd and Ni" **Catalysis. Letter**, vol.141, 2011. pp.784–791.

[43] Buckley E. and Herington E.F.G. “Equilibria in some secondary alcohol+hydrogen+ketone system” **Transactions of the Faraday Society**, vol.61, 1965. pp.1618-1625.

[44] Fang X., Min X., Feng L.X. and Lan H.X. “Experimental study of isopropanol dehydrogenation over amorphous alloy Raney nickel catalysts” **Journal of Thermal Science**, vol.22, 2013. pp.613-618.

[45] Mooksuwan W. and Kumar S. “Study on 2-propanol/acetone/hydrogen chemical heat pump: endothermic dehydrogenation of 2-propanol” **International Journal of Energy Research**, vol.24, 2000. pp.1109-1122.

[46] Rodriguez J.A. and Goodman D.W. “Dissociative adsorption and hydrogenolysis of ethane over clean and Ni-covered Pt(1 1 1)” **Journal of Physical Chemistry**, vol.94, 1990. pp.5342-5347.

[47] Nash P. “Phase diagrams of binary nickel alloys” **ASM International**, 1991.

[48] Solomon H.J., Bliss H. and Butt J.B. “Catalysis of alcohol and ether dehydration on γ–alumina” **Industrial & Engineering Chemistry Fundamentals**, vol.6, 1967. pp.325–333.

[49] Occelli M.L., Hsu J.T. and Galya L.G. “Propylene oligomerization over molecular sieves Part I. Zeolite effects on reactivity and liquid product selectivities” **Journal of Molecular Catalysis**, vol.32, 1985. pp.377–390.

[50] Tago T., Konno H., Ikeda S., Yamazaki S., Ninomiya W., Nakasaka Y. and Masuda T. “Selective production of isobutylene from acetone over alkali metal ion-exchanged BEA zeolites” **Catalysis Today**, vol.164, 2011. pp.158–162.

[51] Cruz-Cabeza A.J., Esquivel D., Jiménez-Sanchidrián C. and Romero-Salguero F.J. “Metal-exchanged β zeolites as catalysts for the conversion of acetone to hydrocarbons” **Materials**, vol.5, 2012. pp.121-134.

Chapter 6

Keto-hydrodeoxygenation of acetic acid to propylene

6.1 Introduction

The controlled deoxygenation of acetic acid to olefins is one of the most challenging due to high oxygen content in the molecule, as compared to other feedstocks. Many works have focused on partially deoxygenation via ketonization over metal oxide catalysts (MgO, CdO, MnO_2, and Fe_2O_3) to acetone, CO_2 and water [1-7]. Alternatively, the dehydration of acetic acid to ethenone, which leads to rapid deactivation of catalyst, was also reported [8-9] Meanwhile, the hydrodeoxygenation (HDO) of acetic acid have been investigated over Pt-Sn alloy, Cu and Co catalysts. In this case, ethanol, acetaldehyde and ethyl acetate are obtained [10-12] The esterification facilitated by acidic support can increase the degree of oxygen removal but inhibit the further hydrogenation to hydrocarbons [13]. Many noble metals including Pt, Pd, Ni, and Rh were found to be effective catalysts for liquid and gas phase hydrogenation of acetic acid to hydrocarbons [1, 11, 14-15]. However, high H_2 pressure (> 4 MPa) or high temperature (typically > 698 K) are required to obtain appreciable activity over these metals [1, 16]. In addition, the hydrocarbons obtained are mainly paraffins (ethane and methane), presumably due to successive hydrogenation, decarboxylation and hydrogenolysis over those metals [11, 14, 17].

According to obstacles mentioned above, a novel approach for obtaining olefins from acetic acid via keto-hydrodeoxygenation process is proposed in this Chapter. Chapter 5 demonstrates that ketone can be hydrodeoxygenation to olefin via a controlled hydrogenation-dehydrogenation [18]. At the same time, acetic acid can be selectively ketonized over various metal oxides that are relatively inert for hydrogenation and dehydration [19-21] Hence, it is possible to incorporate these metal oxides into the hydrodeoxygenation catalysts for a single stage conversion of acetic acid to olefins via ketonization-hydrogenation-dehydration as illustrated below;

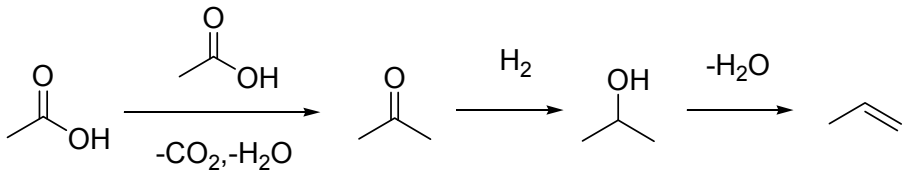

In this Chapter, CeO_2 will be selected as ketonization catalyst due to high activity especially at low temperature [5]. Cu/HY and Cu/HZSM-5, showing high hydrodeoxygenation activity from Chapter 5 (section 5.3.4.3), will be incorporated for hydrogenation-dehydration of the ketone formed. Despite the difference in catalytic parameters for each step, formulation of the three-component catalyst (CeO_2/Cu/zeolites) that works isothermally at relatively mild condition will be optimized. Their effects on the reaction and products are also highlighted, together with the role of water presents in acetic acid feed.

6.2 Experimental details

CeO_2 (99.9%) was purchased from Sigma-Aldrich®. HY and HZSM-5 were commercially obtained from Tohso and Zeochem®, respectively. The CeO_2 and zeolite were calcined in air at 723 K for 5 h before used. 5 %wt Cu/Zeolites were simply prepared by incipient wetness impregnation. Briefly, $Cu(NO_3)_2.3H_2O$ precursor (Ajax Fine Chem) was dissolved in deionized water (~ 0.01 M) and slowly droped onto zeolites until wet. The sample was dried at 333 K in an oven for 15 min, and then the loading was repeated until desired metal content was reached. The samples were kept to dry at 333 K overnight and calcined in air at 723 K for 5 h. The metal oxides were mixed with Cu/zeolites (7-40 %wt Cu/zeolites) then pelletized to the size of 600–850 μm. The three-component catalyst is referred to as CeO_2/Cu/Zeolite(X), where X is %wt of Cu/Zeolite in the mixed catalyst.

Elemental composition of the catalysts was determined by X-ray fluorescence spectrometer (XRF; Siemens). Specific surface area (BET) of catalysts was measured using nitrogen adsorption analyzer (Quantachrome) at 77 K and 0.05–0.30 P/P_0. Reducible metal oxide species in the catalysts were analyzed by temperature programmed reduction (TPR). The catalysts were treated in air at 723 K for 5 hours prior to heating from 323-1173 K in 10% H_2/Ar. The hydrogen consumption was recorded

with an on-line thermal conductivity detector (VICI) [22]. Copper dispersion on zeolites support was also analyzed by surface-selective TPR technique. Briefly after typical TPR, the sample was *in situ* treated with N_2O for selective oxidation of surface copper to copper (I) oxide at 333 K for 2 hours. Then, the surface-oxidized sample was subjected to a secondary TPR, in which the reduction took place only at the copper (I) oxide on the surface. The surface copper could be calculated directly from hydrogen consumption of Cu(I) ⟶ Cu(0) as described by Hoang *et al*. [23]. The Cu dispersion is referred to mole ratio of Cu on the surface over the bulk. Detail of calculations for Cu dispersion using this procedure can be found as described by Sagar *et al*. [24] Acidity of all zeolite samples was quantified by NH_3-TPD. 1% NH_3/He was pre-adsorbed at 323 K. TPD was carried out in He at 10 $K.min^{-1}$ from 323–973 K [25] The particle size of Cu on support was estimated by TEM with LaB_6 emitter (FEI Tecnai G^2 20, 200 kV).

The catalytic testing was conducted in a fixed bed flow reactor (6 mm i.d. Pyrex®) at atmospheric pressure. The CeO_2/Cu/Zeolites catalysts were primarily activated at 723 K (2 $K.min^{-1}$) under stream of air (30 $ml.min^{-1}$) for 5 h. Subsequently, the catalyst was flushed with N_2 and treated in H_2 at 723 K for another 2 h. The system was cooled down to the reaction temperature (573 K) and the acetic acid was introduced by a syringe pump at the rate of 0.5-1.0 g/h. The products were analyzed by an on-line GC-FID. A Hayesep® P (1/8" X 8') was used as separating column. The analysis condition for gas chromatography is shown in Appendix A.

6.3 Result and discussion

6.3.1 Characterization of catalyst

All Cu/zeolite samples possess relatively high surface area (> 360 $m^2.g^{-1}$) with 54-65% dispersion as tabulated in Table 6.1.

Table 6.1 % Dispersion, copper area, surface area, and acidity of copper catalysts and supports

Catalyst	Si/Al	%Cu content	% Dispersion	Cu area	BET surface area	Acidity (μmol/g)	
		%wt		(m^2/g_{Cu})	(m^2/g)	Weak	Strong
CeO_2	-	-	-	-	11	-	-
HY	153	-	-	-	713	54	65
HZSM-5	152	-	-	-	376	56	65
Cu/HY	166	5.1	65	499	568	158	62
Cu/HZSM-5	173	5.2	54	414	361	92	20

In this work, low acidity (low Al_2O_3) zeolites are selected supports for Cu/zeolites catalyst to prevent the aldol-codensation, occurring when acetone intermediate adsorbed on acid site. HZSM-5 and HY are compared at similar Si/Al (150). The copper loading is approximately 5%wt for both zeolites. The loading of copper into zeolite results in the decrease in surface area. This is because bulk metallic copper is obtained. A higher copper surface area of Cu/HY, as compared to Cu/HZSM-5, indicates that the dispersion of copper in HY is better than that in HZSM-5. No significant change in Si-Al is observed after loading the copper onto zeolites. The CeO_2 shows relatively low surface area (< 11 $m^2.g^{-1}$), due to low porosity. The increase in weak acidity of Cu/HY and Cu/HZSM-5, as compared to the parent zeolites (NH_3-TPD), is an evidence for partial exchangeable copper cation in zeolites as described in 5.3.1.

At approximately 5%wt Cu loading, the Cu/HY and Cu/HZSM-5 samples show two reduction peaks at 473 and 520 K (Figure 6.1), corresponding to copper oxide aggregates and highly dispersed copper oxide in the pore of zeolite, respectively [26-27].

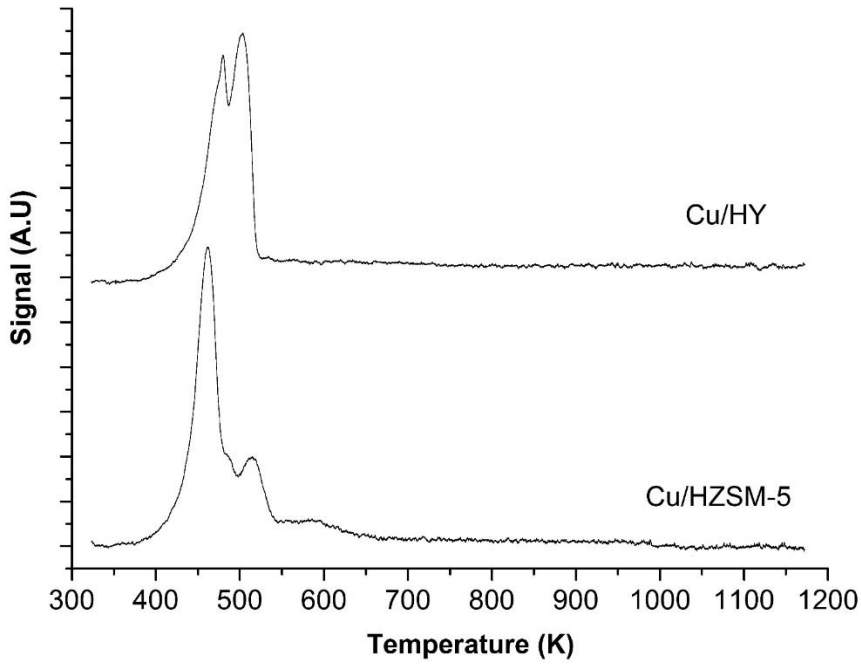

Figure 6.1 Temperature program reduction of Cu/zeolites, 5%wt Cu loading

The Cu dispersion on HY is somewhat higher than that on HZSM-5 (peak at ~ 520 K), presumably due to a better diffusion of the Cu precursor in the larger pore of HY. In consistence with TPR, the TEM results in section 5.3.1 (Chapter 5) reveal that Cu/HY possesses relatively small Cu particles (Figure 5.5a-b, Chapter 5) and some of them (dark spot) are well aligned in the pore of HY (light grey plane) as expressed in Figure 5.5c (Chapter 5). While a relatively lower Cu dispersion on HZSM-5 can be evidenced by large semicircle Cu particles, deposited on the external surface of HZSM-5 crystals (Figure 5.6, Chapter 5).

6.3.2 Catalytic activity testing

From Chapter 5, the ketone as well as alcohol and ether can be deoxygenated by hydrogenation-dehydration. The incorporation of ketonization in the deoxygenation series can improve the upgrading process covering most of oxygenate compounds in the light fraction of bio-oil. However, some preliminary test of acetic ketonization over cerium oxide is necessary to understand the limitation before the process design. As shown in Figure 6.2, only acetone is produced as deoxygenation product.

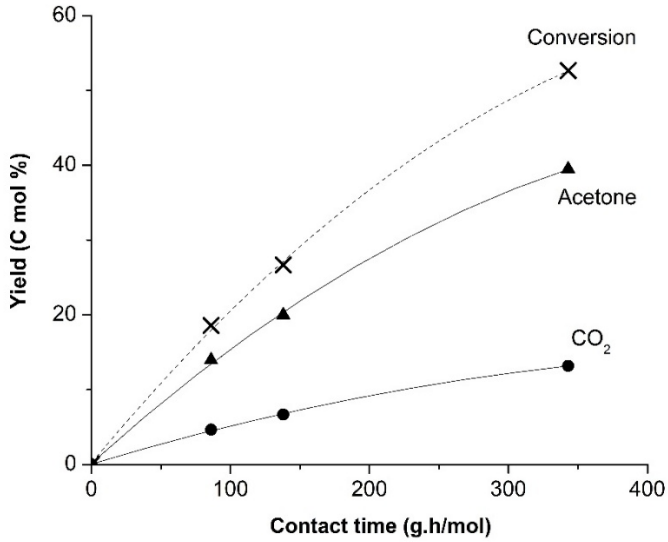

Figure 6.2 Effect of contact time on acetic acid ketonization over CeO_2

578 K, H_2 30 mL.min^{-1}

In this reaction, the oxygens in acetic acid are eliminated via formation of carbon dioxide and water following the scheme below;

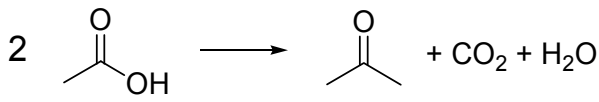

From Figure 6.3, it can be seen that the ketonization can be initially conducted at >523 K. Due to the endothermic nature of this process, a sharp increase in acetic acid conversion is observed when the temperature is increased. Again, only acetone is produced as deoxygenated product up to 623 K.

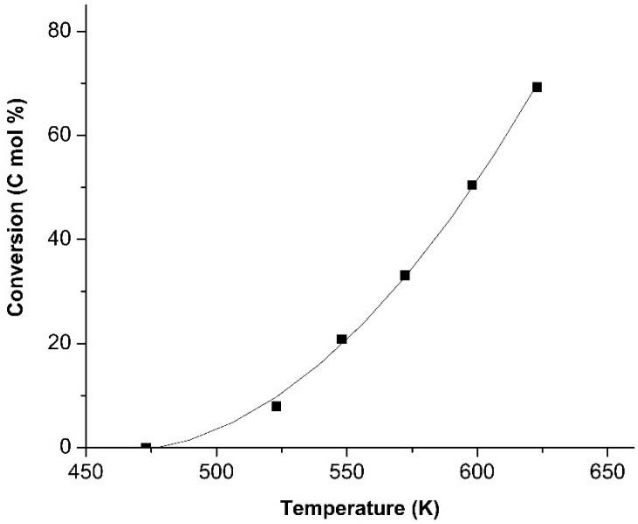

Figure 6.3 Effect of reaction temperature on acetic acid ketonization over CeO_2

138 g.h.mol^{-1}, H_2 30 mL.min^{-1},

selectivity i) acetone = 75 C mol% ii) CO_2 = 25 C mol%

As the hydrodeoxygenation of ketones to olefins takes place at temperature lower than that for ketonization (> 423 K, section 5.3.4.3), the keto-hydrodeoxygenation (KHDO) is limited by the ketonization. Therefore, the KHDO can be conducted at > 523 K as demonstrated below;

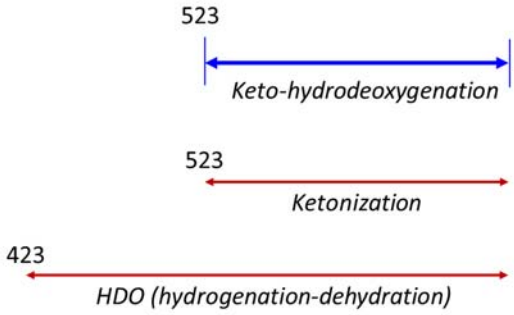

The cerium oxide is selected as ketonization catalyst for this Chapter, due to the outstanding acetone selectivity even at high temperature.

6.3.2.1 Effect of reaction temperature

Due to the difference in thermodynamic nature of the three reactions; ketonization, hydrogenation, and dehydration, the effect of temperature on acetic acid conversion was studied with a three-component catalyst containing 75%wt of CeO_2 and 25%wt of Cu/HY (CeO_2/Cu/HY(25)). It can be seen that the conversion increases gradually with the reaction temperature and reaches 100% at above 598 K (Figure 6.4a).

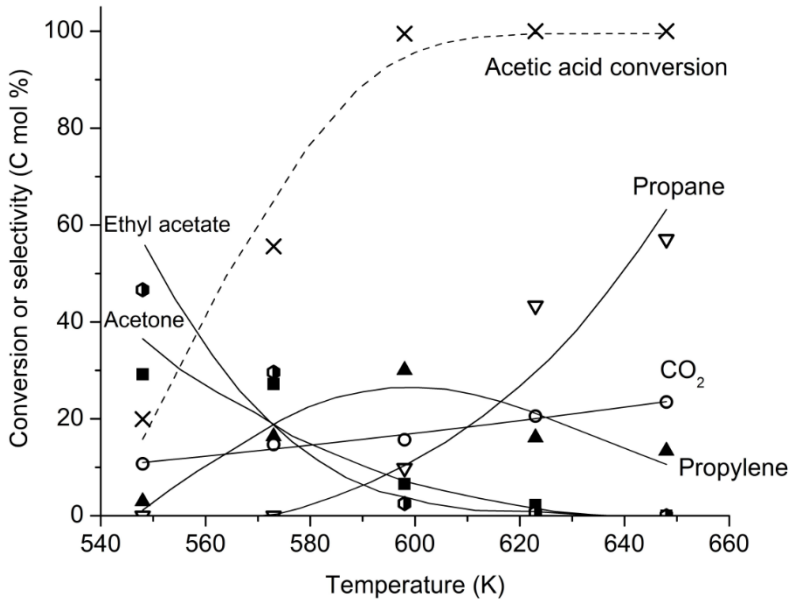

Figure 6.4a Effect of temperature to acetic acid KHDO over CeO_2/Cu/HY(25); conversion, propylene, propane, acetone, ethyl acetate, carbon dioxide

457 g.h.mol^{-1}, H_2 30 mL.min^{-1}

The C_3 products including acetone, propylene, and propane and CO_2 are produced via ketonization of acetic acid and subsequent hydrodeoxygenation of the acetone formed, so called keto-hydrodeoxygenation (KHDO) process as demonstrated below;

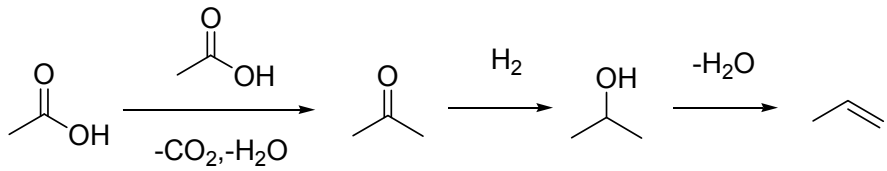

The selectivity to acetone is relatively high at 548 K suggesting that ketonization activity can be readily promoted over the CeO_2 component while the hydrogenation-dehydration of the acetone produced is not facilitated at this temperature. Hence, no propylene can be observed. This is probably due to competitive adsorption by acetic acid over the Cu/HY at low temperature. It is worth noting that, over Cu/zeolites, the hydrogenation-dehydration of acetone alone can be accomplished at > 473 K, as reported in 5.3.4.3 [18]. When the temperature is increased from 548-598 K, the selectivity to propylene increases with the decrease in acetone as expected. This is not only because acetic acid is less competitive at elevated temperature, but also the hydrogenation-dehydration is increasingly promoted by the Cu/HY component. However, the propylene selectivity turns down with a sharp increase in propane at > 598 K despite that the Cu alone cannot promote propylene hydrogenation [18,28]. The observed propane yield in this case is presumably derived from H-transferred to propylene. As propylene is formed, it would be protonated on the acid sites within a proximate vicinity of copper. Hence, some of the protonated propylene is then hydrogenated by H-transfer from the proximate metal sites as expressed below;

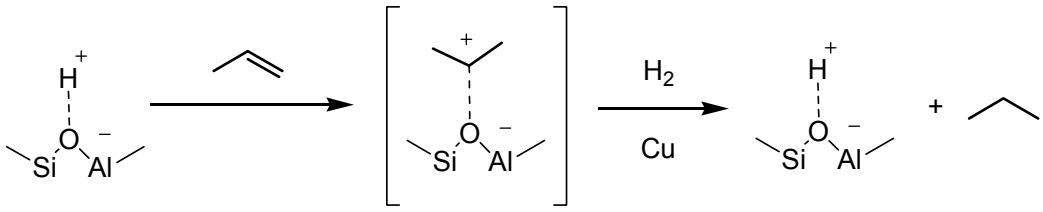

This is particularly the case at high temperature since H-transfer can also be promoted from the hydrocarbon pools [29-31].

As mentioned earlier that acetic acid competitively adsorbed on Cu/HY at low temperature, the C_2 products including acetaldehyde, ethanol, ethylene, and ethane are also observed, together with ethyl acetate as shown in Figure 6.4b.

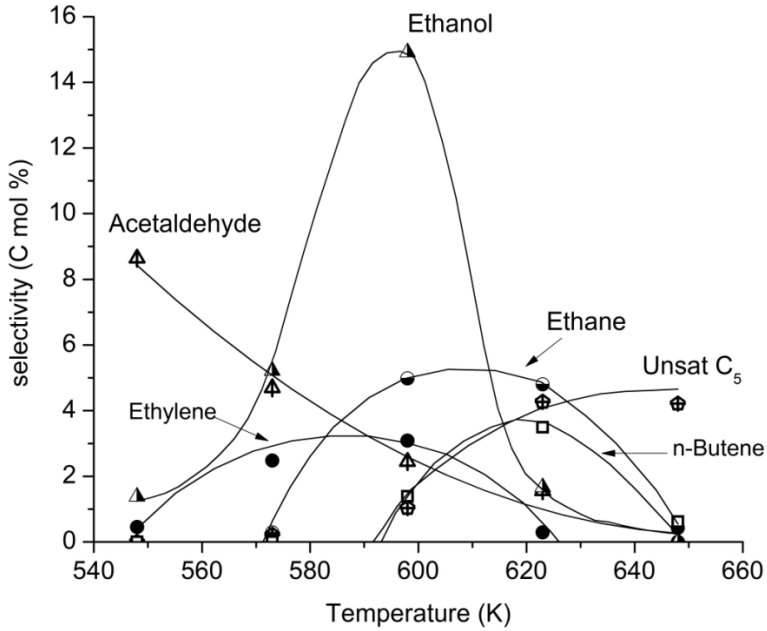

Figure 6.4b Effect of temperature to acetic acid KHDO over CeO_2/Cu/HY(25); ethylene, ethane, *n*-butane, C5 olefins, acetaldehyde, ethanol

457 g.h.mol^{-1}, H_2 30 mL.min^{-1}

The result from acetic acid conversion over Cu/zeolites alone (Table 6.2) reveals that these C_2 products are derived from a direct hydrodeoxygenation (HDO) of acetic acid.

Table 6.2 Direct HDO of acetic acid over Cu/zeolites

	Cu/HY	Cu/HZSM-5
Conversion (C mol%)	24	14
Selectivity (C mol%)		
Acetaldehyde	12	24
Ethanol	3	-
Ethyl acetate	81	43
Ethylene	4	16
Acetone	-	11
Propylene	-	2
CO_2	-	4

48 g.h.mol^{-1} and 573 K, H_2 30 mL.min^{-1}, 1st hour on stream

Over copper catalyst, the acetic acid can be hydrogenated to acetaldehyde and then ethanol as expressed below;

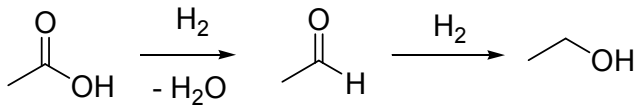

Acetaldehyde selectivity is decreased while ethanol, ethylene, and ethane are increased when the reaction temperature is raised from 548-598 K (Figure 6.4b). As the dehydration is a thermodynamically favored at high temperature, ethanol can be increasingly dehydrated to ethylene over the acid sites;

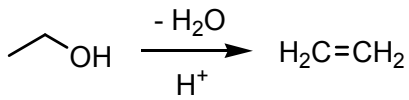

Accordingly, the acetaldehyde-ethanol equilibrium is not limited over Cu/HY because the ethanol produced is immediately dehydrated to ethylene. Hence, acetaldehyde is largely consumed by hydrogenation-dehydration process as the temperature is raised. In a manner similar to propane, ethane can also be produced by H-transfer to ethylene over adjacent copper-acid site at relatively high temperature;

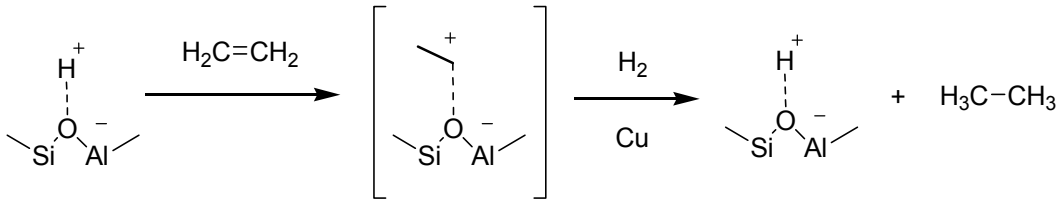

In fact, the observed high selectivity of ethyl acetate at low temperature (Figure 6.4a) suggests that ethanol is readily formed, but captured by acetic acid via esterification as illustrated below;

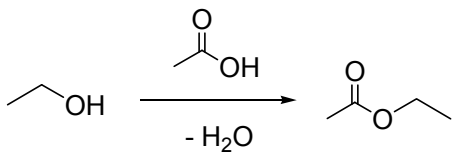

However, the selectivity to ester decreases when the temperature is increased due to the running low of acetic acid retained in the stream. It is noted that no esterification between acetic acid and *i*-propanol was found. This is because the generation of tertiary carbenium ion from *i*-propanol is easier than secondary carbenium ion from ethanol. Therefore, the *i*-propanol is rapidly dehydrated to propylene and no *i*-propanol is detected.

The selectivity to ethanol, ethylene and ethane turn down at > 598 K (Figure 6.4b) while C_3 hydrocarbons is largely observed. As the HDO and KHDO of acetic acid are parallel processes, the direct HDO of acetic acid is suppressed because the KHDO of

acetic acid is more favorable at high temperature. This is consistent with the observed increase in ketonization activity of CeO_2 at high temperature as shown in Figure 6.3. It is worth noting that, as the catalyst contains acidic zeolite (CeO_2/Cu/HY(25)), the ethylene and propylene produced can undergo oligomerization, as observed by the increase in C_4-C_5 olefins at > 598 K;

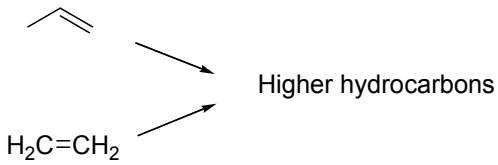

According to the products observed, the overall reaction scheme for conversion of acetic acid can be proposed as shown below;

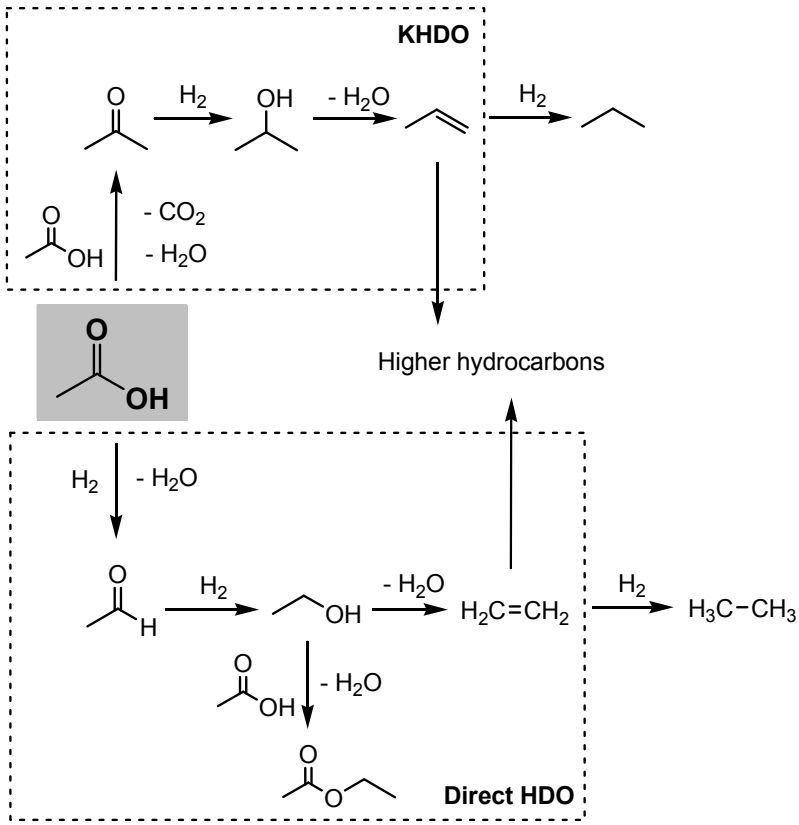

6.3.2.2 Effect of the catalyst composition

The KHDO of acetic acid depends largely on the component of catalyst, as shown by the experiments with various %weight of the CeO_2 in the catalyst composition (Figure 6.5). It is clear that the acetic acid conversion increases when the CeO_2 is increased (Figure 6.5a).

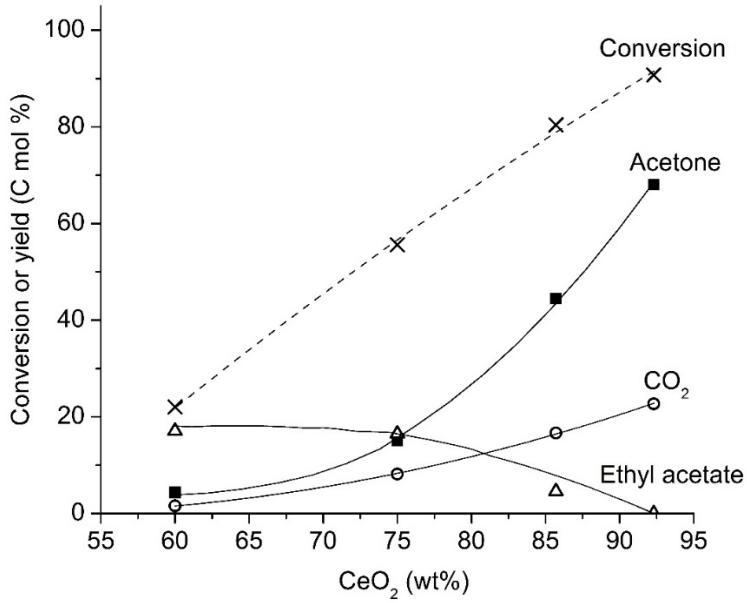

Figure 6.5a Effect of CeO_2/Cu/HY composition (from CeO_2/Cu/HY(40) to CeO_2/Cu/HY(7)) for acetic acid KHDO; conversion, acetone, ethyl acetate, carbon dioxide

457 g.h.mol^{-1} and 573 K, H_2 30 mL.min^{-1}, 1st hour on stream

Since the ketonization of acetic acid is primarily promoted in KHDO, the catalyst with high CeO_2 content would be more active for overall acid conversion. In consistence with this result, yield of KHDO products, including acetone (Figure 6.5a) and propylene (Figure 6.5b), are also increased, together with CO_2.

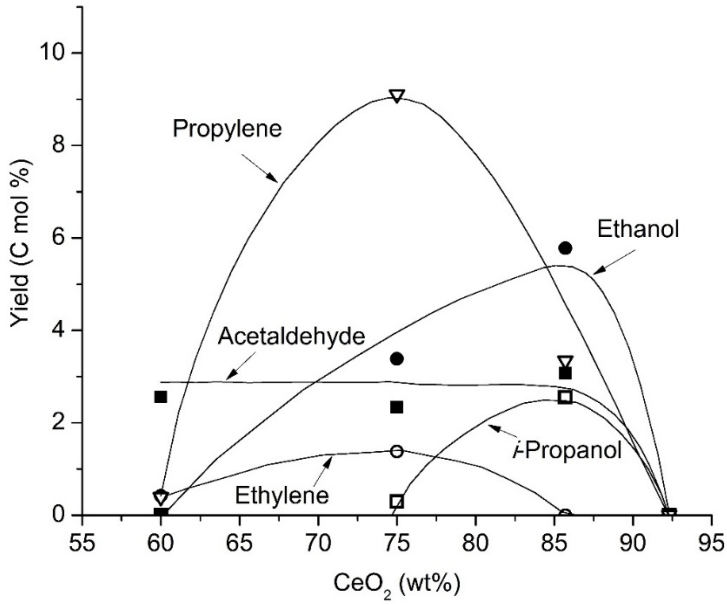

Figure 6.5b Effect of CeO_2/Cu/HY composition (from CeO_2/Cu/HY(40) to CeO_2/Cu/HY(7)) for acetic acid KHDO; propylene, *i*-propanol, ethylene, acetaldehyde, ethanol

457 g.h.mol^{-1} and 573 K, H_2 30 mL.min^{-1}, 1st hour on stream

However, the propylene production depends on both CeO_2 and Cu/zeolite (Figure 6.5b). Insufficient Cu/HY results to a drop of subsequent HDO activity, as seen by a decline in propylene yield when CeO_2 content is higher than 75%wt (CeO_2/Cu/HY(25)). On the other hand, the direct HDO of acetic acid depends on Cu/zeolite only. The increase in CeO_2 plays no significant role for direct HDO of acetic acid initially. Yields of ethyl acetate and acetaldehyde remain similar from 60 to 75%wt CeO_2 (CeO_2/Cu/HY(40) to CeO_2/Cu/HY(25)). The observed increase in ethanol yield (Figure 6.5b) is resulted from i) a decrease in acid site when Cu/HY is decreased ii) drop in esterification activity due to a decrease in retained acetic acid in the reaction stream when ketonization is boosted. As the ethanol is increased, dehydration to ethylene is also promoted initially. However, at CeO_2 content higher than 86%wt (CeO_2/Cu/HY(14)), the overall HDO activity is significantly suppressed. This is seen from drop of propylene, ethyl acetate, ethanol, acetaldehyde and ethylene. According to the results, it is clear that CeO_2 play significant role for initial activation of acetic acid to acetone while CuHY is essentially required for olefin production from both HDO of acetone produced and direct HDO of acetic acid. Hence, the combination of these catalysts would lead to a successful olefin production

from acetic acid. With the reaction conditions used in this study, optimum yields of propylene and ethylene can be obtained over CeO_2/Cu/HY(25) with ~ 55% conversion.

6.3.2.3 Effect of the zeolite framework

It is clear from Figure 6.6a that CeO_2/Cu/HZSM-5(25) is more active for acetic acid conversion, as compared with CeO_2/Cu/HY(25).

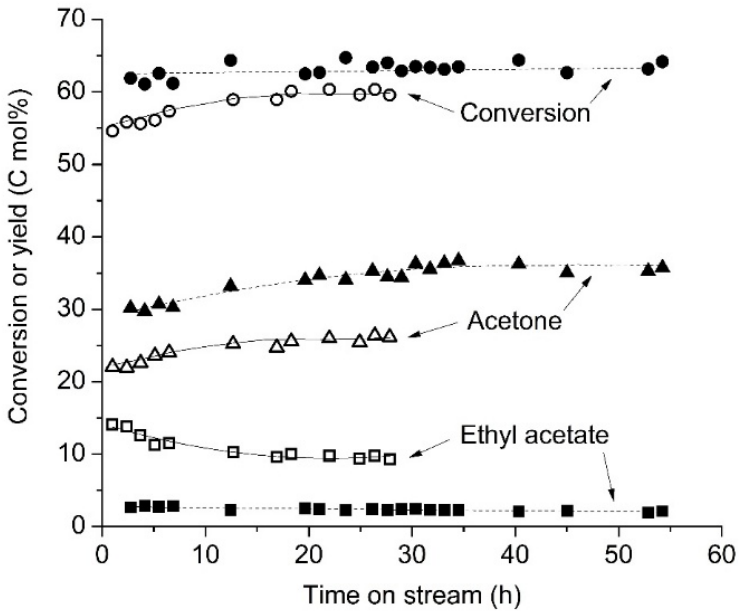

Figure 6.6a Comparison between CeO_2/Cu/HY(25) *(opened symbol)* and CeO_2/Cu/HZSM(25) *(closed symbol)* for acetic acid KHDO; conversion *(circle)*, acetone *(triangle)*, ethyl acetate *(rectangular)*

457 g.h.mol^{-1} and 573 K, H_2 30 mL.min^{-1}

This is because a similar level of conversion is obtained from both catalysts, despite that Cu/HZSM-5 possesses lower acidity (Table 6.1). However, at the similar level of conversion, acetone yield from CeO_2/Cu/HZSM-5(25), (~ 34%) is higher than that from CeO_2/Cu/HY(25) (~ 24%) while propylene yield from both catalysts is not so significantly different (3-5% differences) (Figure 6.6b).

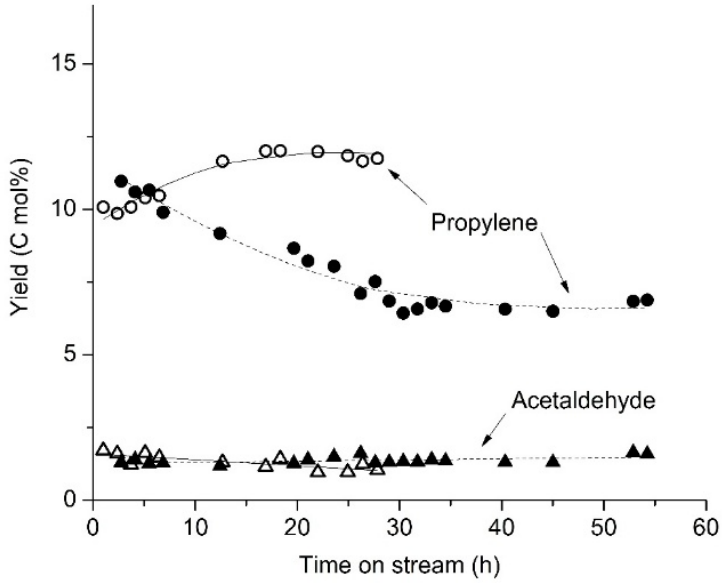

Figure 6.6b Comparison between CeO_2/Cu/HY(25) *(opened symbol)* and CeO_2/Cu/HZSM(25) *(closed symbol)* for acetic acid KHDO; propylene *(circle)*, acetaldehyde *(triangle)*

457 g.h.mol^{-1} and 573 K, H_2 30 mL.min^{-1}

At steady state, one may expect that as higher acetone is left unconverted, yield of propylene should be accordingly lower. Nevertheless, the observed increased yield of acetone without proportional change in propylene yield can be attributed to the fact that ketonization of acetic acid to acetone can also be facilitated by HZSM-5 [32-33], as seen in section 4.3.2.1 (Chapter 4). This is evidenced by a noticeable selectivity of acetone (11.3%) when acetic acid was fed over Cu/HZSM-5 alone (Table 6.2). Accordingly, the ketonization of acetic acid is additionally promoted as seen by higher yield to CO_2 over CeO_2/Cu/HZSM-5(25). However, the further hydrogenation-dehydration of the acetone produced to form propylene is somewhat limited over this catalyst. This is probably due to the competitive adsorption of acetic acid over the acetone in the zeolite and also the lower Cu dispersion as mentioned in 6.3.1 (Figure 5.6, Chapter 5).

Although CeO_2/Cu/HZSM-5(25), seems to be less effective for KHDO to produce propylene, this catalyst provides high selectivity for direct HDO of acetic acid to ethylene. It can be seen from Figure 6.6c that higher yield to ethylene can be obtained

from CeO_2/Cu/HZSM-5(25) while CeO_2/Cu/HY(25) gives mainly ethyl acetate by the esterification (Figure 6.6a).

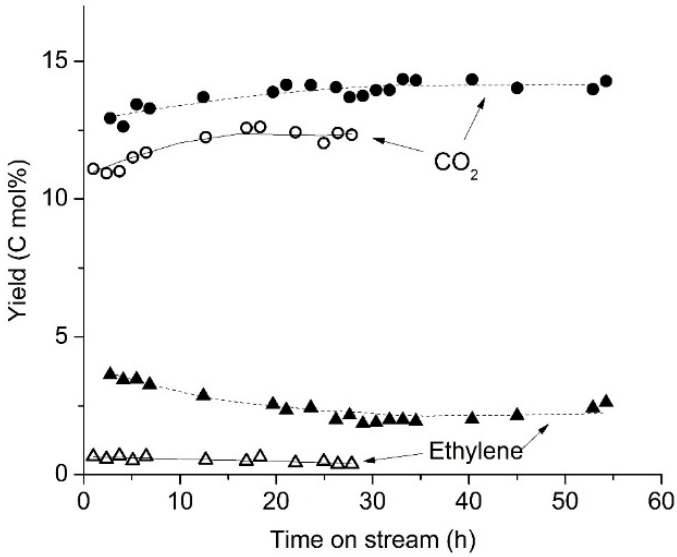

Figure 6.6c Comparison between CeO_2/Cu/HY(25) *(opened symbol)* and CeO_2/Cu/HZSM(25) *(closed symbol)* for acetic acid KHDO; ethylene *(triangle)*, carbon dioxide *(circle)*

457 g.h.mol^{-1} and 573 K, H_2 30 mL.min^{-1}

In a support manner, the results in Table 6.2 provide the same conclusion as above. Over Cu/HY, high selectivity to ethyl acetate is obtained while ethylene selectivity is significantly enhanced over Cu/HZSM-5. This is because the bi-molecular reaction like esterification is simply facilitated in large cavity of HY. While, the esterification is inhibited by the confinement of the medium pore zeolite; HZSM-5, which in turn, promotes mainly monomolecular dehydration of the ethanol formed to ethylene. It is worth emphasizing again that CeO_2/Cu/HZSM-5(25) provides much lower selectivity to ethyl acetate despite that the same level of conversion is obtained for both catalysts. This means that acetic acid must be converted to acetone from both CeO_2 and zeolite component in the CeO_2/Cu/HZSM-5(25). In a different manner, the ketonization is promoted solely by CeO_2 component in the CeO_2/Cu/HY(25) and the

Cu/zeolite component of this catalyst facilitates mainly hydrogenation-dehydration and also the esterification.

Although several reaction networks take place over these three component catalysts, both CeO_2/Cu/HZSM-5(25) and CeO_2/Cu/HY(25) possess relatively high stability up to 60 hours on stream. However, a slightly drop in hydrogenation-dehydration over CeO_2/Cu/HZSM-5(25) can be noticed. This is because ketonization also takes place over the Cu/HZSM-5 component, as discussed earlier. Hence, some of the acetone formed over the acid site may well undergo aldol condensation to higher MW products deposited in the pores [34-35], as discussed in section 4.3.2.3 (Chapter 4). On the opposite manner, only hydrogenation-dehydration is promoted over the Cu/HY component in CeO_2/Cu/HY(25). Together with a high dispersion of Cu active site in this catalyst, acetone can be readily hydrogenated. Hence, the CeO_2/Cu/HY(25) provides relatively higher stability for propylene production, as compared to CeO_2/Cu/HZSM-5(25). As various benefit and disadvantage are shared for both CeO_2/Cu/HY(25) and CeO_2/Cu/HZSM-5(25). Table 6.3 compares performance of these catalyst.

Table 6.3 Comparison the performance of KHDO catalysts

Category	CeO_2/Cu/HY	CeO_2/Cu/HZSM
Dispersion of Cu in zeolite	+	-
Activity of catalyst	-	+
KHDO activity	-	+
Direct HDO activity	+	-
Selectivity to propylene	+	-
Selectivity to ethylene	-	+
Suppress the esterification	-	+
Intermediates retained (ketone, aldehyde)	+	-
Separation of catalyst working function	+	-
Stability	+	-

+ Higher, - Lower

In this Chapter CeO_2/Cu/HY(25) is selected for further study due the outstanding propylene selectivity and stability.

6.3.2.4 Physical mixed bed vs Sequential bed

To minimize direct HDO of acetic acid taking place over Cu/zeolite, two separated beds containing CeO_2 and Cu/HY catalyst was tested at the same total contact time (343+114 g.h.mol^{-1}; the first number refers to contact time of top bed (CeO_2) and the latter is for bottom bed (Cu/zeolite), 457 g.h.mol^{-1} in total) as the physical mixed bed (457 g.h.mol^{-1}). It can be seen from Table 6.4 that the sequential bed gives a relatively higher conversion, as compared to the physical mixed bed system.

Table 6.4 KHDO of acetic acid over CeO_2/Cu/HY(25) by different systems and acetic acid concentrations

	Mixed catalyst (457 g.h.mol^{-1})		Sequential bed (343+114 g.h.mol^{-1})
Acetic acid in H_2 (mol %)	1.2	2.3	1.2
Conversion (C mol%)	56	85	89
Selectivity (C mol%)			
Acetone	27	10	2
Propylene	16	47	49
Propane	-	3	8
Acetaldehyde	3	3	2
Ethanol	5	5	6
Ethyl acetate	30	8	4
Ethylene	3	4	4
Ethane	-	1	4
CO_2	15	19	20

573 K, H_2 30 mL.min^{-1}, 1st hour on stream

This is because, in the physical mixed bed, part of acetic acid is in contact with Cu/zeolite that possesses higher surface area, as compared to the CeO_2 (Table 6.1). Hence, a relatively less fraction of acetic acid is in contact with the CeO_2 and a lower activity can be expected over the physical mixed bed. In a support manner, the reaction with the same contact time but higher acetic acid concentration (2.3%mol) provides a higher activity (Table 6.3). This is because the ketonization over CeO_2 is kinetically second order [21, 36]. For the bi-molecular reaction (two moles of acetic acid), an increase in reactant concentration can increase the collision rate and hence the acetic acid is largely consumed by ketonization. The selectivity to KHDO products (propylene and acetone) is improved. This can suppress the parallel process like direct HDO of acetic acid as well.

For the sequential bed, the acetic acid is solely in contact with CeO_2 in the first bed. Accordingly, a higher conversion of acetic acid to acetone can be expected, as also seen from an increase in CO_2 selectivity. The higher ketonization efficiency in the sequential bed also leads to the higher propylene selectivity after the second bed (Cu/HY). This is because the competitive adsorption by acetic acid over Cu/HY is reduced as more acetone is produced from the first bed and less acetic acid is remained in the reaction stream. Accordingly, hydrodeoxygenation of acetone can be readily promoted while the products from direct HDO of acetic acid are noticeably lower than those obtained from the mixed catalyst (i.e. ethyl acetate selectivity decreases from 29.6 to 4.3%). However, more paraffinic hydrocarbons (propane and ethane) were detected from the sequential bed system, due to higher H-transfer efficiency at high conversion.

6.3.2.5 Effect of water

Together with acetic acid, water is always present in gas stream from the pyrolysis biomass. Hence, the effect of water on the direct HDO is primarily studied as shown in Table 6.5. It can be seen that the conversion of acetic acid is significantly drop when 50%wt acetic acid (aq) is used as feed.

Table 6.5 Direct HDO of glacial acetic acid and aqueous acetic acid over 5%Cu/HY

	Glacial acetic acid	50 wt% aq. acetic acid
Conversion (C mol%)	24	3
Selectivity (C mol%)		
Acetaldehyde	12	16
Ethanol	3	-
Ethyl acetate	81	84
Ethylene	4	-

48 g.h.mol^{-1} and 573 K, H_2 30 mL.min^{-1}, 1st hour on stream

This is due to (i) the effect of feed dilution as mentioned in section 6.3.2.5 and (ii) a competitive adsorption of water on three component catalyst (CeO_2/Cu/HY(25)). To verify the later, an experiment with alternate switching between acetic acid and aqueous acetic acid was tested. From Figure 6.7a, it can be seen that the acetic acid conversion drops markedly after the feed is replaced by aqueous acetic acid.

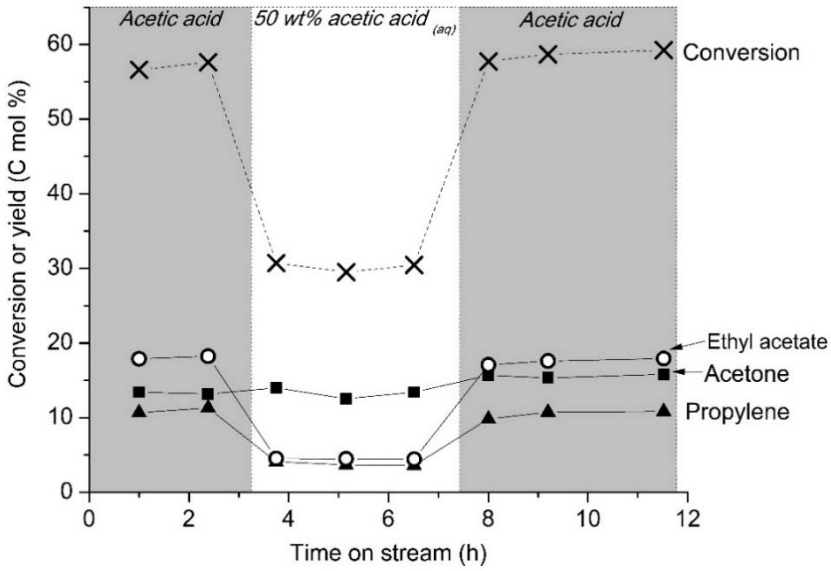

Figure 6.7a Effect of water to acetic acid KHDO over CeO_2/Cu/HY(25); conversion, acetone, propylene, ethyl acetate

457 g.h.mol^{-1} and 573 K, H_2 30 mL.min^{-1}

This is clearly due to the competitive adsorption between acetic acid and water on the catalyst. The decrease in olefin yields including propylene and ethylene indicates that the water would interact preferentially with the acid site in zeolite. Therefore, the dehydration is suppressed. The less effect is expected for the CeO_2 component hence ketonization remains unaffected as the seen from the unchanged of acetone yield. The presence of water also decreases yield of ethyl acetate, as the esterification is a reversible process. The decline in dehydration rate brings back the aldehyde-alcohol limitation. This suppresses the hydrogenation as revealed by a lower in the decrease of acetaldehyde yield, as compared to the ethanol yield, when water is present (Figure 6.7b).

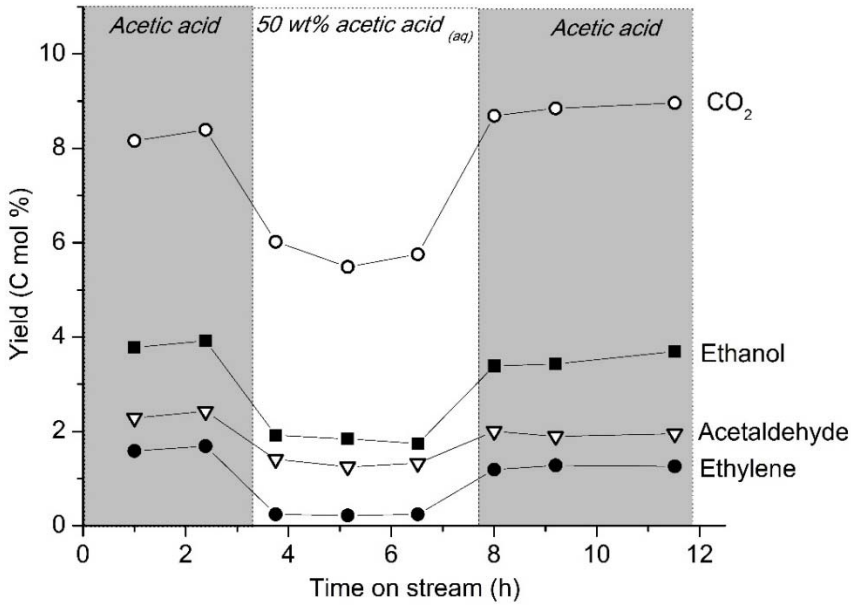

Figure 6.7b Effect of water to acetic acid KHDO over CeO_2/Cu/HY(25); ethylene, ethanol, acetaldehyde, carbon dioxide

457 g.h.mol^{-1} and 573 K, H_2 30 mL.min^{-1}

These results are in agreement with the direct HDO of acetic acid over Cu/HY as tabulated in Table 6.5. However, water does not permanently deactivate the catalyst. As seen in Figure 6.7a-b, the activity and selectivity of all products is recovered after water is removed.

6.3.2.6 Light distillated hydrocarbons from KHDO of acetic acid

In the practical point of view, a separate bed system would provide more advantage in controlling and tuning the catalyst performance. As olefins are obtained from KHDO of acetic acid, another sequential bed of HZSM-5 (Si/Al = 13) is added to convert the olefin to higher hydrocarbons via oligomerization. With excess of catalyst (the sequential beds of CeO_2-CuHY-HZSM-5), nearly 100% conversion is obtained as shown in Figure 6.8a.

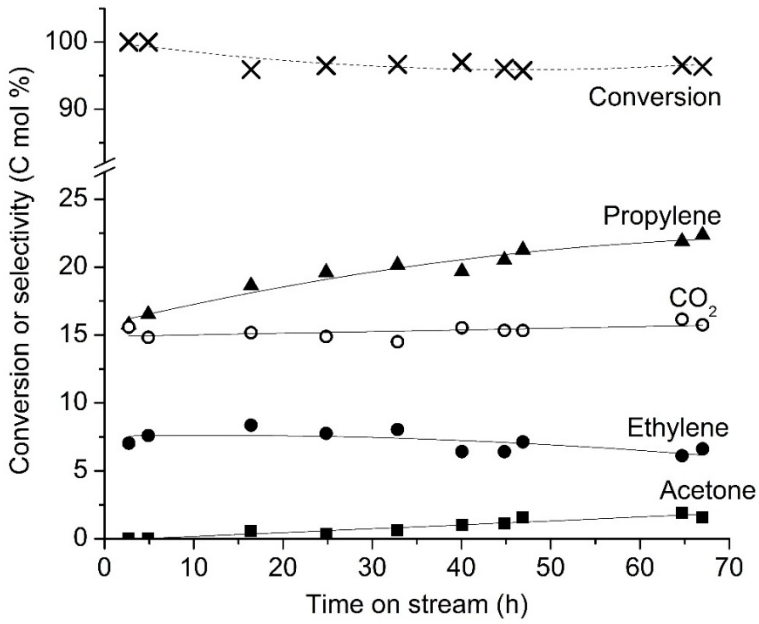

Figure 6.8a Light distillated hydrocarbons from acetic acid over sequential beds of CeO_2-Cu/HY -HZSM-5; conversion, propylene, acetone, ethylene, carbon dioxide

343-114-80 g.h.mol^{-1} and 573 K, H_2 30 mL.min^{-1}, HZSM-5 (Si/Al=13)

The wide range of hydrocarbon products including light olefins (ethylene, propylene, and butylene), LPG (C2-C4 paraffins), gasoline (C5-C10 olefins), and C7-C9 aromatics can be obtained from acetic acid (Figure 6.8a-b).

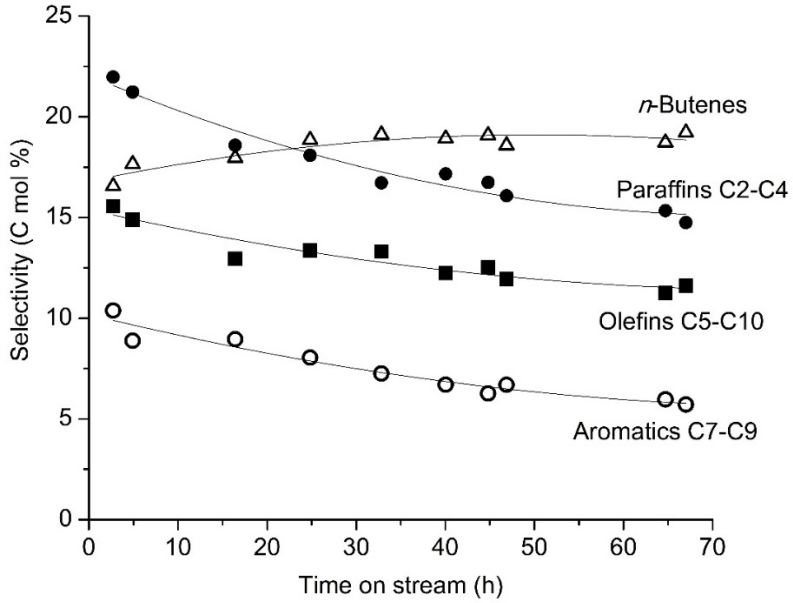

Figure 6.8b Light distillated hydrocarbons from acetic acid over sequential beds of CeO_2-Cu/HY -HZSM-5; butenes, paraffins C2-C4, olefins C5-C10, aromatics C7-C9

343-114-80 g.h.mol^{-1} and 573 K, H_2 30 mL.min^{-1}

These obtained products indicates that the higher hydrocarbons probably generated via hydrocarbon pool, in which the oligomerization, aromatization, cracking, and hydrogen transfer occurred simultaneously. A slight increase in selectivity of the acetone intermediate with the decrease in paraffins production indicates that the deactivation also takes place, presumably over the Cu/HY component. While, the continuous increase in propylene selectivity with a decrease in C5-C10 olefins and C7-C9 aromatics selectivity are evidences for the HZSM-5 deactivation, which is typically observed for acid-catalyzed reaction. Nevertheless, this clearly demonstrates a potential catalyst system/process for conversion of acetic acid to hydrocarbon products.

6.4 Conclusion

The acetic acid can be successfully converted to propylene via keto-hydrodeoxygenation (KHDO) over the three component catalyst containing CeO_2 and Cu

loaded acid zeolites (CeO_2/Cu/HZSM-5(25) or CeO_2/Cu/HY(25)) at relatively low temperature (573 K) and atmospheric pressure. Ketonization of acetic acid to acetone initially takes place and the acetone formed is subsequently hydrogenation-dehydration to propylene. Direct hydrodeoxygenation of acetic acid is also observed producing ethylene and other C_2-oxygenates. With higher Cu dispersion, the catalyst containing CeO_2/Cu/HY(25) provides higher stability and more selective conversion of acetic acid to olefin products, as compared to that over CeO_2/Cu/HZSM-5(25). The presence of water suppresses the overall activity, particularly the hydrogenation-dehydration. With a sequential bed system composing of CeO_2, Cu/HY and HZSM-5, the KHDO can be applicable for the conversion of acetic acid, a biomass derived product, to olefins and higher hydrocarbons.

6.5 References

[1] Bravo-Suarez J.J, Schwartz V. and Kidder M.K., Editors. **Novel Materials for Catalysis and Fuels Processing.** USA: American Chemical Society. 2013.

[2] Mekhemer G.A.H., Halawy S.A., Mohamed M.A. and Zaki M.I. "Ketonization of acetic acid vapour over polycrystalline magnesia: in situ Fourier transform infrared spectroscopy and kinetic studies" **Journal of Catalysis,** vol.230, 2005. pp.109–122.

[3] Kuriacose J.C. and Swaminathan R. "Studies on the Ketonization of Acetic Acid on Chromia 1. The Adsorbate-Catalyst Interaction" **Journal of Catalysis,** vol.14, 1969. pp.348-354.

[4] Swaminathan R. and Kuriacose J.C. "Studies on the Ketonization of Acetic Acid on Chromia II. The Surface Reaction" **Journal of Catalysis,** vol.16, 1970. pp.357-362.

[5] Pham T.N., Sooknoi T., Crossley S.P. and Resasco D.E. "Ketonization of Carboxylic Acids: Mechanisms, Catalysts, and Implications for Biomass Conversion" **ACS Catalysis**, vol.3, 2013. pp.2456-2473.

[6] Martinez R., Huff M.C. and Barteau M.A. "Ketonization of acetic acid on titania-functionalized silica monoliths" **Journal of Catalysis**, vol.222, 2004. pp.404–409.

[7] Snell R.W. and Shanks B.H. "Ceria calcination temperature influence on acetic acid ketonization: Mechanistic insights" **Applied Catalysis A: General**, vol.451, 2013. pp.86– 93.

[8] Waters T., O'Hair R.A.J. and Wedd A.G. "Catalytic gas phase dehydration of acetic acid to ketene" **International Journal of Mass Spectrometry**, vol.228, 2003. pp.599–611.

[9] Vajo J.J., Sun Y.K. and Weinberg W.H. "Catalytic Dehydration of Acetic Acid on a Graphitized Platinum Surface" **Journal of Physical Chemistry**, vol.91, 1987. pp.1153-1158.

[10] Zhang S., Duan X., Ye L., Lin H., Xie Z. and Yuan Y. "Production of ethanol by gas phase hydrogenation of acetic acid over carbon nanotube-supported Pt–Sn nanoparticles" **Catalysis Today**, vol.215, 2013. pp.260– 266.

[11] Cressely J., Farkhani D., Deluzarchi A. and Kiennemann A. "Evolution Des Especes Carboxylates Dans Le Cadre Des Synthesis CO_2-H_2 Reduction De L'acide Acetique Sur Systeme Co, Cu, Fe" **Material Chemistry and Physics**, vol.11, 1984. pp.413-431.

[12] Johnston V.J., Kimmich B., Potts J., Weiner H., Zink J.H., Chapman J.T., Chen L. and Jevtic R. **"Copper Catalysts for Making Ethanol from Acetic Acid"** U.S. patent no. US 2011/0263910 A1, 27 Oct 2011.

[13] Zhu Y. and Shi X.W.L. "Hydrogenation of Ethyl Acetate to Ethanol over Bimetallic Cu-Zn/SiO2 Catalysts Prepared by Means of Coprecipitation" **Bulletin of the Korean Chemical Society,** vol.35, 2014. pp.141-146.

[14] Rachmady W. and Vannice M.A. "Acetic Acid Hydrogenation over Supported Platinum Catalysts" **Journal of Catalysis**, vol.192, 2000. pp.322-334.

[15] Wan H., Chaudhari R.V. and Subramaniam B. "Aqueous Phase Hydrogenation of Acetic Acid and Its Promotional Effect on *p*-Cresol Hydrodeoxygenation" **Energy and Fuels**, vol.27, 2013. pp.487-493.

[16] Zhang K., Li F., Zhang H., Ma H, Ying W. and Fang D. "Hydrogenation of Acetic Acid on Alumina-Supported Pt-Sn Catalysts" **International Scholarly and Scientific Research & Innovation,** vol.7, 2013. pp.488-492.

[17] Kharaca Y.K., Carothers W.W. and Rosenbauer R.J. "Thermal decarboxylation of acetic acid: implications for origin of natural gas" **Geochimica et Cosmochimica Acta**, vol.47, 1982. pp.397-402.

[18] Witsuthammakul A. and Sooknoi T. "Selective hydrodeoxygenation of bio-oil derived products: ketones to olefins" **Catalysis Science and Technology**, vol.5, 2015. pp.3639-3648.

[19] Liu C., Karim A.M., Lebarbier V.M., Mei D. and Wang Y. "Vapor phase ketonization of acetic acid on ceria based metal oxides" **Topic in Catalysis**, vol.56, 2013. pp.1782–1789.

[20] Snell R.W. and Shanks B.H. "$CeMO_x$ promoted ketonization of biomass-derived carboxylic acids in the condensed phase" **ACS Catalysis**, *vol.4,* 2014. pp.512–518.

[21] Pham T.N., Shi D. and Resasco D.E. "Kinetics and mechanism of ketonization of acetic acid on Ru/TiO_2 catalyst" **Topic in Catalysis**, vol.57, 2014. pp.706–714.

[22] Peamaroon N. and Sooknoi T. "Aromatization of cyclopentane over ZSM-5 catalysts: a proposal of reaction pathway" **Petroleum Science and Technology**, vol.30, 2012. pp.1647–1655.

[23] Hoang D.L., Dang T.T.H., Engeldinger J., Schneider M., Radnik J., Richter M. and Martin A. "TPR investigations on the reducibility of Cu supported on Al_2O_3, zeolite Y and SAPO-5" **Journal of Solid State Chemistry**, vol.184, 2011. pp.1915–1923.

[24] Sagar G.V., Rao P.V.R., Srikanth C.S. and Chary K.V.R. "Dispersion and Reactivity of Copper Catalysts Supported on Al_2O_3-ZrO_2" **Journal of Physical Chemistry B,** vol.110, 2006. pp.13881-13888.

[25] Ausavasukhi A., Suwannaran S., Limtrakul J. and Sooknoi T. "Reversible interconversion behavior of Ag species in AgHZSM-5: XRD, ^1H MAS NMR, TPR, TPHE, and catalytic studies" **Applied Catalysis A: General**, vol.345, 2008. pp.89–96.

[26] Strassberger Z., Alberts A.H., Louwerse M.J., Tanase S. and Rothenberg G. "Catalytic cleavage of lignin β-O-4 link mimics using copper on alumina and magnesia–alumina" **Green Chemistry**, vol.15, 2013. pp.768-774.

[27] Huo C., Ouyang J. and Yang H. "CuO nanoparticles encapsulated inside Al-MCM-41 mesoporous materials via direct synthetic route" **Scientific Reports**, vol.4, 2014. pp.1-9.

[28] Frevel L.K., Kressley M.J. and Kressley L.J. "**Selective hydrogenation in the presence of copper catalysts**" U.S. patent no.3076858, 5 Feb 1963.

[29] Ilias S. and Bhan A. "Mechanism of the catalytic conversion of methanol to hydrocarbons" **ACS Catalysis**, vol.3, 2013. pp.18-31.

[30] Ravasio N. and Gargano M. "Selective hydrogenations promoted by copper catalysts. 2. hydrogen-transfer reactions leading to stereoselective hydrogenation of Δ^5-3β-

sterols to 5β-derivatives" **Journal of Organic Chemistry**, vol.58, 1993. pp.1259-1261.

[31] Parravano G. "Equilibrium hydrogen transfer between benzene and C6 hydrocarbons over supported metal catalysts" **Journal of Catalysis**, vol.16, 1970. pp.1-15.

[32] Gumidyala A., Sooknoi T. and Crossley S. "Role of acid site proximity on the mechanism of acetic acid conversion over HZSM-5" **247th ACS National Meeting & Exposition**, 2014. pp.84.

[33] Gumidyala A., Godavarthy M., Sooknoi T. and Crossley S. "Insights into the mechanism of acetic acid ketonization over zeolites" **AIChE Annual Meeting**, 2014.

[34] Novakova J. and Kubelkova L. "Reactions of ^{12}C and ^{13}C acetone mixtures with a HZSM-5 zeolite" **Journal of Catalysis**, vol.126, 1990. pp.689-692.

[35] Tago T., Sakamoto M., Iwakai K., Nishihara H., Mukai S.R., Tanaka T. and Masuda T. "Control of acid-site location of MFI zeolite by catalytic cracking of silane and its application to olefin synthesis from acetone" **Journal of Chemical Engineering of Japan**, vol.42, 2009. pp.s162–s167.

[36] Pham T.N., Shi D. and Resasco D.E. "Reaction kinetics and mechanism of ketonization of aliphatic carboxylic acids with different carbon chain lengths over Ru/TiO_2 catalyst" **Journal of Catalysis**, vol.314, 2014. pp.149–158.

Chapter 7

Deoxygenation of furfural in a presence of acetic acid and water

7.1 Introduction

Furfural is an aldehyde deriving from decomposition of hemi-cellulose by pyrolysis (~ 1 %) [1] or hydrolysis [2] It is reactive and can be polymerized rapidly leading to the storage instability of bio-oil. On the other hand, furfural is an important feedstock for a several industrial monomer e.g. butanediol [3-4], maleic acid [33], and succinic acid [5]. Therefore, the deoxygenation of furfural is necessary to improve the stability and value of product from biomass pyrolysis. The decarbonylation of furfural to furan [6] is a well-known method for furfural deoxygenation. The furan produced will be an intermediate for an important industrial solvent, tetrahydrofuran (THF) [7]. Pd is a preferred catalyst for furan synthesis at > 473 K and atmospheric pressure [8]. Doping K into Pd can enhance the furan selectivity and inhibits the 2-methylfuran formation [9] while alloy with Cu leads to the loss of decarbonylation activity [10]. A good selectivity to furan (> 90%) over Pt catalyst was also reported in case of small particle (< 2 nm) [11] while the Ni can facilitate a further hydrogenation resulting in parafins production [7]. Various mixed metal oxides were choices of cheaper catalysts. The commercial available CoMo and NiMo (15-20%) over Al_2O_3 catalysts are slightly active for decarbonylation (< 30% yield) while the CdMnO and CdMnZnO on Al_2O_3 support show an improved activity (> 80% yield) [12]. However, the metal oxide catalysts require the temperature higher than of the noble metal catalysts (> 623 K) and deactivated rapidly. A study on catalyst deactivation reveals that the two adjacent furfural adsorbed on catalyst surface can be evolved to coke, which is the cause of deactivation [13]. Therefore, the H_2 (for metal catalyst) [8] or water (for metal oxide catalyst) [12] covered on catalyst surface and feed dilution are essential to maintain the catalyst stability.

The hydrogenation of furfural to furfuryl alcohol, which is an important monomer in resin industry [14], is another common furfural upgrading (62% of furfural consumption in global). Cu can hydrogenate the carbonyl selectively at > 503 K (90% selectivity to furfuryl alcohol) [15]. However, high conversion was not achieved due to

the thermodynamic limitation of hydrogenation-dehydrogenation (maximum 60% conversion). The noble metal like Pt can promote the hydrogenation at lower temperature, as compared to Cu (443 K) when the particle size is > 2.6 nm (60 %) [11]. While, the Ni possesses the hydrogenation activity similar to Pt but at temperature < 503 K [7]. It is noted that the furfuryl alcohol is still reactive particularly for the polymerization. Alternatively, the further hydrogenolysis of the furfuryl alcohol produced yields 2-methylfuran, which is more stable than furfuryl alcohol. It can be used as a solvent and alternative octane booster for gasoline [14] (RON=131) [7]. An outstanding 2-methylfuran yield (up to 99%) was obtained over copper chromite catalyst [16] at > 473 K [17]. Recently, it was found that the Ni-Fe alloy can promote 2-methylfuran production at > 483 K (nearly 20% yield) but the parafins are also obtained due to a high hydrogenation activity of nickel (8% yield) [18]. Meanwhile, the alloy of Cu-Fe, Cu-Zn-Al doped with Ca or Na give >95 % yield of 2-methyl furan at 525 K [19]. The 2-methylfuran can be produced in liquid phase system as well, using Ru/C or Pt/C catalyst (40-60 % yield) at similar temperature to the gas phase reaction [20]. However, the system requires high pressure (2.04 MPa of N_2) and reactive solvent (*i*-propanol or *n*-butanol).

Although the deoxygenation of furfural single component was achieved over various metal catalysts as mentioned above, the separation of the furfural in bio-oil to the single component is difficult as it is always found together with acetic acid and water. In the presence of acid, the distillation may lead to rapid polymerization. Meanwhile, the direct upgrading of bio-oil was often failed due to uncontrollable deoxygenation. A low activity and selectivity to product were obtained due to differences in functional groups, interference by other oxygenated compounds, and acidity of the bio-oil [21-24]. It is necessary to provide the practical upgrading technology supporting the bio-oil utility. In this Chapter, the decarbonylation and hydrodeoxygenation (HDO) of furfural were tested over palladium and copper based catalysts in the presence of acetic acid and water, co-products generally found in bio-oil. The stability and change of catalyst were also investigated.

7.2 Experimental details

The 99% furfural and ≥99.7% acetic acid were obtained from Sigma-Aldrich®. The furfural was purified by distillation under atmosphere of N_2 at 473 K and kept in N_2 at 253 K. A commercial 5%Pd/C was purchased from Sigma-Aldrich® and used without modification. All supports (SiO_2 (Carlo Erba®), HY (Si/Al=150; Tohso®), >99.0% CeO_2 (Sigma-Aldrich®), 99.97% γ-Al_2O_3, 99.9%, TiO_2 (anatase), and 99.9% ZnO (Alfa Aesar®)) were calcined in air (60 mL.min^{-1}) at 723 K (2 K.min^{-1}) for 5 hours before used. The 99.98% palladium (II) acetate ($Pd(OAc)_2$, Sigma-Aldrich®) was used as precursor for palladium catalysts by dissolving in acetone (HPLC grade ≥99.8%; Sigma-Aldrich®). The solution was loaded into the calcined supports by incipient wetness impregnation (IWI) and left dried at 303 K overnight. The precursors were decomposed by calcination in air (60 mL.min^{-1}) at 723 K (2 K.min^{-1}) for 5 hours. The calcined palladium catalyst were diluted in their support to 5 %wt of catalyst. The Cu catalysts were also prepared by IWI of aqueous copper (II) nitrate ($Cu(NO_3)_2.3H_2O$, Ajax Fine Chem) onto support (SiO_2 and HY (Si/Al=150)). They were then calcined in the similar manner to Pd catalysts. The copper catalysts were pelletized to 600-850 micron before used.

The specific surface area (BET) of catalysts was measured using nitrogen adsorption technique (Quantachrome) at 77 K and 0.05–0.30 P/P_0. The picture of metals on supports was captured by transmission electron microscopy (TEM; FEI Tecnai G^2 20, 200 kV) with LaB_6 emitter and Formvar coated Cu grid, then measure the size of metal particle by Image J® software. Amount of palladium on supports was quantified instantly after TEM analysis by the energy dispersive X-ray spectroscopy (EDX). Meanwhile, the quantification of copper on support was carried out by X-ray fluorescence spectroscopy (XRF; Siemens). Reducible copper oxide species was analyzed by temperature programmed reduction (TPR). The catalysts were treated in air (30 mL.min^{-1}) at 723 K (2 K.min^{-1}) for 5 hours then cooled down to 303 K. The TPR was performed in 10% H_2/Ar from 323-1173 K (5 K.min^{-1}). The hydrogen consumption is recorded by an on-line thermal conductivity detector (VICI). Copper dispersion on support was analyzed by selective surface TPR technique. Briefly after typical TPR, the sample was *in situ* treated with N_2O at 333 K for 2 hours. Then, the surface-oxidized sample was subjected to a secondary TPR [25]. Moles of surface copper can be calculated as described in literature [26]. Acidity of HY and Cu/HY was quantified by NH_3-TPD. 1 % NH_3/He was pre-adsorbed at 323 K. TPD was carried out in He at 10 K.min^{-1} from 323–973 K.

The catalytic testing was conducted in a fixed bed flow reactor (6 mm i.d. Pyrex®) at atmospheric pressure. The catalysts were primarily activated at 723 K (2 K.min^{-1}) under stream of air zero (30 ml.min^{-1}) for 5 h, except that for Pd/C. The reduction of catalyst was achieved in H_2 at 523 K for Pd/C, 673 K for other Pd catalysts, and 723 K for Cu catalysts for 2 h. The system was cooled down to the reaction temperature (523 K) and the furfural solution was introduced by a syringe pump at the rate of 0.2-1.5 g/h. The products were analyzed by an on-line GC-FID (Agilent 6890). A EC-Wax® (0.25 mm X 30 m) was used as separating column. The analysis condition for gas chromatography is shown in Appendix A.

7.3 Result and discussion

7.3.1 Characterization of catalyst

7.3.1.1 Palladium catalysts

Surface area and palladium content of catalysts is tabulated in Table 7.1. The CeO_2, ZnO anatase TiO_2, and γ-Al_2O_3 exhibit low surface area (< 150 m^2.g^{-1}). In contrast, the SiO_2, HY, and C possess relatively higher surface area (> 240 m^2.g^{-1}). The loading of palladium on to these supports (5%wt) leads to a slight decrease in surface area as the surface area of palladium is much lower that these support.

Table 7.1 Surface area and palladium content catalysts

Catalyst	BET surface area m^2/g	Pd content by ICP, %wt Fresh	Pd content by EDX, %wt Fresh (spent*)	Particle size of Pd Nm Fresh (spent*)
Pd/SiO_2	236	5.1	6.98 (not found)	6.6 (not found)
SiO_2	246	-	-	-
$Pd/\gamma\text{-}Al_2O_3$	115	5.3	7.82 (not found)	8.5 (not found)
$\gamma\text{-}Al_2O_3$	125	-	-	-
Pd/TiO_2	80	4.3	5.83	15.9
TiO_2	88	-	-	-
Pd/HY	693	4.9	7.68	6.2
HY	713	-	-	-
Pd/ZnO	34	5.4	4.35	8.1
ZnO	42	-	-	-
Pd/CeO_2	15	4.9	3.78	5.4
CeO_2	16	-	-	-
Pd/C (com)	746	5.0	not applicable	4.7 (3.3) (6.64, heat to 673)
Charcoal	1009	-	-	-

** furfural decarbonylation in stream of acetic acid*

However, the surface area of the above catalysts are much lower, as compared to the commercial 5%Pd/C catalyst (> 700 $m^2.g^{-1}$). These catalysts contain ~ 5%wt palladium as evaluated by ICP. The particles of Pd on supports (C, SiO_2, $\gamma\text{-}Al_2O_3$, HY, TiO_2, ZnO, and CeO_2) are expressed in Figure 7.1-7.7. It is found that particle size of palladium (Table 7.1) can be rearranged as Pd/C < Pd/CeO_2 < Pd/HY < Pd/SiO_2 < Pd/ZnO < $Pd/\gamma\text{-}Al_2O_3$ < Pd/TiO_2.

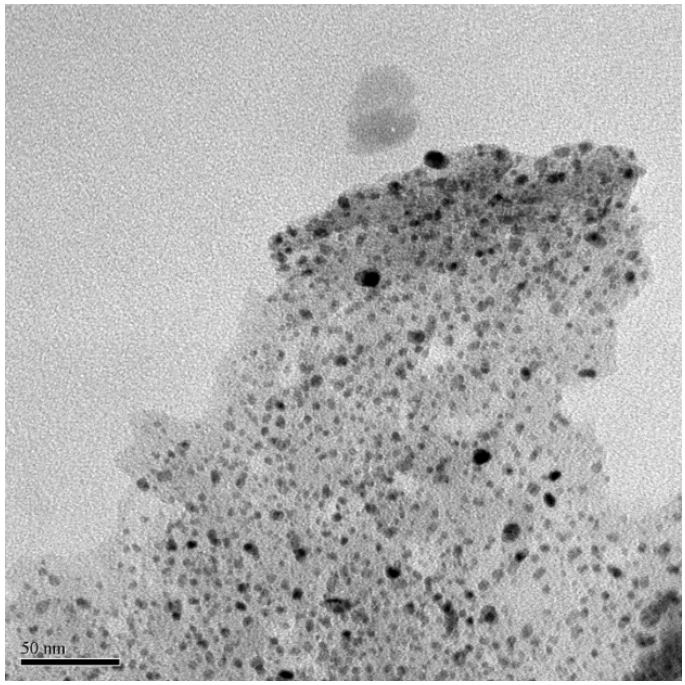

Figure 7.1 TEM image of a commercial Pd/C at 62 kX; 5%wt palladium loading

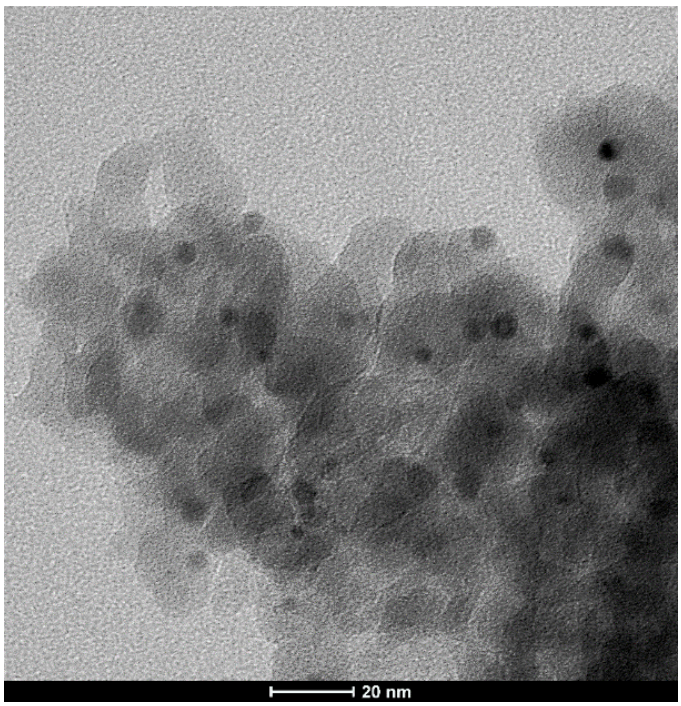

Figure 7.2 TEM image of Pd/SiO_2 at 285 kX; 5%wt palladium loading

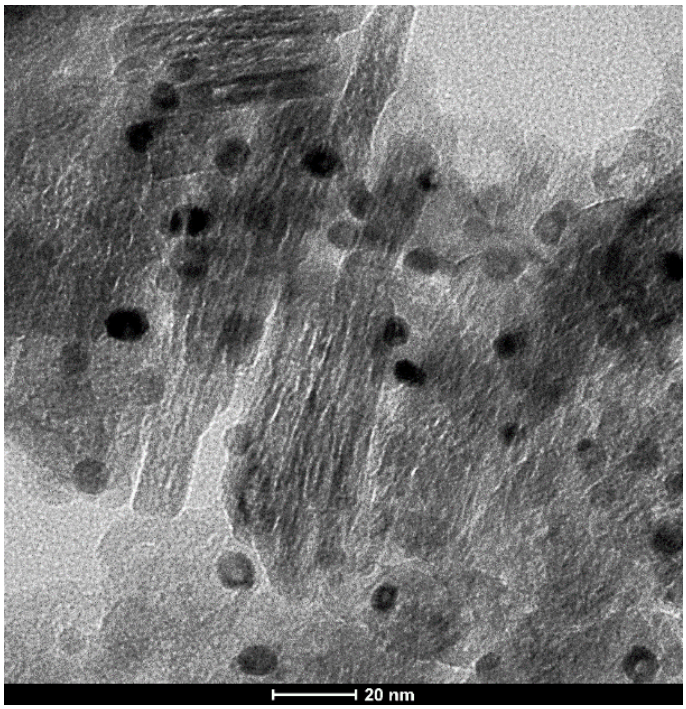

Figure 7.3 TEM image of Pd/γ-Al_2O_3 at 285 kX; 5%wt palladium loading

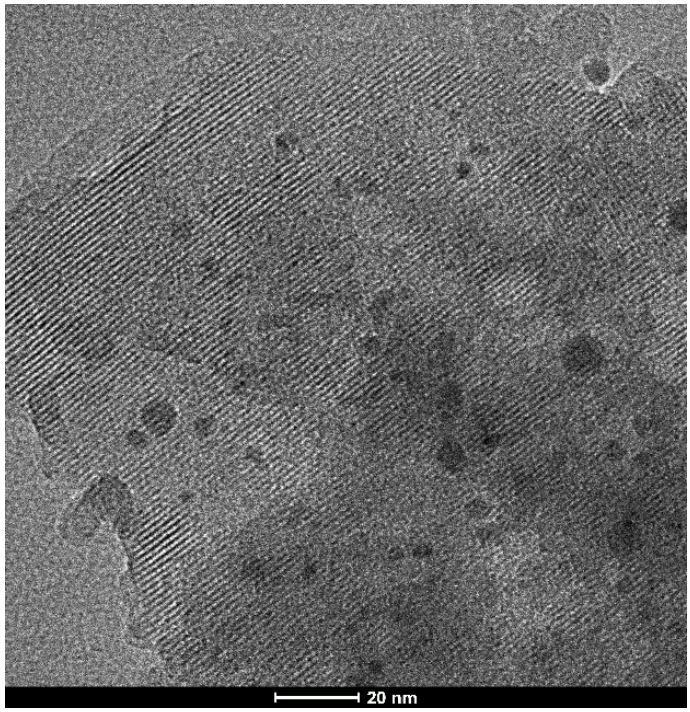

Figure 7.4 TEM image of Pd/HY at 285 kX; 5%wt palladium loading

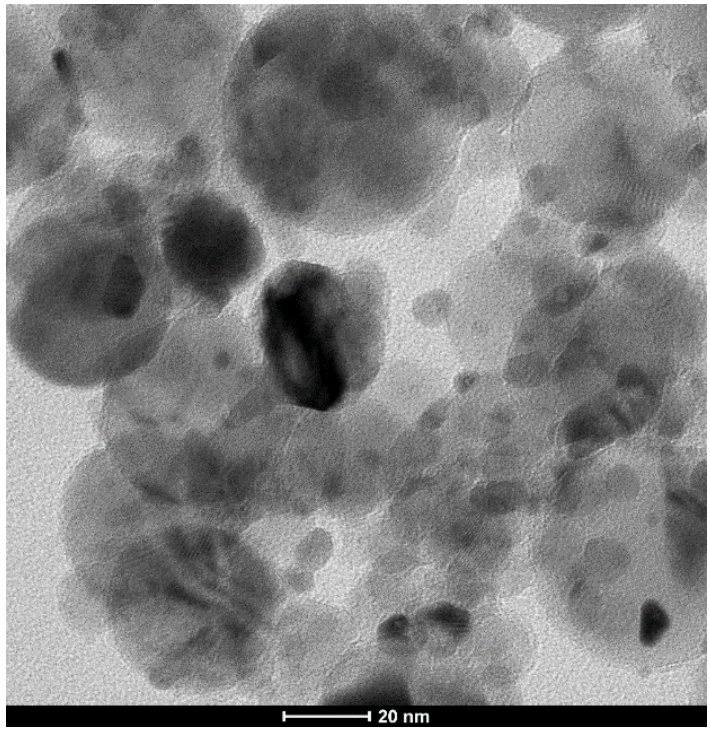

Figure 7.5 TEM image of Pd/TiO_2 at 285 kX; 5%wt palladium loading

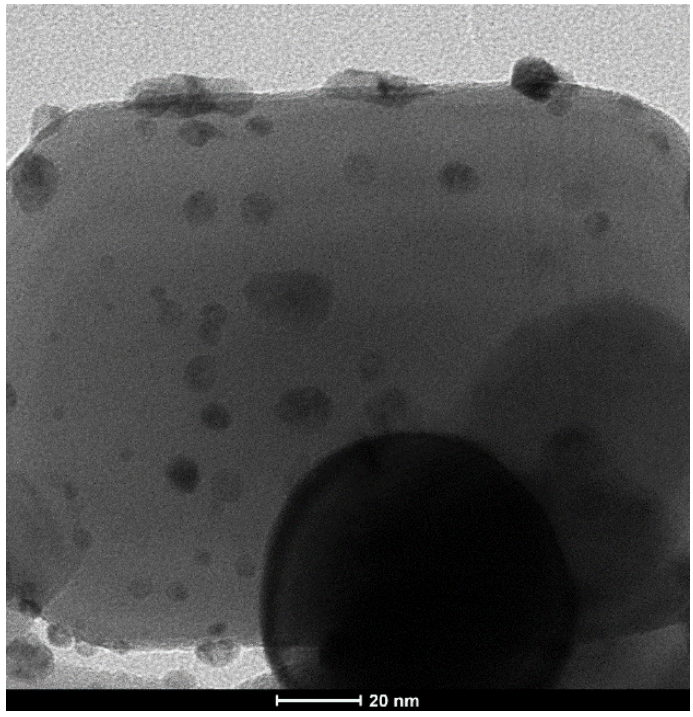

Figure 7.6 TEM image of Pd/ZnO at 285 kX; 5%wt palladium loading

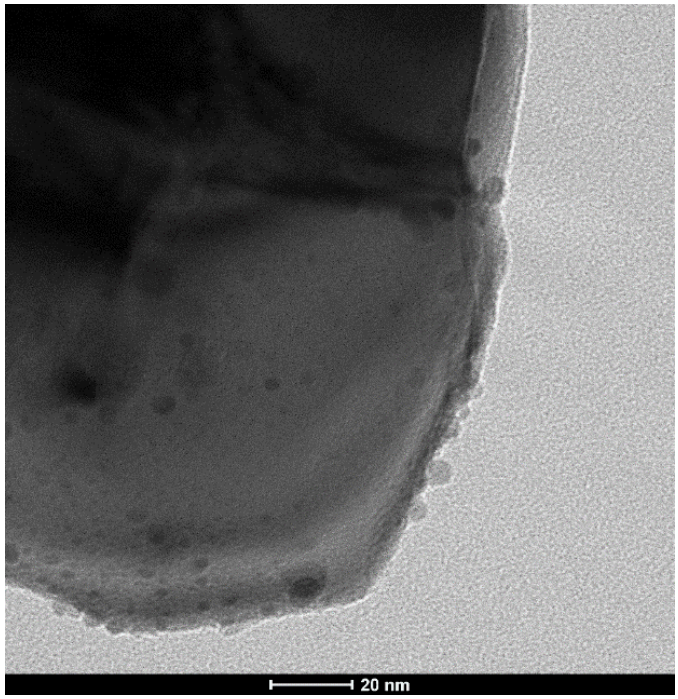

Figure 7.7 TEM image of Pd/CeO_2 at 285 kX; 5%wt palladium loading

The support with high surface area (C, SiO_2, and HY) possesses a large area for palladium dispersion. Therefore, a small palladium particles are obtained, as compared to the particles on low surface supports (ZnO, γ-Al_2O_3, and TiO_2). For CeO_2, although it is a low surface area support, the small palladium particle can be observed. This is probably due to a good metal-support interaction.

7.3.1.2 Copper catalysts

At similar copper loading (5%wt), Table 7.2 shows that the loading of copper on to supports (SiO_2 and HY) slightly decreases the surface area, as compared to the support alone.

Table 7.2 %Dispersion, copper area, copper content, surface area, and acidity of copper catalysts

Catalyst	Si/Al	%Cu content	%Cu dispersion	Particle size of Cu Fresh (spent*)	Cu area	BET surface area	Acidity (μmol/g)	
		%wt		nm	(m^2/g_{Cu})	(m^2/g)	Weak	Strong
SiO_2	-	-	-	-	-	246	-	-
Cu/SiO_2	-	5.1	95	-	646	240	-	-
HY	153	-	-	-	-	713	54	65
Cu/HY	166	5.1	65	2.7 (2.7)	499	568	158	62

** furfural decarbonylation in stream of acetic acid*

As the HY possesses surface area higher than that of the SiO_2, the surface area of Cu/HY is also higher than Cu/SiO_2. The good dispersion of Cu/SiO_2 results in flat and thin copper particle, which is barely visible when observed by TEM (Figure 5.3, Chapter 5). Meanwhile, a lower Cu dispersion (65 %) is observed from Cu/HY due to a part of exchangeable copper as mentioned in section 5.3.1. The copper particle dispersed on HY would be larger than Cu/SiO_2 as it can be seen by TEM (Figure 5.5a-b, Chapter 5). A part of copper (dark spot) are aligned in the pore of HY (light grey plane) as expressed in Figure 5.5 (c) (Chapter 5). TPR of Cu/SiO_2 and Cu/HY are shown in Figure 7.8.

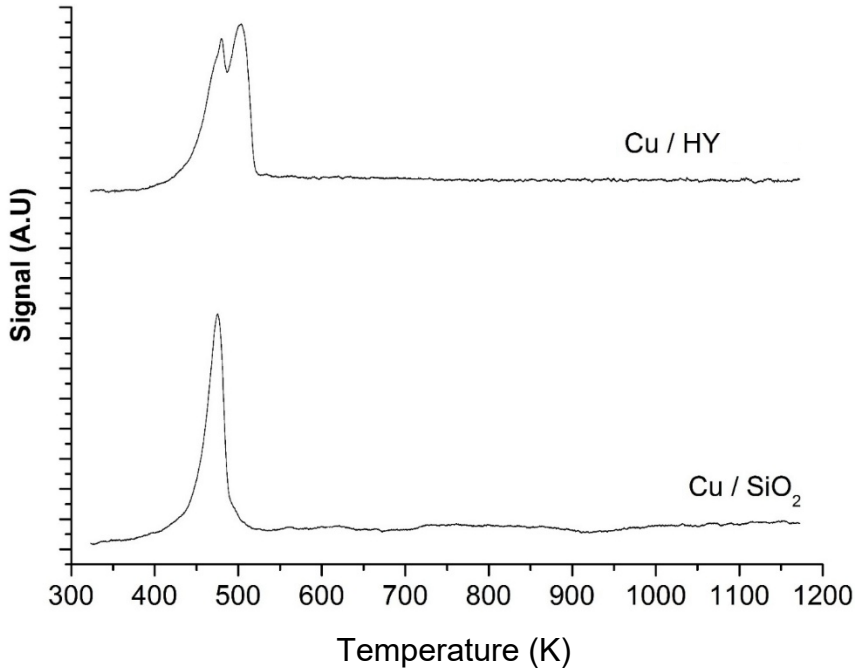

Figure 7.8 Temperature program reduction of Cu/SiO_2 and Cu/HY, 5%wt loading

From Figure 7.8, TPR of Cu/SiO_2 shows the single reduction peaks at 473 K corresponding to CuO aggregates on the surface. While, the Cu/HY exhibits two reduction peaks at 473 and 520 K. The additional peak at higher temperature, as compared to Cu/SiO_2, is highly dispersed copper oxide in the pore of zeolite [27-28].

7.3.2 Catalytic activity testing

7.3.2.1 Decarbonylation of furfural over Pd catalysts

To evaluate the furan production from furfural in bio-oil using the palladium catalyst, the experiment with purified furfural is initially tested. Table 7.3 shows that high furfural conversion (74%) is obtained with high selectivity to furan (68%) at 523 K.

Table 7.3 Decarbonylation of furfural solutions over Pd/C; selectivity at 1st hour on stream

Feed	Conversion	Selectivity (C mol%)				
	(C mol%)	Furan	THF	Fur-OH	THfur-OH	CO
Furfural	74	68	5	5	4	18
7.5%wt Furfural/water	76	74	3	3	0.5	19
7.5%wt Furfural/7.5%wt acetic acid/water	70	73	3	3	2	19

*THF=tetrahydrofuran, Fur-OH=furfuryl alcohol, THfur-OH=tetrahydrofurfuryl alcohol

523 K, 0.15 g.h.mol^{-1}, H_2 60 ml.min^{-1}

The products obtained can be derived from decarbonylation (furan and tetrahydrofuran (THF)) and hydrogenation (furfuryl alcohol and tetrahydrofurfuryl alcohol). No significant change in product selectivity is observed within 8 hours on stream. Over palladium, furfural is decarbonylated to furan that can be subsequently hydrogenated to THF. In parallel, the furfural is directly hydrogenated at the carbonyl group to furfuryl alcohol and further hydrogenated at the furan ring to produce tetrahydrofurfuryl alcohol as demonstrated below [8];

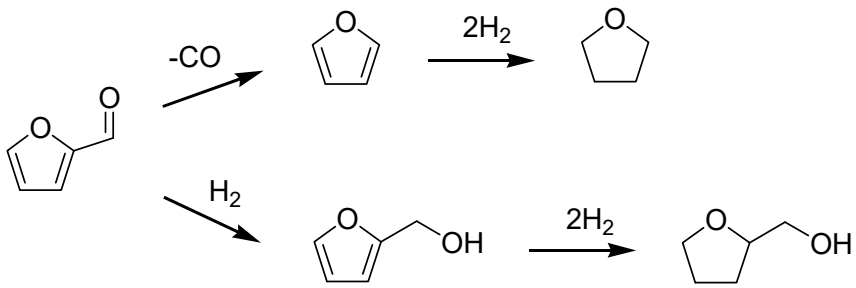

However, a slow deactivation is observed as shown in Figure 7.9.

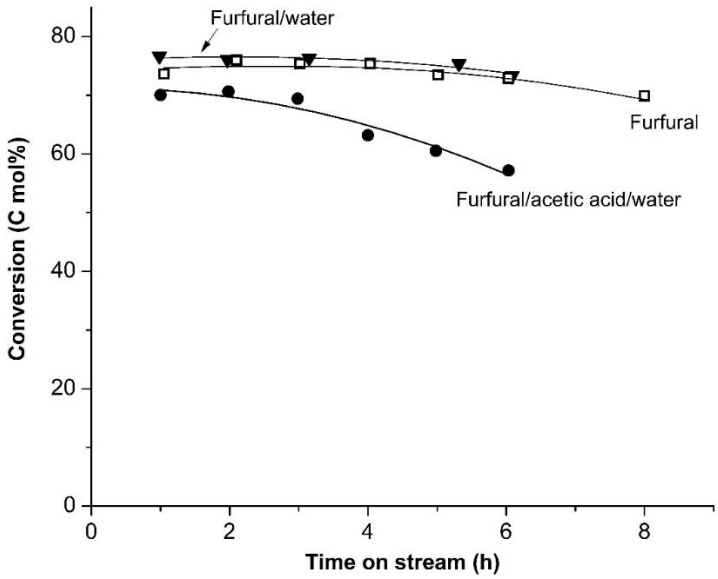

Figure 7.9 Decarbonylation of furfural solutions over Pd/C; conversion

*100% Furfural, 7.5%wt furfural/water, 7.5%wt furfural/7.5%wt acetic acid/water

523 K, 0.15 g.h.mol^{-1}, H_2 60 ml.min^{-1}

As the furfural is highly reactive, it can be polymerized rapidly leading to the carbon deposition on Pd surface [29-30]. No significant difference in furfural conversion when water is used as diluent (Figure 7.9), as compared to furfural alone. However, the selectivity to hydrogenation products is decreased as shown in Table 7.3. As the hydrogenation of furfural to furfuryl alcohol requires η^1 (O) adsorption at the edge of palladium [31], it is possible that the adsorption of carbonyl of furfural is competitive with water [32-33]. Hence, the η^1 (O) adsorption mode is suppressed.

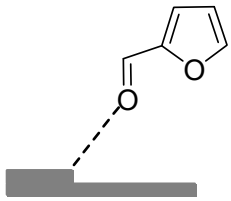

η^1 (O) adsorption of furfural at edge of Pd

In contrast, when acetic acid is added to the aqueous furfural, the conversion of furfural is notably decreased but the product selectivity is quite similar to aqueous furfural. It is probably due to a competitive adsorption of acetic acid onto palladium surface. To verify the competitive adsorption, an experiment with feed alternation between furfural and 50% furfural/acetic acid was performed over Pd/C as shown in Figure 7.10.

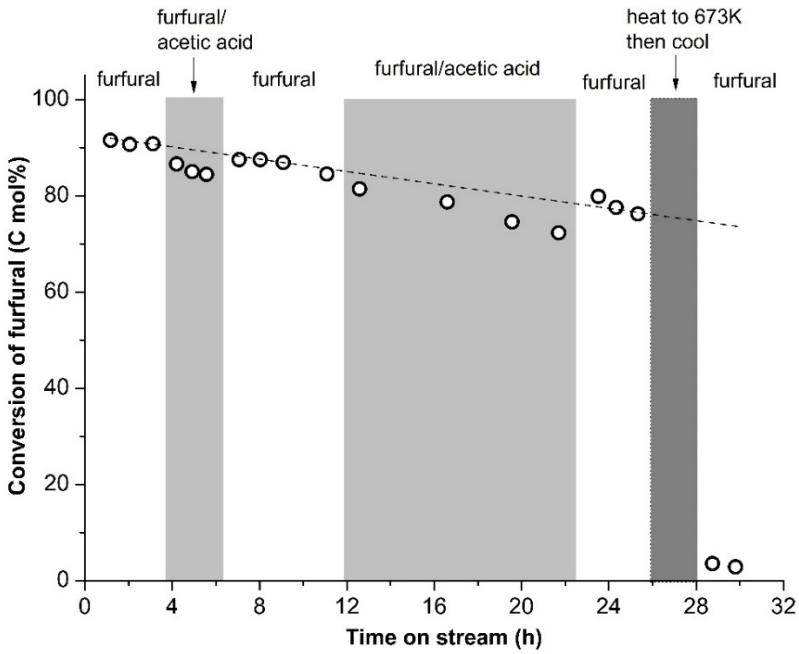

Figure 7.10 Decarbonylation of alternated furfural - 50%wt furfural/acetic acid over Pd/C

523 K, 0.17 g.h.mol^{-1}(furfural), H_2 60 ml.min^{-1}, 0% acetic acid conversion

It can be seen that the conversion of furfural slowly drop, when the furfural is fed, due to the carbon deposit as mentioned earlier. The introduction of acetic acid into the system by switching furfural/acetic acid feed results in a marked decrease in furfural conversion. However, the conversion is obviously recovered to the trend when the acetic acid is removed (by re-introduce the pure furfural). The process can be repeated and the conversion can be recovered with the same trend. These also take place with palladium over other supports (SiO_2, γ-Al_2O_3, HY, TiO_2, and CeO_2) as shown in Figure 7.11.

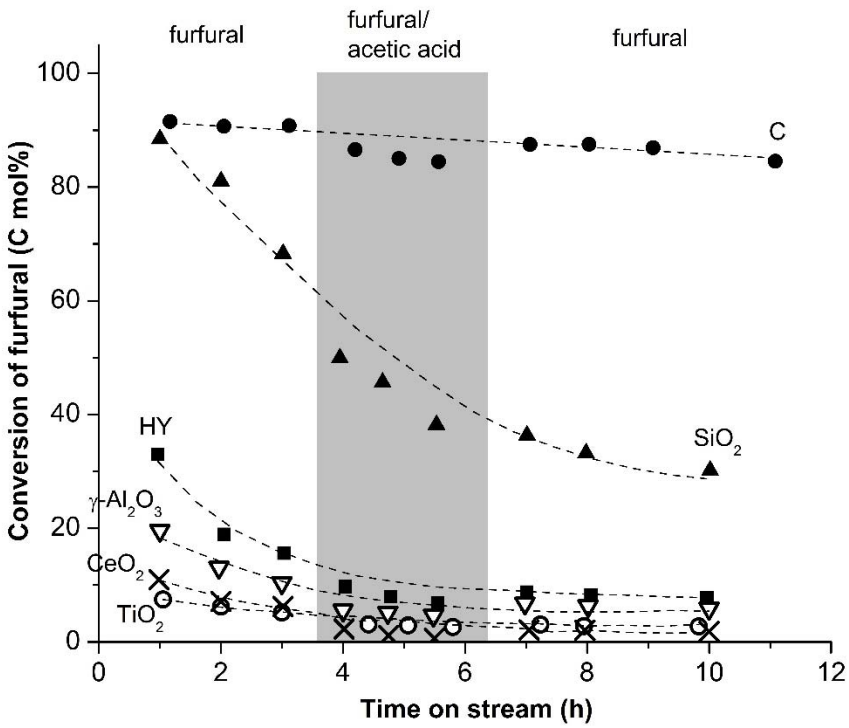

Figure 7.11 Decarbonylation of alternated furfural - 50%wt furfural/acetic acid over various Pd support catalysts

523 K, 0.17 g.h.mol^{-1}(furfural), H_2 60 ml.min^{-1}, 5%wt Pd loading, 0% acetic acid conversion

These results are evidences for temporary deactivation of catalyst due to competitive adsorption by acetic acid. For Pd/ZnO, no activity is observed. This is due the formation of PdZn alloy when treat the palladium with zinc oxide in H_2 at > 523 K [34-35].

However, a further heat up of Pd/C in H_2 to 673 K results in a severe drop of activity (< 5 %). This is a result of agglomeration of palladium as evidenced by the increase in palladium particle, as compared to the fresh catalyst (TEM, Figure 7.12 and Table 7.1).

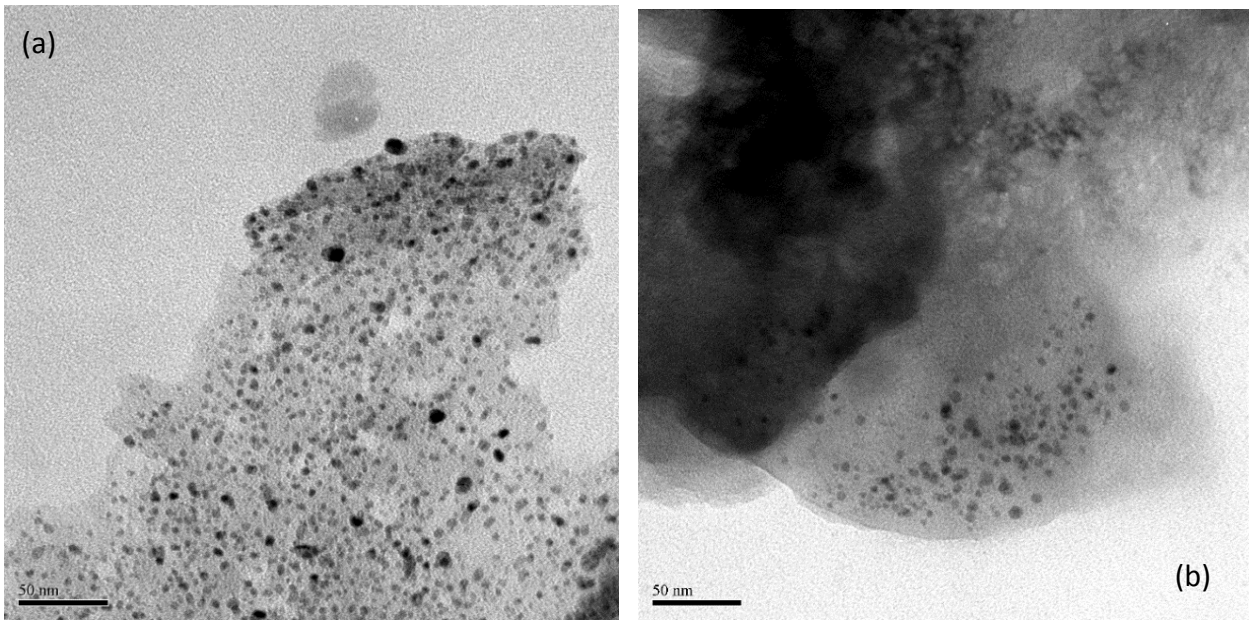

Figure 7.12 TEM image of Pd/C at 62 kX a) fresh b) after heated to 673 K; 5%wt palladium loading

The presence of acetic acid in the feed does not only decrease the conversion via competitive adsorption , but also leads to a more severe deactivation as shown in Figure 7.9. One could expect that as furfural is competitively adsorbed by acetic acid, polymerization and coke deposit would be suppressed. Hence, the observed

deactivation may be a result of active site loss. This can be verified by an experiment with alternated feeding as shown in Figure 7.13.

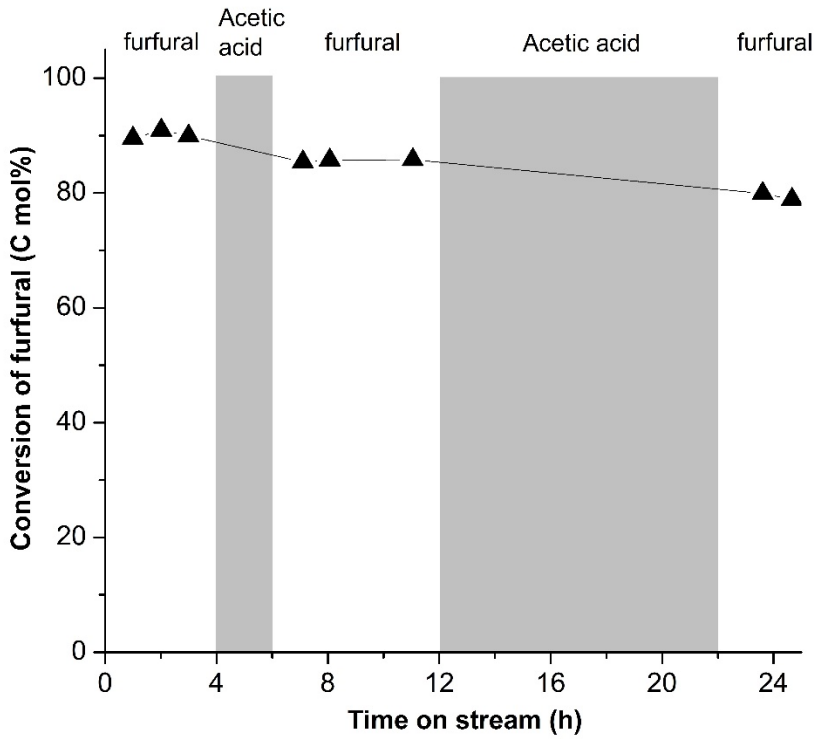

Figure 7.13 Decarbonylation of alternated furfural - acetic acid over Pd/C

523 K, 0.17 g.h.mol^{-1}(furfural), H_2 60 ml.min^{-1}, 0% acetic acid conversion

It can be seen that a furfural conversion level is decreased after feeding acetic acid over catalyst for a period of time. As furfural is absent, deactivation due to coke deposit shall not be the case for the observed decline in conversion when furfural is re-introduced. The catalyst must be deactivated during acetic acid feeding. TEM of spent catalysts show that the number of particle and particle size of palladium are decreased for Pd/C while no palladium is observed from Pd/ SiO_2 and Pd/γ-Al_2O_3, as compared to the fresh catalysts (Figure 7.14-7.16 and Table 7.1).

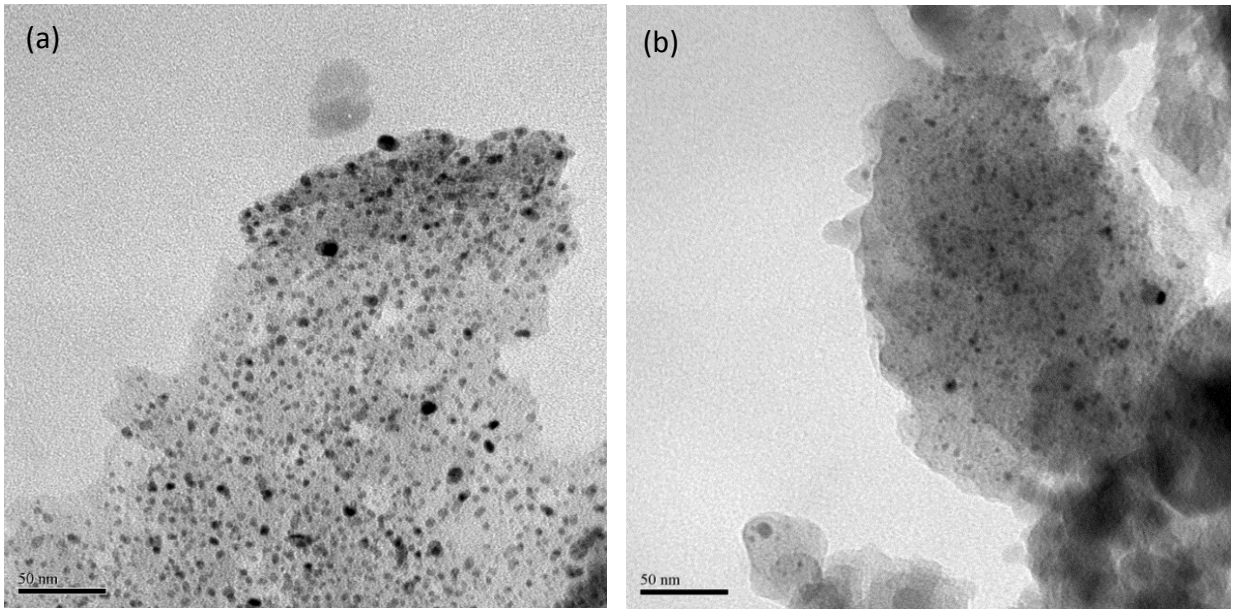

Figure 7.14 TEM image of Pd/C at 62 kX a) fresh b) after exposed in furfural/acetic acid at 523 K; 5%wt palladium loading

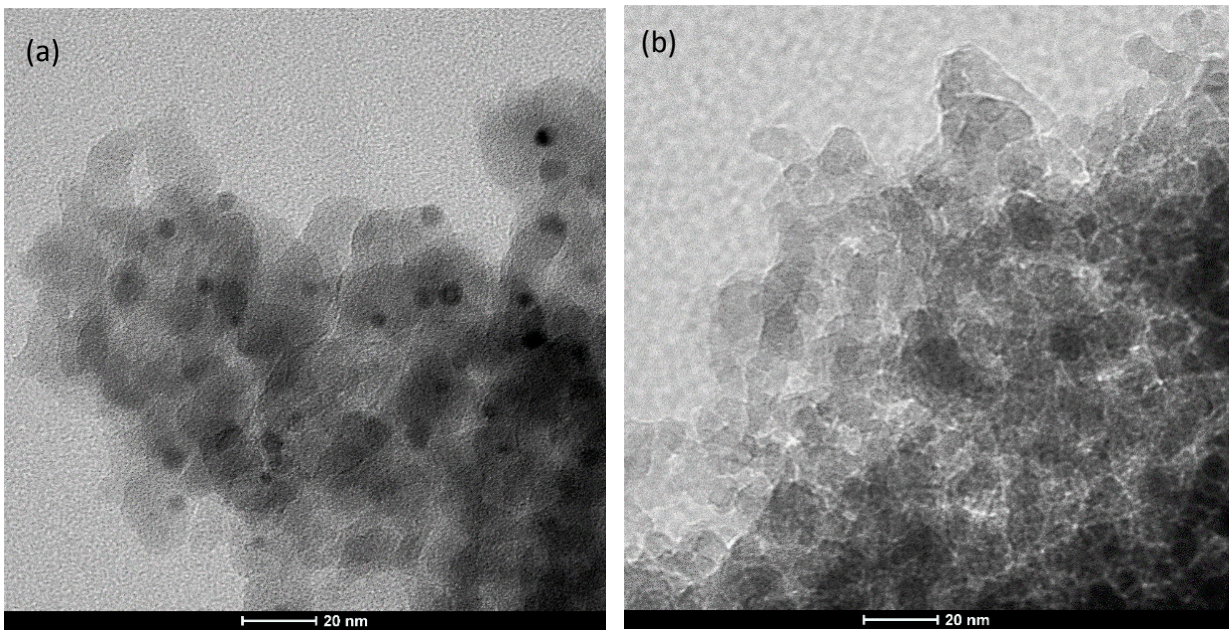

Figure 7.15 TEM image of Pd/SiO_2 at 285 kX a) fresh b) after exposed in furfural-50%wt furfural/acetic acid; 5%wt palladium loading

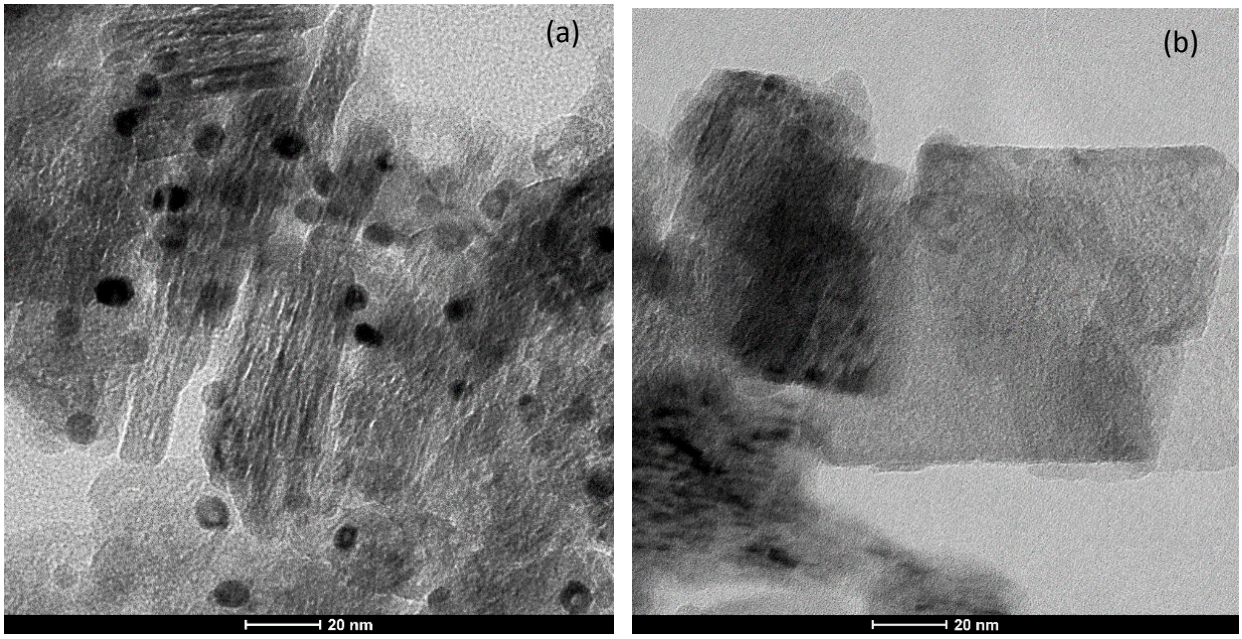

Figure 7.16 TEM image of Pd/γ-Al_2O_3 at 285 kX a) fresh b) after exposed in furfural-50%wt furfural/acetic acid; 5%wt palladium loading

These results indicate the corrosion of palladium by acetic acid, presumably forming of volatile palladium acetate, is a cause of permanent deactivation.

7.3.2.2 Hydrodeoxygenation of furfural over Cu/zeolite

As the corrosion is an obstacle for utilization of palladium catalysts under acid condition, the copper catalyst is instead tested for HDO of furfural. However, the copper catalysts does not facilitate the decarbonylation of furfural. Figure 7.17a shows that the hydrogenation furfural to furfuryl alcohol is selectively promoted (> 90% at 70-80 % conversion) over Cu/ SiO_2 catalyst.

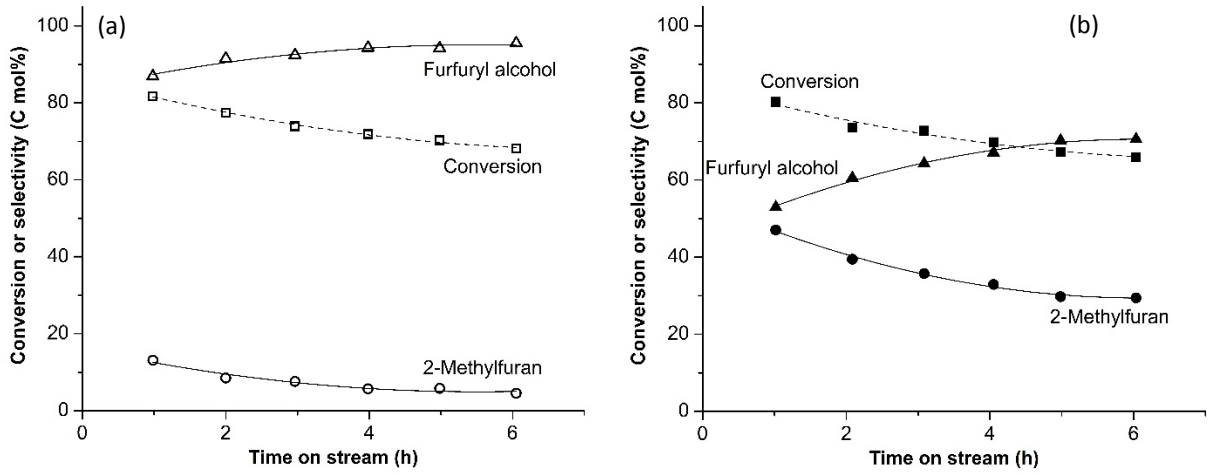

Figure 7.17 HDO of furfural over a) Cu/SiO_2 b) Cu/HY

523 K, 8 g.h.mol^{-1}, H_2 as carrier at 60 ml.min^{-1}, 5%wt Cu loading

Meanwhile, small amount of 2-methylfuran, which is a high octane fuel, is obtained as by-product from further hydrogenolysis of the furfuryl alcohol (< 10% selectivity) [7]. The hydrogenation pathway of furfural hydrogenation over Cu/SiO_2 can be illustrated below;

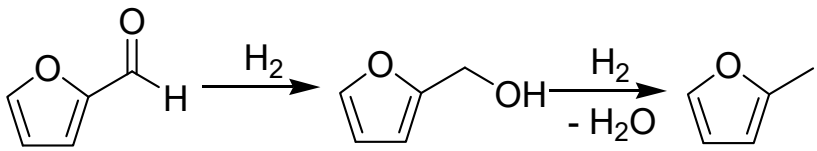

The selectivity to 2-methylfuran can be improved to 30-40 % when the Cu/HY is used (Figure 7.17b). This is because the acid function on support promotes the dehydration of furfuryl alcohol produced. From Figure 7.18, it is found that when the contact time is increased. Yield of furfuryl alcohol increases then declines at > 5 g.h.mol^{-1}.

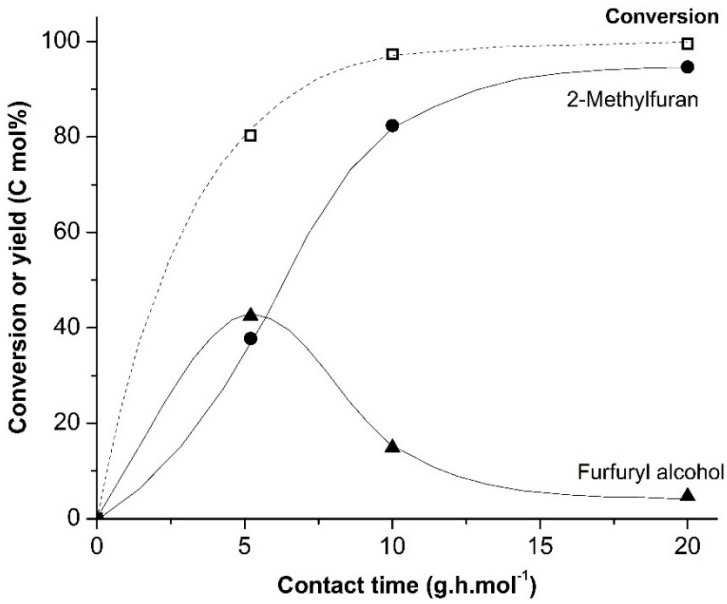

Figure 7.18 Effect of contact time to HDO of furfural over Cu/HY

543 K and atm, H_2 as carrier at 60 ml.min^{-1}, 5%wt Cu loading

This points out that the furfuryl alcohol is generated first then consumed by the other process. The continuous increase in 2-methylfuran yield reveals that this is a secondary product derived from furfuryl alcohol as shown below;

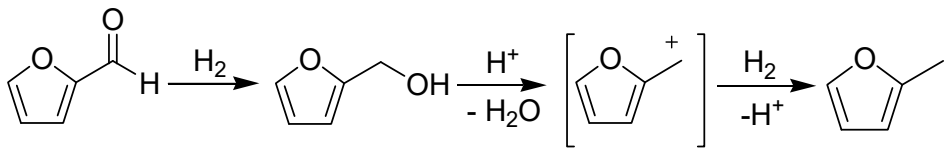

This is consistent with the result when feeding the furfuryl alcohol. The 2-methylfuran is readily formed [18]. Hence, the HDO of furfural to 2-methylfuran over Cu/zeolite is a sequential process of hydrogenation-dehydration-hydrogenation. This requires synchronization between the metal and the Brønsted acid function, in a manner similar to HDO of acetone to propane mentioned in section 5.3.4.3 (Chapter 5). The furfural is primarily hydrogenated to furfuryl alcohol over copper. The alcohol produced is subsequently protonated at the hydroxyl that undergoes dehydration over Brønsted

acid site. The carbenium ion generated is pretty stable over the acid site due to the resonance effect from pi-electron of the furan ring. It can be further hydrogenated to 2-methylfuran via hydrogen transfer from adjacent copper site.

A decline in conversion over both Cu/SiO_2, Cu/HY (Figure 7.17) points out that deactivation takes place over these catalysts. The TGA of spent Cu/SiO_2 in air (Table 7.4) reveals that the carbon deposit on copper may well be responsible for the deactivation of hydrogenation activity.

Table 7.4 Thermo-gravimetric analysis of spent Cu/SiO_2 and Cu/HY after HDO of furfural

Catalyst	Testing gas	Weight loss (%)		
		473-603 K	>603 K	Total
Cu/SiO_2	Air	2.5	4.8	7.3
	N_2	7.5 (not separated)		7.5
Cu/HY	Air	5.0	5.6	10.6

A TGA of the spent Cu/SiO_2 in nitrogen (Table 7.4) also shows the similar amount of carbon deposit, as tested in air. As the oxygen is not required to decompose the carbon deposit, it is suggested that the carbon deposit is high molecular weight products strongly adsorbed on the metal surface probably derived from the polymerization of furfural. They cannot be flushed at the catalytic testing temperature and blocking the accessibility of feed to copper surface. On the other side, when Cu/HY is used, an additional carbon deposit is observed, as compared to Cu/SiO_2. This indicates that the carbon is not only deposits on the copper surface but also on the zeolite. This is common as Brønsted acid is highly reactive, particularly with unsaturate and oxygenate compounds. The polymerization of furfural as well as furfuryl alcohol is rapidly promoted.

As the acetic acid and water obviously interfere the furfural conversion over palladium catalysts, they were also tested with copper catalyst. Surprisingly, it is found that the presence of acetic acid in stream leads to improvement of the conversion and selectivity to 2-methylfuran, as compared to furfural alone (Figure 7.19a-b).

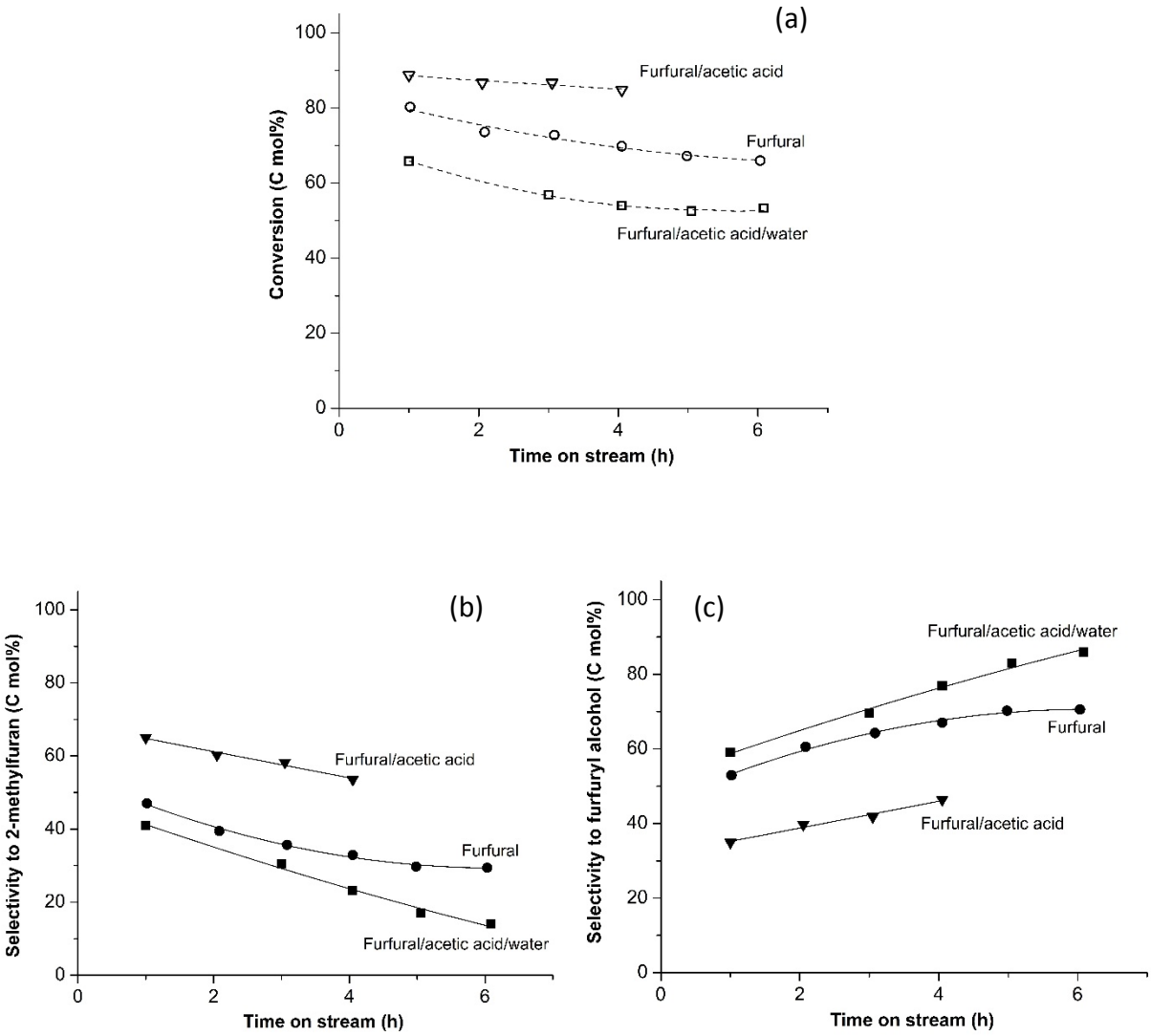

Figure 7.19 HDO of furfural, 50%wt furfural/acetic acid, and 7.5%wt furfural/7.5%wt acetic acid/water over Cu/HY

a) conversion
b) selectivity to 2-methylfuran
c) selectivity to furfuryl alcohol

523 K, 8 g.h.mol^{-1}, H_2 60 ml.min^{-1}, 5%wt Cu loading, 0% acetic acid conversion

This is probably due to the proton shuttling process when acetic acid is presented in the reaction stream [36]. Acetic acid can undergo dissociative adsorption over copper surface generating the surface hydrogen as illustrated below;

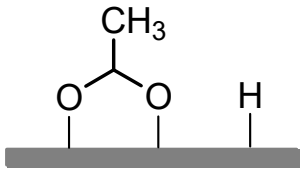

With this, the copper surface does not only acts as hydrogen storage, but also the proton donor to any adsorbed species. This would facilitate hydrogenation of the furfural, particularly at carbonyl group by the surface hydrogen and proton donor. Hence, the total rate is increased. The dissociated hydrogen from gas phase can be compensated when the acetic acid is desorbed.

Although the severe corrosion has been observed with palladium (section 7.3.2.1), one could expect that the strong interaction of acetic acid with copper as mentioned earlier, could also lead to copper leaching. The TEM of the spent Cu/HY in furfural/acetic acid is then checked as shown in Figure 7.20.

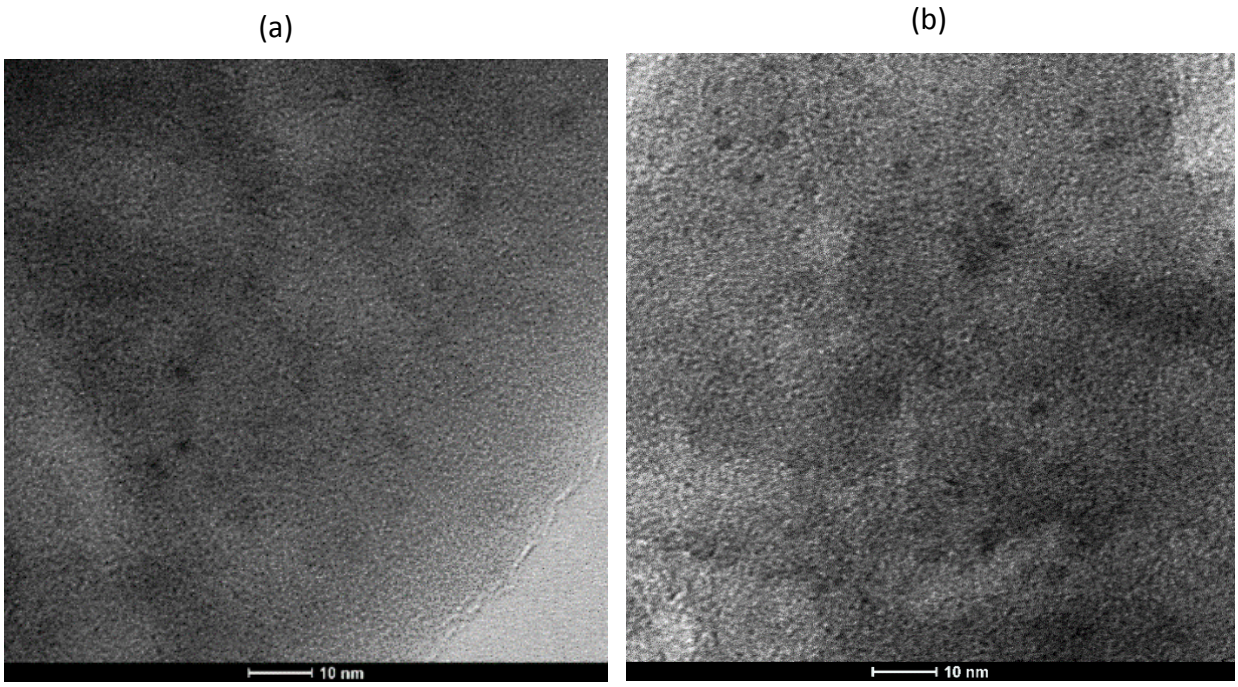

Figure 7.20 TEM image of Cu/HY at 440 kX a) fresh b) after exposed in furfural/acetic acid; 5%wt copper loading

No significant change in copper particle size from Cu/HY catalyst is observed after exposed to acetic acid, as compared to fresh catalyst (Figure 5.5a-b, Table 7.1). The Cu/HY seems to possess an outstanding corrosion resistance. In opposite manner to acetic acid, the water obviously decreases the dehydration rate as seen from the increase in furfuryl alcohol left unconverted (Figure 7.19c) and a lower in 2-methylfuran selectivity (Figure 7.19b). The furfural conversion is also decreased, as compared to furfural/acetic acid fed (Figure 7.19a). This is due to the competitive adsorption of water with furfural, as mentioned earlier.

From Figure 7.19a, no conversion of acetic acid is observed at low contact time (8 g.h.mol^{-1}) despite that acetic acid alone can be direct HDO over Cu/HY at this temperature, as shown in section 6.3.2.1 (Chapter 6). This indicates that the furfural possesses stronger adsorption on copper surface, as compared to acetic acid. Therefore, no acetic acid shall be converted unless all furfural is consumed. With higher contact

time (83 g.h.mol^{-1}), it is found that conversion of acetic acid (3%) is observed with 100% furfural conversion at 523 K, as shown in Figure 7.21.

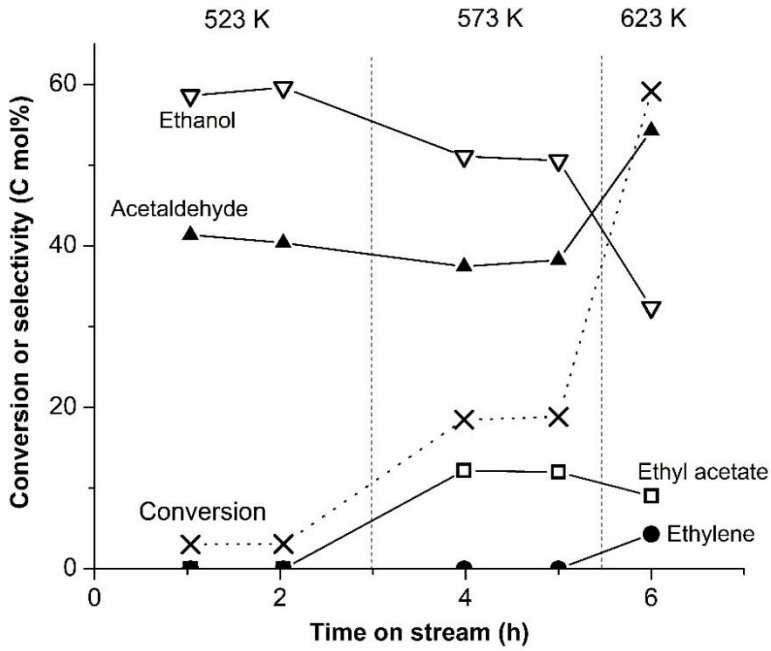

Figure 7.21 HDO 50%wt furfural/acetic acid over Cu/HY at 523-623 K

Furfural 83 g.h.mol^{-1}, acetic acid 52 g.h.mol^{-1}, H_2 60 ml.min^{-1},

100% furfural conversion and 100% 2-methylfuran selectivity for all test

Only acetaldehyde and ethanol are obtained from HDO of acetic acid. No ethylene and ethyl acetate are observed because the temperature is not enough to promote the subsequent dehydration. The increase in reaction temperature to 573 K results in the increase in conversion of acetic acid (20%). While, selectivity to ethanol is declined because it is consumed in esterification with acetic acid to form ethyl acetate. However, the ethylene cannot be produced due to competitive adsorption of acetic acid feed over the ethanol produced. The increase in reaction temperature to 623 K can further increase acetic acid conversion to 58%. The running low of acetic acid leads to some ethylene production from ethanol dehydration. The esterification is suppressed as seen from the drop of ethyl acetate selectivity. It is worth noting that HDO of furfural

over Cu/HY at this temperature gives 100 % of 2-methylfuran yield. With these results, the simultaneously conversion of furfural and acetic acid by HDO can be achieved producing high value chemicals with high stability of catalyst.

7.4 Conclusion

The palladium (on C, SiO_2, γ-Al_2O_3, HY, TiO_2, ZnO, and CeO_2) are not suitable catalyst for deoxygenation of furfural from bio-oil due to the corrosion and competitive adsorption by acetic acid present. Meanwhile, the copper catalysts exhibit the excellent stability. The bi-functional 5%Cu/HY catalyst can be successfully used to upgrade bio-oil by transforming the all furfural to 100% of 2-methylfuran at >523 K via hydrogenation-dehydration-hydrogenation. Moreover, the acetic acid present can be subsequently upgraded to ethylene, ethanol, acetaldehyde, and ethyl acetate at the same catalyst and reaction conditions. However, it is notified that competitive adsorption by water composed in bio-oil can decrease the catalyst performance.

7.5 References

[1] Mullen C.A. and Boateng A.A. "Chemical Composition of Bio-oils Produced by Fast Pyrolysis of Two Energy Crops" **Energy & Fuels,** vol.22, 2008. pp.2104-2109.

[2] Seidel A., Editor. "Furan derivatives" **Kirk-Othmer encyclopedia of chemical technology.** vol.12: 259-281.

[3] Kamm B., Gruber P.R. and Kamm M., Editors. **Biorefineries-Industrial Processes and Products Volume 2.** Darmstadt: Wiley-VCH. 2006.

[4] Kunioka M., Masuda T., Tachibana Y., Funabashi M. and Oishi A. "Highly selective synthesis of biomass-based 1, 4-butanediol monomer by alcoholysis of 1, 4-diacetoxybutane derived from furan" **Polymer Degradation and Stability**, vol.109, 2014. pp.393-397.

[5] Choudhary H., Nishimura S. and Ebitani K. "Metal-free oxidative synthesis of succinic acid from biomass-derived furan compounds using a solid acid catalyst with hydrogen peroxide" **Applied Catalysis A: General,** vol.458, 2013. pp.55– 62.

[6] Wang S., Vorotnikov V. and Vlachos D.G. “Coverage-Induced Conformational Effects on Activity and Selectivity: Hydrogenation and Decarbonylation of Furfural on Pd (111)” **ACS Catalysis,** vol.5, 2015. pp.104-112.

[7] Sitthisa S. and Resasco D.E. “Hydrodeoxygenation of Furfural Over Supported Metal Catalysts: A Comparative Study of Cu, Pd and Ni” **Catalysis Letter,** vol.141, 2011. pp.784–791.

[8] Sitthisa S., Pham T., Prasomsri T., Sooknoi T., Mallinson R.G. and Resasco D.E. “Conversion of furfural and 2-methylpentanal on Pd/SiO_2 and $Pd–Cu/SiO_2$ catalysts” **Journal of Catalysis,** vol.280, 2011. pp.17–27.

[9] Zhang W., Zhu Y., Niu S. and Li Y. “A study of furfural decarbonylation on K-doped Pd/Al_2O_3 catalysts” **Journal of Molecular Catalysis A: Chemical,** vol.335, 2011. pp.71–81.

[10] Lesiak M., Binczarski M., Karski S., Maniukiewicz W., Rogowski J., Szubiakiewicz E., Berlowska J., Dziugan P. and Witonska I. “Hydrogenation of furfural over $Pd–Cu/Al_2O_3$ catalysts. The role of interaction between palladium and copper on determiningcatalytic properties” **Journal of Molecular Catalysis A: Chemical,** vol.395, 2014. pp.337–348.

[11] Pushkarev V.V., Musselwhite N., An K., Alayoglu S. and Somorjai G.A. “High Structure Sensitivity of Vapor-Phase Furfural Decarbonylation/Hydrogenation Reaction Network as a Function of Size and Shape of Pt Nanoparticles” **Nano Letters,** vol.12, 2012. pp.5196-5201.

[12] Coca J., Morrondo E.S. and Sastre H. “Catalytic Decarbonylation of Furfural in a Fixed-Bed Reactor” **Journal of Chemical Technology and Biotechnology**, vol.32, 1982. pp.904-908

[13] Srivastava R.D. and Guha A.K. “Kinetics and Mechanism of Deactivation of Pd/Al_2O_3 Catalyst in The Gaseous Phase Decarbonylation of Furfural” **Journal of Catalysis,** vol.91, 1985. pp.254-262.

[14] Yan K., Wu G., Lafleur T. and Jarvis C. “Production, properties and catalytic hydrogenation of furfural to fuel additives and value-added chemicals” **Renewable and Sustainable Energy Reviews**, vol.38, 2014. pp.663–676.

[15] Sitthisa S., Sooknoi T., Ma Y., Balbuena P.B. and Resasco D.E. “Kinetics and mechanism of hydrogenation of furfural on Cu/SiO_2 catalysts” **Journal of Catalysis,** vol.277, 2011. pp.1–13.

[16] Burnette L.W., Johns I.B., Holdren R.F. and Hixon R.M. “Production of 2-Methylfuran by Vapor-Phase Hydrogenation of Furfural” **Industrial and Engineering Chemistry,** vol.40, 1948. pp.502-505.

[17] Brown H.D. and Hixon R.M. “Vapor Phase Hydrogenation of Furfural to Furfuryl Alcohol” **Industrial and Engineering Chemistry,** vol.41, 1949. pp.1382-1385.

[18] Sitthisa S., An W. and Resasco D.E. “Selective conversion of furfural to methylfuran over silica-supported Ni-Fe bimetallic catalysts” **Journal of Catalysis,** vol.284, 2011. pp.90–101.

[19] Lessard J., Morin J., Wehrung J., Magnin D. and Chornet E. “High Yield Conversion of Residual Pentoses into Furfural via Zeolite Catalysis and Catalytic Hydrogenation of Furfural to 2-Methylfuran” **Topics in Catalysis**, vol.53, 2010. pp.1231–1234.

[20] Panagiotopoulou P. and Vlachos D.G. “Liquid phase catalytic transfer hydrogenation of furfural over a Ru/C catalyst” **Applied Catalysis A: General**, vol.480, 2014. pp.17–24.

[21] Elliott D.C., Hart T.R., Neuenschwander G.G., Rotness L.J. and Zacher A.H. “Catalytic Hydroprocessing of Biomass Fast Pyrolysis Bio-oil to Produce Hydrocarbon Products” **Environmental Progress & Sustainable Energy,** vol.28, 2009. pp.441-449.

[22] Fisk C.A., Morgan T., Ji Y., Crocker M., Crofcheck C. and Lewis S.A. “Bio-oil upgrading over platinum catalysts using in situ generated hydrogen” **Applied Catalysis A: General,** vol.358, 2009. pp.150–156.

[23] Wildschut J., Melián-Cabrera I. and Heeres H.J. “Catalyst studies on the hydrotreatment of fast pyrolysis oil” **Applied Catalysis B: Environmental,** vol.99, 2010. pp.298-306.

[24] Bernardes M.A., Editor. Biofuel's Engineering Process Technology. Rijeka: InTech. 2011.

[25] Hoang D.L., Dang T.T.H., Engeldinger J., Schneider M., Radnik J., Richter M. and Martin A. “TPR investigations on the reducibility of Cu supported on Al_2O_3, zeolite Y and SAPO-5” **Journal of Solid State Chemistry**, vol.184, 2011. pp.1915–1923..

[26] Sagar G.V., Rao P.V.R., Srikanth C.S. and Chary K.V.R. “Dispersion and Reactivity of Copper Catalysts Supported on Al_2O_3-ZrO_2” **Journal of Physical Chemistry B,** vol.110, 2006. pp.13881-13888..

[27] Strassberger Z., Alberts A.H., Louwerse M.J., Tanase S. and Rothenberg G. "Catalytic cleavage of lignin β-O-4 link mimics using copper on alumina and magnesia–alumina" **Green Chemistry**, vol.15, 2013. pp.768-774.

[28] Huo C., Ouyang J. and Yang H. "CuO nanoparticles encapsulated inside Al-MCM-41 mesoporous materials via direct synthetic route" **Scientific Reports**, vol.4, 2014. pp.1-9.

[29] Singh H., Prasad M. and Srivastava R.D. "Metal support interactions in the palladium catalysed decomposition of furfural to furan" **Journal of Chemical Technology and Biotechnology**, vol.30, 1980. pp.293-296.

[30] Bitemirova A.E., Alihanova H.B., Spabekova R.S., Shagrayeva B.B. and Ermahanov M.N. "Regeneration of spent catalysts for furfural decarbonylation" **Modern Applied Science**, vol.9, 2015. pp.358-366.

[31] Pang S.H., Schoenbaum C.A., Schwartz D.K. and Medlin J.W. "Directing reaction pathways by catalyst active-site selection using self-assembled monolayers" **Nature Communications**, vol.4, 2013. pp.1-6.

[32] Rivelino R. and Canuto S. "Conformational stability of furfural in aqueous solution: The role of hydrogen bonding" **Brazilian Journal of Physics**, vol.34, 2004. pp.84-89

[33] Gatta G.D., Badea E. and Saczuk M. "Thermodynamics of solvation of some linear and branched aliphatic aldehydes in water and heptane" **Journal of Chemical Thermodynamics**, vol.42, 2010. pp.1204–1208.

[34] Yanhua W., Jingchang Z. and Hengyong X. "Interaction between Pd and ZnO during reduction of Pd/ZnO catalyst for steam reforming of methanol to hydrogen" **Chinese Journal of Catalysis**, vol.27, 2006. pp.217-222.

[35] Yanhua W., Jingchang Z., Hengyong X. and Xuefeng B. "Reduction of Pd/ZnO catalyst and its catalytic activity for steam reforming of methanol" **Chinese Journal of Catalysis**, vol.28, 2007. pp.234-238.

[36] Pingen D. **Hydrogen shuttling as a tool in the catalytic synthesis of amines: development and scope**. UK: Eindhoven University. 2010.

Chapter 8

Conclusions and suggestions

8.1 Conclusions

As the light fraction of bio-oil obtained from pyrolysis consists of a several oxygenate compounds that are limited in utilization, this thesis has accomplished approach for the upgrading of those components (totally >15 % constituent in bio-oil) to high value fuels and petrochemical. Acetone (Chapter 4-5), acetic acid (Chapter 6) and furfural (Chapter 7), a model compound for ketones, carboxylic acid and aldehyde, respectively, are selectively deoxygenated to olefins at mild condition (448-573 K and atmospheric pressure).

In Chapter 4, acetones can be self-deoxygenated to *i*-butylene and acetic acid over proton zeolites at > 448 K. This is a sequential process occur in pore of the zeolites. Briefly, two acetones are activated by Brønsted acid results in aldol condensation to a diacetone alcohol. The dehydration of diacetone alcohol takes place readily via concerted mechanism (E2) generating a mesityl oxide. This compound can be decomposed when protonated at the C=C, primarily producing *i*-butylene and ethenone. Water from aldol condensation is then react with ethenone to form acetic acid. The additional deoxygenation can be employed by increasing the reaction temperature (> 498 K). The two acetic acid produced can be ketonized regenerating acetone for further self-deoxygenation. The oxygens composed in acetic acid is removed by the formation of carbon dioxide and water. However, the *i*-butylene produced is highly reactive. The secondary reactions including oligomerization, aromatization, dealkylation, and cracking via hydrocarbon pools formation are promoted, particularly at high temperature. These pools can be evolved to coke leading to severe deactivation. As the self-deoxygenation is a multi-step process, the low Si/Al zeolite is an outstanding catalyst. This is because it can provide a short range proximity facilitating the adsorption of reactant and re-adsorption of the intermediates. Meanwhile, the mass transfer of reactant and products through the catalyst would be promoted using the large three dimensional pore zeolite with channel structure, such as β. A test with asymmetry ketone namely ethyl methyl ketone reveals that pore of zeolite (HZSM-5)

can constrain the intermediates generated during the self-deoxygenation. Hence, an excellence selectivity to C5 olefins is obtained.

The use of hydrogen as a reactant is an optional deoxygenation when hydrogen is available. The acetone upgrading via hydrodeoxygenation (HDO) is achieved in Chapter 5. A sequential process of hydrogenation-dehydration is employed to produce the propylene. The individual study of acetone hydrogenation to *i*-propanol over a several metal catalyst (Cr, Fe, Co, Ni, Cu, and Pd) reveals that the copper is an outstanding catalyst as the *i*-propanol produced is never converted at 473 K. While, the nickel provides good activity even at low temperature (448 K). The alloy of copper into nickel can partially decrease the hydrogenolysis activity, as compared to the nickel alone. The increase in metal loading onto silica support leads to the agglomeration, hence the normalized hydrogenation rate is dropped. The hydrogenation activity is generally limited by thermodynamic. However, some secondary reaction, such as hydrogenolysis of *i*-propanol to methane can increase the level of hydrogenation over the thermodynamic limitation as the concentration of alcohol is reduced. Moreover, the *i*-propanol can be either directly dehydrated to propylene or diisopropyl ether in pore of zeolite. The zeolite with good mass transfer (large three dimensional pore with channel structure), such as H-β is an excellent catalyst in term of activity. While, the smaller pore of HZSM-5 is a suitable catalyst for diisopropyl ether suppression. The HDO by hydrogenation-dehydration using Ni/SiO_2-HZSM-5 catalyst can be achieved only in sequential bed system at < 448 K to prevent the hydrogenation and hydrogenolysis of the olefin produced. Over these sequential catalyst, the acetone and ethyl methyl ketone (MEK) can be converted to propylene and *n*-butylene, respectively. However, some deactivation is observed over Brønsted acid site in zeolite via carbon deposition. In contrast, there is no hydrogenation of propylene produced over copper. The HDO of ketone using Cu/SiO_2-zeolites can be carried out over physical mixed catalyst with wide range of temperature (423-473 K). Acetone, MEK, and cyclohexanone are selectively converted to their corresponded olefins (propylene, *n*-butylene, and cyclohexene, respectively) over a single bed of Cu/SiO_2-HZSM-5 mixture. A slightly higher activity, when compared to the use of copper alone, is derived from the decrease in alcohol concentration via the further dehydration to olefin. However, isomerization of the olefin produced is obtained as the Brønsted acid is excessively used. The catalyst formulation is a major concern as the aldol condensation of ketone fed is detected when highly active zeolite, such as H-β is instead used. The incorporation of copper into zeolite forming bi-functional catalyst would eliminate the problem derived from the balancing

between metal and acid site. At a certain amount of each catalyst function (5%wt Cu on HZSM-5 or HY (acidity ~ 120 μmol/g), a significant increase in activity is obtained, as compared to the mixed catalyst. This is a result of a short range proximity between the metal and the acid sites. However, this leads to some hydrogenation of olefin adsorbed on acid site via H-transfer from adjacent copper sites. The use of HY as support can provide a good dispersion of copper into its large pore, as compared to the external pore copper obtained from the HZSM-5 support, leading to an improved activity. The order of reactivity is acetone > cyclohexanone > MEK.

As the bi-functional catalyst of Cu/zeolites exhibits an outstanding performance in olefin production from ketone, they can be participated in acetic acid upgrading via a sequential process so called "keto-hydrodeoxygenation" (KHDO) over mixture of CeO_2-Cu/zeolites catalyst at 573 K in Chapter 6. Briefly, two acetic acid is ketonized to a ketone over cerium (IV) oxide catalyst and the oxygens are eliminated as a carbon dioxide and a water. The acetone produced is subsequently HDO (hydrogenation-dehydration) to propylene over Cu/zeolites bi-functional catalyst, in a manner similar to discussion in Chapter 5. However, the acetic acid is also activated over the Cu/zeolites generating co-products from direct hydrogenation (ethylene, ethanol, acetaldehyde, and ethyl acetate). The increase in reaction temperature can increase the KHDO products (propylene and acetone) but the propylene produced is largely hydrogenated to propane via the H-transfer at adjacent copper-acid site, as mentioned earlier. A formulation of catalyst (75%wt CeO_2 + 25%wt Cu/zeolite) can improve the selectivity to KHDO product without paraffin production. Moreover, additional increase in KHDO products is accomplished by an increase in ketonization rate via the increase in acetic acid concentration. Alternatively, the use of sequential bed can provide high selectivity to KHDO products by minimize the contact between the acetic acid and the copper. The CeO_2-Cu/HY catalyst exhibits a better selectivity to KHDO products as well as the stability, as compared to CeO_2-Cu/HZSM-5. The KHDO with CeO_2-Cu/HY catalyst is extremely stable up to 30 hours on stream. However, a temporary deactivation by the water, adsorbed on the acid site, is a major concern. The KHDO can be extend to use in a production of light distillated hydrocarbons from acetic acid by adding another sequential bed of HZSM-5 catalyst.

In Chapter 7, the decarbonylation of furfural to furan in a presence of acetic acid and water is selected as model reaction for bio-oil upgrading. At 523 K, the decarbonylation of furfural over Pd/C gives decarbonylation products (furan,

tetrahydrofuran, and carbon monoxide) and hydrogenation products (furfuryl alcohol, tetrahydrofurfural alcohol). The presence of water can slightly improve the selectivity to decarbonylation product without any effect to the activity. However, the presence of acetic acid severally decreases the activity of palladium support catalysts (on C, SiO_2, γ-Al_2O_3, HY, TiO_2, ZnO, and CeO_2). The palladium can be corroded by the acid as well as support in case of ZnO leading to permanent deactivation. Moreover, the acetic acid can be competitively adsorbed on to palladium surface resulting in temporary deactivation. In contrast, the copper catalysts possess the excellent resistance to acetic acid. Over Cu/SiO_2, furfural is hydrogenated to furfuryl alcohol. Adding the acid function by using Cu/HY results in 2-methyl furfural production (maximum 100% yield) from subsequent dehydration-hydrogenation of the furfuryl alcohol produced. The water can competitively adsorbed onto acid site as mentioned earlier, leading to temporary deactivation. Surprisingly, the presence of acetic acid can enhance the hydrogenation of furfural via proton shuttling process. The sequential conversion of furfural and acetic acid is accomplished over Cu/HY catalyst at higher the contact time or reaction temperature. The deactivation by carbon deposition is noticed over both copper and palladium catalysts.

8.2 Suggestions

8.2.1 As the HDO can upgrade a several oxygenate in light fraction of bio-oil successfully, the test in mixture of furfural/acetic acid reveals that there is a sequent of oxygenate conversion. This thesis will be more complete if a larger series of oxygenate e.g. mixture of aldehyde, carboxylic acid, ketone as well as the compound with multi-functional group is tested. The understand in HDO sequent may leads to the better catalyst design covering the upgrading of every component in bio-oil light fraction. Then, a test with actual bio-oil light fraction would be evaluated.

8.2.2 The TEM result shows that copper can be deposited in pore of zeolite forming the clusters. However, the pore contains a number of proton. It possible that the copper clusters may be induced by the proton. Therefore, the adsorptivity of reactant to the copper would be modified. A characterization of copper by XPR is required to prove that phenomenon by a comparison between Cu/zeolite and Cu/SiO_2.

8.2.3 Copper is a well-known cheap catalyst. A synchronization between copper-acid adjacent site in Cu/zeolite leads to an improvement in hydrogenation activity of olefin to paraffin. This exhibits an opportunity to develop this catalyst replacing various noble metal catalyst, especially nickel, palladium and platinum. Furthermore, the Cu/zeolite may avoid the problem in thermodynamic limitation as the hydrogenation mechanism over metal-acid is absolutely different to over metal alone.

8.2.4 The deactivation by higher olefins is a most important obstacle in ketone self-deoxygenation. As higher olefins are derived from oligomerization of *i*-butylene. It is possible to use water suppress the oligomerization similar to coventional catalytic cracking process. Hence, an experiment with acetone/water fed is need. Alternatively, an operation in fluidized bed reactor may increase the life time of zeolite as the catalyst is always regenerated.

Appendices

Appendix A

Chromatography condition

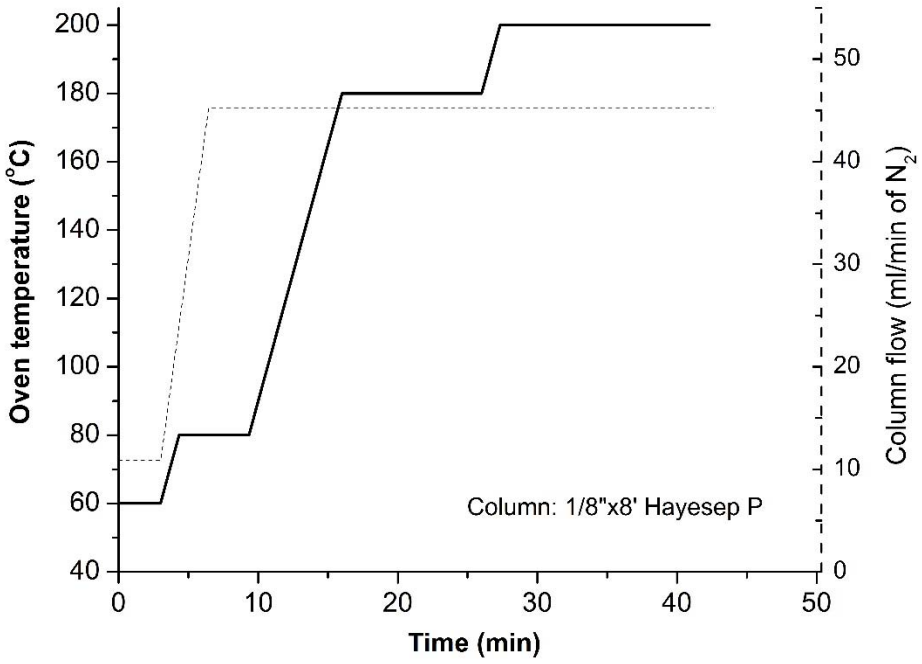

Figure A1 Analysis parameter for acetone and MEK self-deoxygenation

** Injector: 200 °C, FID: 230 °C*

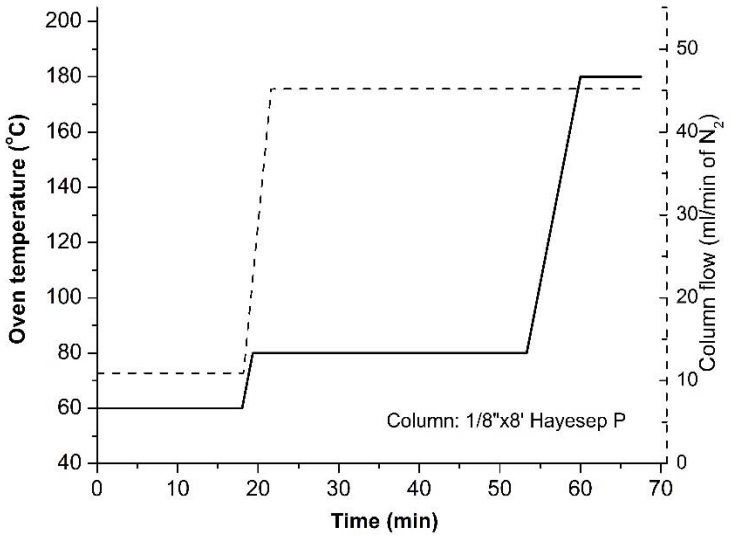

Figure A2 Analysis parameter for acetone hydrogenation, *i*-propanol dehydration acetone HDO, acetic acid KHDO, and acetic HDO

** Injector: 200 °C, FID: 230 °C*

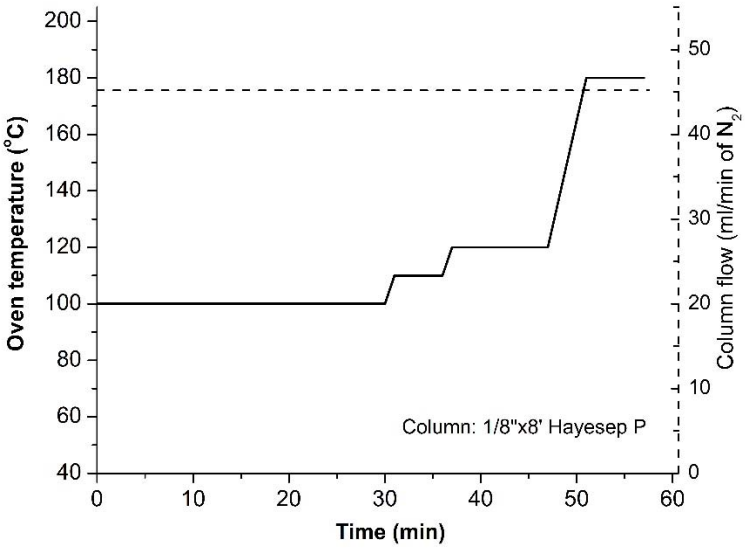

Figure A3 Analysis parameter for ethyl methyl ketone HDO

** Injector: 200 °C, FID: 230 °C*

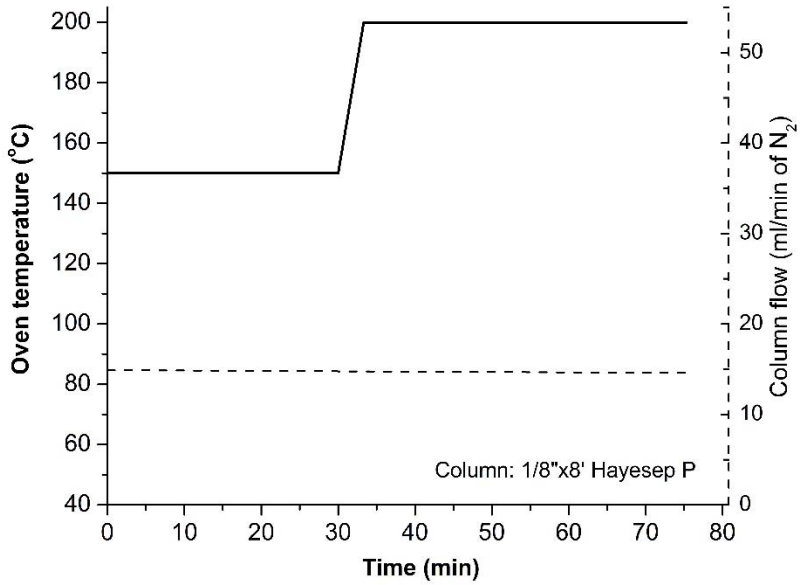

Figure A4 Analysis parameter for cyclohexanone HDO

** Injector: 200 °C, FID: 230 °C*

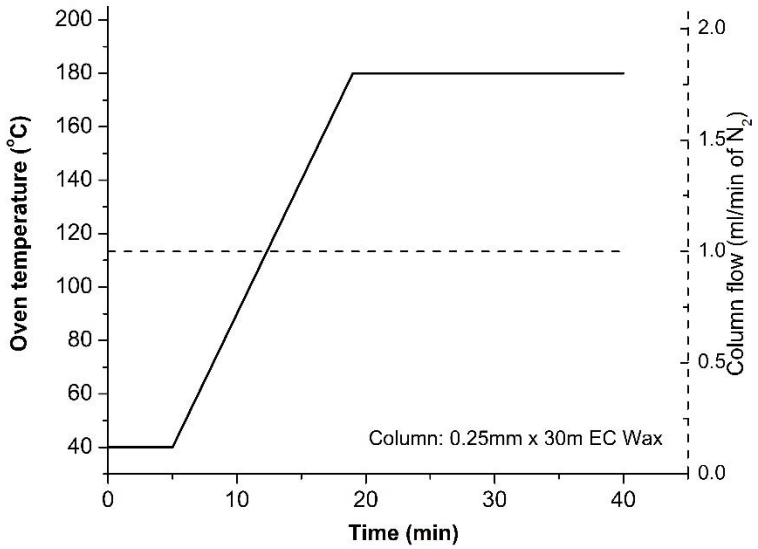

Figure A5 Analysis parameter for furfural decarbonylation and HDO

** Injector: 250 °C, FID: 300 °C*

Appendix B

Calculation

B1. Contact time

$$\text{Contact time (W/F)} = \frac{\text{Weight of catalyst (g)}}{\text{Mole feed rate of reactant (mol.hour}^{-1}\text{)}}$$

For example, in case of acetone HDO over 0.025 g of Cu/HY using 1.35 X 10^{-3} mol.h^{-1} (0.0.078 g.h^{-1})

$$\textit{Contact time} = \textit{0.025 (g) / 1.35 x } 10^{-3} \textit{ (mol.}h^{-1}\textit{)}$$

$$= \textit{18.5 g.h.mol}^{-1}$$

B2. Quantitative analysis of product

Prior analysis, the structure of products in sample was identified the by GC-MS (gas chromatography with mass spectrometer detector). Then, the quantitative analysis of products was carried out by GC-FID (gas chromatography with flame ionization detector). The chromatogram were integrated to obtain the peak area. According to the certain injection volume (by on-line sampling loop) of sample to GC, the quantitative calculation is carried out by normalization. Yield percentage can be calculated by adjusting the peak area (from chromatogram) with response factor then normalization following the equation below

$$\text{Yield of } a \text{ (C mole \%)} = \frac{(\text{area}_a \times \text{response factor}_a)}{\sum_{i=a}^{n} (\text{area}_i \times \text{response factor}_i)} \times 100$$

For example, in case of propylene

$$\text{Yield of propylene} = \frac{(801 \times 8.46) \times 10^{-5} \times 100}{(801 \times 8.46)+(56.7 \times 8.46)+(53.5 \times 11.5)+(33.5 \times 12.9) \times 10^{-5}}$$

$$= 81.6 \text{ C mole \%}$$

Conversion of reactant can be derived from the differential between staring feed (always 100%) and unconverted reactant, therefore,

Conversion (C mole %) = % reactant in feed - % unconverted reactant

For example, in case of acetone HDO

$$\text{Conversion of acetone} = 100.00\% - 7.43\%$$

$$= 92.6 \text{ C mole \%}$$

Then, selectivity to product is computed from percentage of product in converted part only, so,

$$\text{Selectivity to } a \text{ (C mole \%)} = \frac{\text{Yield of } a}{\text{Conversion}} \times 100$$

For example, in case of propylene

$$\text{Selectivity of propylene} = (81.6 / 92.6) \times 100$$

$$= 88.3 \text{ C mole \%}$$

Table B1 The area, response factor, and quantitative calculation of products HDO of acetone over Cu/HY

Products	Retention time	Area	Response factor	Yield	Selectivity
	min		C mol x10^{-5}/area	C mol %	C mol %
Propylene	16.3	801	8.46	81.6	88.3
Propane	18.2	56.7	8.46	5.78	6.24
Acetone	52.8	53.5	11.5	7.43	-
i-Propanol	56.2	33.5	12.9	5.19	5.60
Conversion				***92.6***	

473 K, 19 g.h.mol^{-1}, 6th hour

B3. Copper dispersion

The mole of hydrogen consumption for copper reduction can be calculate from TPR area of sample comparing to standard copper oxide. *In this calculation, Cu/HY is a selected example. It consumes 0.89 mmol of H_2 for completed oxide reduction and 0.290 mmol of H_2 for surface oxide reduction per 1 gram of catalyst.* From stoichiometry of copper reduction,

$Cu^{2+} + H_2 \longrightarrow Cu^0$, for complete oxide reduction

$2\ Cu^{1+} + H_2 \longrightarrow 2\ Cu^0$, for surface oxide reduction

So, mole of Cu in catalyst = mole of H_2 consumption

= *0.89 mmol/g_{cat}*

and mole of surface Cu = 2 x mole of H_2 consumption

= *0.58 mmol/g_{cat}*

Hence, dispersion of copper is

$$\% \text{ Dispersion} = \frac{\text{surface Cu}}{\text{total Cu}} \times 100$$

$$= 0.58 \text{ (mmol)} / 0.89 \text{ (mmol)} \times 100$$

$$= 65 \%$$

Then, surface area of copper can be calculated from

$$\text{Surface Cu area } (m^2/g_{Cu}) = (mol_{Cu} \times N_A) / (10^4 \times C_M \times W_{Cu})$$

where, mol_{Cu} is μmole of surface Cu per gram of catalyst

N_A is Avogadro number (6.022×10^{23} atom/mol)

C_M is number of surface Cu atom per m^2 (1.4×10^{19} atom/m^2, average from (110), (100), (111) planes)

W_{Cu} is Cu content by %wt in catalyst

$$\textit{Surface Cu area} = \frac{\textit{580 (μmol) x 6.022 x } 10^{23} \textit{ (atom/mol)}}{\textit{}10^4 \textit{ x 1.4 x } 10^{19} \textit{ (atom/m}^2\textit{) x 5 (\%wt)}}$$

$$= \textit{499 } m^2/g_{Cu}$$

B4. Turnover frequency (TOF)

From data in B3, turnover frequency can be subsequently calculated from

$$\text{TOF } (s^{-1}) = \frac{\text{conversion per gram of catalyst (mol/s)}}{\text{mole of active site per gram of catalyst (mol)}}$$

For example, in case of acetone HDO over Cu/HY at 473 K and 19 g.h.mol^{-1}, acetone conversion is 6.8 x 10^{-6} mol/s (derive from %conversion x mole feed rate) if 1 gram of catalyst is used, So

$TOF = (6.8 \times 10^{-6}) / (0.58 \times 10^{-3})$

$= 11.7 \times 10^{-3}\ s^{-1}$

B5. Normalized reaction rate

The normalized reaction rate is defined as the mole of reactant converted per mole of catalyst in a unit of time.

$$\text{Normalized rate } (t^{-1}) = \frac{\text{reactant converted (mol/t)}}{\text{catalyst used (mol)}}$$

For example, in case of acetone hydrogenation over 5%Cu/SiO_2 at 473 K and 30 g.h.mol^{-1}, acetone conversion is 0.6 mmol/h (derive from %conversion x mole feed rate) and 16 x 10^{-6} mole of copper is used, So

$Normalized\ rate = (0.6 \times 10^{-3}) / (16 \times 10^{-6})$

$= 38\ h^{-1}$

Appendix C

X-ray diffraction pattern of zeolites and metal oxide supports

All reference X-ray diffraction pattern data of zeolites are provided by the official website of International Zeolite Association (http://izasc.fos.su.se/fmi/xsl/IZA-SC/xrd.xsl). While, the diffraction patterns of metal oxides are verified with the reference database in XRD program.

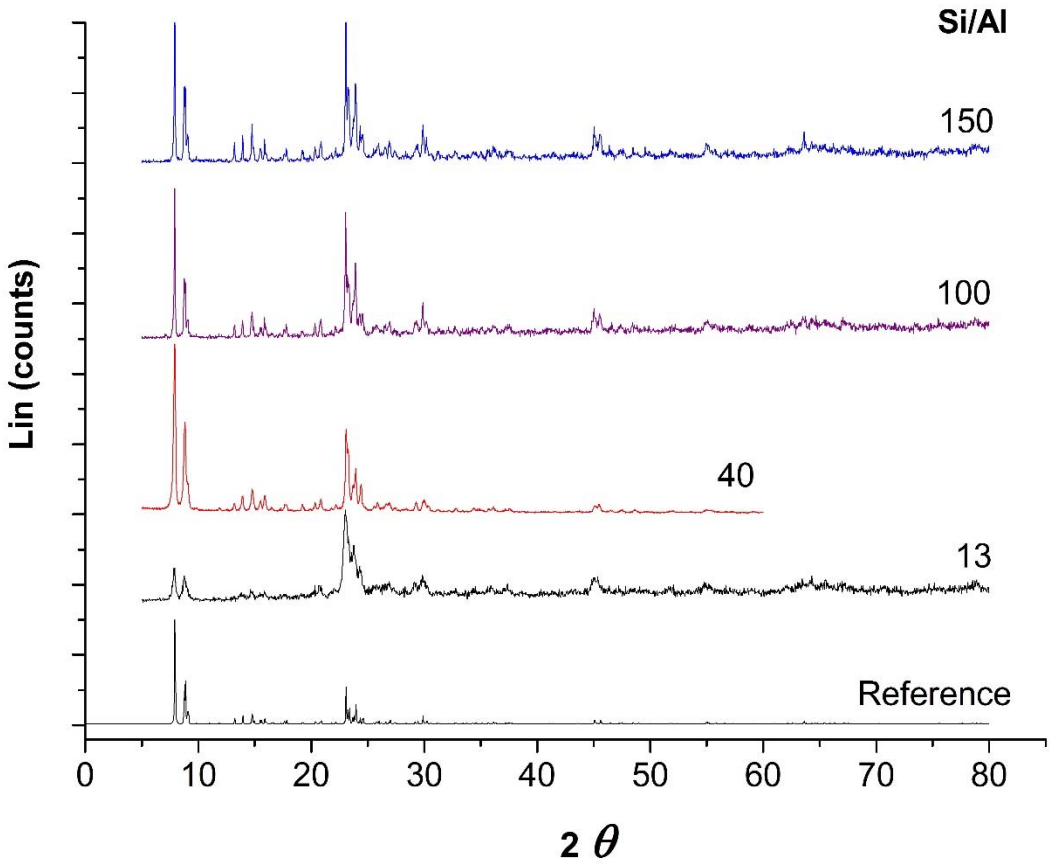

Figure C1 X-ray diffraction pattern of HZSM-5 (Si/Al=13, 40, 100, and 150)

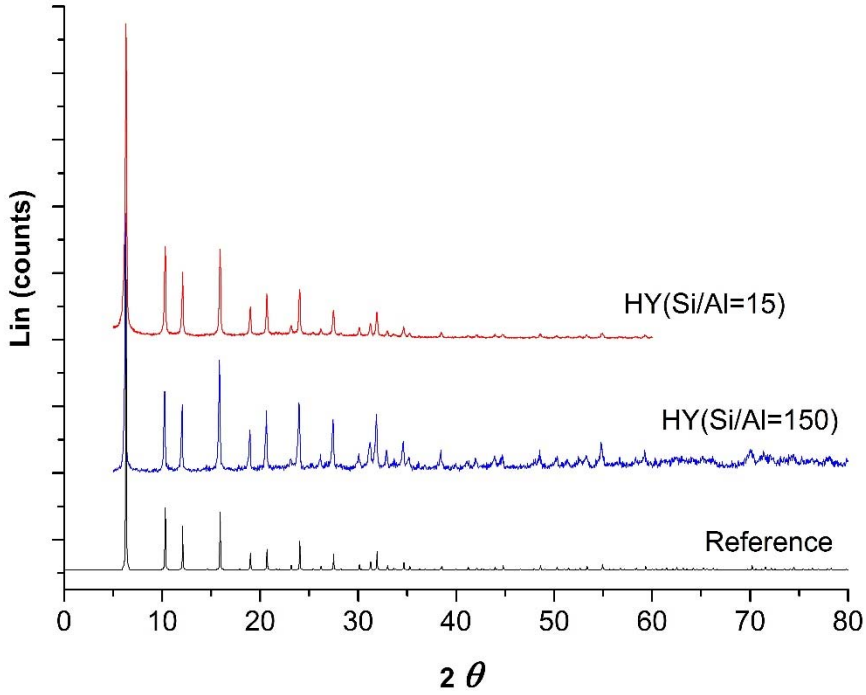

Figure C2 X-ray diffraction pattern of HY (Si/Al=15 and 150)

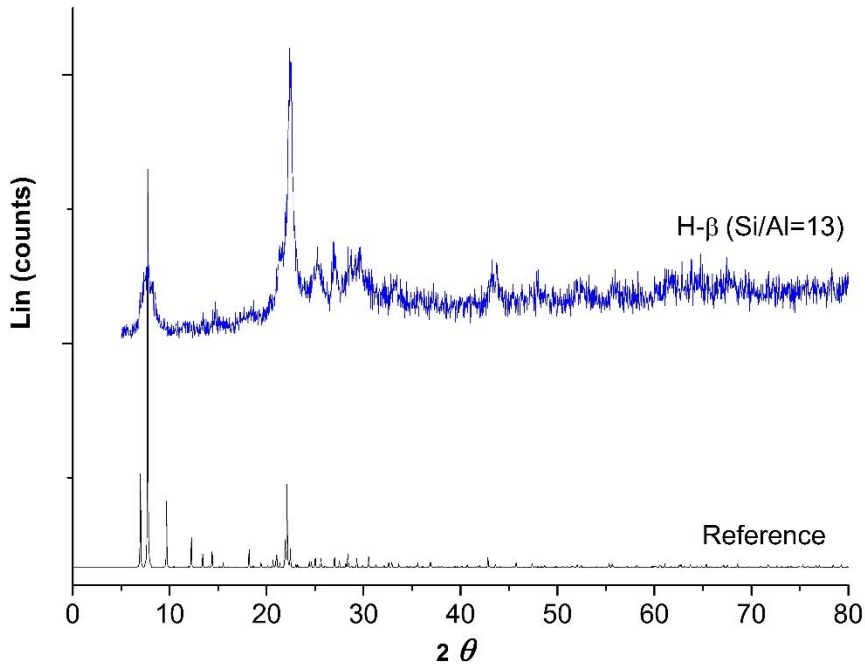

Figure C3 X-ray diffraction pattern of H-β (Si/Al=13)

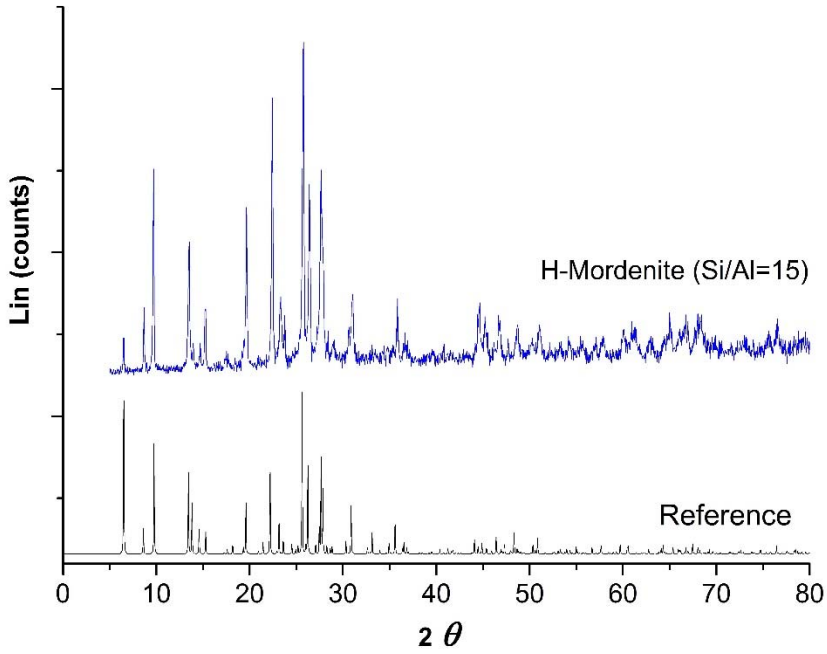

Figure C4 X-ray diffraction pattern of H-Mordenite (Si/Al=15)

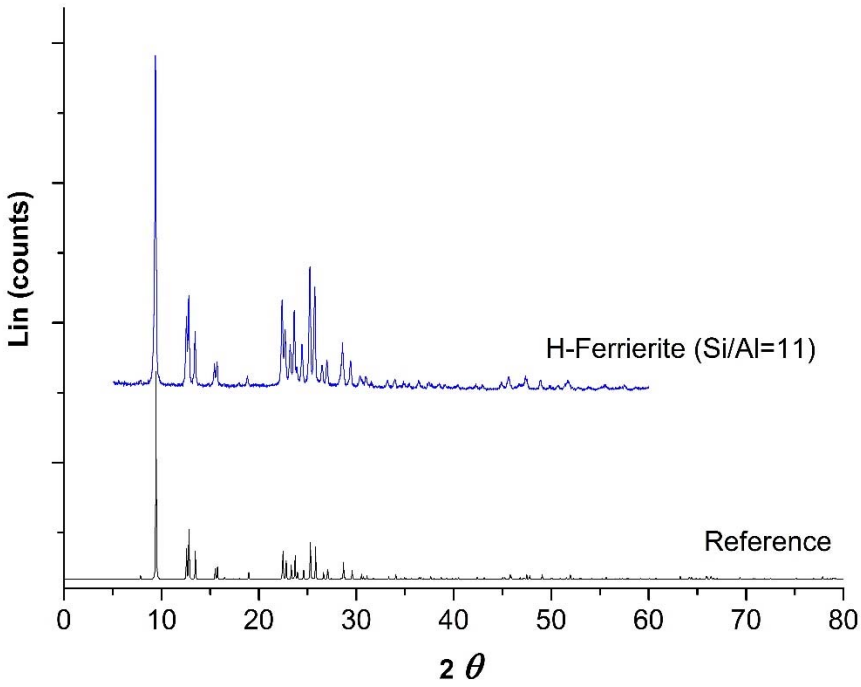

Figure C5 X-ray diffraction pattern of H-Ferrierite (Si/Al=11)

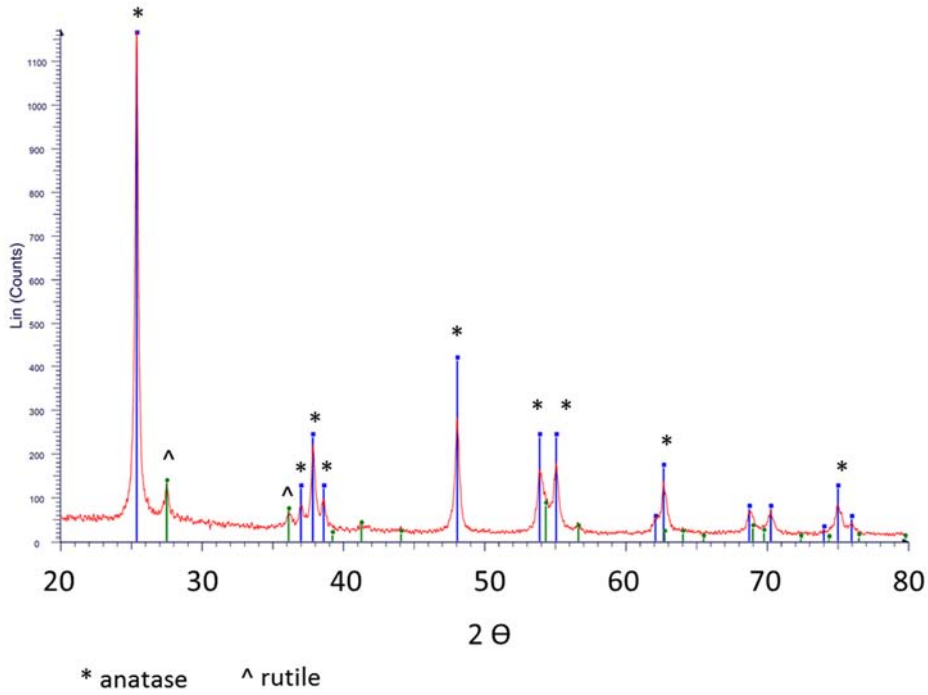

Figure C6 X-ray diffraction pattern of TiO_2

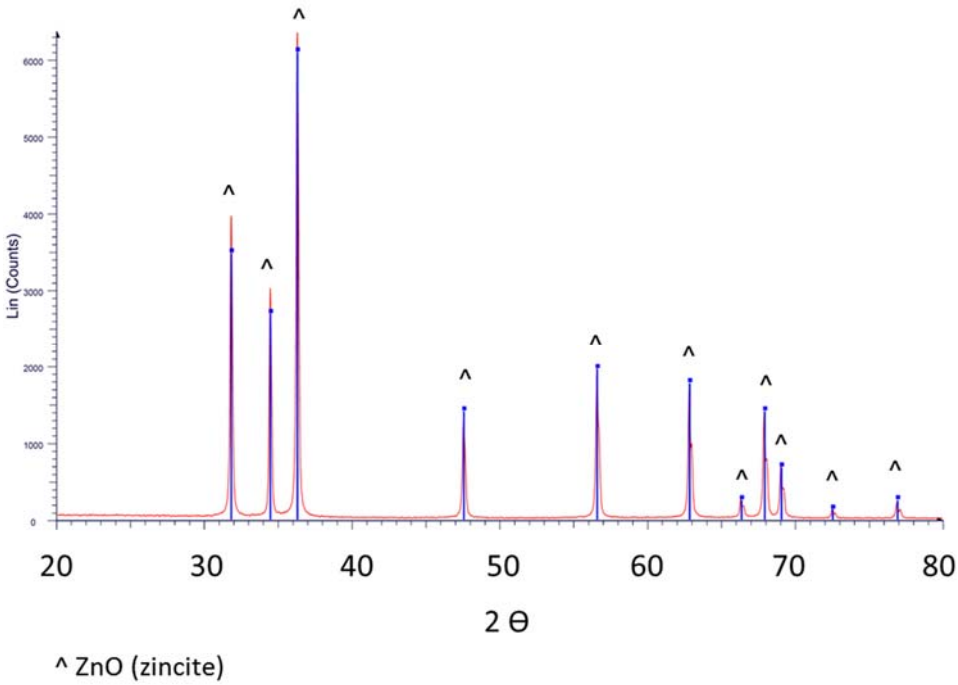

Figure C7 X-ray diffraction pattern of ZnO

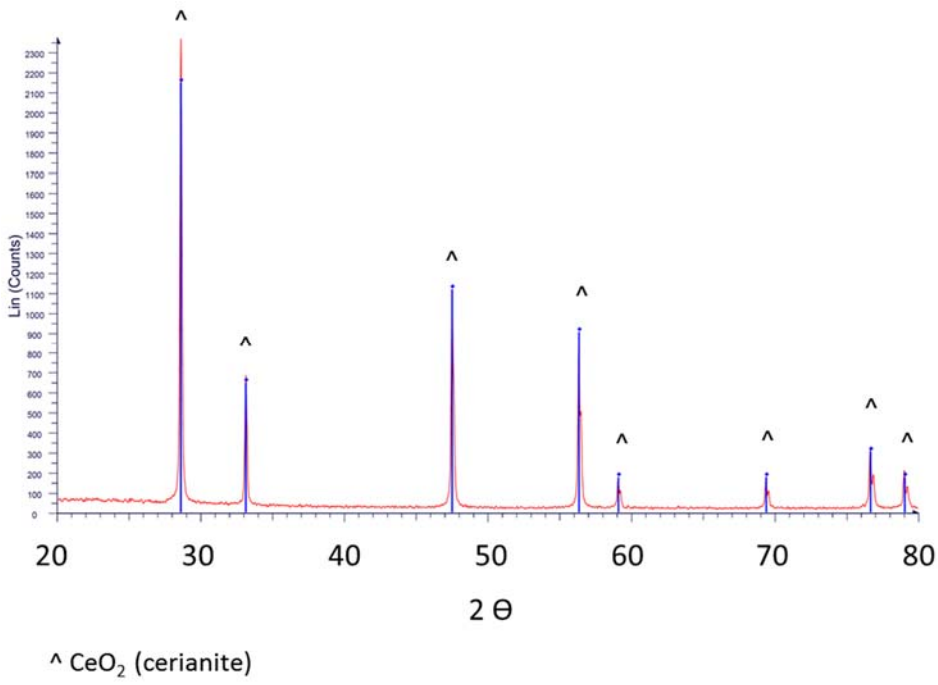

Figure C8 X-ray diffraction pattern of CeO_2

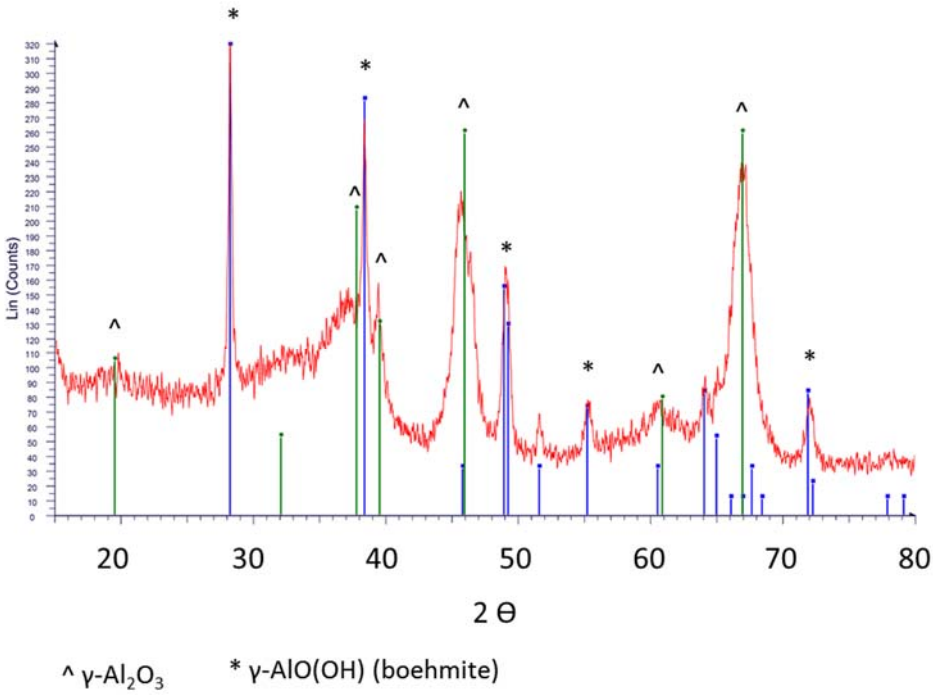

Figure C9 X-ray diffraction pattern of **γ**-Al_2O_3

Appendix D

Surface TPR and TPR of copper catalysts

The TPR is employed to determine the copper dispersed on support. The first TPR represents the total mole of copper. Meanwhile, the second TPR, after surface oxidation of copper by nitrous oxide, corresponds to the mole of surface copper (see also the calculation in Appendix B3).

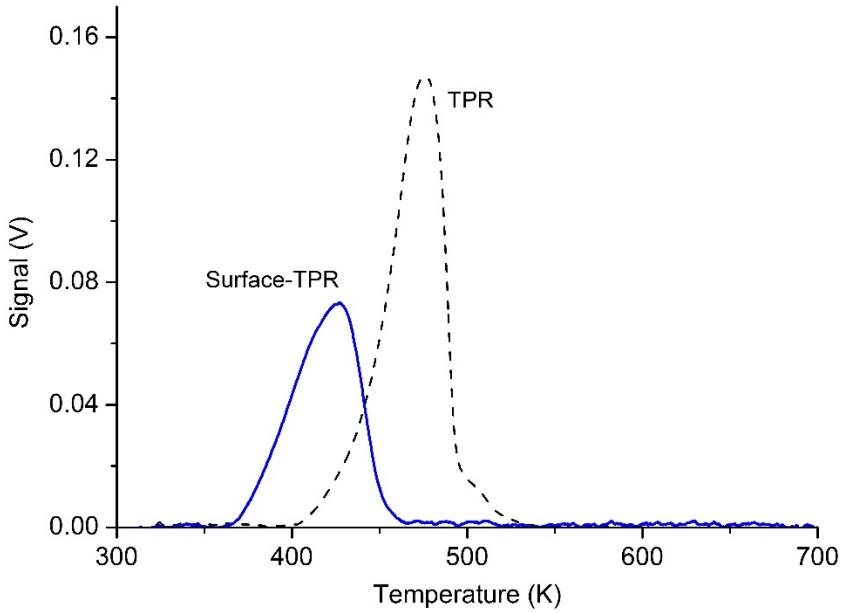

Figure D1 Surface TPR and TPR of 5%Cu/SiO_2 (sample 0.1 g)

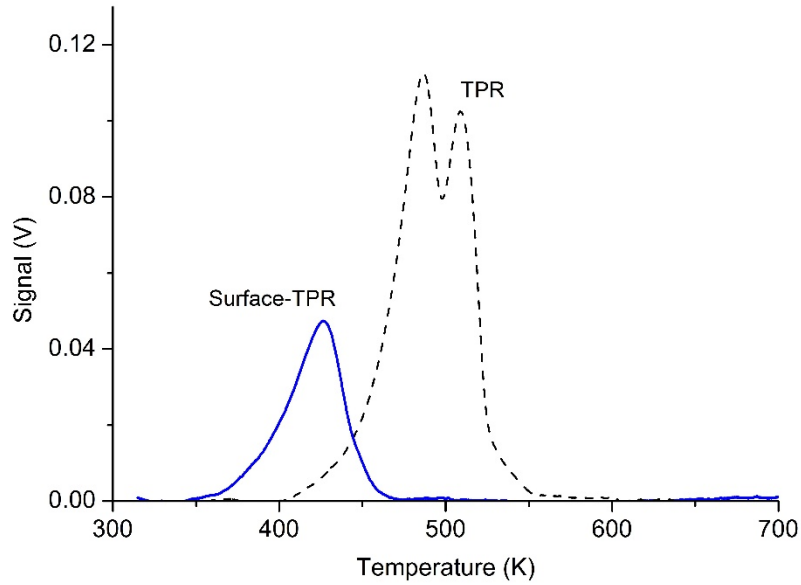

Figure D2 Surface TPR and TPR of 10%Cu/SiO_2 (sample 0.05 g)

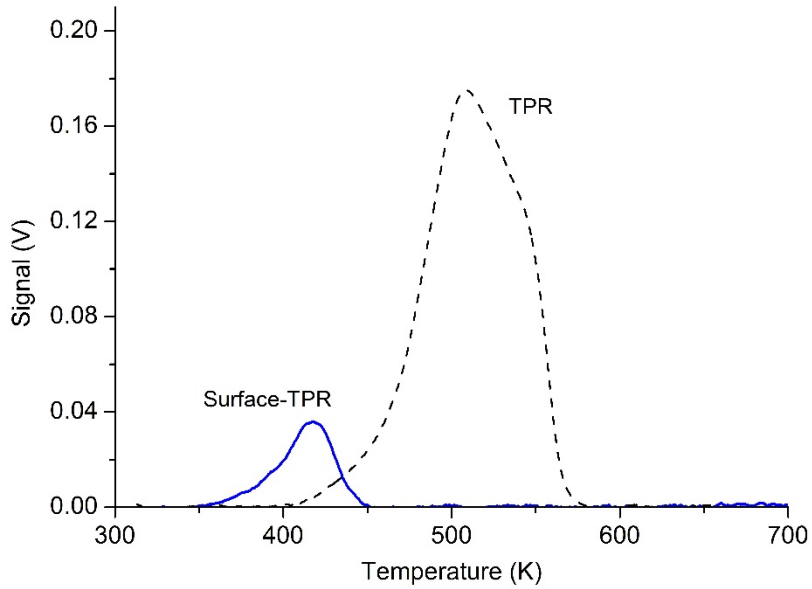

Figure D3 Surface TPR and TPR of 15%Cu/SiO_2 (sample 0.05 g)

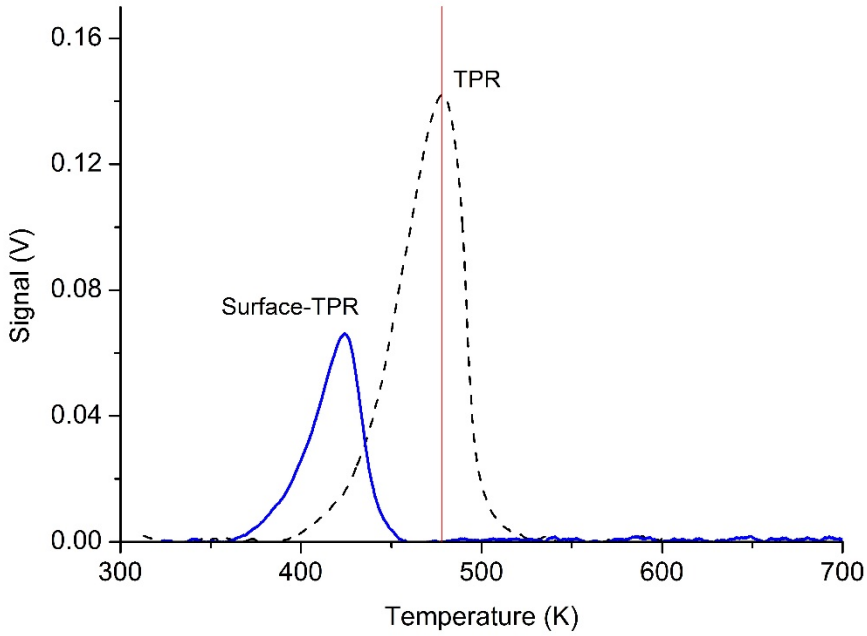

Figure D4 Surface TPR and TPR of 5%Cu/HY (sample 0.1 g)

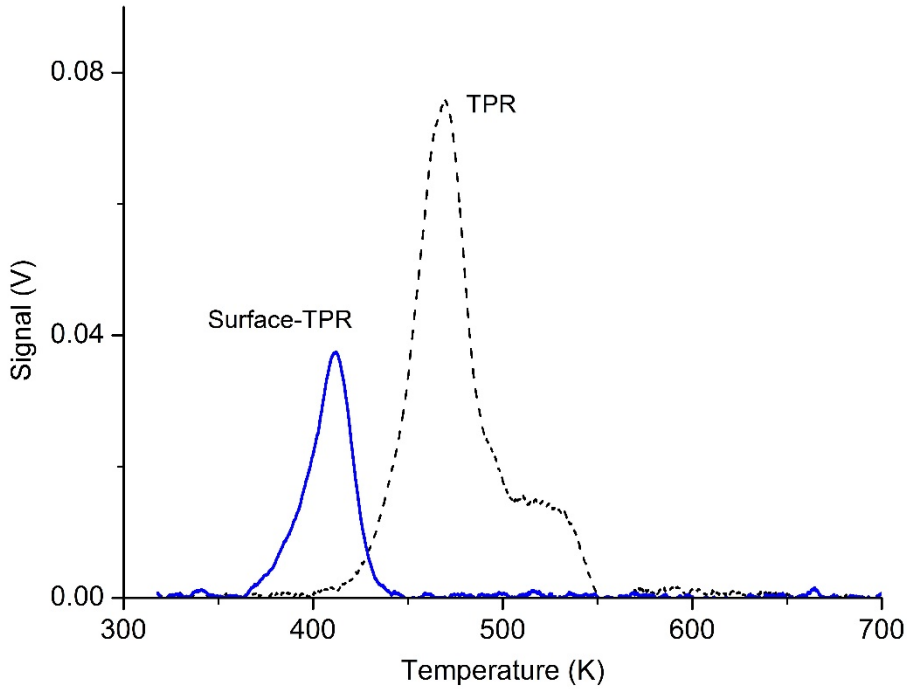

Figure D5 Surface TPR and TPR of 5%Cu/HZSM-5 (sample 0.1 g)

Author biography

Mr. Ayut Witsuthammakul was born on 16 November 1983 in Bangkok. He received a Bachelor of Science in Industrial Chemistry and a Master of Science in Petrochemical and Hydrocarbon Chemistry from the Department of Chemistry, Faculty of Science, King Mongkut's Institute of Technology Ladkrabang in 2006 and 2011, respectively. He also received a Bachelor Degree in General Management from the Faculty of Business Administration, Ramkhamhaeng University in 2006. Currently, he is an assistant researcher under a contract with the Royal Golden Jubilee Ph.D. Program (grant no. PHD/0137/2553) and working under vision of Assoc. Prof. Dr. Tawan Sooknoi at Department of Chemistry, Faculty of Science, King Mongkut's Institute of Technology Ladkrabang, Thailand and Prof. Daniel E. Resasco from the University of Oklahoma, USA.

Academic Publications

1. Selective hydrodeoxygenation of bio-oil derived products: ketones to olefins
   Catalysis Science & Technology, vol.5 (2015) p.3639-3648.
2. Selective hydrodeoxygenation of bio-oil derived products: acetic acid to propylene over hybrid CeO_2-Cu/zeolite catalysts
   Catalysis Science & Technology, Published online, (October, 2015)